NORTHWESTERN UNIVERSITY

Sustainable Polyurethane and Polyurethane-like Network Materials with Excellent Reprocessability and Stress Relaxation and Stiffness in Acrylic Random Copolymer Films

A DISSERTATION

SUBMITTED TO THE GRADUATE SCHOOL

IN PARTIAL FULFILLMENT OF THE REQUIREMENTS

for the degree

DOCTOR OF PHILOSOPHY

Chemical Engineering

By

Sumeng Hu

EVANSTON, ILLINOIS

September 2022

ABSTRACT

Conventional polymer networks are composed of strong, fixed covalent cross-links. The covalent cross-links render polymer networks with outstanding mechanical properties, heat stability, and chemical resistance; however, they also prevent polymer networks from being decross-linked or/and recycled into similar-value products at the end of their life, leading to environmental and economic concerns.

Polyurethanes (PUs) are one of the most widely used commodity polymers. However, the effective recycling of PUs, especially the cross-linked ones, has never been well established. The first part of this dissertation describes two approaches to improve the recyclability of PU and PU-like network materials. In the first approach, the intrinsic dynamic nature of urethane linkages is utilized to achieve excellent reprocessability of conventional PU networks. The property recovery of PU networks after reprocessing is enhanced by judicious molecular design, off-stoichiometry reactions, and proper choice of catalyst. In the second approach, polyhydroxyurethanes (PHUs), which are a class of non-isocyanate PU-like materials, are synthesized from bio-based precursors. Hydroxyurethane dynamic chemistry involves dual dissociative and associative mechanisms. Exploiting this dynamic chemistry, we develop bio-based PHU networks that exhibit complete recovery of cross-link density and tensile properties after multiple reprocessing cycles. We also demonstrate that the mechanical and thermal properties of reprocessable PHU networks can be enhanced by using polyhedral oligomeric silsesquioxanes (POSS) with cyclic carbonate end groups as reactive nanofillers to fabricate dynamic PHU network composites. The intrinsic reprocessability of PHU networks is not impacted by POSS incorporation. With up to 10 wt%

POSS loading, PHU–POSS network composites can undergo multiple reprocessing cycles with 100% recovery of cross-link density.

The second part of this dissertation focuses on understanding the residual stress relaxation behavior and stiffness of supported acrylic random copolymer films. The residual stress relaxation process in spin-coated poly(styrene/*n*-butyl acrylate) (P(S/nBA)) random copolymer films is characterized by ellipsometry and fluorescence. Both techniques show that stress relaxation occurs over a period of hours in the rubbery state and that the presence of a very small amount of nBA units vastly changes the relaxation behavior from neat polystyrene films. Fluorescence characterizations show that the interfacial stiffness of supported P(S/nBA) films is enhanced by attractive hydrogen bonding interactions between polymer films and substrates. The length scale over which substrate perturbations modify the average stiffness of a P(S/nBA) film near a hydrophilic substrate interface increases with increasing nBA molar content. In contrast, studies associated with supported poly(styrene/2-ethylhexyl acrylate) (P(S/EHA)) random copolymer films reveal that the interfacial stiffness and stiffness gradient length scales in supported P(S/EHA) films are independent of interfacial hydrogen bonding interactions. For P(S/EHA)s and P(S/nBA)s with similar bulk glass transition temperatures, the stiffness gradient length scales associated with P(S/EHA) films are substantially longer than those of P(S/nBA) films.

ACKNOWLEDGEMENT

There are many people who I need to acknowledge, but none more so than my advisor, Professor John M. Torkelson. John has played an enormous role in both my professional and personal development. His dedication to excellence has a profound influence on me. Without him, I would not be where I am today. I am deeply grateful for his guidance and support during my time in graduate school.

A special acknowledgement also goes out to the Dow scientists that I have worked with in the Dow-Northwestern UPI project, namely, Dr. Sipei Zhang, Dr. Asghar Peera, Dr. Saswati Pujari, Dr. Alan Nakatani, and Dr. John Reffner. This collaboration was a unique experience to me, and I benefited a lot from it.

I would like to thank my parents, Hongli Tang and Fan Hu, for their love and support during my past nine years studying abroad. I thank them for always being understanding and caring about me. I am lucky to be their daughter.

Finally, I would like to thank all polymer crew members who I had the pleasure to meet and work with, especially those I collaborated with, including Xi Chen, Tong Wei, Tong Wang, Mohammed Bin Rusayyis, Nathan Purwanto, and Jeremy Wang. Graduate school would not have been the same without you. I hope our paths cross again in the future.

TABLE OF CONTENTS

LIST OF SCHEMES

LIST OF FIGURES

LIST OF TABLES

CHAPTER 1

Introduction

Covalently cross-linked polymers are used in a broad range of high-value applications. The covalent cross-links in these materials render them with outstanding mechanical properties, heat stability, and chemical resistance (Sperling, 2006). Unfortunately, the covalent linkages also prevent cross-linked polymers from being reprocessed or recycled into similar value products, leading to significant sustainability and economic losses (Chen et al., 2002; Denissen et al., 2016; Kloxin et al., 2010; Montarnal et al., 2011; Scheutz et al., 2019; Zou et al., 2017). Therefore, developing materials with both desired properties and excellent recyclability remains a scientific and technological challenge.

In recent years, much effort has focused on the development of reprocessable polymer networks, also known as covalent adaptable networks (CANs) (Kloxin et al., 2010; Kloxin & Bowman, 2013) or dynamic covalent polymer networks (DCPNs) (Zou et al., 2017), which contain sufficient dynamic bonds or structures that allow the cross-linked polymers to change their chemical structures or physical shapes under certain conditions (Brandt et al., 2014; Chakma & Konkolewicz, 2019; Denissen et al., 2016; Kloxin et al., 2010; Kloxin & Bowman, 2013; McBride et al., 2019; Podgórski et al., 2020; Schneiderman & Hillmyer, 2017; Wojtecki et al., 2011; Y. Yang et al., 2015; Zou et al., 2017). Since the landmark study by Wudl and coworkers on a thermally re-mendable network designed with the Diels–Alder (DA) reaction (X. Chen et al., 2002), there has been considerable progress in developing CANs with numerous dynamic chemistries. These include dissociative chemistries such as hindered urea exchange (Bin Rusayyis & Torkelson, 2022; Ying et al., 2014; Y. Zhang et al., 2016), alkoxyamine chemistry (Jin et al.,

2016; Li et al., 2021; Otsuka, 2013), and bis(hindered amino) disulfide chemistry (Bin Rusayyis & Torkelson, 2021; Bin Rusayyis & Torkelson, 2020), and associative chemistries such as transesterification (Li et al., 2018; Montarnal et al., 2011; Snyder et al., 2018; B. Zhang et al., 2018), boronic ester interchange (Y. Chen et al., 2018; Soman & Evans, 2021; Tajbakhsh et al., 2021), and transamination of vinylogous urethanes (Denissen et al., 2015, 2017), among others (Anaya et al., 2021; Y. Hu et al., 2021; Ishibashi & Kalow, 2018; Li et al., 2020). However, many of the published studies on CANs require complicated, multi-step synthesis, and full recovery of properties associated with cross-link density after reprocessing has been achieved only in limited cases.

The first part of this dissertation is focused on developing simple strategies to achieve excellent property recovery of CANs after reprocessing. Studies are primarily focused on polyurethanes (PUs) and PU-like materials. Polyurethanes are one of the most widely used commodity polymers; however, efficient recycling of PUs, especially the cross-linked ones, has never been well established. Urethane linkages are intrinsically dynamic, and the dynamic process involves both associative and dissociative mechanisms (X. Chen et al., 2020; Scheutz et al., 2019). Because isocyanate groups liberated from the dissociative reactions at the reprocessing conditions are active and prone to side reactions, PU networks commonly suffer from property loss after reprocessing. Some studies have tried to incorporate extrinsic dynamic functionalities such as hindered urea bonds and disulfide bonds into PU networks to improve the reprocessability (J.-H. Chen, Hu, Li, Meng, et al., 2018; Gao et al., 2018; Y. Zhang et al., 2016; Z. P. Zhang et al., 2018); however, this strategy typically involves complicated monomer synthesis, which is not ideal for industrial applications. Therefore, the main objective of the first part of this dissertation is to develop simple strategies to improve the reprocessability of PU and PU-like network materials.

The second part of this dissertation is focused on understanding the role of the substrate interface in perturbing the stiffness of supported acrylic random copolymer films. Nanoconfined polymers typically do not exhibit bulk properties, and research has shown that surfaces and interfacial effects are responsible for such behavior. Confinement effects on modulus and stiffness have been investigated for more than two decades, and numerous techniques have been employed to study stiffness-confinement effects for a variety of polymer−substrate pairs (Askar et al., 2015; Askar & Torkelson, 2016; Brune et al., 2016; Cheng et al., 2007; Delcambre et al., 2010; Evans et al., 2012; Forrest et al., 1998; Gomopoulos et al., 2010; Inoue et al., 2005; Song et al., 2019; Stafford et al., 2004, 2006; Tweedie et al., 2007; Watcharotone et al., 2011; Xia et al., 2016; Ye et al., 2015). In 2016, Askar and Torkelson (Askar & Torkelson, 2016) used fluorescence to characterize perturbations associated with substrate and free-surface interfaces to stiffness of polystyrene films supported on glass and demonstrated that deviations in polymer stiffness upon confinement originate from the combined perturbations from the substrate and free-surface interfaces. The perturbations were attributed to a general phenomenon of molecular caging and were related to the rigidity of substrates (Askar & Torkelson, 2016). The role of interfacial interactions between polymer films and substrates on polymer stiffness has never been studied. A major motivation of the second part of this dissertation is to understand substrate perturbations to stiffness of polymer films when attractive interfacial interactions are present in the polymer−substrate interfacial region.

Chapter 2 introduces and provides background on the core concepts involved in this dissertation regarding dynamic covalent polymer networks, PUs, and PU-like materials. Chapter 3, 4, and 5 focus on the development of strategies to improve the reprocessability and thermomechanical properties of PU and PU-like network materials. In Chapter 3, we demonstrate

that the intrinsic dynamic nature of urethane linkages can be utilized to achieve excellent reprocessability of cross-linked PU networks. We discovered that the property recovery and thermal stability of dynamic PU networks can be enhanced by incorporating excess free hydroxyl groups or increasing the cross-linker functionality from three to four (X. Chen et al., 2020). While free hydroxyl groups suppress the reversion of urethane linkages and minimize side reactions associated with isocyanate groups generated from the dissociative reactions during reprocessing, tetrafunctional cross-linkers help to maintain network integrity in the presence of small levels of side reactions. Using these strategies, we demonstrated via a model PU network that the intrinsic dynamic nature of urethane linkages enables full recovery of cross-link density and tensile properties of PU networks after multiple reprocessing cycles. We also showed via a proof-of-principle demonstration that PU networks can be depolymerized by alcoholysis under relatively mild conditions, which can potentially lead to monomer recovery and help to achieve a closed loop recycling of PUs.

Besides recycling, PU synthesis involves another problem which is the use of isocyanates. Isocyanates are hazardous and have been facing increasing constraints on storage and transportations in recent years. In Chapter 4, we employed bio-based feedstocks to synthesize polyhydroxyurethane (PHU) networks, which are a class of non-isocyanate PU materials. Besides the non-isocyanate nature, PHU has an additional important advantage which is that the dynamic nature of hydroxyurethane linkages can be utilized to achieve reprocessability of PHU networks. In Chapter 4, renewable, dynamic PHU networks were synthesized by reacting bio-derived polyfunctional cyclic carbonates, carbonated soybean oil (CSBO) and sorbitol ether carbonate (SEC), with either a synthetic diamine or a bio-based diamine (S. Hu et al., 2019). With relatively mild reprocessing conditions, CSBO-based PHU networks exhibit complete recovery of cross-link

density and associated properties after multiple melt-state reprocessing steps, which is achieved via three concurrent dynamic chemistries. In contrast to the excellent property recovery achieved by CSBO-based PHU networks, as a result of disadvantageous monomer molecular design, SEC-based networks exhibit poor reprocessability even with increased catalyst load and reprocessing temperature and time. This work reveals the important role of monomer structure on the reprocessability of dynamic polymer networks and highlights the effectiveness of CSBO to serve as a precursor of robust, sustainable non-isocyanate polyurethane (NIPU) networks with excellent reprocessability.

The rapid development of CANs shows promise for addressing the long-standing recycling issue associated with conventional, permanently cross-linked polymers. At the same time, it is important to demonstrate that properties of CANs can be optimized to meet the ongoing demands for high-performance materials. In Chapter 5, we demonstrate that the properties of reprocessable PHU networks can be enhanced by using reactive polyhedral oligomeric silsesquioxane (POSS) as reinforcing fillers to fabricate dynamic PHU network composite. With functionalized POSS serving as both nanofillers and a fraction of the cross-linkers, the PHU−POSS network composites exhibit significantly enhanced storage modulus and thermal stability relative to the neat PHU network. With up to 10 wt% POSS loading, the network composites can undergo melt-state reprocessing at 140 °C with 100% property recovery associated with cross-link density. We also show that hydroxyurethane dynamic chemistry leads to excellent creep resistance at elevated temperature up to 90 °C and is unaffected by reactive incorporation of POSS. This study demonstrates the effectiveness of POSS as nanofillers for designing high-performance, dynamic PHU networks with excellent reprocessability.

Chapter 6 introduces core concepts involved in this dissertation regarding residual stress, stiffness, and stiffness-confinement effects in polymers. Chapter 7, 8 and 9 focus on developing an understanding of effects of substrate interface on stiffness of supported acrylic random copolymer films in the interfacial region. Stiffness characterizations described in this dissertation were achieved using a fluorescence technique, which relies on the sensitivity of a measurable intensity ratio I_1/I_3 of a pyrenyl label that is responsive to molecular caging. For a pyrene-labeled polymer film, I_1/I_3 values are influenced by both the stress state and the stiffness of a material (Askar et al., 2015); therefore, prior to stiffness characterization, sufficient annealing in the rubbery state needs to be done to ensure all residual stresses in polymer films are apparently removed, so that I_1/I_3 values only reflect information on stiffness. Chapter 7 demonstrates that residual stress relaxation in spin-coated polymer films can be characterized using both ellipsometry and fluorescence techniques. We show that the residual stress relaxation timescale of bulk poly(styrene/*n*-butyl acrylate) (P(S/nBA)) random copolymer films depends significantly on the molar content of nBA in the copolymers.

Chapter 8 focuses on investigating the role of substrate interface in perturbing the local stiffness of supported P(S/nBA) films when attractive hydrogen bonding interactions are present in the interfacial region. We discovered that the stiffness of P(S/nBA) films is enhanced near hydrophilic substrates, and the length scale over which substrate perturbations enhance the average stiffness is highly dependent on nBA content due to the ability of ester groups in nBA units to form hydrogen bonds with hydroxyl groups on a hydrophilic glass surface. When the hydroxyl groups on the glass surface are removed, the perturbation length scales decrease and become independent of nBA content. Thus, our study shows that in addition to substrate rigidity, interfacial

effects are another important contributor to stiffness-confinement effects in supported polymer films.

Chapter 9 focuses on understanding the effect of a slight change in monomer structure on stiffness and stiffness gradient lengths scales of acrylic-based random copolymer films in the interfacial region. We investigated the substrate perturbations to stiffness of another acrylic-based random copolymer, poly(styrene/2-ethylhexyl acrylate) (P(S/EHA)), and compared the results with those of P(S/nBA)s. We discovered that for P(S/EHA)s and P(S/nBA)s with similar bulk glass transition temperatures, the stiffness gradient length scales near the substrate interface associated with P(S/EHA) films are substantially longer than those of P(S/nBA)s. The stiffness gradient length scales in P(S/EHA)s remain constant regardless of whether attractive hydrogen bonding interactions are possible or not in the interfacial region.

Finally, Chapter 10 provides a summary of this dissertation and offers recommendations for future studies.

CHAPTER 2

Background

This chapter introduces core concepts involved in this dissertation regarding dynamic covalent polymer networks and polyurethanes.

2.1 Conventional and Reprocessable Cross-linked Polymers

2.1.1 Conventional cross-linked polymers

Polymers can be divided into two types based on their response to heating: thermoplastics and thermosets (Brazel & Rosen, 2012; Chanda, 2013; Rubinstein & Colby, 2003). The primary physical difference between these two types of materials is that thermoplastics can be re-melted back into a liquid when heated above the glass transition temperature, T_g, if amorphous or above the melt transition temperature, or T_m, if semi-crystalline. In contrast, thermosets remain in a permanent solid state once they are cured. The reason why thermoplastics and thermosets behave differently is that they have different structures. Thermoplastics are typically made of linear or sometimes branched polymer chains. The chains can slide past each other upon heating and allow thermoplastics to be remolded and recycled without affecting their material properties. Thermosets, on the other hand, have covalent cross-links. These cross-links often afford thermosets properties that are superior to thermoplastics, including improved mechanical properties, better heat stability, and solvent resistance (Brazel & Rosen, 2012). A schematic representation of thermoplastics and thermosets is given in Figure 2-1.

Thermosets are synthesized by three general routes (Sperling, 2006). The first route is step-growth polymerization with at least one monomer species having a functionality greater than two

(Flory, 1953; Lodge & Hiemenz, 2020). A typical example is the reaction between diisocyanates and multifunctional polyols to form polyurethane network materials (Akindoyo et al., 2016). The second route is chain-growth polymerization which involves polymerizing monomers with multiple polymerizable moieties which can serve as branching units (Rubinstein & Colby, 2003). One example is the copolymerization of styrene and ethylene glycol dimethacrylate, the latter of which contains two carbon-carbon bonds and serves as the branching unit. Finally, thermosets can also be achieved through post-polymerization modifications. For example, the vulcanization process in the tire industry uses sulfur to cross-link linear polymers of polyisoprene or styrene-butadiene copolymers and make the tires more durable (Coran, 2003).

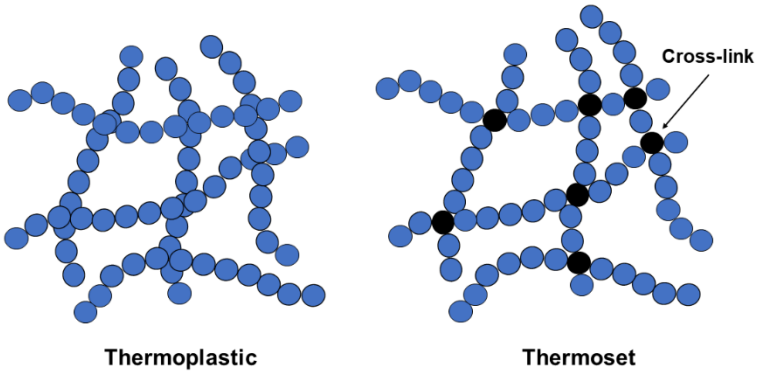

Figure 2-1. Schematic structures of linear polymers (thermoplastics) and cross-linked polymers (polymer networks or thermosets).

2.1.2 Dynamic covalent polymer networks

Despite their high durability, thermosets have one major disadvantage which is that they cannot be recycled for high-value applications because the permanent, fixed cross-links that make these materials strong and useful also prevent them from being melt-reprocessed. This has led to significant economic losses and environmental concerns. To address the problems associated with the recycling of conventional thermosets, research began over a decade ago to develop dynamic

covalent polymer networks (DCPNs) (Zou et al., 2017), also known as covalent adaptable networks (CANs) (Kloxin et al., 2010; Kloxin & Bowman, 2013) or reprocessable polymer networks, that are self-healable or recyclable (Brandt et al., 2014; Chakma & Konkolewicz, 2019; Denissen et al., 2016; Kloxin et al., 2010; Kloxin & Bowman, 2013; McBride et al., 2019; Podgórski et al., 2020; Scheutz et al., 2019; Schneiderman & Hillmyer, 2017; Wojtecki et al., 2011; Y. Yang et al., 2015; Zou et al., 2017). DCPNs are polymer networks that contain sufficient dynamic covalent bonds or structures that allow the materials to reconfigure or rearrange under appropriate conditions. Such materials can change their structures and shapes in response to external stimuli (e.g., heat, light, pH) and have the potential to be recycled in an analogous way to thermoplastics.

2.1.3 Dynamic chemistries

Dynamic covalent polymer networks have generally been considered to undergo structural reconfiguration by one of two general mechanisms (Denissen et al., 2016; Kloxin et al., 2010; Scheutz et al., 2019) (Figure 2-2). The first is a dissociative bond exchange mechanism in which dynamic bonds break under an applied stimulus such as high temperature or light; after that, the network segment that bears the reactive moiety will diffuse through the network until it encounters its complementary reactive moiety and forms a new bond there (Scheutz et al., 2019). This dissociation, diffusion, and association process occurs repeatedly until the applied stimulus is removed from the system. The second mechanism is an associative bond exchange mechanism, in which case free reactive groups in the network system can undergo substitution reactions with existing cross-links in the system (Scheutz et al., 2019). In this case, bond breaking and bond forming always happen simultaneously; therefore, the total number of cross-links is considered to remain constant during the entire process. In most cases, DCPNs undergo structure reconfiguration

by only one of the two mechanisms, although a few studies show that some specific types of dynamic chemistries involve dual dissociative and associative mechanisms; examples include urethane chemistry (X. Chen et al., 2020), thiourethane chemistry (Li et al., 2019; Wen et al., 2020) and hydroxyurethane chemistry (X. Chen et al., 2017; S. Hu et al., 2019). DCPNs based solely on associative bond exchange are termed "vitrimers" by Leibler and coworkers (Capelot, Montarnal, et al., 2012). Regardless of the underlying mechanism, in the absence of external stimuli, the dynamic process in DCPNs are commonly considered to be dormant, which allows DCPNs to be used as conventional cross-linked polymers.

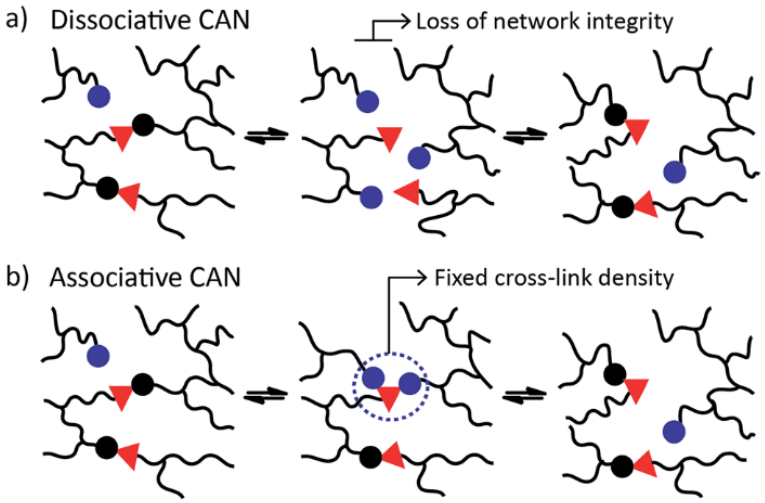

Figure 2-2. Dynamic chemistries in DCPNs or CANs are divided into two groups: (a) dissociative and (b) associative. (Figure adapted from reference ((Denissen et al., 2016)).)

2.1.3.1 Dissociative dynamic chemistry

In DCPNs based on dissociative mechanisms, upon proper external stimulus (in most cases, heat), the dynamic bonds will dissociate and reach a new dynamic equilibrium between the dissociated moieties and the combined moieties (Scheutz et al., 2019). At sufficiently high temperatures, the dynamic equilibrium highly favors the cross-link dissociation, which leads to the

partial decross-linking of the networks. As a result, the fully cross-linked polymer transitions to a system with many branched and linear chains which can flow under stress like thermoplastics and therefore are intrinsically reprocessable.

Many dissociative chemistries such as Diels−Alder (DA) cycloadditions (X. Chen et al., 2002), hindered urea exchange (Bin Rusayyis & Torkelson, 2022; Ying et al., 2014; Y. Zhang et al., 2016), aminal bond exchange (Chao & Zhang, 2019), and persistent radical approaches using nitroxide (Jin et al., 2016) or thionitroxide (Bin Rusayyis & Torkelson, 2020; Takahashi et al., 2017) radicals have been explored and used successfully for DCPN synthesis. DA reactions are one the earliest and most commonly used dynamic chemistries for dissociative DCPNs. In 2002, Wudl and coworkers designed a thermally re-mendable network using DA cycloaddition of multi-furan and multi-maleimide monomers; this work is considered as the seminal study in the research field of DCPNs (X. Chen et al., 2002). Since this work, numerous DA-crosslinked materials with various reconfiguration abilities have been developed for different applications (Adzima et al., 2008; Bai et al., 2015; Oehlenschlaeger et al., 2014; Polgar et al., 2015; Reutenauer et al., 2009; Tanasi et al., 2019; Toncelli et al., 2012; Truong et al., 2019; Yamashiro et al., 2008).

Radical-based approaches involving nitroxide or thionitroxide radicals are dissociative dynamic chemistries that are also very effective in developing DCPNs with excellent reprocessability. Jin et al. (Jin et al., 2016) developed a one-step strategy that can be used to synthesize recyclable cross-linked polymers from any monomers or polymers that contain carbon–carbon double bonds using a polymerizable nitroxide radical 2,2,6,6-tetramethyl-1-piperidinyloxy methacrylate (TEMPO methacrylate). The nitroxide radicals incorporated in the network can reversibly cap/uncap, thus allowing the material to undergo thermally triggered dissociation-combination reactions and achieve reprocessability. More recently, Bin Rusayyis and Torkelson

(Bin Rusayyis & Torkelson, 2020) developed a reprocessable polymethacrylate network using a bifunctional bis(dialkylamino) disulfide cross-linker (BiTEMPS methacrylate), which is a sulfur analogue of TEMPO methacrylate. BiTEMPS can dissociate into thionitroxide radicals upon heating, allowing the network to undergo multiple melt-reprocessing steps with full recovery of cross-link density. One particular advantage of the BiTEMPS methacrylate over the TEMPO methacrylate is that networks cross-linked with BiTEMPS do not generate any carbon-centered radicals during reprocessing; therefore, the irreversible termination of carbon-centered radicals that potentially leads to property loss of TEMPO-methacrylate-cross-linked networks is prevented (Bin Rusayyis & Torkelson, 2020).

2.1.3.2 Associative dynamic chemistry

Dynamic covalent polymer networks based on associative bond exchange mechanisms are cross-linked polymers with exchangeable covalent bonds that enter a dynamic equilibrium for cross-link exchange when activated (Scheutz et al., 2019). Unlike DCPNs based on dissociative chemistries, bond breaking and bond forming in associative DCPNs occur simultaneously in a single-step exchange reaction rather than in discrete dissociation, diffusion, and association steps. Significant research effort has been devoted to design healable or reprocessable materials based on associative dynamic chemistries. Because of the nature of exchange reactions, the chemical entities on both sides of the equilibrium are essentially the same, so neither side of the reaction is thermodynamically favored. At higher temperatures, only the exchange rate is accelerated.

Examples of associative chemistries include transesterification (Li et al., 2018; Montarnal et al., 2011; Snyder et al., 2018; B. Zhang et al., 2018), transamination (Denissen et al., 2015, 2017), boronic ester interchange (Y. Chen et al., 2018; Soman & Evans, 2021; Tajbakhsh et al., 2021), sulfide exchange reaction (Li et al., 2020; Rekondo et al., 2014), trans-siloxanification (P.

Zheng & McCarthy, 2012), and olefin metathesis (Lu et al., 2012; Lu & Guan, 2012). The most-commonly studied associative chemistry to date is the transesterification reactions of esters in the presence of free alcohols, commonly catalyzed by Lewis acids or organocatalysts. In 2011, Leibler and coworkers first developed a transesterification-based DCPN containing a $Zn(acac)_2$ catalyst (Montarnal et al., 2011). This DCPN can be reprocessed to yield materials with properties similar to the as-synthesized resins. In a later study, Leibler and coworkers coined the term "vitrimers" to describe DCPNs solely based on associative exchange reactions to highlight the Arrhenius relationship between viscosity and temperature (Capelot, Montarnal, et al., 2012), although later others questioned the use of this term because the viscosity of most dissociative DCPNs seems to also exhibit an Arrhenius dependence of temperature over broad temperature ranges typically used for reprocessing (Elling & Dichtel, 2020).

2.2 Polyurethanes and Polyurethane-like Materials

2.2.1 Conventional polyurethanes

Polyurethanes (PUs) were first developed in 1937 by Dr. Otto Bayer and coworkers in Germany (Bayer, 1947). Polyurethanes are among the most widely used commodity polymers. World-wide production of PUs accounts for approximately 5% of global polymer production (Blattmann et al., 2014; Delebecq et al., 2013; Engels et al., 2013). Polyurethanes are synthesized from the step-growth polymerization of isocyanates and alcohols. If both reactants are difunctional, the resulting PUs are linear. If one or both reactants have a functionality that is greater than two, the resulting PUs may be cross-linked. Isocyanates are highly reactive toward nucleophilic reagents, because the electronegativity of the oxygen and nitrogen imparts a large electrophilic character to the carbon in the isocyanate group (Chattopadhyay & Raju, 2007; Kathalewar et al.,

2013). Commonly used isocyanates for PU manufacturing include toluene diisocyanate (TDI), methylene diphenylene isocyanate (MDI), xylene diisocyanate (XDI), isophorone diisocyanate (IPDI), norbornane diisocyanate (NBDI), hydrogenated MDI (HMDI), etc. Commonly used polyols for PU manufacturing include polyethylene glycol (PEG), polypropylene glycol (PPG), poly(tetramethylene ether) glycol (PTMEG), etc. Because there are many possible combinations of the isocyanates and alcohols, a broad range of PUs with different properties can be obtained, and these materials are used in a broad array of applications such as foams, coatings, sealants, and adhesives (Blattmann et al., 2014; Nohra et al., 2013).

Polyurethane foams constitute 67% of global PU production (Engels et al., 2013). Two main types of blowing agents used for PU foams production are (i) physical blowing agents such as low-boiling-point solvent which blows the polymers by vaporization, and (ii) chemical blowing agents such as water which blows the polymers by reacting with isocyanates to form amines and carbon dioxide (Gama et al., 2018). Depending on the molecular weight and functionality of the reactants, PU foams are classified as flexible foams and rigid foams. Flexible foams are mostly used for fabricating furniture cushions, mattresses, and acoustic dampers (Engels et al., 2013). Rigid foams exhibit excellent insulating properties and are commonly used as structural materials (Engels et al., 2013).

Polyurethane elastomers are also a very important class of PUs although their global production is much lower than that of PU foams. Polyurethane elastomers are typically segmented and consist of alternating soft and hard segments (Engels et al., 2013). Soft segments consist of polyols, and hard segments consist of all non-polyol components. Because of rigidity and hydrogen bonding, hard segments associate into hard domains which act as physical cross-links to afford

PUs elastomeric characteristics. PU elastomers are, thus, two-phase polymers, and their elastomeric properties are highly dependent on the degree of the phase separation.

2.2.2 Polyhydroxyurethanes

The synthesis of conventional PUs involves isocyanates, which present serious issues for human health. Overexposure to isocyanates may cause sensitization and occupational asthma (Elms et al., 2001; Fisseler-Eckhoff et al., 2011). Due to these health concerns, many isocyanates are listed as dangerous chemicals and are under increasing regulatory scrutiny regarding safe transport and use. In view of the trend toward green chemistry, research efforts have intensified in recent years to find routes to non-isocyanate PU (NIPU) materials (Blattmann et al., 2014; Guan et al., 2011; Kathalewar et al., 2013). Common reactions include transurethanization between alcohols and carbamates (Deng et al., 2014; Ochiai & Utsuno, 2013; Z. Wang et al., 2016) and cyclic carbonate aminolysis reaction between cyclic carbonates and amines (Beniah, Chen, et al., 2017; Beniah et al., 2016; Beniah, Fortman, et al., 2017; Beniah, Heath, et al., 2017; Beniah, Uno, et al., 2017; Leitsch et al., 2016; Lombardo et al., 2015; Nohra et al., 2013; Steblyanko et al., 2000; Tomita et al., 2001).

The cyclic carbonate aminolysis reaction is nowadays seen as one of the most promising approaches to synthesize NIPUs (Blattmann et al., 2014; Cornille, Auvergne, et al., 2017; Guan et al., 2011; Kathalewar et al., 2013; Maisonneuve et al., 2015). The five-, six-, seven-, or eight-membered cyclic carbonates undergo reactions with amines resulting in the formation of polyhydroxyurethanes (PHUs), which are structurally similar to PUs, except that there is a pendent primary or secondary hydroxyl group next to each urethane linkage in PHUs. The cyclic carbonate aminolysis reaction has significant sustainability benefits, not only because it circumvents the use

of isocyanates, but also because five-membered cyclic carbonates can be easily obtained by sequestering carbon dioxide into epoxies, so this chemistry also contributes to carbon neutrality.

2.2.3 Dynamic PUs and PHUs

Conventional cross-linked PUs cannot be effectively remolded or reprocessed when reaching their end of life. The urethane bond is a dynamic bond, and its dynamic chemistry has a dual-mechanism nature (Scheme 2-1). When exposed to heat, dynamic urethane bonds can undergo simultaneous dissociative and associative reactions; the urethane linkages can dissociative into isocyanate and alcohol moieties, and if there are free hydroxyl groups present in the system, these free hydroxyl groups can undergo associative transcarbamoylation exchange reactions with urethane linkages (X. Chen et al., 2020). Both mechanisms can be utilized to achieve reprocessability of cross-linked PUs. However, because transcarbamoylation reactions are "sluggish" (Fortman et al., 2015), and isocyanate groups generated from the dissociative reactions are reactive and are prone to side reactions, PU thermosets commonly suffer from property loss after recycling. To solve this problem, many studies have incorporated extrinsic dynamic bonds such as hindered urea bonds and disulfide bonds to enhance the recyclability of cross-linked PUs (J.-H. Chen, Hu, Li, Meng, et al., 2018; Gao et al., 2018; Y. Zhang et al., 2016; Z. P. Zhang et al., 2018); however, these synthetic strategies usually involve complicated monomer synthesis and sometimes can even lead to changes in bulk properties relative to neat PUs, which is impractical for commercial applications.

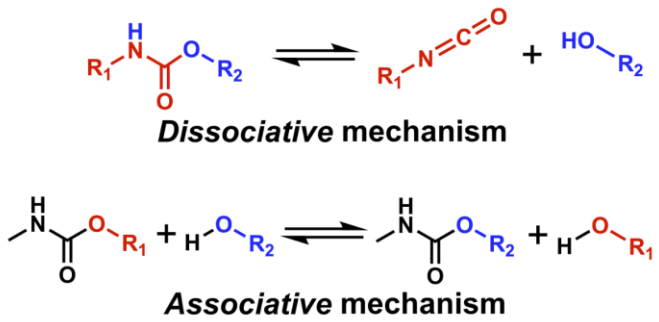

Scheme 2-1. Two mechanisms associated with urethane dynamic chemistry.

As one of the most promising alternatives for conventional PUs, PHUs have the potential to become an important class of DCPNs and provide an alternative approach to achieve reprocessability of PU-like materials. Similar to urethane linkages, hydroxyurethane linkages are also intrinsically dynamic. Cyclic carbonate aminolysis reactions are reversible. In addition, the pendent, secondary *β*-hydroxyl groups or methylol groups along the PHU backbones can undergo associative transcarbamoylation exchange reactions with the urethane linkages (X. Chen et al., 2017; S. Hu et al., 2019) (Scheme 2-2). Because the cyclic carbonate aminolysis route completely bypasses the use of isocyanates, side reactions associated with isocyanates that lead to property loss of dynamic PU networks after reprocessing no longer present an issue for PHU reprocessing. In addition, catalysts can be embedded into the polymers to accelerate the transcarbamoylation exchange reactions during the reprocessing process. Therefore, PHUs generally exhibit an enhanced intrinsic reprocessability relative to conventional PUs.

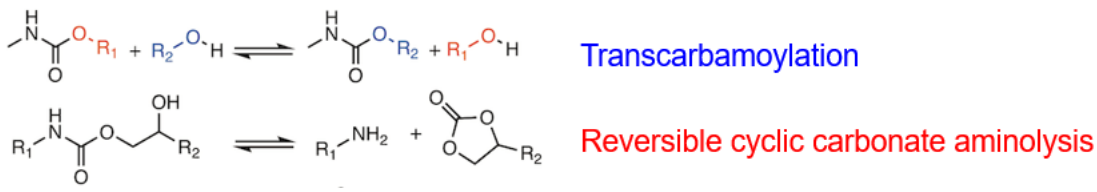

Scheme 2-2. Two mechanisms associated with hydroxyurethane dynamic chemistry.

In 2015, Dichtel, Hillmyer, and coworkers first reported that PHU networks derived from bis(six-membered cyclic carbonates) and amines can undergo network rearrangement at elevated temperatures via associative transcarbamoylation exchange reactions between the carbamate groups and the free hydroxyl groups (Fortman et al., 2015). In 2017, Torkelson and coworkers discovered that in addition to the transcarbamoylation reactions, PHU networks also undergo reversible cyclic carbonate aminolysis reactions at the reprocessing condition, so the dynamic process of PHUs has a dual-mechanism nature and involves concurrent dissociative and associative dynamic reactions (X. Chen et al., 2017). In the presence of a catalyst 4-(dimethylamino)pyridine (DMAP), they developed a PHU network that exhibits full property recovery associated with cross-link density after multiple reprocessing steps (X. Chen et al., 2017).

CHAPTER 3

Dynamic Covalent Polyurethane Networks with Excellent Property and Cross-link Density Recovery after Recycling and Potential for Monomer Recovery

3.1 Introduction

Cross-linked polymers are used in many high-value applications owing to their outstanding stability and performance. However, permanent covalent bonds in traditional cross-linked polymers prevent them from being reprocessed in the melt state, leading to major sustainability and economic losses. To address this problem, research has been dedicated to incorporating dynamic covalent bonds into polymer networks, which enable the rearrangement of network chains under proper stimulus, thus allowing for reprocessing or recycling of these cross-linked polymers (Chakma & Konkolewicz, 2019; Denissen et al., 2016; Kloxin & Bowman, 2013; McBride et al., 2019; Scheutz et al., 2019; Zou et al., 2017). The dynamic chemistries are commonly classified into two types: (1) dissociative dynamic chemistries based on dissociative reversible reactions, including Diels–Alder addition (X. Chen et al., 2002; Trovatti et al., 2015) and alkoxyamine chemistry (Jin et al., 2016; Otsuka, 2013); (2) associative dynamic chemistries based on associative exchange reactions, including transesterification (Li et al., 2018; Lossada et al., 2020; Montarnal et al., 2011; Self et al., 2018), transamination (Denissen et al., 2015; Lessard et al., 2019) and dioxaborolane metathesis (Röttger et al., 2017; Wu et al., 2020). In some cases, the dynamic chemistry involves both dissociative and associative mechanisms, e.g., hydroxyurethane (X. Chen et al., 2017; X. Chen, Li, & Torkelson, 2019; X. Chen, Li, Wei, & Torkelson, 2019; X. Chen, Li,

Wei, Venerus, et al., 2019; S. Hu et al., 2019) and thiourethane (Li et al., 2019; Wen et al., 2020) dynamic chemistries.

Polyurethanes (PUs) are among the most widely used polymers worldwide, with 2020 annual production estimated to be ~29 billion kg (Hicks & Austin, 2017). The applications of PUs include elastomers, adhesives, coatings and foams, and commonly involve cross-linked architectures (Akindoyo et al., 2016; Engels et al., 2013). To address the recycling issue associated with PU thermosets reaching their end of life, many previous studies have adopted different extrinsic dynamic chemistries to achieve reprocessability in cross-linked PU or PU-like materials (J.-H. Chen, Hu, Li, Zhu, et al., 2018; L. Chen et al., 2020; Fortman et al., 2015; Fortman, Snyder, et al., 2018; Fu et al., 2018; Gao et al., 2018; W.-X. Liu et al., 2017; Y. Zhang et al., 2016; Z. P. Zhang et al., 2018). In some studies, PU networks are synthesized from the traditional isocyanate–alcohol reaction, with additional dynamic functional groups incorporated during synthesis, e.g., hindered urea bonds (L. Chen et al., 2020; Y. Zhang et al., 2016), reversible C–C bonds (Z. P. Zhang et al., 2018) and disulfide bonds (J.-H. Chen, Hu, Li, Zhu, et al., 2018; Gao et al., 2018). In other studies, reprocessable PU-like materials are synthesized with formation of dynamic covalent bonds that have some structurally similarity to urethanes groups, e.g., hydroxyurethane bonds (X. Chen et al., 2017; X. Chen, Li, & Torkelson, 2019; X. Chen, Li, Wei, & Torkelson, 2019; X. Chen, Li, Wei, Venerus, et al., 2019; Fortman et al., 2015; S. Hu et al., 2019), thiourethane bonds (Li et al., 2019; Wen et al., 2020) and oxime–carbamate bonds (Fu et al., 2018; W.-X. Liu et al., 2017). However, these synthetic strategies lead to changes in molecular structure and sometimes bulk properties relative to conventional cross-linked PUs, and some strategies involve complicated monomer synthesis (Fortman, Snyder, et al., 2018; W.-X. Liu et al., 2017; Z. P. Zhang et al., 2018). It would be ideal, especially for the commercial PU industry, if excellent reprocessability could be

achieved in PU networks solely by taking advantage of the intrinsic dynamic nature of conventional urethane linkages.

Stress relaxation of PU networks at elevated temperatures was first reported by Tobolsky and co-workers in 1956 (Offenbach & Tobolsky, 1956), which was attributed to the dissociation of urethane linkages to isocyanates and alcohols (Colodny & Tobolsky, 1957; Offenbach & Tobolsky, 1956). Recently, the dynamic nature of urethane bonds has been exploited to achieve advanced characteristics in conventional PU networks, including self-healing (Kuhl et al., 2018; Bonab et al., 2019), plasticity (Wen et al., 2018; N. Zheng et al., 2016, 2017), and reprocessability (although without full property and cross-link density recovery) (Fortman et al., 2019; W. Liu et al., 2019; Y. Wang et al., 2019; Yan et al., 2017). For example, Lei and co-workers reported that multifunctional PU-vitrimers synthesized from renewable castor oil can be reprocessed at 180 °C in 2 h with the presence of dibutyltin dilaurate (DBTDL) catalyst (Yan et al., 2017). Dichtel and co-workers investigated the use of several Lewis acid catalysts in cross-linked PU networks to achieve reprocessability under mild conditions (Fortman et al., 2019). The use of phenol–carbamate bonds has also been explored, which involves non-traditional synthesis of PU networks from phenols (Shi et al., 2019, 2020). Despite these efforts attempting to develop PU networks with intrinsic reprocessability, no study has reported full recovery of cross-link density and tensile properties after reprocessing. Here, we have investigated factors that affect the property recovery of PU networks after reprocessing and accordingly have developed a PU network that exhibits full property recovery within error after multiple reprocessing steps. We have also demonstrated the alcoholysis of the PU network toward the potential recovery of alcohol monomers under relatively mild conditions.

3.2 Experimental

3.2.1 Materials

Tolylene 2,4-diisocyanate terminated poly(propylene glycol) (PPG Diisocyanate, average M_n ~2,300 g/mol, narrow molecular weight distribution, isocyanate group ~3.6 wt%), trimethylolpropane (Triol, ≥98.0%), pentaerythritol (Tetraol, 99%), 4-(dimethylamino)pyridine (DMAP, *ReagentPlus*®, ≥99%), dibutyltin dilaurate (DBTDL, ≥96.0%), ethylene glycol (anhydrous, 99.8%), *N*,*N*-dimethylformamide (DMF, anhydrous, 99.8%), tetrahydrofuran (THF, anhydrous, 99.9%), and dichloromethane (DCM, anhydrous, 99.8%) were from Sigma-Aldrich. All chemicals were used without further purification. PPG Diisocyanate, DBTDL and DMF were dried on molecular sieves before use.

3.2.2 Synthesis of polyurethane (PU) networks

In a typical synthesis of Tetraol-20OH network, 250 mg Tetraol and 149.6 mg DMAP were added to a 20-mL scintillation vial with the total mass of vial + cap recorded prior to weighing. Then 5 mL DMF was added into the vial, and the mixture was heated on a hot plate at 125 °C until complete dissolution to obtain a Tetraol stock solution. The mass of stock solution was determined by subtracting the mass of empty vial from the total mass of solution and vial. The proper amount of stock solution (containing 230.9 mg Tetraol and 138.1 mg DMAP) was then weighed in a Max20 cup (Flacktek) containing 6.5 g PPG Diisocyanate. The concentration of isocyanate groups was adjusted to 1 M by adding another 1.03 mL DMF into the cup, assuming the density of stock solution is 1 g/mL. The reactant mixture was then homogenized in a speed mixer (Flacktek DAC 150.1 FVZ-K) at 3200 rmp for 1 min. Afterward, the reactant mixture was poured into an aluminum pan (96 mm diameter) and cured on a hot plate at 60 °C. After gelation (typically within minutes), the sample was transferred to an oven at 80 °C for overnight reaction and then dried for

48 h at 80 °C under vacuum. For details on the formulation of other PU networks, please refer to Table 3-S1.

3.2.3 Reprocessing procedure

Reprocessing of PU networks was performed using a PHI hot press. After obtaining DMA or tensile test samples from as-synthesized materials, residual materials were cut into small pieces and then pressed into ~1 mm thick sheets using a 7-ton ram force, which were considered as 1st molded samples. Similarly, 1st molded materials were then cut into small pieces and pressed again to obtain 2nd molded materials. All PU networks containing DMAP were reprocessed at 140 °C for 70 min. The PU network containing DBTDL was reprocessed at 120 °C for 15 min.

3.2.4 Alcoholysis of PU networks

In a 20 mL scintillation vial, ~300 mg of the as-synthesized Tetraol-20OH network was added, together with 15.4 mg DMAP (0.5 eq with respect to urethane groups in the PU network) and 1 mL ethylene glycol. The mixture was heated on a hot plate at 130 °C for 8 h, during which time the network materials were gradually “dissolved”.

3.2.5 Characterization

Dynamic mechanical analysis (DMA) was performed with a TA Instruments RSA III. Specifically, storage modulus (E'), loss modulus (E''), and damping ratio $\tan\delta$ (E''/E') were recorded as functions of temperature on the heating scan from −60 to 60 °C at a 3 °C/min heating rate. The measurement was performed in tension mode under a 0.03% oscillatory strain at 1 Hz frequency. For each sample, at least three measurements were performed, and the E' value at 40 °C was reported as the average rubbery plateau modulus with errors given by standard deviations. The high-temperature DMA measurement was performed on as-synthesized PU samples, in which samples underwent temperature ramps set from −60 to 300 °C. The measurement was stopped

when the equipment started to report inconsistent results due to the flow of sample. The corresponding temperature was recorded as T_{flow} of the material.

Uniaxial tensile testing was performed with a TA Instruments RSA-G2 at room temperature. Dog-bone-shaped samples were cut from as-synthesized and molded films using a Dewes-Gumb die. Samples underwent a uniaxial extension at a rate of 1 mm/s until break, with the data collected at a 40 pts/s rate. Tensile properties including Young's modulus, tensile strength and elongation at break were reported as average values of at least five specimens with errors representing the standard deviations.

Attenuated total reflectance–Fourier transform infrared (ATR–FTIR) spectroscopy was performed using a Bruker Tensor 37 FTIR spectrophotometer equipped with a diamond/ZnSe ATR attachment. All samples were scanned at a resolution of 2 cm^{-1}, and 16 scans were collected in the range of 4000–600 cm^{-1}. Spectra were normalized with respect to the aliphatic ether stretching peak at ~1100 cm^{-1}.

Swelling tests were carried out for all as-synthesized and molded PU networks to determine the swelling ratio and gel fraction. Samples (~100 mg) were immersed in 20 mL of DCM in glass vials and were left to swell at room temperature for 72 h. The liquid phase was replaced with fresh DCM every day. After swelling, the liquid phase was decanted, and the residual solvent on sample surface was carefully wiped off using filter paper. Masses of swollen networks were recorded. Samples were then dried at 60 °C under vacuum until no weight change could be measured. For each sample, three specimens were measured. The gel fraction was determined as m_d/m_0, and the swelling ratio was calculated as $(m_s-m_d)/m_d$, where m_0 is the original mass of the sample before swelling and m_s and m_d are the masses of the swollen sample and dried sample, respectively.

3.3 Results and Discussion

As shown in Scheme 3-1, PU networks were synthesized from a poly(propylene-glycol)-based diisocyanate (PPG Diisocyanate) and a trifunctional alcohol trimethylolpropane (Triol) or a tetrafunctional alcohol pentaerythritol (Tetraol). For each type of cross-linker, the reaction was performed both at stoichiometric balance (0OH) and with 20 mol% hydroxyl group in excess (20OH). Urethane dynamic chemistry involves both associative and dissociative mechanisms (Scheutz et al., 2019). When excess free hydroxyl groups are present, associative transcarbamoylation exchange reactions can occur between carbamate groups and hydroxyl groups (Fortman et al., 2015). As well, urethane linkages can dissociate, thereby forming alcohols and isocyanates at elevated temperature (Fortman et al., 2019; Wen et al., 2018). Here, we consider that this dual-mechanism nature exists in both 0OH and 20OH samples because the reversion of urethane bonds releases free hydroxyl groups that can participate in the associative pathway (Scheme 3-1).

All PU networks were synthesized with 20 mol% 4-(dimethylamino)pyridine (DMAP) catalyst with respect to isocyanate functional groups, which accounts for ~2 wt% of the total material. As-synthesized samples were obtained by curing the reactant mixture (some minutes at 60 °C and then overnight at 80 °C) in an aluminum pan, followed by 48-h vacuum drying at 80 °C to remove solvent. The isocyanate peak at ~2270 cm^{-1} observed in the Fourier-transform infrared (FTIR) spectrum of PPG Diisocyanate (Figure 3-S1) disappeared in all as-synthesized PU networks (Figure 3-S2, 3-S3), indicating complete conversion within error of isocyanate groups. The as-synthesized materials were reprocessed for two cycles at 140 °C for 70 min using compression molding. The same reprocessing condition was applied for all samples to ensure fair comparison of reprocessability and resulting properties. In all cases, consolidated and

homogeneous films were obtained after reprocessing, indicating effective network rearrangement enabled by the dynamic chemistry. Images of as-synthesized (top) and reprocessed (bottom) Tetraol-20OH samples are shown in Scheme 3-1. We note that the surface of network samples became rougher after reprocessing, which is likely due to the thermodynamic incompatibility between PU networks and the polyimide substrate film used during reprocessing via compression molding. In our previous studies on dynamic polyhydroxyurethane and polythiourethane networks (X. Chen et al., 2017; X. Chen, Li, & Torkelson, 2019; X. Chen, Li, Wei, & Torkelson, 2019; X. Chen, Li, Wei, Venerus, et al., 2019; S. Hu et al., 2019), we observed similar surface roughness after reprocessing, which did not affect the property recovery of remolded samples.

Figure 3-1(a) shows the dynamic mechanical analysis (DMA) results of as-synthesized, 1st molded and 2nd molded Triol-0OH networks. In all three samples, a rubbery plateau in the storage tensile modulus E' is observed at temperatures well above the glass transition temperature (T_g), confirming their cross-linked nature. The E' rubbery plateau moduli determined at 40 °C are summarized in Table 3-1, which indicate a 76% recovery in the 1st molding step (relative to the as-synthesized material) and a 67% recovery in the 2nd molding step (relative to the 1st molded sample). According to ideal rubbery elasticity theory, at constant temperature the rubbery plateau modulus is proportional to cross-link density (Flory, 1953). This incomplete cross-link density recovery after reprocessing is likely due to side reactions associated with isocyanate groups at elevated temperatures. During the molding process at 140 °C, highly reactive free isocyanate groups are generated from the dissociative reaction of urethanes. These liberated isocyanate groups may then undergo undesired side reactions in the presence of moisture (in air and absorbed by the network) at high temperature, leading to property losses in molded Triol-0OH networks. We tried to minimize the contact between PU samples and moisture by drying all reactants on activated

molecular sieves and molding as-synthesized materials right after the vacuum drying process, but it would be nearly impossible to completely eliminate the occurrence of side reactions given that we performed multiple molding and sample-cutting processes for each PU network sample.

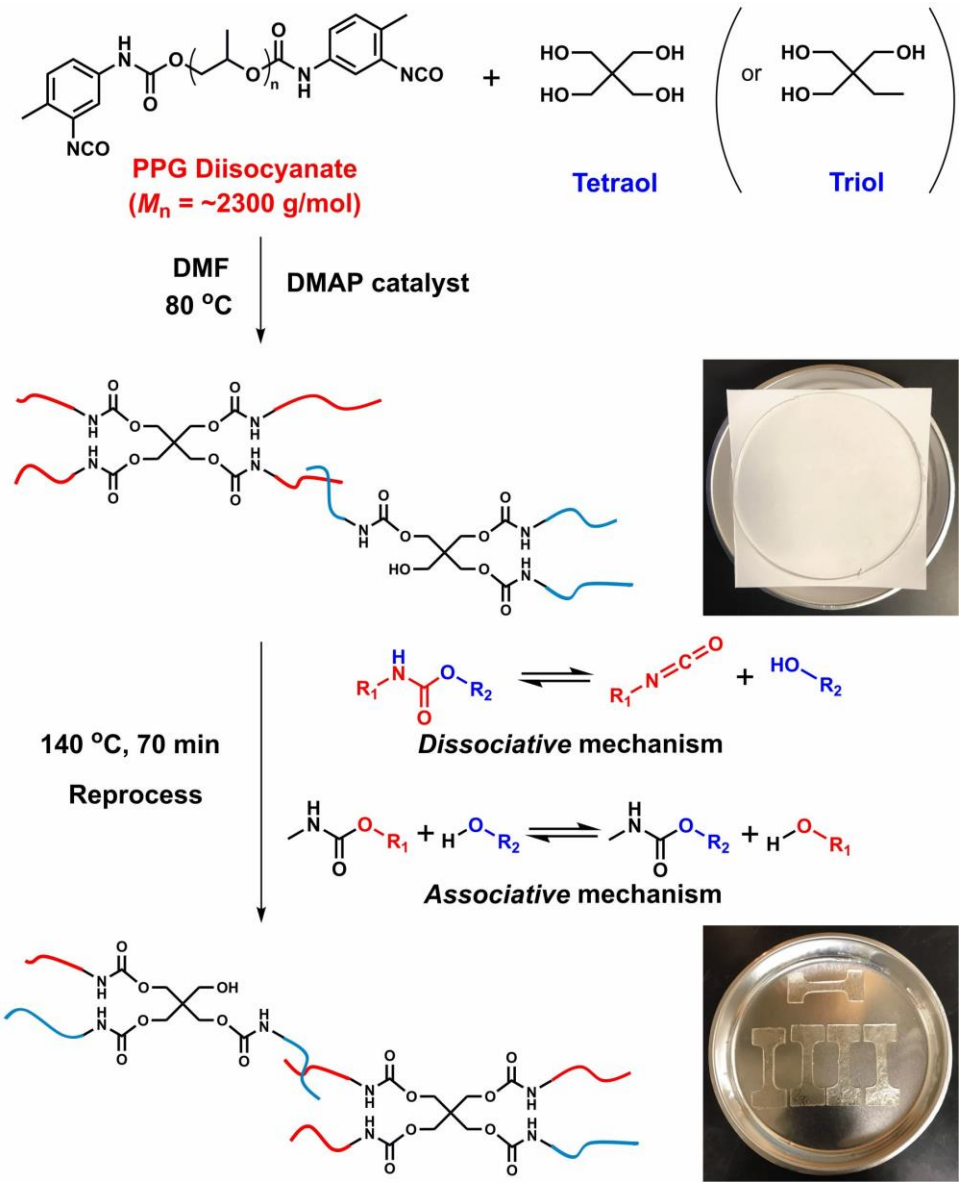

Scheme 3-1. Mechanism of synthesis and rearrangement of PU networks.

To suppress side reactions of isocyanate groups during reprocessing, we incorporated 20 mol% free hydroxyl groups in the PU network by running the reaction slightly off-stoichiometry, similar to the strategy that Li et al. adopted to achieve reprocessable thiourethane networks with full cross-link density recovery (Li et al., 2019). The DMA results of as-synthesized and molded Triol-20OH networks are shown in Figure 3-1(b). Compared with the Triol-0OH network, the as-synthesized Triol-20OH network has a slightly decreased *E'* rubbery plateau modulus because of the unbalanced stoichiometry. However, we obtained much better recovery of *E'* rubbery plateau modulus and thus cross-link density (86% in the 1st molding (relative to as-synthesized) and 93% in the 2nd molding (relative to the 1st molding)) in molded Triol-20OH networks; see Table 3-1.

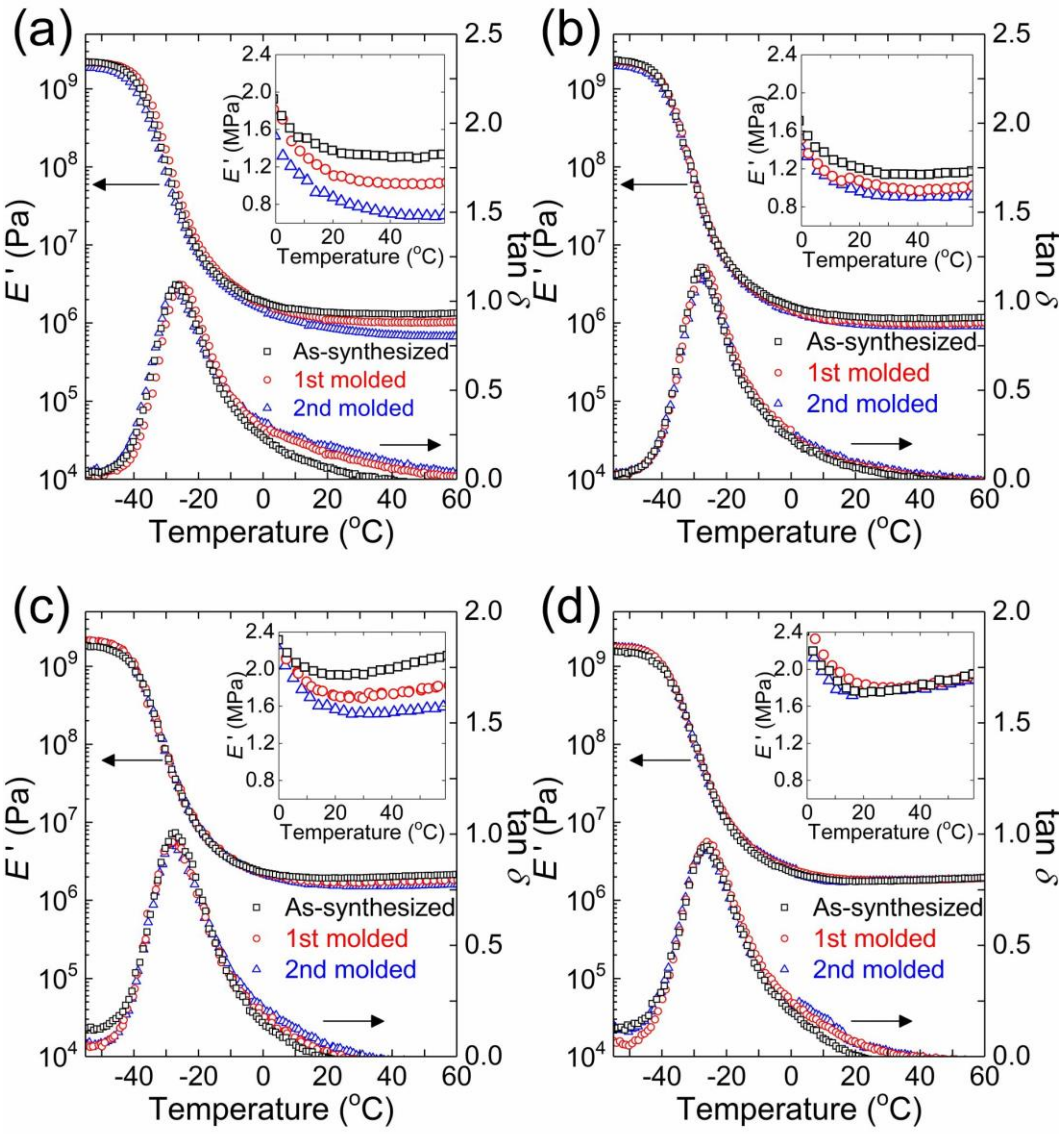

Figure 3-1. Dynamic mechanical responses of DMAP-containing (a) Triol-0OH, (b) Triol-20OH, (c) Tetraol-0OH and (d) Tetraol-20OH networks: E' and tan δ (E''/E') as functions of temperature for as-synthesized, 1st molded, and 2nd molded samples. Inset: zoomed-in rubbery plateau moduli as a function of temperature.

Table 3-1. Rubbery-plateau tensile storage moduli and room-temperature tensile properties of as-synthesized and molded PU networks.

Sample		*E′* at 40 °C (MPa)	Young's modulus (MPa)	Tensile strength (MPa)	Strain at break (%)
Triol-0OH	**As-synthesized**	1.30 ± 0.04	1.46 ± 0.04	1.12 ± 0.03	349 ± 12
	1st molded	0.99 ± 0.05	1.19 ± 0.03	0.67 ± 0.10	212 ± 52
	2nd molded	0.66 ± 0.04	0.92 ± 0.10	0.57 ± 0.04	243 ± 36
Triol-20OH	**As-synthesized**	1.13 ± 0.04	1.20 ± 0.03	1.05 ± 0.03	464 ± 43
	1st molded	0.97 ± 0.03	1.19 ± 0.02	0.85 ± 0.03	344 ± 45
	2nd molded	0.90 ± 0.07	0.99 ± 0.03	0.81 ± 0.08	326 ± 45
Tetraol-0OH	**As-synthesized**	2.00 ± 0.04	2.35 ± 0.07	1.35 ± 0.11	195 ± 14
	1st molded	1.72 ± 0.01	2.37 ± 0.09	1.17 ± 0.04	162 ± 21
	2nd molded	1.53 ± 0.05	2.13 ± 0.03	1.01 ± 0.07	138 ± 21
Tetraol-20OH	**As-synthesized**	1.79 ± 0.03	1.90 ± 0.03	1.16 ± 0.07	200 ± 19
	1st molded	1.76 ± 0.05	2.01 ± 0.10	1.19 ± 0.17	152 ± 20
	2nd molded	1.71 ± 0.06	1.99 ± 0.12	1.11 ± 0.07	157 ± 27
Tetraol-20OH-Tin	**As-synthesized**	2.16 ± 0.05	2.23 ± 0.01	1.68 ± 0.04	228 ± 8
	1st molded	0.96 ± 0.02	0.94 ± 0.00	0.64 ± 0.04	212 ± 20
	2nd molded	0.50 ± 0.01	0.40 ± 0.03	0.33 ± 0.02	249 ± 22

The presence of free hydroxyl groups during reprocessing is expected to have two effects. First, hydroxyl groups could reduce side reactions by reacting promptly with free isocyanate groups released in the dissociative reaction and pushing the reaction equilibrium toward urethane moieties. Second, hydroxyl groups would promote the associative mechanism relative to the dissociative mechanism of urethane bonds and thereby reduce the level of side reactions. Thus, adding free hydroxyl groups beyond stoichiometric balance is an effective way to enhance cross-link density and property recovery of PU networks after reprocessing.

Polyurethane networks were also synthesized using a tetrafunctional alcohol Tetraol as the cross-linker. Figure 3-1(c) shows DMA results of Tetraol-0OH samples synthesized at stoichiometric balance. By increasing the cross-linker functionality from three to four, the *E′* rubbery plateau modulus (at 40 °C) of the resulting as-synthesized PU network increases from 1.30 MPa to 2.00 MPa (Table 3-1). More importantly, as evidenced by *E′* plateau values, the property recovery of recycled Tetraol-0OH networks is improved compared with recycled Triol-0OH networks. The use of Tetraol cross-linker is beneficial for property recovery in two ways. First, compared to networks formed with trifunctional cross-linker, at the reprocessing condition, networks formed with tetrafunctional cross-linker have a higher fraction of chains that remain cross-linked and a lower fraction of free-moving linear chains generated from the dissociative reaction. As a result, the networks have more restricted mobility, and isocyanate groups are less exposed to conditions that may induce side reactions. Second, the network structure formed with tetrafunctional cross-linker has more tolerance towards side reactions. Even if one of the four branches at the junction point cannot be recovered due to the loss of isocyanate functionality during reprocessing, the remaining three branches still afford a cross-linked structure, and the resulting network would not exhibit significant reduction in properties associated with cross-link density.

In contrast, if the network formed with trifunctional cross-linker loses one branch at the junction point, the cross-linked structure would become a (locally) linear structure, leading to substantial property losses. Thus, the property recovery of recycled PU networks can also be improved by replacing trifunctional cross-linker with tetrafunctional cross-linker.

We then prepared a Tetraol-20OH PU network, which is formed using the tetrafunctional cross-linker and contains 20 mol% free hydroxyl groups in excess. As shown in Figure 3-1(d) and Table 3-1, within error, the Tetraol-20OH network exhibits full recovery of the rubbery plateau E' value after multiple reprocessing steps. Although average E' values at 40 °C are different from each other, when taking into account the error bars (which represent standard deviations from at least three measurements), these results are identical. This very positive outcome is in contrast with outcomes obtained in the other three PU networks and indicates that replacing the trifunctional cross-linker with a tetrafunctional cross-linker and adding a small amount of excess free hydroxyl groups can lead to full property and cross-link density recovery in reprocessable PU networks. Even if degradation happens in one chain of some tetrafunctional cross-linkers during reprocessing, changes in mechanical properties of the bulk network may not be significant enough to be determined outside of experimental error.

Also, the inset of Figure 3-1(d) shows a linear increase in storage modulus with increasing temperature. This is in accordance with Flory's ideal rubber elasticity theory, which predicts that the rubbery plateau tensile modulus, E, is proportional to absolute temperature in the rubbery plateau regime (Flory, 1953). Since the values of E'' are negligibly small compared with E' in the rubbery plateau regime, the rubbery plateau E' values are essentially the same as E.

Notably, we observed no apparent changes in FTIR spectra (Figure 3-S2, 3-S3) and T_g values (from the peak of E'' curves, Figure 3-S4) of all four PU networks after reprocessing.

Despite evident reductions observed in *E′* plateau moduli of recycled Triol-0OH, Triol-20OH and Tetraol-0OH samples, changes in molecular structures of these samples may be insufficient to cause differences in FTIR spectra and T_gs.

We also performed high-temperature DMA on the as-synthesized PU network samples; see Figure 3-2. At temperatures between 25 °C and 150 °C, rubbery plateaus can be observed in all samples. In the rubbery plateau regime, *E′* values increase with increasing temperature, consistent with expectations from the ideal rubber elasticity theory. With increasing temperature above 150 °C, *E′* values start to decrease gradually, indicating losses in the total number of cross-links. At sufficiently high temperature, the rates of dynamic chemistries become more rapid, and the cross-link density change resulting from the dissociative reaction manifests in the sample moduli. As temperature is further increased, the material loses mechanical integrity and flows like a liquid, with the DMA equipment reporting inconsistent *E′* values. Measurements were stopped at this point, and the corresponding temperature recorded as T_{flow}. Figure 3-S5 shows a PU sample after the high-temperature DMA test, in which the deformation and flow is clearly evident.

Compared with the Triol-0OH sample, which has T_{flow} = 234 °C, the T_{flow} values of Triol-20OH and Tetraol-0OH are enhanced by ~28 °C, and the T_{flow} of Tetraol-20OH is enhanced by 41 °C. These results indicate that the thermal stability of PU networks can be enhanced by incorporating excess free hydroxyl groups in the network and/or by replacing Triol with Tetraol. In the presence of free hydroxyl groups, the reversion of urethane is suppressed, and more chains remain in the cross-linked network at elevated temperatures. With Tetraol replacing Triol, the network can withstand the loss of more chains in the dissociative reaction while maintaining a cross-linked nature, thereby remaining mechanically robust to somewhat higher temperature. These thermal stability results are in good agreement with the property recovery results.

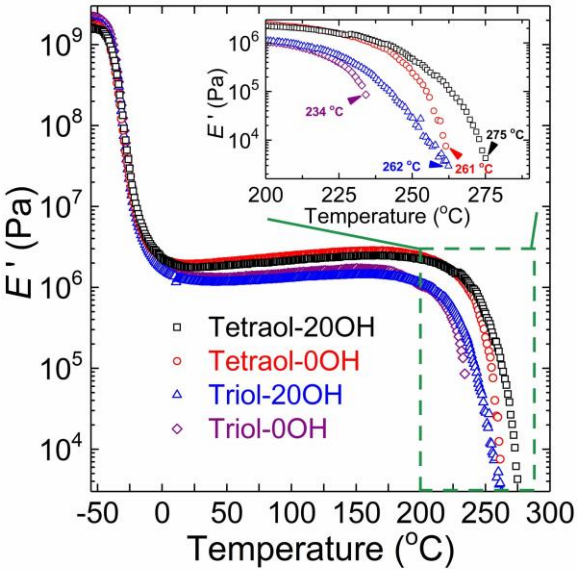

Figure 3-2. High-temperature dynamic mechanical responses of as-synthesized PU networks containing DMAP: *E'* as a function of temperature. Inset: zoomed-in *E'* results with T_{flow} labeled for each sample.

In addition to DMA measurements, we also used tensile and swelling tests to evaluate the recovery of mechanical properties and cross-link density in PU networks. Table 3-1 gives Young's modulus, tensile strength, and strain at break results of as-synthesized and molded PU networks. Among the four networks, Tetraol-20OH shows the best property recovery after reprocessing, with the 2nd molded sample fully recovering all properties within experimental error. In accordance with DMA results, both Tetraol-0OH and Triol-20OH networks exhibit moderate recovery of Young's modulus and tensile strength after reprocessing, and the Triol-0OH network exhibits the worst property recovery. Because the tensile tests were performed at room temperature, which is substantially higher than T_gs of all PU networks, these mechanical property results describe elastomeric responses that are related to cross-links. Table 3-S2 shows swelling ratio and gel fraction results of as-synthesized and molded PU networks. Due to its highest susceptibility to side reactions, Triol-0OH is the only network that exhibits an increase in swelling ratio and decrease

in gel content after reprocessing, consistent with a significant loss in cross-links. In spite of the stoichiometric imbalance in synthesis, the Tetraol-20OH network is in a highly effectively cross-linked state (gel fraction ≈ 99%), which was maintained after each molding cycle. In all, with the incorporation of excess hydroxyl groups and the substitution of the trifunctional cross-linker by the tetrafunctional cross-linker, fully reprocessable, conventional PU networks can be obtained with excellent recovery of cross-link density and tensile properties after multiple molding cycles. This is the first time that the full recovery of both cross-link density and tensile properties is achieved in conventional PU networks.

In previous studies on reprocessable, conventional PU networks (which were done at stoichiometric balance of hydroxyl and isocyanate groups and did not result in full cross-link density recovery after reprocessing), DBTDL catalyst was commonly used to achieve the dynamic characteristic of urethane linkages (Fortman et al., 2019; W. Liu et al., 2019; Y. Wang et al., 2019; Yan et al., 2017). We explored the use of this catalyst in our best-performing PU network (with excess hydroxyl groups) and synthesized a Tetraol-20OH-Tin network containing 1 mol% DBTDL with respect to isocyanate groups. We used the same level of DBTDL as Fortman et al. applied in their study, in which an 83% recovery of cross-link density was obtained after the 1st reprocessing step (Fortman et al., 2019). We first applied the same condition (140 °C, 70 min) to reprocess this Tetraol-20OH-Tin network. However, the sample became very sticky and was hardly able to be removed from the Kapton substrate film without breaking (Figure 3-S6(a)), suggesting a significant extent of decross-linking during reprocessing. Thus, we used a milder condition (120 °C, 15 min) to obtain intact molded films (Figure 3-S6(b)).

The Tetraol-20OH-Tin network shows poor recovery of properties after reprocessing, which is evidenced by major reductions in rubbery plateau E' values (Figure 3-3(a) and Table 3-

1), the shifting of tan δ and E'' peaks (Figure 3-S7) towards lower temperatures, the loss in tensile properties (Table 3-1), and the increase in swelling ratio as well as decrease in gel fraction (Table 3-S2). In addition, compared with the Tetraol-20OH network, T_{flow} of the as-synthesized Tetraol-20OH-Tin network decreases by 91 °C (Figure 3-3(b)). The poor thermal stability and property retention are possibly due to the overly strong catalytic activity of DBTDL for the urethane dynamic chemistry, leading to significant levels of side reactions and loss of urethane cross-links during reprocessing. The FTIR spectra of Tetraol-20OH-Tin networks (Figure 3-S8) reveal obvious decreases in characteristic peaks of urethane linkages after reprocessing, including the C=O stretching band at 1728 cm^{-1}, the amide II combination band at 1533 cm^{-1}, and the amide III combination band at 1225 cm^{-1}. The significant difference between property recovery efficiencies of Tetraol-20OH and Tetraol-20OH-Tin networks suggests the importance of catalyst selection in forming dynamic PU networks with good reprocessability. Moreover, our Tetraol-20OH-Tin network gives much inferior property recovery compared with the previous study which used the same level of DBTDL catalyst but involved a different molecular structure (Fortman et al., 2019). Future studies will be focused on investigating the effect of molecular structures and catalyst uses on reprocessability of PU networks.

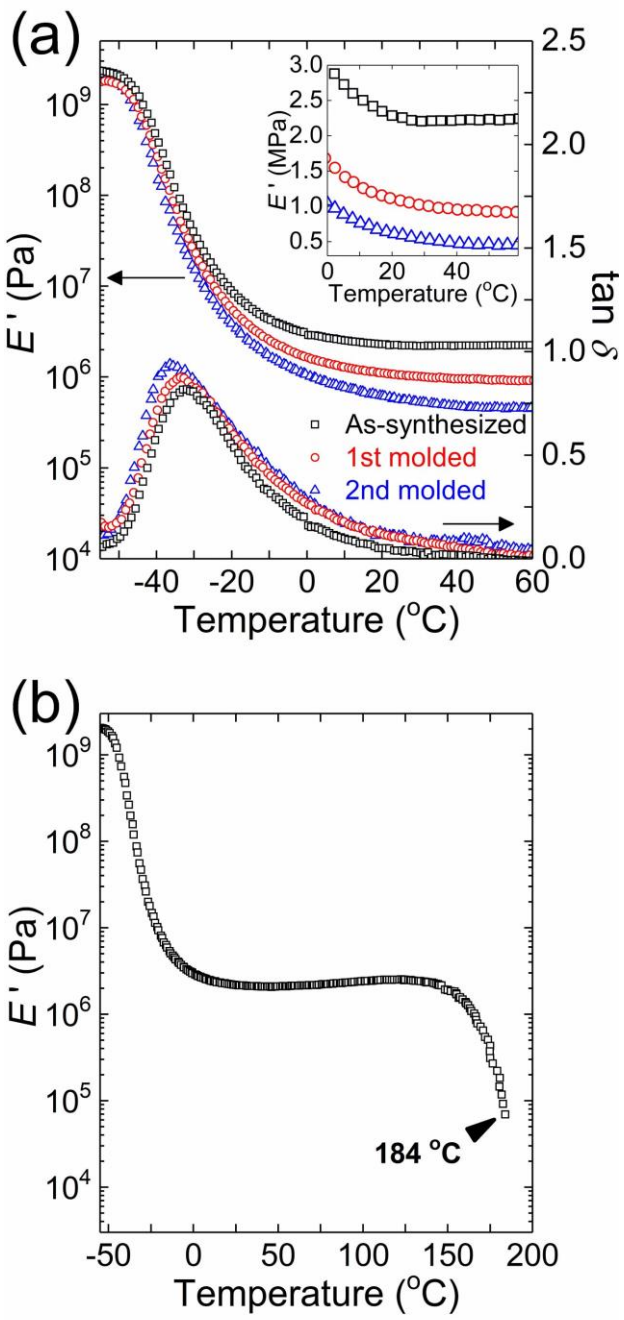

Figure 3-3. (a) E' and tan δ (E''/E') as functions of temperature for as-synthesized, 1st molded, and 2nd molded Tetraol-20OH-Tin samples. Inset: zoomed-in rubbery plateau moduli as a function of temperature. (b) High-temperature dynamic mechanical response of the as-synthesized Tetraol-20OH-Tin network: E' as a function of temperature. ("Tin" refers to the DBTDL catalyst.)

Apart from reprocessability, we have shown via a proof-of-principle demonstration that the dynamic nature of urethane bonds can also be used to decross-link or depolymerize the network,

which could potentially lead to recovery of alcohol monomers. We mixed 300 mg of as-synthesized Tetraol-20OH with 0.5 eq DMAP (with respect to urethane linkages) and 1 mL ethylene glycol and heated the mixture at 130 °C for 8 h. As shown in Figure 3-4, a phase-separated liquid mixture was obtained after heating, which can be completely dissolved in tetrahydrofuran. The decross-linking is a result of alcohols participating in dynamic chemistries at elevated temperature. Compared with previous studies on alcoholysis of PU networks (Simón et al., 2018; W. Yang et al., 2012), the condition we used in our study is much milder, likely due to the use of DMAP catalyst and different molecular structures of PU networks. Future studies are warranted to optimize decross- linking conditions and to purify and characterize alcoholysis products.

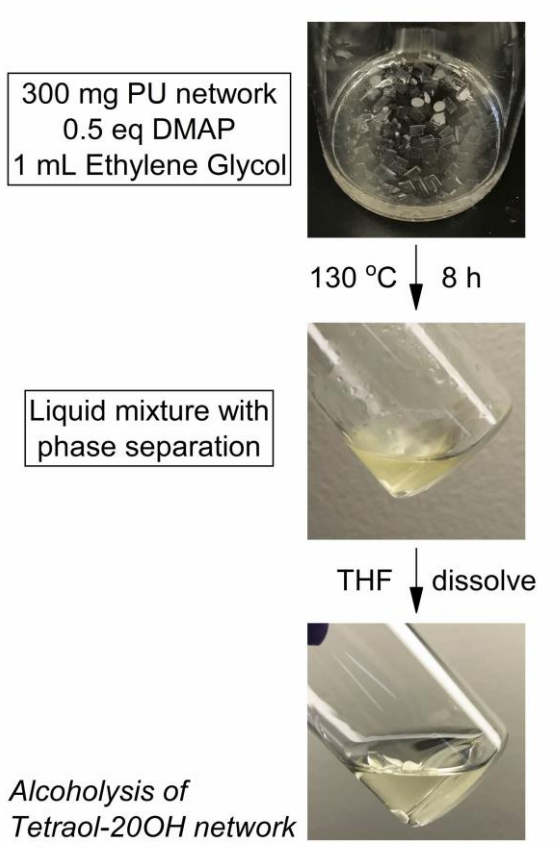

Figure 3-4. Alcoholysis of the as-synthesized Tetraol-20OH network in ethylene glycol.

3.4 Conclusions

We have demonstrated that property recovery and thermal stability of reprocessable, conventional PU networks made with DMAP catalyst can be improved by incorporating excess free hydroxyl groups and/or replacing trifunctional cross-linker with tetrafunctional cross-linker. We have developed a Tetraol-20OH PU network that exhibits full recovery of cross-link density and tensile properties within error after multiple reprocessing cycles. While such full recovery has been reported recently for reprocessable polyhydroxyurethane networks and polythiourethane networks, our study provides the first demonstration of full recovery of cross-link density and tensile properties within error after reprocessing of conventional PU networks. When DMAP catalyst is replaced by DBTDL, the resulting PU network shows poor property recovery after reprocessing, indicating the important role of catalyst selection in preparing dynamic PU networks with excellent reprocessability. We have also provided a proof-of-principle demonstration that alcohol monomers in PU networks can potentially be recovered by alcoholysis under mild conditions.

Acknowledgements

This work was done in collaboration with Xi Chen from the Torkelson research group at Northwestern University. This research is now published (X. Chen et al., 2020): *ACS Appl. Polym. Mater.* 2020, 2, 2093-2101 (DOI: 10.1021/acsapm.0c00378).

3.5 Supporting Information

Table 3-S1. Formulations for the synthesis of PU networks.

Sample	PPG Diisocyanate (g)	Triol (mg)	Tetraol (mg)	DMAP (mg)	DBTDL (mg)	DMF (mL)
Triol-0OH	6.5	252.8	0	138.1	0	5.65
Triol-20OH	6.5	303.3	0	138.1	0	5.65
Tetraol-0OH	6.5	0	192.4	138.1	0	5.65
Tetraol-20OH	6.5	0	230.9	138.1	0	5.65
Tetraol-20OH-Tin	6.5	0	230.9	0	35.7	5.65

Table 3-S2. Swelling ratio and gel content of as-synthesized and molded PU networks.

Sample		Swelling ratio (%)	Gel content (%)
Triol-0OH	**As-synthesized**	731 ± 16	97.0 ± 0.2
	1st molded	760 ± 41	93.7 ± 0.7
	2nd molded	879 ± 18	90.4 ± 1.3
Triol-20OH	**As-synthesized**	710 ± 9	96.8 ± 1.0
	1st molded	663 ± 43	95.9 ± 0.3
	2nd molded	688 ± 30	95.5 ± 2.3
Tetraol-0OH	**As-synthesized**	483 ± 25	99.3 ± 0.7
	1st molded	483 ± 25	98.8 ± 0.2
	2nd molded	498 ± 8	98.3 ± 0.6
Tetraol-20OH	**As-synthesized**	481 ± 60	99.1 ± 0.4
	1st molded	481 ± 19	99.2 ± 0.4
	2nd molded	505 ± 14	98.8 ± 0.9
Tetraol-20OH-Tin	**As-synthesized**	430 ± 5	97.4 ± 0.8
	1st molded	585 ± 8	88.4 ± 2.8
	2nd molded	798 ± 40	78.3 ± 7.8

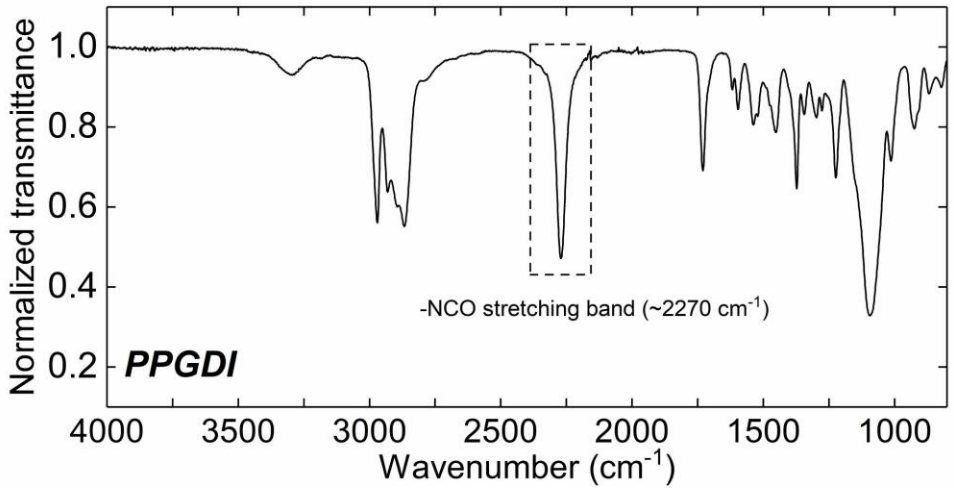

Figure 3-S1. FTIR spectrum of PPG Diisocyanate.

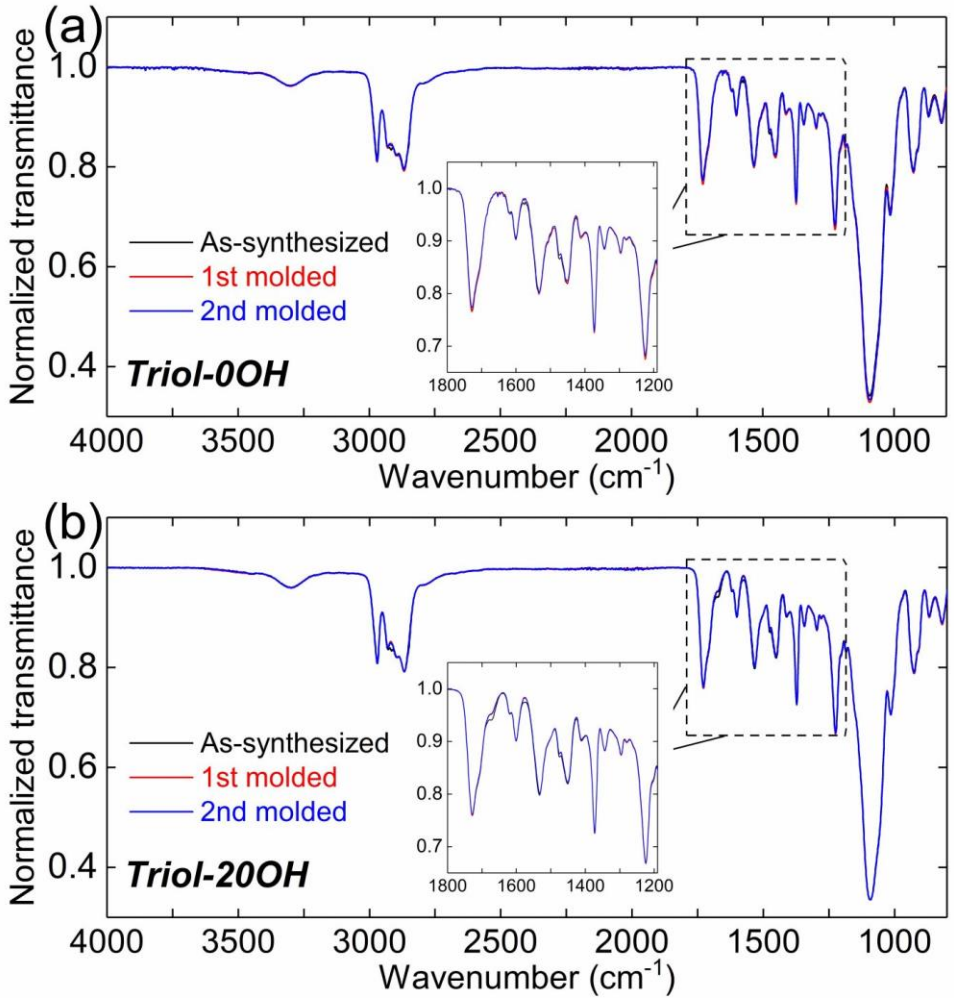

Figure 3-S2. FTIR spectra of (a) Triol-0OH and (b) Triol-20OH networks.

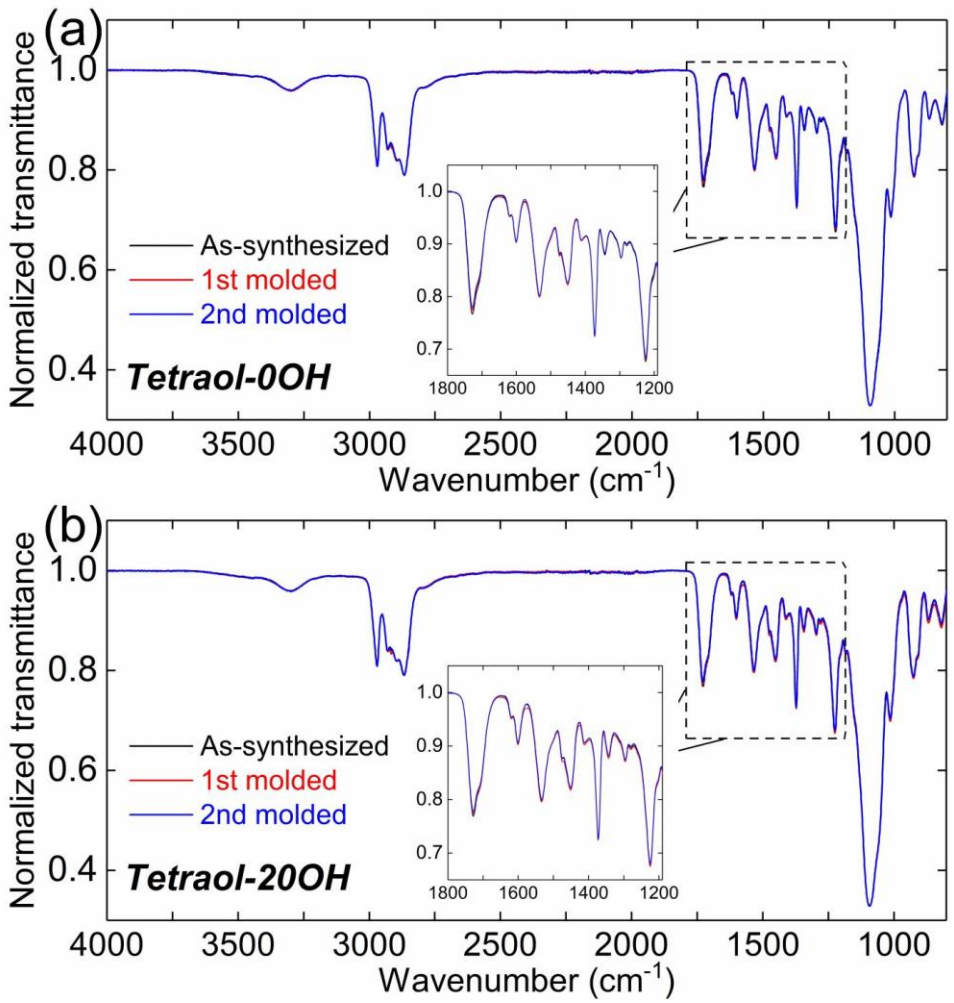

Figure 3-S3. FTIR spectra of (a) Tetraol-0OH and (b) Tetraol-20OH networks.

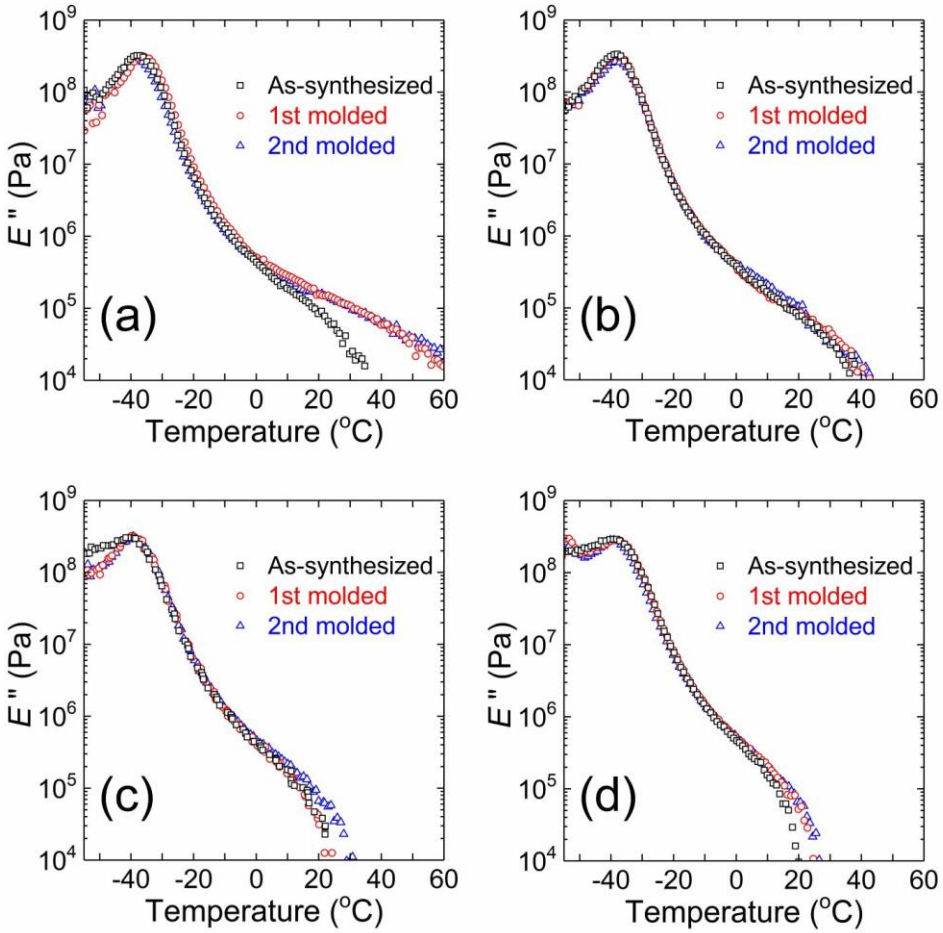

Figure 3-S4. *E''* as a function of temperature for as-synthesized and molded (a) Triol-0OH, (b) Triol-20OH, (c) Tetraol-0OH, and (d) Tetraol-20OH networks. (All samples used DMAP as catalyst.

Figure 3-S5. Image of a PU sample after the high-temperature DMA test.

Figure 3-S6. Images of 1st molded Tetraol-20OH-Tin networks reprocessed under different conditions: (a) 140 °C, 70 min; (b) 120 °C, 15 min.

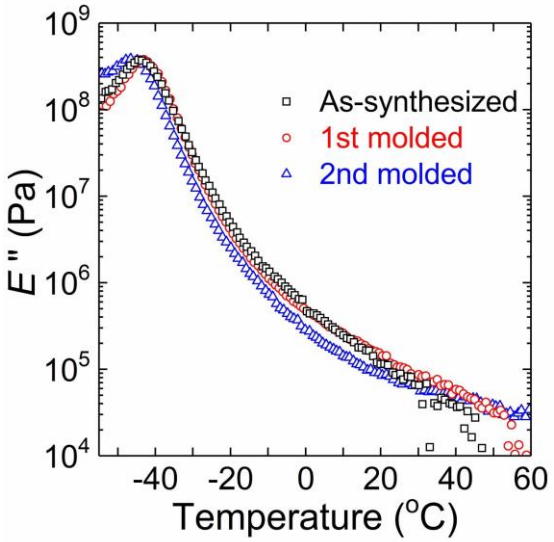

Figure 3-S7. *E''* as a function of temperature for as-synthesized and molded Tetraol-20OH-Tin networks. ("Tin" refers to DBTDL as catalyst.)

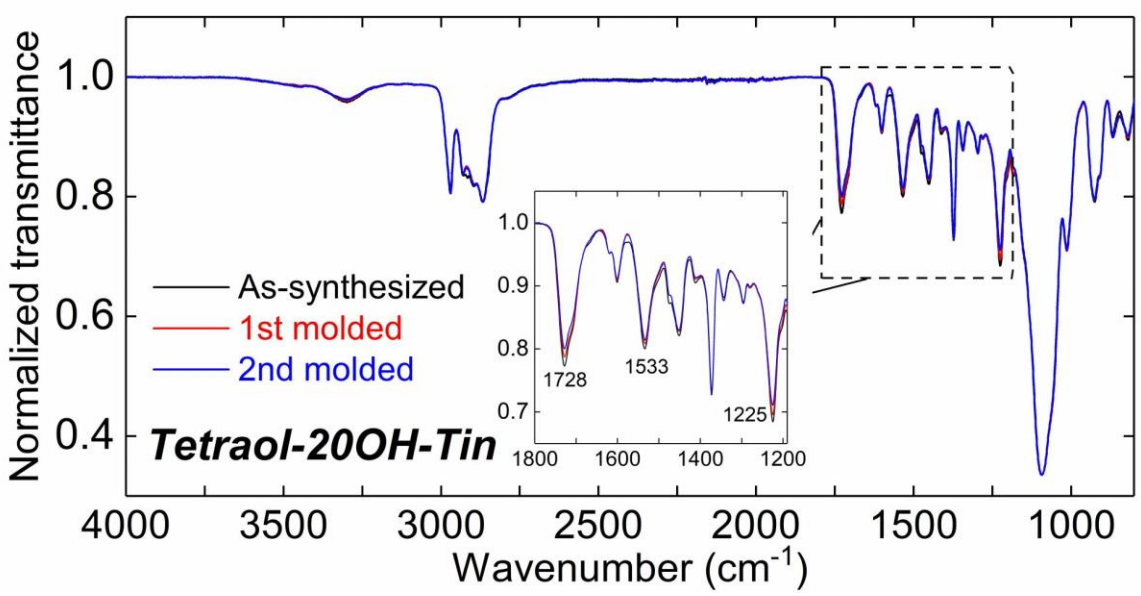

Figure 3-S8. FTIR spectra of Tetraol-20OH-Tin networks. Inset: zoomed-in spectra for characteristic peaks of the urethane linkage.

CHAPTER 4

Bio-based Reprocessable Polyhydroxyurethane Networks: Full Recovery of Cross-link Density with Three Concurrent Dynamic Chemistries

4.1 Introduction

Polyurethane (PU) is a commercially important material, ranking sixth in overall worldwide annual production among all polymer species (Delebecq et al., 2013; Engels et al., 2013; Nohra et al., 2013). Because of the range of attainable material properties, PUs are used in a broad array of applications such as coatings, foams, sealants, and adhesives (Delebecq et al., 2013; Engels et al., 2013; Nohra et al., 2013). Conventional PU synthesis involves the use of isocyanates, which present issues for human health and are under increasing regulatory scrutiny regarding safe transport and use (Beniah et al., 2016; Leitsch et al., 2016). In view of the trend toward green chemistry, research efforts have intensified in finding routes to non-isocyanate PU (NIPU), with cyclic carbonate aminolysis leading to polyhydroxyurethane (PHU) being a very promising chemistry (Blattmann et al., 2014; Guan et al., 2011; Kathalewar et al., 2013; Maisonneuve et al., 2015; Nohra et al., 2013). Besides circumventing the use of isocyanates, the cyclic carbonate aminolysis synthetic route to PHU has an additional sustainability advantage of utilizing or sequestering carbon dioxide, as cyclic carbonates are commonly prepared by carbon dioxide fixation of epoxies (Blattmann et al., 2014; Darensbourg & Holtcamp, 1996; Foltran et al., 2012, 2013; North et al., 2010).

Because of a range of sustainability and economic driving forces, there is increasing interest in developing renewable polymeric materials that reduce or eliminate the use of reactants derived from petroleum or natural gas. Many studies have utilized renewable resources including

epoxidized plant seed oils and other bio-derived compounds as intermediates to synthesize NIPUs via cyclic carbonate aminolysis (Bähr et al., 2012; Bähr & Mülhaupt, 2012; Cornille, Blain, et al., 2017; Furtwengler & Avérous, 2018; Javni et al., 2013; Poussard et al., 2016; Schmidt et al., 2017; Tamami et al., 2004). In 2004, Tamami et al. developed a set of cross-linked PHUs based on carbonated soybean oil (Tamami et al., 2004). Depending on the functionality and molecular weight of the amine curing agents, the resulting PHUs exhibited tensile strengths ranging from 0.4 to 1.6 MPa and elongation at break ranging from 40 to 200% (Tamami et al., 2004). In 2012, Mülhaupt and coworkers reported a route to synthesize linear or cross-linked terpene-based PHUs from high purity limonene dioxide, which is a renewable material originated from orange peels (Bähr et al., 2012). Limonene dicarbonate was obtained by carbon dioxide fixation of limonene dioxide under tetrabutylammonium bromide catalysis and further cured with polyfunctional amines to afford a variety of linear, branched and networked NIPUs. They reported increases in both stiffness and T_g with increasing amine functionality (Bähr et al., 2012).

In addition to the use of bio-based reactants, the effective recycling and reprocessing of networks for high-value reuse provides another means of improving the sustainability associated with polymeric materials, albeit one with many challenges (Schneiderman & Hillmyer, 2017). Conventional cross-linked polymeric materials have limited recyclability, and typically no recyclability for high-value products, because the permanent, fixed covalent cross-links prevent the materials from being melt-reprocessed (Wojtecki et al., 2011; Y. Yang et al., 2015). Beginning more than fifteen years ago, numerous studies have addressed this challenge by incorporating dynamic covalent bonds into cross-linked materials to form dynamic covalent polymer networks (DCPNs) (Capelot, Montarnal, et al., 2012; Chakma & Konkolewicz, 2019; Denissen et al., 2016; Fortman, Brutman, et al., 2018; Kloxin et al., 2010; Z. P. Zhang et al., 2018; Zou et al., 2017) (also

called covalent adaptable networks (CANs) (Kloxin et al., 2010)) and network composites (de Luzuriaga et al., 2016; Kuang et al., 2018; Y. Liu et al., 2018). Such networks have generally been reported to undergo reconfiguration by one of two mechanisms (Denissen et al., 2016). The first is a dissociative bond exchange mechanism in which dynamic bonds break under applied stimulus (commonly high temperature) and reform with stimulus removal. Dissociative mechanisms include the Diels–Alder reaction (Fang et al., 2018; Oehlenschlaeger et al., 2014; Polgar et al., 2015; Shao et al., 2017) and alkoxyamine chemistry (Jin et al., 2016; Otsuka, 2013). The second is an associative bond exchange mechanism, e.g., transesterification (Capelot, Montarnal, et al., 2012; Li et al., 2018), in which dynamic bonds undergo exchange reactions so that the total number of bonds remains invariant. DCPNs based solely on associative bond exchange are termed vitrimers (Capelot, Montarnal, et al., 2012).

Unlike conventional PU networks, PHU networks synthesized by cyclic carbonate aminolysis contain primary and secondary hydroxyl groups adjacent to urethane groups, which afford the materials novel, high-levels of reprocessability that are not present with conventional PU networks (Fortman et al., 2015, 2017). In 2015, Fortman et al. reported that PHU networks synthesized from *bis*(six-membered cyclic carbonates) (6CCs) and polyfunctional amines rearrange at elevated temperature via associative transcarbamoylation exchange reactions between carbamate linkages and the free hydroxyl groups (Fortman et al., 2015). In 2017, the same research team compared the reprocessability and stress relaxation of PHUs derived from difunctional 6CCs and *bis*(five-membered cyclic carbonates) (5CCs) (Fortman et al., 2017). The authors concluded that 5CC-derived PHUs are poor candidates for reprocessable networks due to thermal decomposition and side reactions accompanying transcarbamoylation at elevated temperature (Fortman et al., 2017). In 2017, Chen et al. demonstrated that 5CC-derived PHU networks with

appropriate catalysis exhibit both transcarbamoylation exchange chemistry and reversible cyclic carbonate aminolysis chemistry (X. Chen et al., 2017) (Scheme 4-1). Importantly, this work also shows that such PHU networks can undergo multiple reprocessing steps with full property retention associated with cross-link density. Thus, PHU networks that do not fall strictly in the category of vitrimers because of the presence of concurrent dissociative and associative dynamic reactions can exhibit reprocessability with complete cross-link density recovery.

Despite past efforts aimed at exploiting green, bio-derived precursors and improving the recyclability of PHU networks, no single study has yet addressed the reprocessability of bio-based PHU networks, which could lead to further advances in the sustainability of NIPU networks and network composites. Here, we have investigated the reprocessability of four PHU networks prepared with two types of bio-based cyclic carbonates, carbonated soybean oil (CSBO) and sorbitol ether carbonate (SEC), and two types of amines, Priamine^{TM} 1074 (1074) and diethylene glycol bis(3-aminopropyl) ether (DGBE). Priamine^{TM} 1074 is a bio-based difunctional amine derived from oleic and/or linoleic acid (Duval et al., 2016), so PHU networks synthesized with 1074 in this study are fully bio-based. We find that CSBO-based PHU networks can undergo multiple reprocessing steps with full property recovery related to cross-link density. In addition, besides the simultaneous presence of the reversible cyclic carbonate aminolysis and transcarbamoylation exchange reactions, CSBO-based PHU networks also undergo a third dynamic chemistry based on transesterification exchange reactions between ester groups in the CSBO backbone and the free hydroxyl groups. Finally, by comparison of CSBO-based and SEC-based networks we show that cross-link density/architecture of monomers can play a major role in the reprocessability of dynamic polymer networks, sometimes making otherwise fully reprocessable networks unable to achieve full reprocessability.

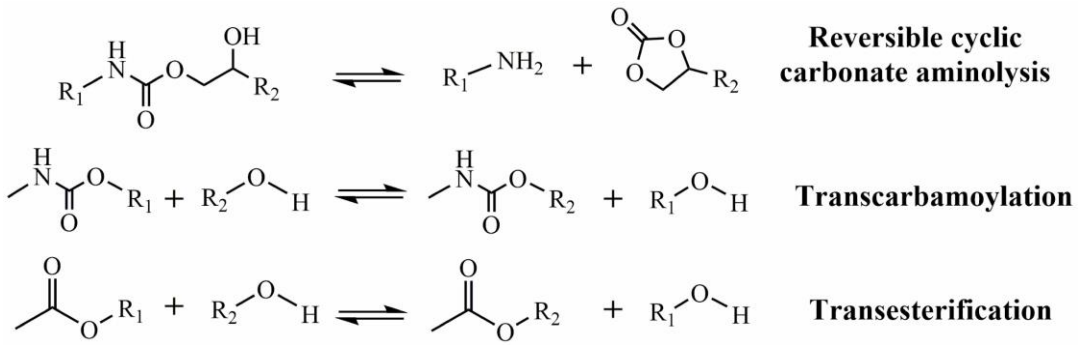

Scheme 4-1. Reversible cyclic carbonate aminolysis, transcarbamoylation, and transesterification reaction.

4.2 Experimental

4.2.1 Materials

Epoxidized soybean oil (Paraplex G-62, oxirane oxygen content 7.13 wt%), subsequently referred to as ESBO, was supplied by Hallstar. Tetrabutylammonium iodide (TBAI, reagent grade, 98%), *N*,*N*-dimethylacetamide (DMAc, anhydrous, 99.8%), 4-(dimethylamino)pyridine (DMAP), chloroform-d ($CDCl_3$, 99.8 atom % D), dimethyl sulfoxide (DMSO, anhydrous, ≥99.9%), dimethylformamide (DMF, anhydrous, 99.8%), 1,6-hexanedithol (96%) and tetrahydrofuran (THF, anhydrous, ≥99.9%) were from Sigma-Aldrich. Diethylene glycol bis(3-aminopropyl ether (≥98%) was from TCI America. D-Sorbitol polyglycidyl ether (SGE) was purchased from Carbosynth. Priamine^{TM} 1074 was supplied by Croda. Chemicals were used as received.

4.2.2 Synthesis

Synthesis of Multifunctional Cyclic Carbonate Monomers

Carbonated soybean oil was prepared by catalytic CO_2 fixation of ESBO in the presence of TBAI (5 mol% with respect to epoxy groups). In a typical synthesis, ESBO (20.0 g, containing 89.1 mmol of epoxy groups) and TBAI (1.65 g, 4.47 mmol) were placed in a test tube along with

5 mL DMAc that helped to dissolve TBAI, and the mixture was heated in an oil bath at 110 °C. CO_2 gas was then bubbled through the mixture until complete conversion of epoxy groups to carbonate groups was achieved (~70 h). The level of conversion was monitored via both FTIR and ^{1}H NMR spectroscopy by the disappearance of the band or proton signals associated with the epoxy moiety. Upon completion, TBAI was removed by dissolving the mixture in ethyl acetate and extracting five times with distilled water. ^{1}H NMR spectroscopy confirmed the complete removal of TBAI. The organic layer was then rotary evaporated and placed overnight in an 80 °C vacuum oven to remove all remaining solvent. The dried CSBO was collected and stored for use.

Sorbitol ether carbonate was prepared by catalytic CO_2 fixation of SGE in the presence of TBAI (10 wt% with respect to SEC). In a typical synthesis, SGE (20.0 g) and TBAI (2.00 g) were placed in a test tube along with 15 mL DMAc that helped to dilute the reaction mixture. The test tube was heated to 80 °C in an oil bath. CO_2 gas was then bubbled through the mixture until achievement of complete conversion of epoxy groups to carbonate groups. The conversion level was monitored by ^{1}H NMR spectroscopy via the disappearance of bands or peaks associated with the epoxy group. After ~90 h, the mixture became a highly viscous liquid. To remove the solvent and catalyst from the system, the mixture was diluted with 20 mL acetone and washed with 250 mL water for five cycles. Full removal of TBAI was confirmed by ^{1}H NMR spectroscopy. The purified product was dried in a heated oven (80 °C) under vacuum overnight to remove all remaining solvents and then stored. The carbonate content in SEC was characterized via ^{1}H NMR spectroscopy using DMSO as solvent with 1,2,4,5-tetrachlorobenzene as an internal reference. Equation 4-1 was used to calculate the moles of carbonate groups per gram of SEC (Schmidt 2017):

$$\text{carbonate content } \left[\frac{\text{mol}}{\text{g}}\right] = \frac{I_{\text{cc}} \times n_{\text{ref}}}{\frac{I_{\text{ref}}}{2} \times m_{\text{SEC}}} \tag{4-1}$$

where I_{cc} is the intensity of the peak associated with one of the three protons on cyclic carbonate in SEC (~4.92 ppm), n_{ref} is the molar amount of 1,2,4,5-tetrachlorobenzene in the sample, I_{ref} is the peak intensity associated with the two protons on 1,2,4,5-tetrachlorobenzene (~8.07 ppm), and m_{SEC} is the weight of SEC in the sample.

Synthesis of PHU Networks

Preparation of all PHU networks was performed by reacting equivalent weights of multifunctional carbonate monomer with difunctional amine under DMAP catalysis. In a typical synthesis of CSBO-DGBE network, 95.6 mg DMAP (0.78 mmol, 6 mol% with respect to cyclic carbonate) was dissolved in 1.44 g DGBE (6.52 mmol) in a 20-mL scintillation vial. After complete solubilization, 3.50 g CSBO (containing 13.04 mmol of cyclic carbonate) was added into the vial. The mixture was reacted at 80 °C for 24 h with stirring to yield complete conversion within error as determined by FTIR spectroscopy. The CSBO-1074 network was synthesized in a similar manner. In a typical synthesis of SEC-DGBE network, 1.00 g SEC (containing 4.30 mmol of cyclic carbonate) and 0.47 g of DGBE (2.15 mmol) were added to a 20-mL scintillation vial. 2 mL anhydrous DMF was then added to reduce the mixture viscosity and enable homogeneous mixing. 94.5 mg DMAP (0.77 mmol, 18 mol% with respect to cyclic carbonate) was dissolved in the solution, and the vial was transferred to a preheated oil bath at 80 °C. Within less than 2 h, the sample formed gels, which were allowed to remain in oil bath for additional 20 h to ensure complete crosslinking. The samples were then heated in an 80 °C oven under vacuum for 24 h to evaporate any remaining solvent. Synthesis of SEC-1074 networks followed a procedure similar to that of SEC-DGBE networks, except that THF instead of DMF was used as solvent to make the polar SEC and non-polar Priamine^{TM} 1074 compatible with each other. Structures of all monomers used for the synthesis of PHU networks are shown in Figure 4-1.

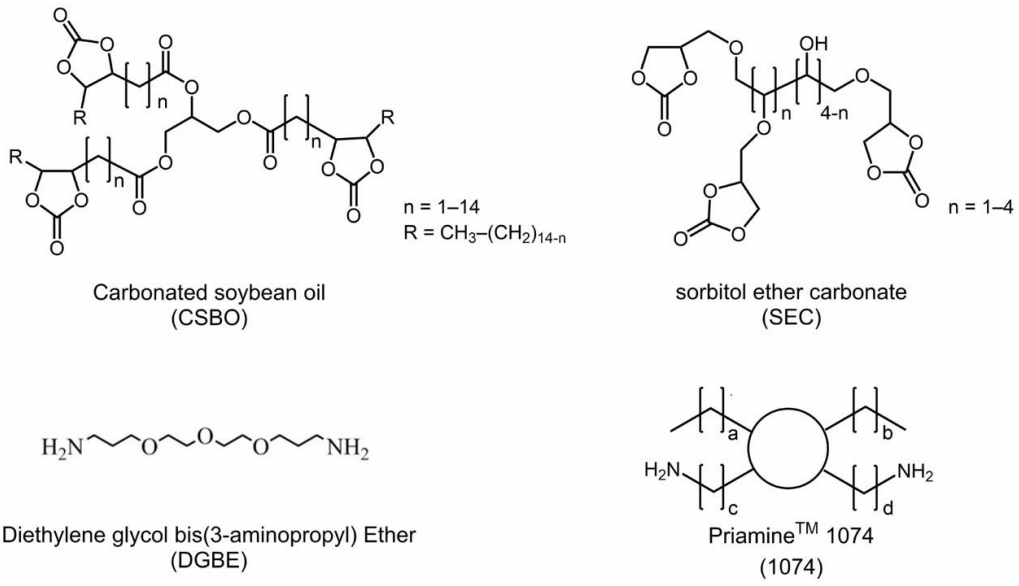

Figure 4-1. Monomers used for the synthesis of PHU networks.

Synthesis of ESBO-SH_2 Network (Model Reaction)

The ESBO-SH_2 network was prepared via thiol-epoxy click reaction by reacting ESBO with a stoichiometric amount of 1,6-hexhanedithiol under DMAP catalysis. In a typical synthesis, 49.0 mg DMAP (6 mol% with respect to epoxide) was dissolved with 0.50 g dithiol in a FlackTek cup, followed by adding 1.50 g of ESBO. This mixture was homogenized using a SpeedMixer (FlackTek, DAC 150.1 FVZ-K) at 2500 rpm for 1 min and then transferred to a 20-mL scintillation vial and allowed to react at 80 °C for 24 h to ensure full conversion.

4.2.3 Reprocessing procedure

Reprocessing of CSBO-based PHU networks was carried out by cutting networks into small pieces and remolding in a PHI press (Model 0230C-X1) at 110 °C with a 7-ton ram force (11 MPa). The minimum required reprocessing times were 30 min and 40 min for CSBO-DGBE and CSBO-1074 networks, respectively. After remolding, samples were cooled to room temperature in a cold compression mold with a 3-ton ram force.

4.2.4 Characterization

^{1}H NMR spectroscopy was done at room temperature using a Bruker Avance III 500 MHz NMR spectrometer with a direct cryoprobe. Solutions were in deuterated chloroform ($CDCl_3$) or dimethyl sulfoxide (DMSO), and spectra were reported relative to tetramethylsilane or tetrachlorobenzene. Attenuated total reflectance-Fourier transform infrared (ATR–FTIR) spectroscopy employed a Bruker Tensor 37 MiD IR FTIR spectrophotometer with a diamond/ZnSe attachment. Thirty-two scans were collected at room temperature over the 4000 to 600 cm^{-1} range with a 4 cm^{-1} resolution. Conversion of cyclic carbonate groups was determined by analyzing the carbonate peak at ~1780 cm^{-1}.

Dynamic mechanical analysis (DMA) employed a TA Instruments Rheometrics Stress Analyzer-III. Samples measuring ~0.9 mm in thickness and ~7 mm in width were mounted and underwent temperature ramps from –50 °C to 80 °C at a 3 °C/min heating rate. Tension-mode measurements of the storage modulus (E'), loss modulus (E''), and tan δ (E''/E') were done at 1 Hz frequency and 0.03% strain.

Room-temperature tensile tests (ASTM D1780) were done using an MTS Sintech 20/G tensile tester. Specimens were cut using a Dewes-Gumbs die from molded samples and subjected to extension at a rate of 130 mm/min until break. Tensile properties are reported as average values of at least five tests with error bars representing plus/minus one standard deviation.

The glass transition temperature (T_g) of each network was characterized by differential scanning calorimetry (DSC) employing a Mettler Toledo DSC822e. Samples were maintained at 80 °C for 20 min, followed by cooling to –60 °C at a rate of –40 °C/min. The T_gs were obtained from a second heating ramp at a 10 °C /min rate using the 1/2 ΔC_p method.

Equilibrium swelling experiments were conducted at room temperature using chloroform as swelling solvent. The samples were swollen for 3 days to equilibrium. Swollen samples were weighed immediately after removing excess solvent at the surface of the samples with tissues. Finally, the swollen samples were dried at 80 °C under vacuum for 3 days to evaporate the swelling solvent and the weight of all de-swollen samples were recorded. The swelling ratio is estimated by $(m_{sw}\text{-}m_{dry})/m_{dry}$ and the gel content is estimated by m_{dry}/m_0, where m_0, m_{sw}, and m_{dry} are the masses of the as-prepared samples, swollen samples, and dried samples, respectively.

4.3 Results and Discussion

4.3.1 Synthesis of cyclic carbonate monomers and PHU networks

Carbonated soybean oil is a commonly used, low-cost vegetable oil that has been employed in several previous studies as a precursor for NIPU (Bähr & Mülhaupt, 2012; Javni et al., 2013; Poussard et al., 2016; Tamami et al., 2004). Here, CSBO was synthesized from its bio-based epoxy precursor ESBO following Scheme 4-S1(a) by CO_2 fixation in the presence of TBAI catalyst. Conversion was monitored as a function of time via FTIR and ^{1}H NMR spectroscopy, with complete conversion being reached after ~70 h at 110 °C. Figure 4-2(a) shows the FTIR spectra of the mixture before and after reaction. Epoxy groups underwent full conversion to cyclic carbonate groups as characterized by the disappearance of oxirane C–O bands at 823 and 845 cm^{-1} (Tamami et al., 2004) as well as by appearance of a strong carbonate carbonyl stretching band at 1780 cm^{-1}. Conversion of ESBO into CSBO was further confirmed by ^{1}H NMR spectroscopy by the disappearance of peaks at 2.70–3.00 ppm associated with epoxy units and the appearance of peaks at 4.50–4.87 ppm associated with the cyclic carbonate moiety as shown in Figure 4-2(b) (Poussard et al., 2016).

Only one previously published study has investigated the use of SEC as an intermediate in NIPU synthesis (Schmidt et al., 2017). Here, SEC was prepared from its bio-based epoxy precursor SGE (commercially available, synthesized from the reaction between sorbitol and epichlorohydrin) following Scheme 4-S1(b) by CO_2 fixation in the presence of TBAI catalyst. Before reaction, 15 mL DMAc was added to ensure that CO_2 could flow well through the mixture when viscosity increased with conversion. Complete conversion was reached after ~90 h at 80 °C, as indicated by ^{1}H NMR spectra (Figure 4-2(c)), in which the proton signals associated with epoxide groups in SGE at 3.10, 2.74, and 2.57 ppm disappeared and signals corresponding to cyclic carbonates at 4.92, 4.55, and 4.30 ppm appeared in the carbonated product. Cyclic carbonate content of the purified SEC product was determined to be 0.0043 mol/g using Equation 4-1.

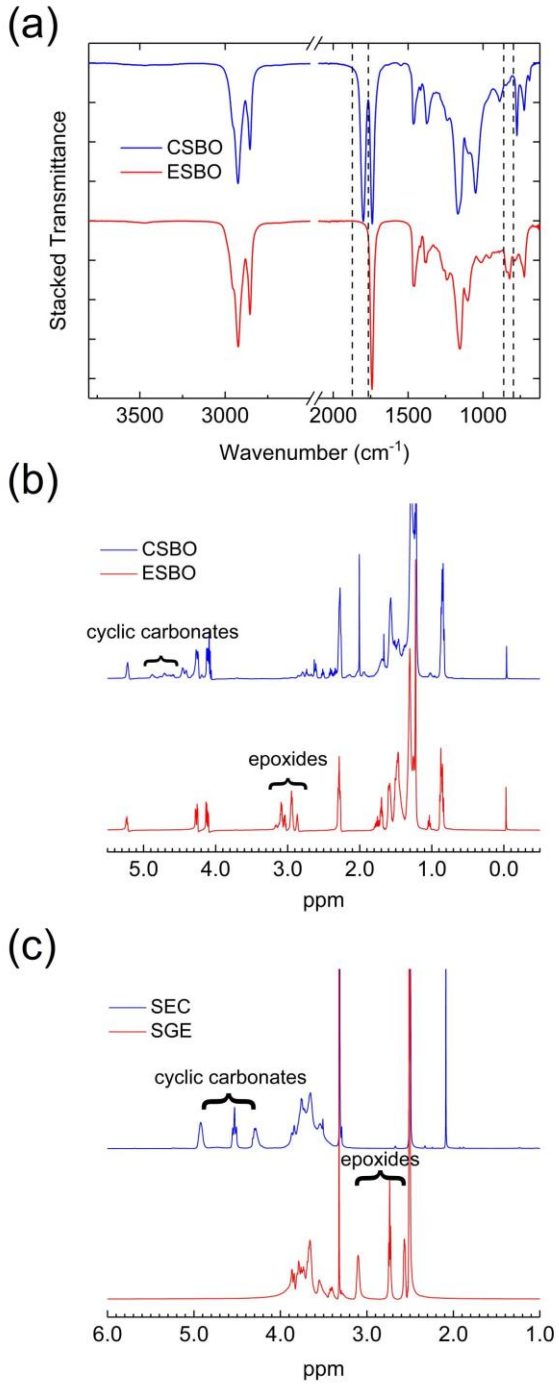

Figure 4-2. (a) Stacked FTIR transmittance of ESBO and CSBO. ^{1}H NMR spectra of (b) ESBO and CSBO, and (c) SGE and SEC.

Renewable PHU networks were prepared by reacting two types of bio-derived multifunctional cyclic carbonate monomers, CSBO and SEC, with either a synthetic diamine, DGBE, or a bio-based diamine, Priamine^{TM} 1074. Chen et al. have shown that because of the presence of the reversible cyclic carbonate aminolysis reaction, volatile components generated by the reverse reaction can evaporate during the reprocessing step, which leads to limited reprocessability of the material (X. Chen et al., 2017). To suppress or eliminate volatilization in the present study, both types of diamine were chosen in consideration of their low volatility. Synthesis of CSBO-based PHU networks was done via solvent-free bulk polymerization; in contrast, with SEC-based PHU networks, synthesis was done via solution polymerization with either DMF or THF as solvent. As reported previously (Schmidt et al., 2017), SEC has a high functionality and short chain length between adjacent functional groups, which makes it a highly reactive material as evidenced by the short gelation time when cured with multifunctional amines. The rapid gelation rate, in addition to the high viscosity of SEC, makes it difficult to achieve a homogeneous reaction mixture in the absence of solvent. Therefore, to ensure sufficient mixing, a pre-calculated amount of DMF was added to all SEC-DGBE networks to adjust the initial reacting group concentration to 2.15 M. In the case of SEC-1074 networks, in order to make the polar SEC and non-polar Priamine^{TM} 1074 compatible with each other, a minimal amount of THF was added that allowed for miscibility of reactants and products during polymerization.

The synthesis of PHU networks was followed by FTIR spectroscopy. The spectra of the as-synthesized CSBO-DGBE, CSBO-1074, SEC-DGBE, SEC-1074 networks are shown in Figure 4-3. For both CSBO-DGBE and CSBO-1074, complete conversion within error of cyclic carbonate groups was achieved as indicated by the disappearance of the carbonate peak at ~1780 cm^{-1} and the appearance of the urethane carbonyl stretch at 1700–1730 cm^{-1} and the hydroxyl stretch at

3500–3100 cm^{-1}. In contrast, in all cases of SEC-based networks, a small but significant amount of unreacted cyclic carbonate remained in the dried sample as shown in the FTIR spectra (Figure 4-3(b)). The incomplete conversion of functional groups in SEC-based PHU networks could possibly be attributed to the steric hindrance caused by the short chain length between adjacent cyclic carbonate groups in SEC.

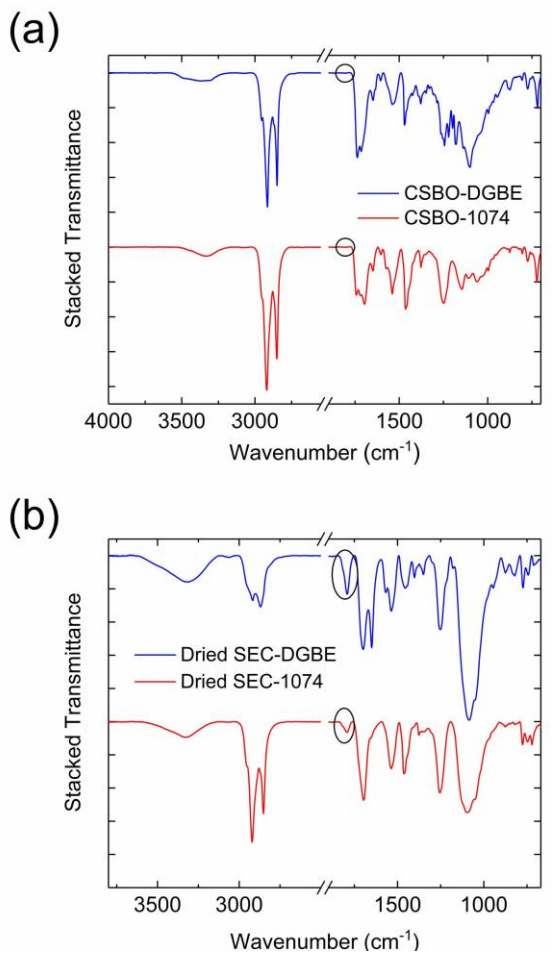

Figure 4-3. Stacked FTIR transmittance of the original (as-synthesized) (a) CSBO-DGBE and CSBO-1074 networks, and (b) SEC-DGBE and SEC-1074 networks.

4.3.2 Reprocessability and reprocessing mechanism of CSBO-based PHU networks

Reprocessing of PHU networks was achieved by cutting samples into small pieces and compressing them into ~1 mm thick sheets at 110 °C with a 7-ton ram force using a PHI press. The reprocessing times were 30 min and 40 min for CSBO-DGBE and CSBO-1074 networks, respectively, which are minimum times required to yield well-consolidated films. Representative images of CSBO-DGBE networks before and after reprocessing are shown in Figure 4-4.

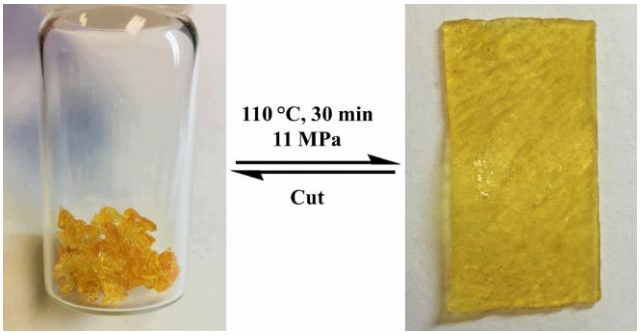

Figure 4-4. CSBO-DGBE networks, original (as synthesized) and remolded sample.

The reprocessability of CSBO-based PHU networks was investigated using DMA. Figure 4-5(a) shows DMA results for the 1st, 2nd, and 3rd molded CSBO-DGBE networks. The *E′* curves for all three samples display a rubbery plateau region above T_g, which is in accordance with the cross-linked nature of the materials. In the rubbery plateau region, all three curves show identical *E′* values within error. Because the rubbery plateau modulus is proportional to the cross-link density of polymer networks (Flory, 1953), this result indicates that CSBO-DGBE networks are able to achieve full property recovery of cross-link density (relative to the 1st molded sample) after multiple molding steps. The tan δ curves of all three samples also overlapped well, consistent with unchanged glass transition behavior as a function of molding steps. This result was further confirmed using DSC, with all three molded samples exhibiting an identical T_g value of –21 °C.

Similar results were observed for the 100% bio-based CSBO-1074 networks. As shown in Figure 4-5(b), the E' and tan δ curves for all three molded CSBO-1074 samples are very similar; DSC analysis revealed that T_g = –14 °C was invariant with reprocessing steps. Values of E' in the rubbery plateau region for the two CSBO-based PHU networks are summarized in Table 4-1 as a function of molding step. The cross-link density (v_e) can be directly calculated from the rubbery plateau E' value according to Flory's ideal rubber elasticity theory (Flory, 1953), and the values are summarized in Table 4-1. Overall, these results indicate that CSBO is a highly effective starting material for the synthesis of renewable PHU networks that exhibit excellent recyclability and reprocessability with complete property recovery of cross-link density.

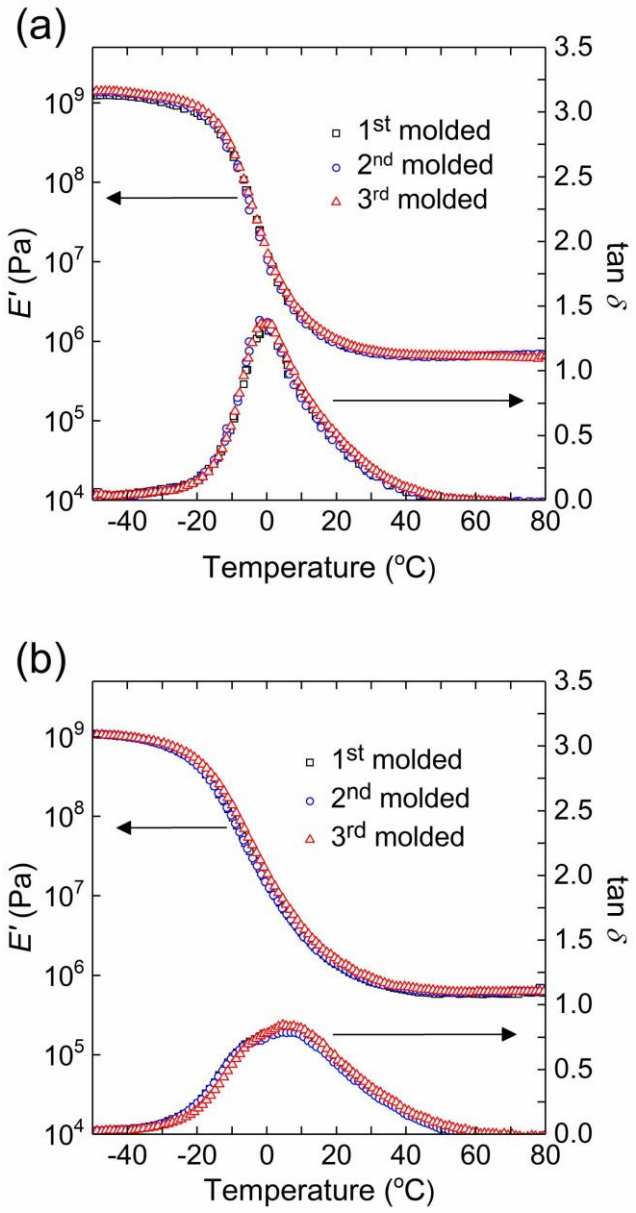

Figure 4-5. Dynamic mechanical responses of (a) CSBO-DGBE networks and (b) CSBO-1074 networks: *E'* and tan δ as functions of temperature for the 1st molded (squares), 2nd molded (circles), and 3rd molded (triangles) samples.

Table 4-1. Rubbery plateau storage modulus at 80 °C and cross-link density of CSBO-based networks.

Sample	Molding step	E' (MPa)	$\nu_e \times 10^5$ (mol cm^{-3})
CSBO-DGBE	1st	0.69 ± 0.03	7.9 ± 0.4
	2nd	0.67 ± 0.02	7.7 ± 0.2
	3rd	0.67 ± 0.02	7.6 ± 0.2
CSBO-1074	1st	0.63 ± 0.02	7.2 ± 0.2
	2nd	0.67 ± 0.03	7.6 ± 0.4
	3rd	0.67 ± 0.06	7.6 ± 0.7

Room-temperature tensile properties are provided in Table 4-2 for the 1st, 2nd, and 3rd molded samples, showing behavior consistent with elastomeric polymer networks. CSBO-DGBE samples exhibit Young's modulus of ~0.8 MPa, tensile strength of ~0.9 MPa and elongation at break of ~160 %. The tensile properties of CSBO-1074 samples are generally better than CSBO-DGBE samples (Young's modulus of ~1.2 MPa, tensile strength of ~1.1 MPa, and elongation at break of ~220%), possibly associated with the slightly higher T_g of CSBO-1074. Within experimental error, both CSBO-based networks are able to maintain consistent tensile properties after multiple molding steps (representative stress-strain curves are shown in Figure 4-S1), indicating excellent reproduction of mechanical response.

Table 4-2. Room-temperature tensile properties of 1st, 2nd, and 3rd molded CSBO-DGBE and CSBO-1074 samples.

Sample	Molding step	Young's modulus (MPa)	Tensile strength (MPa)	Elongation at break (%)
CSBO-DGBE	1st	0.85 ± 0.04	0.85 ± 0.08	145 ± 3
	2nd	0.78 ± 0.07	0.82 ± 0.22	156 ± 34
	3rd	0.75 ± 0.10	0.92 ± 0.12	174 ± 28
CSBO-1074	1st	1.14 ± 0.26	0.92 ± 0.09	233 ± 8
	2nd	1.34 ± 0.07	1.13 ± 0.11	209 ± 26
	3rd	1.18 ± 0.27	1.22 ± 0.19	216 ± 27

Scheme 4-2 shows the hypothesized formation and rearrangement mechanisms of CSBO-based networks. Chen et al. has shown that, with appropriate catalysis, associative transcarbamoylation reactions and dissociative reversible cyclic carbonate aminolysis reactions are both present in the rearrangement of PHU networks (X. Chen et al., 2017). In the current study, we hypothesize that there are three dynamic chemistries involved during the reprocessing step of CSBO-based PHU networks. In addition to transcarbamoylation reactions and reversible cyclic carbonate aminolysis, the ester groups present in CSBO should be able to undergo transesterification reactions with pendent hydroxyl groups (see Scheme 4-1).

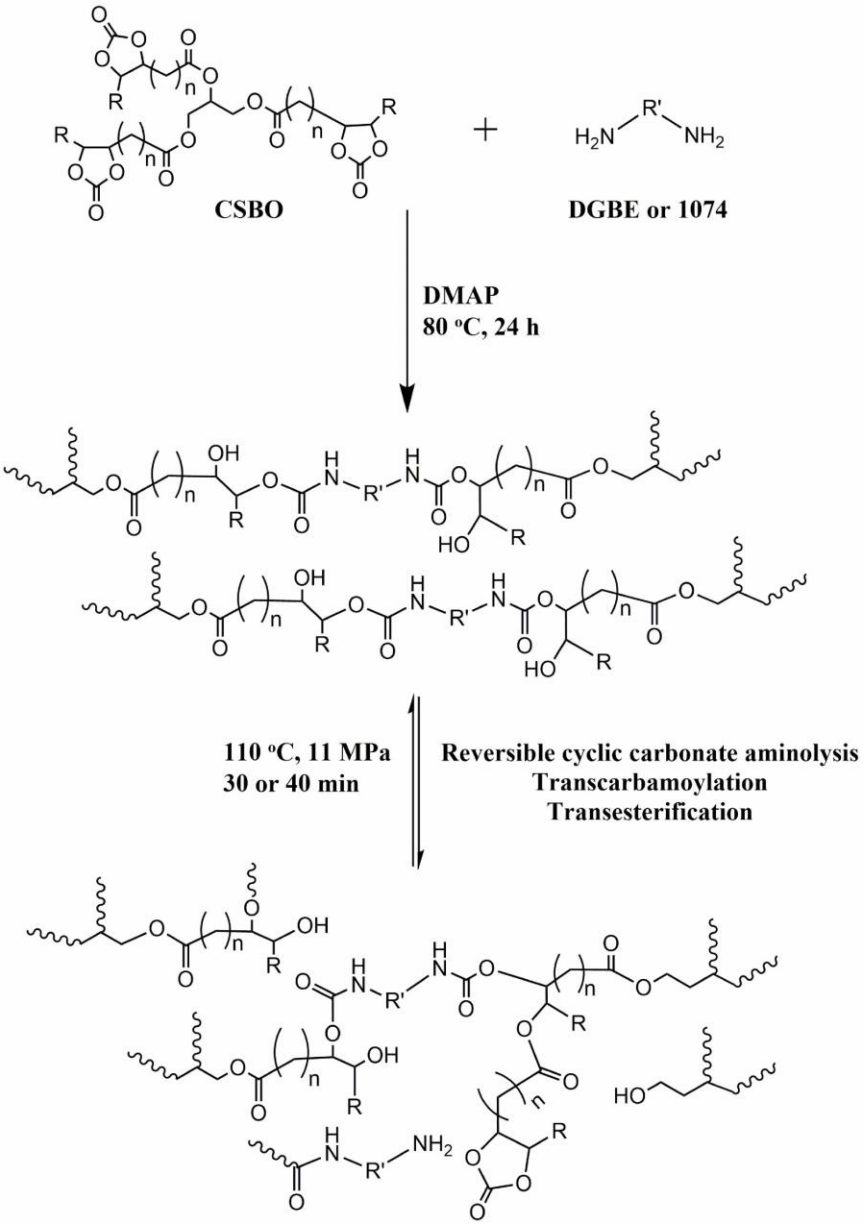

Scheme 4-2. Mechanism of the synthesis and rearrangement of CSBO-based PHU networks.

To test our hypothesis that the transesterification reaction can occur in CSBO-based networks under the experimental conditions used in our study, we designed a model experiment based on thiol-epoxy "click" chemistry in which ESBO and 1,6-hexanedithiol were reacted in stoichiometric balance under DMAP catalysis (6 mol% with respect to epoxide). Complete conversion was confirmed by the disappearance of the thiol peak at ~2570 cm^{-1} (Figure 4-S2). The

resulting network was cut into pieces and reprocessed at 110 °C for 40 min. The catalyst concentration and reprocessing temperature were exactly the same as in CSBO-DGBE networks. The presence of transesterification reactions in soybean oil-based networks under these conditions is confirmed if the broken pieces are able to form a consolidated film after being remolded, since transesterification between ester groups in ESBO and hydroxyl groups generated during thiol-epoxy reaction is the only possible dynamic chemistry involved in this system. As shown in Figure 4-6, after being remolded at 110 °C for 40 min, the sample formed a rough film with many cracks or fractures, showing some signs of healing. We then increased the reprocessing time to 2 h. The resulting sample became smoother and more robust than before, indicating that transesterification was indeed happening under these experimental conditions, but at a relatively slow rate. When we increased the reprocessing time to 8 h, an intact film was formed, indicating that the cross-linked chains rearranged via transesterification so that dynamic covalent bonds were successfully reformed at a 110 °C reprocessing temperature.

Based on the slow healing process observed in the model experiment, the shorter reprocessing time and lower reprocessing temperature for CSBO-based PHU networks (30–40 min at 110 °C) compared to previous studies on reprocessable PHU networks (X. Chen et al., 2017; Fortman et al., 2015, 2017; Fortman, Snyder, et al., 2018) is unlikely to be caused by the presence of the transesterification dynamic chemistry during CSBO-based network rearrangement. Instead, it is likely that the relatively short-time, low-temperature reprocessing conditions needed for the CSBO-based PHU networks are significantly associated with the more flexible CSBO structure and the lower T_g values of the corresponding networks relative to the PHU networks investigated in previous reprocessability studies (X. Chen et al., 2017; Fortman et al., 2015, 2017; Fortman, Snyder, et al., 2018).

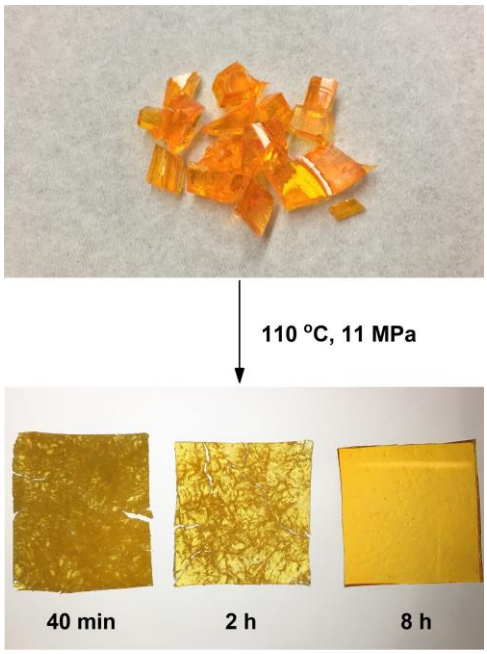

Figure 4-6. ESBO-SH_2 networks, original (as synthesized) and remolded samples.

4.3.3 Reprocessability of SEC-based PHU networks

All SEC-based PHU networks were synthesized following Scheme 4-S2. Initially, SEC-DGBE was prepared with 6 mol% DMAP (with respect to cyclic carbonate group) following the procedures in the experimental session. The resulting network was cut into pieces and reprocessed. After molding the broken pieces at 110 °C for 40 min, a poorly formed film resulted that broke easily upon being touched. In an attempt to improve reprocessability, we increased the catalyst load from 6 mol% to 18 mol%; however, a macroscopically similar sample was obtained after reprocessing. Finally, we prepared the SEC-DGBE network with 18 mol% DMAP and reprocessed it at 180 °C for 3 h. A rough film with significant cracks was formed, which was insufficiently robust to withstand DMA characterization (Figure 4-7). Similar results were observed for the SEC-1074 network.

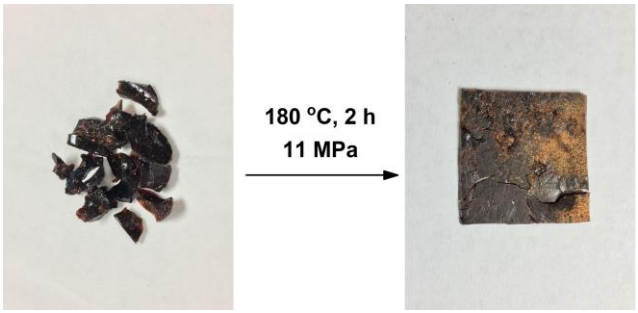

Figure 4-7. SEC-DGBE networks, original (as synthesized) and remolded sample.

The poor reprocessability of the SEC-based PHU network can be attributed to the SEC molecular structure. Because of the high functionality of SEC, SEC-derived networks have the potential for high cross-link density, which could result in higher T_gs relative to CSBO-based networks. In fact, DSC measurements indicate that the T_g of the as-synthesized SEC-DGBE network is 10 °C, roughly 30 °C higher than that of the as-synthesized CSBO-DGBE network. A direct comparison of the molecular structures of CSBO and SEC (Figure 4-1) indicate that functional groups in CSBO are relatively far apart from each other, separated by long fatty acid chains, whereas in SEC as many as six cyclic carbonate groups may be present in side chains on adjacent carbon atoms in the SEC backbone. Thus, when some of these cyclic carbonate groups participate in network formation, a highly dense and inflexible network structure is formed. Based on steric effects and reduced mobility, that highly dense network structure will make it very difficult for remaining unreacted cyclic carbonate groups to participate in reaction. These effects are likely the cause of the incomplete conversion obtained in the as-synthesized SEC-based networks (see Figure 4-3(b)), whereas complete conversion was obtained in the CSBO-based networks. These effects make it much more difficult for SEC-based PHU networks to be effectively reprocessed with cross-link density recovery than CSBO-based networks.

Equilibrium swelling tests at room temperature were performed for the as-synthesized CSBO-based networks and SEC-based networks to confirm their cross-linked architecture. After immersing the samples in chloroform for 3 days, networks were insoluble and maintained their intact forms, manifesting their cross-linked structures. The gel contents and swelling ratios are detailed in Table 4-S1. The high gel content of SEC-based networks (~96%) further indicates that the materials possess a high degree of cross-linking and that the incomplete conversion of cyclic carbonate group observed in FTIR spectra was due to the inflexible nature of the network.

It will be important to consider structural factors in future studies of reprocessable polymer networks. As demonstrated here, failure to achieve reprocessability of a dynamic polymer network with full cross-link density recovery can occur not only because of deficiencies associated with the chemistry but also because of steric effects and mobility issues associated with the molecular design of the monomers. When the chemistry itself is intrinsically able to achieve full conversion and recover cross-link density, as demonstrated with the well-designed CSBO monomer, poor molecular design, as with SEC monomer, can limit conversion of as-synthesized networks and the ability to recover cross-link density.

4.4 Conclusions

We have investigated the reprocessability and cross-link density recovery of four renewable PHU networks derived from two bio-based polyfunctional carbonates, CSBO and SEC. Both carbonates were prepared from their epoxy precursors by direct CO_2 fixation in the presence of catalyst. DMA results have revealed that CSBO-based PHU networks are able to undergo multiple reprocessing steps under mild conditions (110 °C, 30–40 min) with full property recovery associated with cross-link density relative to the 1^{st} molded sample. Under the experimental

condition used in this study and because of the presence of ester groups in the backbone of CSBO, CSBO-based PHU networks are able to undergo network rearrangement via three dynamic chemistries: reversible cyclic carbonate aminolysis, transcarbamoylation exchange reaction, and transesterification exchange reaction. Further study is warranted to determine the rate and extent of each reaction during reprocessing. In sharp contrast to the excellent reprocessability of CSBO-based systems, SEC-based PHU networks exhibit poor reprocessability even with much higher catalyst loading (18 mol% with respect to cyclic carbonate) and increased reprocessing time and temperature (180 °C, 2 h). This poor reprocessability is attributed to the disadvantageous molecular design of SEC, which combines a high functionality of groups involved in cross-linking with short chain lengths between adjacent groups. This molecular design leads to steric effects and low chain mobility after partial reaction which severely limit achievable functional group conversion during synthesis and reprocessing. Thus, potential property advantages afforded by high cross-link density related to high and dense functionality of a monomer may come at the expense of reprocessability of dynamic covalent polymer networks. This finding applies not only to reprocessable PHU networks but is applicable to reprocessable polymer networks in general.

Acknowledgements

This work was done in collaboration with Xi Chen from the Torkelson research group at Northwestern University. This research is now published (S. Hu et al., 2019): *ACS Sustainable Chem. Eng.* 2019, 7, 10025-10034 (DOI: 10.1021/acssuschemeng.9b01239).

4.5 Supporting Information

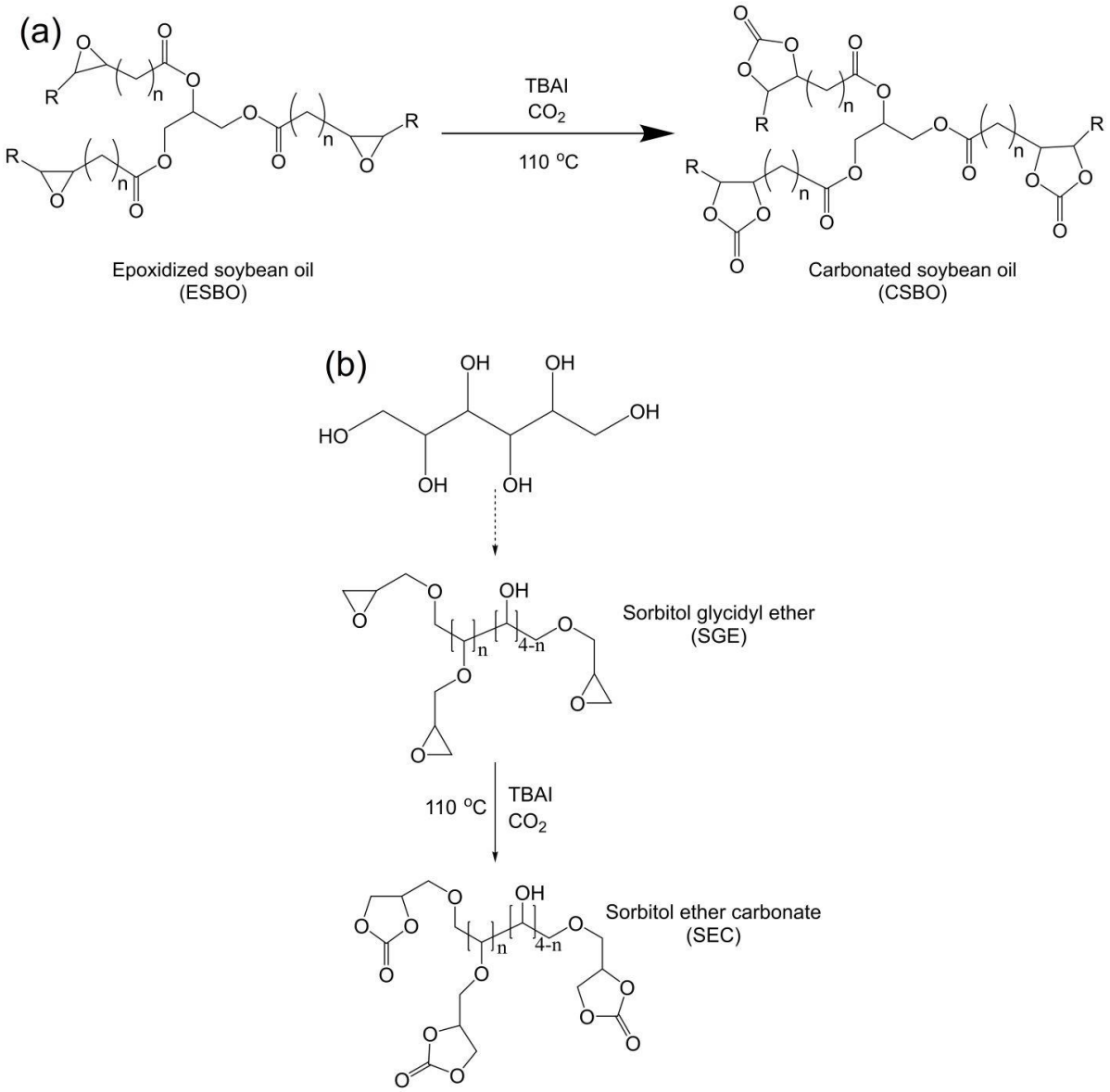

Scheme 4-S1. Schematic of the reaction of (a) ESBO with CO_2 to form CSBO and (b) SGE with CO_2 to form SEC.

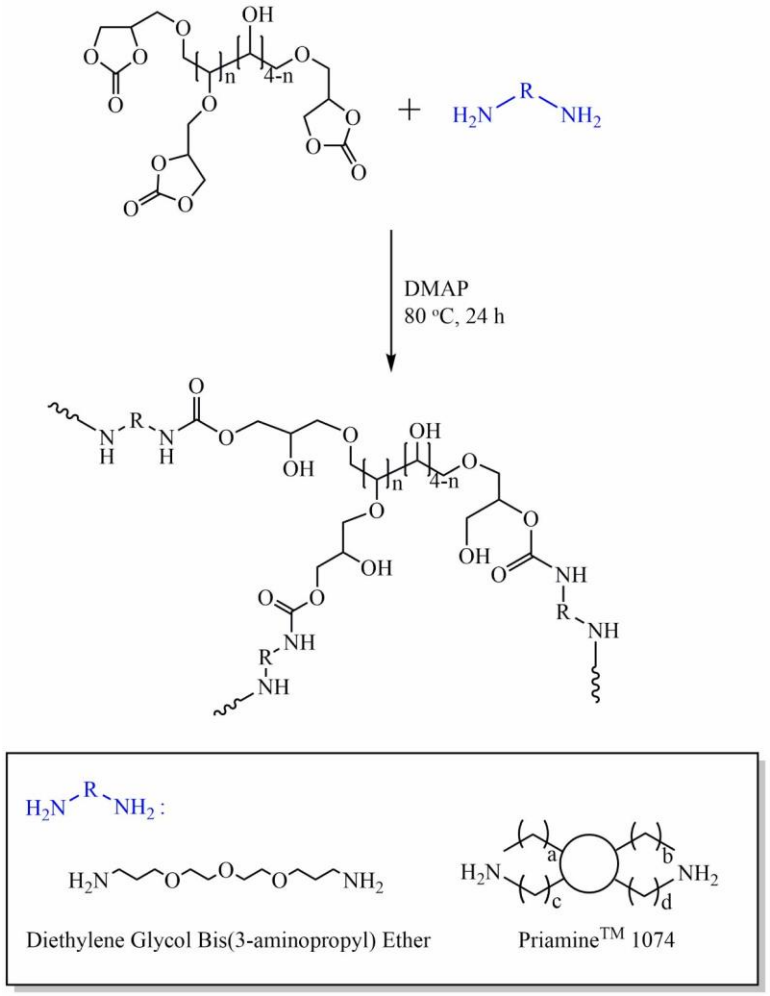

Scheme 4-S2. Mechanism of the synthesis of SEC-based PHU networks.

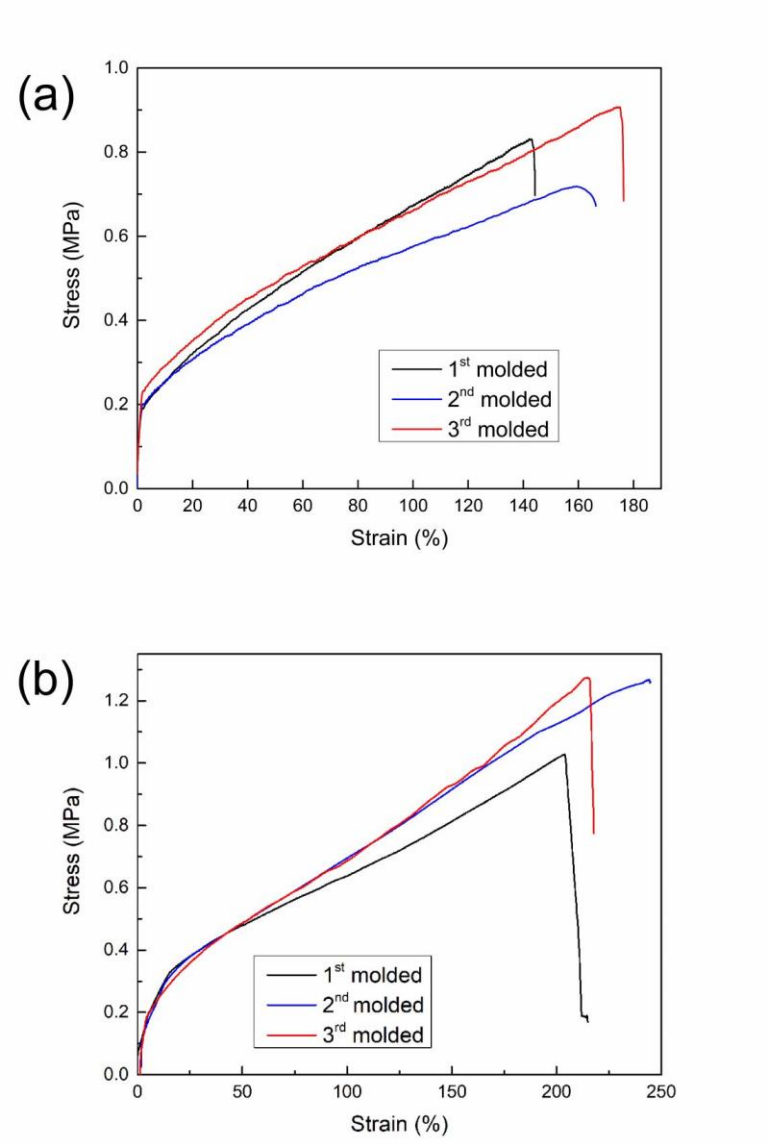

Figure 4-S1. Representative tensile stress-strain curves for 1st, 2nd, and 3rd molded (a) CSBO-DGBE networks and (b) CSBO-1074 networks.

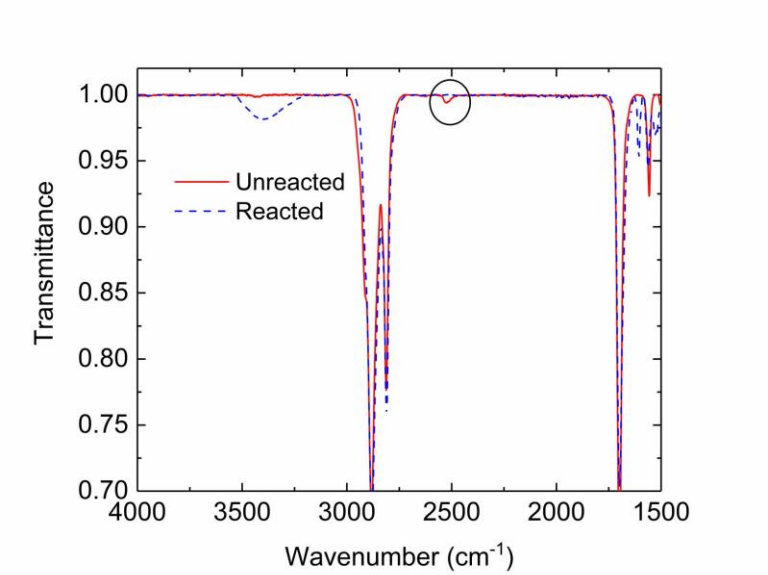

Figure 4-S2. FTIR transmittance of the unreacted and reacted ESBO-hexanedithiol networks.

Table 4-S1. Swelling ratio and gel content of as-synthesized PHU samples.

Sample	Swelling ratio (%)	Gel content (%)
CSBO-DGBE	556 ± 2	97.6 ± 1.5
CSBO-1074	852 ± 8	96.7 ± 2.2
SEC-DGBE	169 ± 3	96.4 ± 1.9
SEC-1074	247 ± 6	95.2 ± 3.4

CHAPTER 5

Reprocessable Polyhydroxyurethane Networks Reinforced with Reactive Polyhedral Oligomeric Silsesquioxanes (POSS) and Exhibiting Excellent Elevated Temperature Creep Resistance

5.1 Introduction

Thermosets have many advantages over thermoplastic materials including improved heat stability, solvent resistance, and enhanced physical properties because of their permanent network structures. However, the proper disposition of end-of-use thermosets remains a key challenge because the permanent cross-links that make these materials strong and useful prevent them from being melt-reprocessed or reshaped. In recent years, covalent adaptable networks (CANs) (Kloxin & Bowman, 2013; Kloxin et al., 2010), also called dynamic covalent polymer networks (DCPNs) (Zou et al., 2017), have been developed to overcome the recyclability challenges associated with conventional thermosets. CANs contain a sufficient number of dynamic linkages to allow the materials to undergo network reconfiguration and thus to achieve recyclability under appropriate conditions (Kloxin et al., 2010). Since the landmark study by Wudl and coworkers on a thermally re-mendable network designed with the Diels–Alder (DA) reaction (X. Chen et al., 2002), there has been considerable progress in developing CANs with numerous dynamic chemistries. These include dissociative chemistries such as hindered urea exchange (Ying et al., 2014; Q. Zhang et al., 2021; Y. Zhang et al., 2016), alkoxyamine chemistry (Jin et al., 2016; Li et al., 2021; Otsuka, 2013), and bis(hindered amino) disulfide chemistry (Bin Rusayyis & Torkelson, 2020, 2021), and associative chemistries such as transesterification (Li et al., 2018; Montarnal et al., 2011; Snyder et al., 2018; B. Zhang et al., 2018), boronic ester interchange (Y. Chen et al., 2018; Soman &

Evans, 2021; Tajbakhsh et al., 2021), and transamination of vinylogous urethanes (Denissen et al., 2015, 2017), among others (Anaya et al., 2021; Y. Hu et al., 2021; Ishibashi & Kalow, 2018; Li et al., 2020). CANs based on associative dynamic chemistries are often called vitrimers (Montarnal et al., 2011). Some CANs have dual dynamic chemistries, e.g., polyhydroxyurethanes undergo associative transcarbamoylation and dissociative reversible cyclic carbonate aminolysis (X. Chen et al., 2017), and polythiourethanes undergo associative exchange reactions with free thiols and dissociative reversion to isocyanates and thiols (Li et al., 2019; Wen et al., 2020). The rapid development of CANs has bridged the gap between thermoplastics and thermosets (X. Chen et al., 2020; McBride et al., 2019; Scheutz et al., 2019) and shown promise for addressing the long-standing issue associated with the irreversible buildup of thermoset wastes. Reviews on the topic of sustainable, recyclable CANs, DCPNs, and vitrimers include refs. (Denissen et al., 2016; Fortman, Brutman, et al., 2018; Hayashi, 2021; McBride et al., 2019; Samanta et al., 2021; Scheutz et al., 2019; Watuthanthrige et al., 2021; Wemyss et al., 2021; N. Zheng et al., 2021).

Fabrication of polymer nanocomposites by nanofiller incorporation is a common strategy to enhance the properties of polymeric materials (Iyer et al., 2015; Paul & Robeson, 2008; Qiu et al., 2018; Valentín et al., 2010; Wei et al., 2019; Y. Yang et al., 2020). The performance of nanocomposites is highly dependent on filler dispersion state and interfacial interactions between fillers and the matrix (Iyer & Torkelson, 2015; Legrand & Soulié-Ziakovic, 2016; Romo-Uribe & Lichtenhan, 2021; Z. Tang et al., 2014). Covalent modification of the filler surface for compatibilized polymer−filler interfaces is an effective method to achieve both high levels of filler dispersion and strong interfacial adhesion (Iyer & Torkelson, 2015; Y. Liu et al., 2018). However, if CANs are used as the matrix, the restricted chain mobility induced by the improved adhesion of polymer chains onto the filler surface can impede topological rearrangement which is essential for

relaxation-related properties such as self-healing ability and reprocessability (Huang et al., 2018). Under such circumstances, surface-modified nanofillers with relatively small surface-to-volume ratios are desirable to balance the stress relaxation and mechanical property enhancement of dynamic network composites.

Polyhedral oligomeric silsesquioxanes (POSS) comprise cage-like organosilicon core $(SiO_{1.5})_n$ and external functional groups attached to each silicon atom (Cordes et al., 2010; J. Wang et al., 2021; Z. Xu et al., 2013). Because the average POSS core diameter is only ~0.5 nm, POSS are considered to be the smallest possible particles of silica (Z. Xu et al., 2013). POSS are important building blocks to obtain organic–inorganic nanocomposites with enhanced properties because the reactive functional groups attached to the core provide a unique advantage for POSS molecules to be covalently bonded to the matrix and thus prevent filler aggregation. Several studies have applied functionalized POSS as reinforcing fillers to fabricate dynamic network composites. Xu et al. (Z. Xu et al., 2013) reported a tough, thermally mendable POSS nanocomposite synthesized from bismaleimide and octafunctional furan-terminated POSS via the DA reaction. Because of the thermally reversible nature of the DA reaction, upon being cracked, the nanocomposite self-healed at appropriate temperatures. Zhou et al. (Zhou et al., 2019) developed a mechanically strong, disulfide-based self-healable network composite by oxidative coupling of small-molecule thiols and octathiol-POSS. Although the composite relaxed stress more slowly than the matrix at lower temperatures, the difference in relaxation rate was lessened above 140 °C. As a result, the composite could be fully healed at higher temperatures or with longer healing time. Yang et al. (H. Yang et al., 2020) prepared a series of epoxy-POSS dynamic network composites by reacting dodecanedioic acid with a mixture of difunctional epoxy and octafunctional glycidyl ether-terminated POSS. The composites exhibited improved tensile strength with increasing POSS

loading. With the help of the efficient transesterification exchange reaction, the composites could be reprocessed with little degradation in mechanical properties. Related studies using functionalized POSS in developing dynamic covalent network composites have been done by Hajiali et al. (Hajiali et al., 2021) and Shen et al. (Shen et al., 2022). These studies highlight the advantages and effectiveness of POSS for fabricating high-performance dynamic covalent network composites.

Polyhydroxyurethane (PHU) is synthesized by aminolysis of cyclic carbonates and is an environmentally friendly alternative to conventional isocyanate-based polyurethane (PU) (Beniah et al., 2016; Blattmann et al., 2014; Cornille, Auvergne, et al., 2017; Gomez-Lopez et al., 2021, 2022; Guan et al., 2011; Kathalewar et al., 2014; Lambeth & Henderson, 2013; Leitsch et al., 2016; Maisonneuve et al., 2015). In recent years, a number of studies have explored the inherent dynamic nature of cross-linked PHU and its effectiveness in developing CANs (X. Chen et al., 2017; X. Chen, Li, Wei, Venerus, et al., 2019; Fortman et al., 2015; S. Hu et al., 2019). In 2015, Fortman et al. (Fortman et al., 2015) reported that PHU networks derived from six-membered cyclic carbonates and amines can relax stress and be reprocessed at elevated temperatures. Their study showed the promise of cross-linked PHUs as a new class of reprocessable networks. In 2017, Torkelson and coworkers discovered that with appropriate catalysis, PHU networks derived from five-membered cyclic carbonates and amines can be reprocessed multiple times with 100% recovery of cross-link density (X. Chen et al., 2017). Such reprocessability was also retained in some biobased PHU networks (S. Hu et al., 2019). Torkelson and coworkers also developed reprocessable PHU network nanocomposites reinforced with silica nanoparticles with different surface functionalities (X. Chen, Li, Wei, Venerus, et al., 2019). When silica nanoparticles with surface hydroxyl and amine functional groups that can participate in dynamic chemistries with the

matrix were used as fillers, reprocessing led to losses in cross-link density. Even when using superhydrophobic silica nanoparticles with surface hydroxyl groups mostly absent, the nanocomposite exhibited a ~10% loss in cross-link density relative to the as-synthesized material after the third reprocessing cycle due to the incomplete elimination of surface hydroxyl groups. These results indicate that an effective nanofiller species is still needed for the development of mechanically strong dynamic PHU network composites with excellent reprocessability.

A few studies have explored the use of POSS as reinforcing fillers to prepare PHU nanocomposites. Blattmann and Mülhaupt reported the preparation of organic–inorganic hybrid PHU thermosets using multifunctional POSS cyclic carbonates (Blattmann & Mülhaupt, 2016). Zhao et al. investigated the use of well-defined difunctional POSS macromers to synthesize physically cross-linked thermoplastic PHUs (Zhao et al., 2020). However, neither study focused on the influence of reactive POSS incorporation on the reprocessability of dynamic covalent PHU networks. Very recently, Liu et al. (W. Liu et al., 2022) synthesized PHUs using reactive trifunctional POSS cyclic carbonates as nanofiller, which led to nanocomposites with 20–40 nm POSS aggregates even at only 5 wt% POSS content. Compared with the original samples, the samples reprocessed by hot pressing exhibited decreases in tensile properties, which was attributed to the decrease in dynamic bond density after POSS incorporation and the restriction on segmental motion caused by POSS aggregation. Here, we have developed dynamic PHU network nanocomposites and investigated the effect of covalent incorporation of multifunctional POSS (with eight to twelve functional groups) on thermomechanical properties, reprocessability, and stress relaxation of dynamic PHU networks. PHU–POSS composites are synthesized by reacting difunctional amine JEFFAMINE D-400 with tris(4-hydroxyphenyl)methane tricarbonate (THPMTC) and POSS-cyclic carbonate (POSS-CC) (structures are shown in Figure 5-1). With

increasing POSS loading, the composites exhibit improved thermal stability and enhanced rubbery plateau modulus. More importantly from a sustainability standpoint, the as-synthesized composites containing up to 10 wt% multifunctional POSS can undergo multiple reprocessing cycles with 100% property recovery associated with cross-link density. This study highlights the potential of POSS for fabricating fully recyclable, cross-linked PU-like materials made by non-isocyanate chemistry.

5.2 Experimental

5.2.1 Materials

Tris(4-hydroxyphenyl)methane triglycidyl ether (THPMTE), tetrabutylammonium iodide (TBAI, reagent grade, 98%), *N*,*N*-dimethylacetamide (DMAc, anhydrous, 99.8%), dimethylformamide (DMF, anhydrous, 99.8%), 4-(dimethylamino)pyridine (DMAP), and dimethyl sulfoxide-d6 (DMSO-d6, 99.9 atom% D) were purchased from Sigma-Aldrich and used as received. Methylene chloride (DCM) was purchased from Fisher Chemical and used as received. JEFFAMINE D-400 (D400) was supplied by HUNTSMAN and was kept on activated molecular sieve before use. POSS glycidyl ether (EP0409), consisting of a mixture of POSS glycidyl ethers with different cage sizes, was purchased from Hybrid Plastics and used as received.

5.2.2 Synthesis of POSS-CC and THPMTC

POSS-CC was synthesized by CO_2 fixation of EP0409 in the presence of TBAI. EP0409 (13.00 g, containing 77.84 mmol of epoxy groups) and TBAI (0.58 g, 1.56 mmol, 2 mol% relative to epoxy groups) were placed in a 50-mL test tube along with 20 mL DMAc that helped to dissolve TBAI. The test tube was placed in an oil bath at 80 °C, and CO_2 gas was bubbled through the mixture until complete conversion of epoxy groups to cyclic carbonate groups was achieved (~5 days). The reaction progress was periodically checked by ^{1}H NMR spectroscopy by observing the

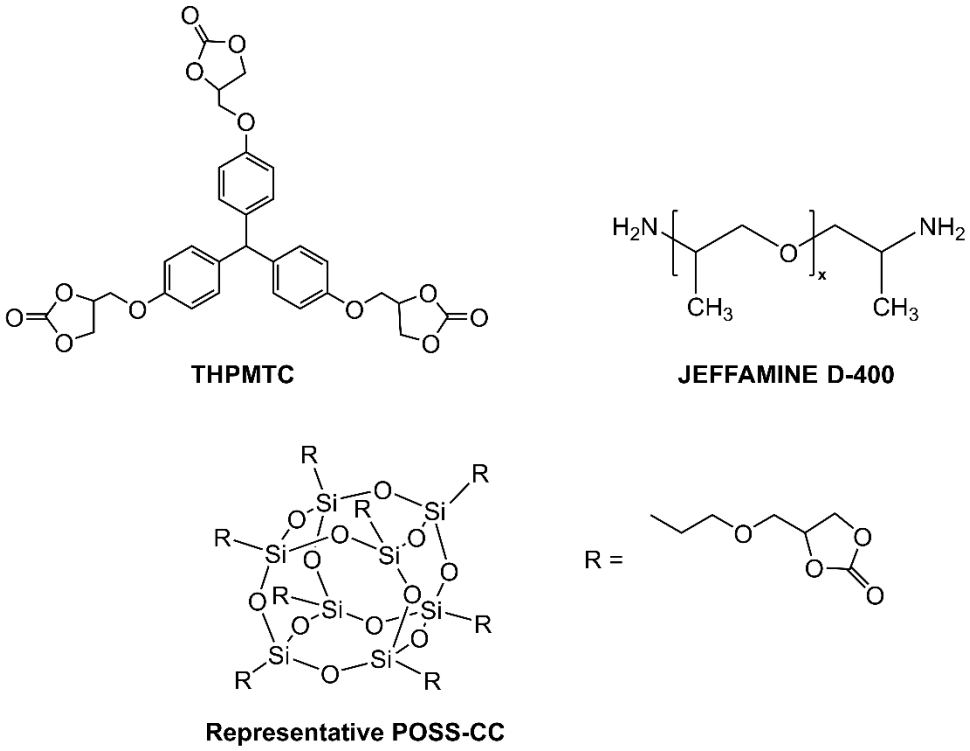

Figure 5-1. Structures of the compounds used for PHU−POSS synthesis.

disappearance of proton signals associated with the epoxy moiety. Upon completion, the mixture became a highly viscous liquid. TBAI was removed by dissolving the mixture with acetone and precipitating with distilled water for seven times. The purified product was dried in an 80 °C vacuum oven for 48 h. The carbonate content in POSS-CC was determined via ^{1}H NMR spectroscopy using DMSO as solvent and 1,2,4,5-tetrachlorobenzene as an internal reference. The following equation was used to calculate the moles of carbonate groups per gram of POSS-CC:

$$\text{carbonate content } [\frac{\text{mol}}{\text{g}}] = \frac{I_{\text{cc}} \times n_{\text{ref}}}{\frac{I_{\text{ref}}}{2} \times m_{\text{POSS-CC}}} \quad (5\text{-}1)$$

where I_{cc} is the intensity of the peak associated with one of the three protons on cyclic carbonate in POSS-CC (~4.89 ppm), n_{ref} is the molar amount of 1,2,4,5-tetrachlorobenzene in the ^{1}H NMR sample, I_{ref} is the peak intensity associated with the two protons on 1,2,4,5-tetrachlorobenzene

(~8.07 ppm), and $m_{POSS\text{-}CC}$ is the weight of POSS-CC in the sample.

THPMTC was synthesized following a similar procedure that used to prepare POSS-CC. In a typical synthesis of THPMTC, THPMTE (20.00 g, 43.43 mmol) and TBAI (1.60 g, 4.34 mmol) were placed in a test tube along with 20 mL DMAc that helped to dilute the reaction mixture. The test tube was heated in an oil bath at 80 °C. CO_2 gas was continuously bubbled through the mixture until full conversion of epoxy groups into cyclic carbonate groups was confirmed by ^{1}H NMR (Figure 5-S3). After the reaction was completed, TBAI was removed by dissolving the product with acetone and washing with water for seven times. The final product was completely dried in a vacuum oven at 80 °C for 48 h.

5.2.3 Synthesis of neat PHU network and PHU−POSS composites

PHU−POSS composites were prepared by reacting the mixture of THPMTC and POSS-CC with difunctional amine D400 under DMAP catalysis. In a typical synthesis of PHU−POSS composite containing 10 wt% POSS-CC, 0.878 g THPMTC (containing 4.45 mmol cyclic carbonate), 0.238 g POSS-CC (containing 1.42 mmol cyclic carbonate), and 71.6 mg DMAP (0.587 mmol) was dissolved with 1.5 mL DMF in a 20-mL scintillation vial. After complete solubilization, 1.26 g D400 (containing 5.87 mmol of primary amine groups) was added into the vial dropwise. The mixture was reacted at 85 °C for 20 h in an oil bath. Then, dry nitrogen gas was flowed through the vial for 4 h to evaporate some DMF before the gelled product was cut into small pieces and further dried in a nitrogen-purged 85 °C vacuum oven for 48 h. Neat PHU networks were synthesized in a similar manner without the addition of POSS-CC.

5.2.4 Reprocessing procedure for neat PHU network and PHU−POSS nanocomposites

Reprocessing of neat PHU networks and PHU−POSS composites was performed using a PHI press (model 0230C-X1). The dried, as-synthesized materials in the form of small pieces were

pressed into ~1-mm-thick sheets at 140 °C with a 7-ton ram force (generating a pressure of ~11 MPa). After the first reprocessing cycle, the uniform, flat sheets were considered as the 1st molded samples. The 1st molded samples were further cut into small pieces and pressed again to give another batch of flat sheets, which are considered as the 2nd molded samples. A 2.0 h reprocessing time was used for the neat PHU network and PHU−POSS composites containing 5 wt% POSS-CC (PHU-POSS-5). For PHU−POSS composites containing 10 wt% POSS-CC (PHU-POSS-10), the reprocessing time from the original materials to the 1st molded materials was 2.5 h, and that from the 1st molded materials to the 2nd molded materials was 1.5 h.

5.2.5 Equilibrium swelling experiments

Swelling experiments were conducted at room temperature using DCM as solvent. Small network pieces were placed in ~20 ml DCM in a glass vial and swollen for 3 days to equilibrium. Swollen samples were immediately weighed after removing the remaining solvent on the network surface. The networks were then dried at 80 °C in a vacuum oven for 3 days and weighed afterwards. The gel fraction is calculated as m_{dry}/m_0, and the swelling ratio is calculated as $(m_{sw} - m_{dry})/m_{dry}$, where m_0, m_{sw}, and m_{dry} are the masses of the original samples, swollen samples, and dried samples, respectively.

5.2.6 Characterization

Attenuated total reflectance-Fourier transform infrared (ATR-FTIR) spectroscopy was performed using a Bruker Tensor 37 MiD IR FTIR spectrophotometer equipped with a diamond/ZnSe ATR attachment. Thirty-two scans were collected at room temperature over the 4000 to 800 cm^{-1} range with a 2 cm^{-1} resolution. ^1H NMR spectroscopy was performed at room temperature using a Bruker Avance III 500 MHz NMR spectrometer with a direct cryoprobe.

Dynamic mechanical analysis (DMA) was performed using a TA Instruments RSA G2

DMA. Rectangular samples measuring ~0.9 mm in thickness and ~3 mm in width were mounted on the fixture and underwent temperature ramps from –10 °C to 80 °C at a 3 °C/min heating rate. The tensile storage modulus (*E'*), tensile loss modulus (*E"*), and tan δ (*E"*/*E'*) were measured in tension mode at 1 Hz frequency and 0.03% strain.

Stress relaxation experiments were performed using a TA Instruments RSA G2 DMA. Rectangular samples measuring ~0.9 mm in thickness and ~3 mm in width were mounted on the fixture and allowed to equilibrate at the desired temperature for 15 min before being subjected to an instantaneous strain of 5%. The stress relaxation modulus at 5% strain was recorded until it decayed to ~20% of its initial value. Stress relaxation experiments were carried out at 140–170 °C at 10 °C increments.

Shear creep experiments at 3.0 kPa stress were performed on 1st molded, ~2 mm-thick disk samples using an Anton-Paar MCR 302 rheometer with 25-mm parallel-plate fixtures. Samples were equilibrated at the test temperature for 10 min before starting the experiment. Each test was carried out for 50000 s.

The glass transition temperature (T_g) of each network was characterized by differential scanning calorimetry (DSC) employing a Mettler Toledo DSC822e. Samples were maintained at 50 °C for 20 min, followed by cooling to –20 °C at a rate of –40 °C/min. The T_gs were determined from the second heating ramp at a 10 °C /min rate using the 1/2 ΔC_p method.

Thermogravimetric analysis (TGA) was performed using a Mettler Toledo TGA/DSC3+. Samples were heated under a nitrogen atmosphere from 25 °C to 600 °C at a 20 °C /min heating rate. The change in weight was recorded as a function of temperature.

Scanning electron microscopy (SEM) samples were prepared by fracturing the PHU−POSS composites and coating them with an 8-nm-thick layer of osmium using an OPC osmium coater.

The morphologies of the fractured section of the composites were obtained using a Hitachi SU8030 scanning electron microscope.

Wide-angle X-ray scattering (WAXS) measurements were performed using a Rigaku SmartLab X-ray diffractometer in transmission mode. CuK_α radiation was operated at 40 kV and 35 mA. The scattering angle (2θ) covered the range from 3° to 60° with a 0.05° step. The *d*-spacing can be calculated using Bragg's law, where $\lambda = 2d\sin\theta$; $\lambda = 0.154$ nm for CuK_α radiation.

5.3 Results and Discussion

5.3.1 Synthesis of POSS-CC and PHU-POSS network nanocomposites

POSS-CC was synthesized by CO_2 fixation of EP0405 in the presence of a catalytic amount of TBAI at 80 °C. EP0405 is a commercially available glycidyl-ether-terminated POSS consisting of a mixture of POSS with different cage sizes (containing 8–12 silicon atoms per cage and thus 8–12 functional groups). The reaction progress was periodically checked by ^{1}H NMR spectroscopy. Figure 5-S2 shows the ^{1}H NMR spectrum of POSS-CC. After ~5 days of reaction, the complete disappearance of proton signals at 2.70–3.00 ppm associated with epoxy units and the appearance of signals at 4.50–4.87 ppm associated with the cyclic carbonate moiety indicate complete conversion of epoxy groups into cyclic carbonate groups. POSS-CC was obtained as a light-yellow, high-viscosity liquid. The exact cyclic carbonate content of POSS-CC was determined via ^{1}H NMR spectroscopy with 1,2,4,5-tetrachlorobenzene as an internal reference to be 0.006 mol/g.

The PHU-POSS network composites were synthesized following the synthesis route shown in Figure 5-S1. The FTIR spectra of the as-synthesized materials are shown in Figure 5-S4 and Figure 5-S5. PHUs were successfully synthesized as indicated by the disappearance of the carbonate peak at ~1780 cm^{-1} and the appearance of the urethane carbonyl stretch at 1700−1730

cm^{-1} and the hydroxyl stretch at 3500−3100 cm^{-1}. In Figure 5-S5, nearly no signal associated with cyclic carbonates can be observed at ~1780 cm^{-1} in the as-synthesized PHU-POSS-5, indicating a nearly 100% conversion. In Figure 5-S4, a small peak exists at ~1780 cm^{-1} in the as-synthesized PHU-POSS-10, indicating that a small level of unreacted cyclic carbonate remained. This slightly reduced conversion of PHU-POSS-10 relative to PHU-POSS-5 can be explained by the fact that PHU-POSS-10 contains a higher fraction of the multifunctional POSS-CC cross-linker (with 8−12 reactive cyclic carbonate groups). After most of the functional groups undergo cross-linking, the reduced network mobility will make it more difficult for remaining unreacted cyclic carbonate groups to participate in the reaction.

5.3.2 Microstructure of PHU-POSS network nanocomposites

It is possible that POSS can aggregate and crystallize. To address the microstructure of the PHU-POSS network composites, WAXS analysis was performed to determine the crystalline degree of the samples. Figure 5-S6 shows the WAXS patterns of the neat PHU and PHU-POSS network composites. The intensity trace of the neat PHU network shows no peak up to a 2θ value of 60°, indicating the absence of crystalline order. For both PHU-POSS-5 and PHU-POSS-10, the WAXS patterns exhibit a broad peak at ~20° 2θ, which corresponds to a *d*-spacing of ~0.44 nm. Since the average core size of POSS is ~0.50 nm, this broad, amorphous peak is consistent with the presence of POSS nanofillers. Regardless of the POSS loading content, sharp, distinct peaks corresponding to crystalline phases are not present in the WAXS patterns of the PHU−POSS composites, indicating that the nanocomposites are amorphous. The lack of crystalline order associated with high POSS loading content in our samples is consistent with the results reported by Romo-Uribe, in which the POSS-methyl methacrylate nanocomposites remain amorphous with up to 45 wt% POSS content (Romo-Uribe, 2018).

The morphology of the 1st molded PHU-POSS-10 network which contains 10 wt% POSS-CC was further examined using SEM. The SEM images (see Figure 5-S7) show no indication of POSS phase separation or aggregation. The POSS-CCs are covalently attached to the PHU matrix and serve as both nanofillers and cross-linkers within the matrix. The fact that each nanofiller can be covalently attached at up to 8–12 reactive sites with the matrix rather than doped into the matrix is conducive to a well-dispersed state. Indeed, Blattmann and Mülhaupt (Blattmann & Mülhaupt, 2016) have used the same multifunctional POSS-CC used in this study to synthesize hybrid PHU–POSS thermosets and reported that minor or no phase separation was present with 13.5 wt% POSS-CC; significant phase separation was only observed with 23 wt% POSS-CC, far above the 10 wt% POSS loading in our study. Thus, it is reasonable that our systems are not exhibiting POSS nanoaggregates. We note that the number of reactive sites associated with each nanofiller can also be important in the dispersion state. Liu et al. (W. Liu et al., 2022) synthesized PHUs with reactive trifunctional POSS cyclic carbonates; their nanocomposites exhibited 20–40 nm POSS aggregates at 5 wt% POSS content.

5.3.3 Effect of POSS incorporation on thermal properties of PHU networks

Neat PHU networks and PHU−POSS network composites were synthesized following the reaction route shown in Figure 5-S1. 10 mol% DMAP with respect to amine functional groups was added into the reaction mixture to facilitate the dynamic chemistries during the reprocessing process. POSS-CC was used as covalently attached nanofillers and was incorporated into neat PHU matrix at 0 wt%, 5 wt% (1.2 wt% of Si−O), and 10 wt% (2.5 wt% of Si−O) loading (weight percentage is with respect to the total weight of network).

The cross-linked nature of the networks was confirmed by equilibrium swelling tests in DCM (Table 5-S1). Figure 5-2 shows the glass transition temperatures (T_gs) of as-synthesized

networks determined by DSC. According to DSC characterization results, T_g decreases from 21°C for the neat PHU network to 14 °C for PHU-POSS-5 and further to 10 °C for PHU-POSS-10. The decrease in T_g with increasing POSS loading is related to the long-chain, flexible structure of the side groups connected to the POSS core. Low T_g is a desirable characteristic for thermosets used for elastomer applications. The incorporation of conventional fillers generally leads to an increase in T_g, which could negatively impact the performance of elastomers at lower temperatures. In our systems, the employment of POSS-CC offers an advantage of improving the mechanical properties of neat PHU networks while maintaining relatively low T_gs of the materials. In addition, as shown in Table 5-S2, no change in T_g breadth was observed with increasing POSS content, indicating that there is no significant change in overall network homogeneity associated with POSS incorporation.

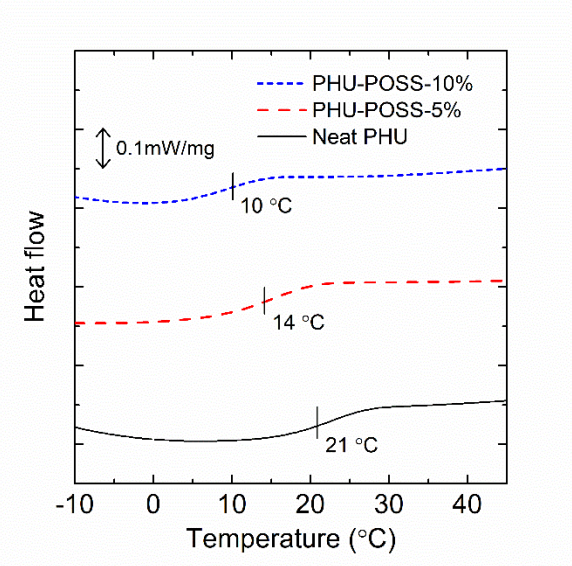

Figure 5-2. Glass transition temperatures of as-synthesized neat PHU and PHU−POSS network composites determined by differential scanning calorimetry.

Thermogravimetric analysis (TGA) was conducted to evaluate the effect of POSS incorporation on thermal decomposition temperatures and thermal stability of dynamic PHU

networks (Figure 5-3). The decomposition temperatures (T_d) corresponding to a 5 % weight loss for the neat PHU network is 288 ± 3 °C. With the addition of POSS, T_d increases to 296 ± 1 °C for PHU-POSS-5 and further increases to 305 ± 3 °C for PHU-POSS-10. These results suggest that the thermal stability of PHU networks can be enhanced by incorporating POSS as nanofillers. Upon heating, dynamic PHU networks can undergo two types of dynamic chemistries, which are associative transcarbamoylation exchange reactions and dissociative reversible cyclic carbonate aminolysis reactions (Figure 5-4) (X. Chen et al., 2017; X. Chen, Li, Wei, Venerus, et al., 2019). The reversion of hydroxyurethane linkages to carbonate and amine moieties will decross-link the network structure and accelerate the decomposition process of the materials. By replacing a small part of the trifunctional carbonate cross-linker THPMTC with POSS-CC possessing eight to twelve reactive carbonate functional groups, the materials can withstand the loss of more chains upon heating while maintaining a cross-linked nature.

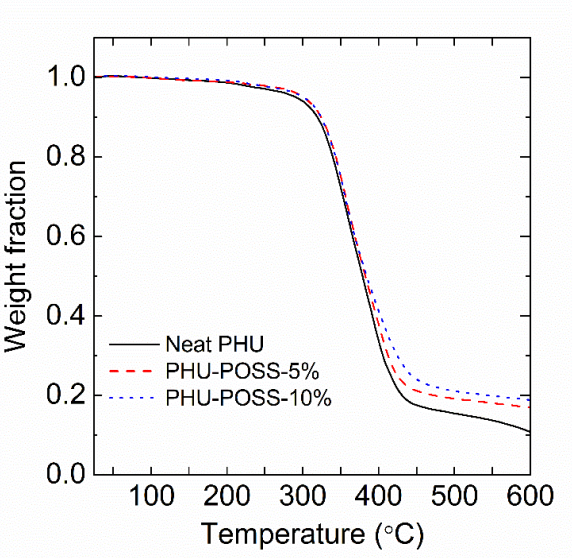

Figure 5-3. Thermogravimetric analysis of as-synthesized neat PHU and PHU−POSS network composites.

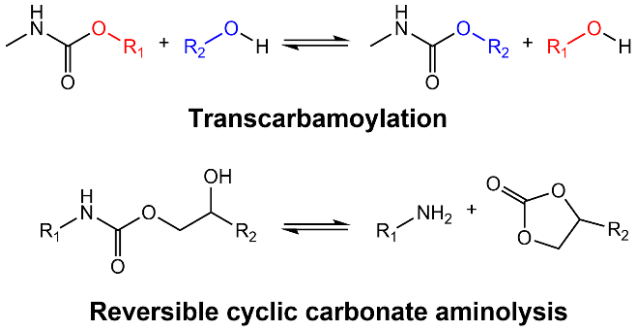

Figure 5-4. Transcarbamoylation and reversible cyclic carbonate aminolysis reactions.

5.3.4 Effect of POSS incorporation on thermomechanical properties and reprocessability of PHU networks

Reprocessing of neat PHU networks and PHU−POSS network composites was performed by cutting the materials into small pieces and compressing them into films using a high-temperature compression mold. DMA characterizations were performed to evaluate the recovery of thermomechanical properties after each reprocessing step. Figure 5-5 shows the DMA results of the 1st molded and 2nd molded neat PHU networks. The reprocessing time and temperature for neat PHU networks was 2 h at 140 °C, and the same condition was employed for both the 1st and the 2nd reprocessing cycles. As shown in Figure 5-5, the *E*' curves for both samples display a rubbery plateau region a few tens of degrees above T_g, confirming their cross-linked nature. The *E*' rubbery plateau moduli determined at 60 °C, 70 °C, and 80 °C are summarized in Table 5-1. Within experimental error, the rubbery plateau *E*' values of the 2nd molded sample are identical to the values of the 1st molded sample at all three temperatures. According to Flory's ideal rubber elasticity, the rubbery plateau modulus is proportional to the cross-link density of a network material (Flory, 1953). Therefore, these results indicate that neat PHU networks derived from THPMTC and D400 can undergo at least two molding or reprocessing cycles with complete recovery of cross-link density.

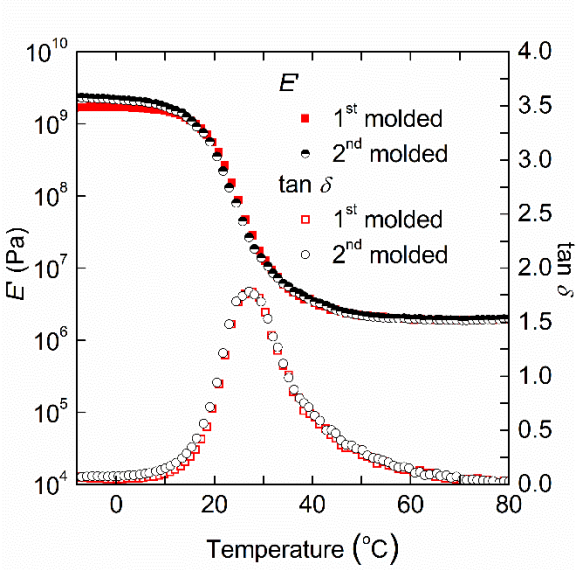

Figure 5-5. Dynamic mechanical analysis results of 1st and 2nd molded neat PHU networks.

Table 5-1. Rubbery plateau moduli (*E*') of the neat PHU network and PHU-POSS network composites at 60 °C, 70 °C, and 80 °C.

Sample		*E*' at 60 °C	*E*' at 70 °C	*E*' at 80 °C
Neat PHU	1st molded	1.98 ± 0.02	1.90 ± 0.01	1.93 ± 0.01
	2nd molded	1.96 ± 0.10	1.85 ± 0.11	1.89 ± 0.11
PHU-POSS-5	1st molded	2.04 ± 0.03	2.06 ± 0.02	2.11± 0.01
	2nd molded	2.03 ± 0.16	2.08± 0.15	2.13 ± 0.14
PHU-POSS-10	1st molded	2.43 ± 0.11	2.49 ± 0.02	2.56 ± 0.03
	2nd molded	2.35 ± 0.06	2.42 ± 0.05	2.45 ± 0.06

Figure 5-6 shows the DMA curves of the 1st and 2nd molded PHU-POSS-5 samples. The same reprocessing condition of 2 h at 140 °C that was used for neat PHU networks was employed for PHU-POSS-5. As evidenced by the well-overlapped *E*' curves on Figure 5-6 and the identical rubbery plateau *E*' values (within error) determined at 60 °C, 70 °C, and 80 °C shown in Table 5-1, PHU-POSS-5 can also undergo reprocessing without any loss in cross-link density. With 5 wt% POSS incorporated into the materials, PHU-POSS-5 samples exhibit comparable reprocessability

to neat PHU networks, indicating that the introduction of a small amount of POSS as nanofillers into a dynamic covalent PHU matrix does not lead to negative impacts.

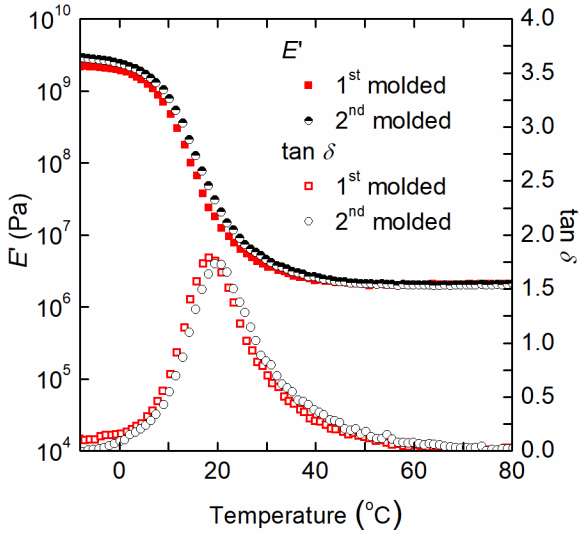

Figure 5-6. Dynamic mechanical analysis results of 1st and 2nd molded PHU-POSS-5 samples.

To reprocess the composite PHU-POSS-10 containing 10 wt% POSS, we first used the reprocessing condition of 2.5 h at 140 °C for both the 1st and the 2nd reprocessing cycles, where 2.5 h is the minimum time that is required for the as-synthesized materials to heal into a consolidated film without visible defects (considered as 1st molded samples). The reprocessing time is slightly increased relative to neat PHU networks and PHU-POSS-5, indicating that POSS incorporation introduces additional barriers for chain dynamics at relatively high POSS loading. DMA characterization of the reprocessed samples suggests that there is a small but significant ~10% decrease in rubbery plateau *E*' (Figure 5-S8) from the 1st molded PHU-POSS-10 samples to the 2nd molded PHU-POSS-10 samples. Without changing the 2.5 h reprocessing time from as-synthesized PHU-POSS-10 to 1st molded PHU-POSS-10, we shortened the reprocessing time from the 1st molded materials to the 2nd molded materials by 1 h. We note that based on our previous

experience of reprocessing dynamic PHU networks by compression molding, the minimum time that is required to compress as-synthesized materials into 1st molded materials always appears longer than the minimum time that is required to compress 1st molded materials into 2nd molded materials. This may occur because the as-synthesized materials are in the form of chunks, whereas the 1st molded materials are in the form of thin sheets and hence are easier to be compressed into films again. Therefore, even though 2.5 h is the minimum time that is necessary to obtain well-healed 1st molded PHU-POSS-10 samples, we can still obtain consolidated, well-healed 2nd molded materials by reprocessing the 1st molded samples for only 1.5 h.

After we shortened the reprocessing time of the 2nd cycle, we performed DMA characterization again to determine if there was any improvement in property recovery. As shown in Figure 5-7, the *E*' curve of the 2nd molded PHU-POSS-10 samples overlaps reasonably well with the curve of the 1st molded samples, indicating that after shortening the reprocessing time of the 2nd cycle relative to the 1st cycle, PHU-POSS-10 can successfully undergo two reprocessing cycles with 100% recovery of cross-link density. To reveal the underlying cause of the loss in cross-link density associated with long reprocessing time, we performed FTIR spectroscopy on as-synthesized PHU-POSS-10, 1st molded PHU-POSS-10 reprocessed by 2.5 h, 2nd molded PHU-POSS-10 reprocessed by 1.5 h, and 2nd molded PHU-POSS-10 reprocessed by 2.5 h. As shown in Figure 5-S4, on the FTIR spectrum of as-synthesized PHU-POSS-10, no peak exists near ~1660 cm^{-1} (related to C=O stretching vibrations of urea groups). After the materials are reprocessed at 140 °C for 2.5 h to yield 1st molded samples, a shoulder appears at ~1660 cm^{-1} in the spectrum of the 1st molded PHU-POSS-10, indicating the appearance of a small amount of urea groups. The urea peak becomes more obvious when the 1st molded materials are further reprocessed for 1.5 h (the red curve in Figure 5-S4). In the spectrum of the 2nd molded sample obtained with 2.5 h of

reprocessing which exhibits significant property loss (the blue curve in Figure 5-S4), the urea peak is even more prominent.

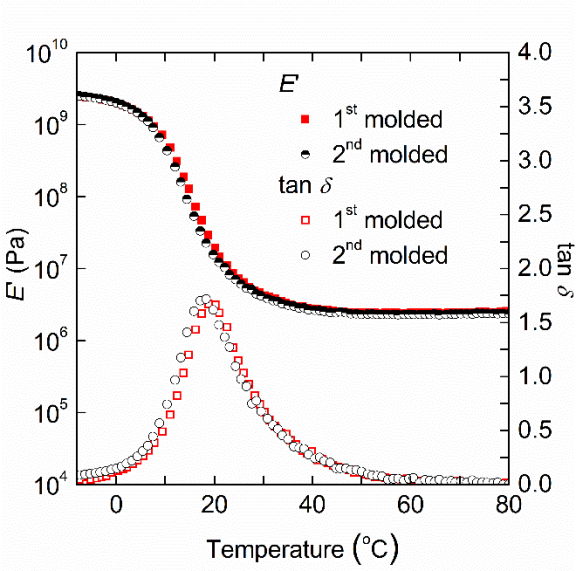

Figure 5-7. Dynamic mechanical analysis results of 1st and 2nd molded PHU-POSS-10 samples.

Boisson et al. has reported the formation of urea in the presence of basic catalysts during PHU synthesis at elevated temperatures (Bossion et al., 2018). According to the mechanism they proposed, free amine groups liberated from the reverse cyclic carbonate aminolysis reactions can further be deprotonated by a basic catalyst and attack the electrophilic center of another urethane linkage, leading to the formation of urea groups and difunctional alcohols. We hypothesized that in our systems, the property loss in 2nd molded PHU-POSS-10 associated with long reprocessing time is also caused by urea formation at high reprocessing temperature. Figure 5-S5 shows the FTIR spectra of as-synthesized and reprocessed PHU-POSS-5 samples. As the total reprocessing time increases with more reprocessing cycles, the urea peak progressively grows. However, based on the relatively small size of the urea peak and the 100% property recovery of PHU-POSS-5 determined by DMA characterization, such a low level of side reactions does not significantly

affect the reprocessability of the materials. In the case of PHU-POSS-10, when 2.5 h of reprocessing time is used for both reprocessing cycles, the total reprocessing time is 5 h; such extended exposure of the materials at high temperature (140 °C) leads to a significant level of urea formation and consequently to a decrease in cross-link density after recycling. When the total reprocessing time is shortened to 4 h, even though there is still a small amount of urea formed during reprocessing, such a small level of side reactions does not influence the bulk thermomechanical properties of PHU networks similar to the case of PHU-POSS-5.

Figure 5-8 compares the *E*' curves of 1st molded neat PHU, PHU-POSS-5, and PHU-POSS-10. With increasing POSS content, the storage modulus in both the glassy state (i.e., ≤ 0 °C) and the rubbery plateau region (i.e., ≥ 60 °C) increases significantly. As determined from the *E*' values summarized in Table 5-1, at 80 °C where the materials are well in the rubbery plateau regime, 1st molded PHU-POSS-5 exhibits slightly enhanced *E*' (by ~9%) compared to the neat PHU network, whereas 1st molded PHU-POSS-10 exhibits a significant enhancement of ~30% in *E*'. Equilibrium swelling tests (Table 5-S1) also show that the networks swell less with increasing POSS loading, consistent with a higher degree of cross-linking after POSS incorporation. These results indicate that the incorporation of POSS as nanofillers is an effective way to improve the modulus of dynamic PHU networks well into the glassy state or the rubbery plateau regime while maintaining good reprocessability. (The fact that *E*' is significantly higher for neat PHU than for the nanocomposites in the temperature range of 5–45 °C simply reflects the higher T_g of neat PHU, which is caused by the long-chain, flexible structure of the side groups connected to the POSS core resulting in plasticization of the nanocomposites.) To understand how these materials respond to large tensile stresses, future studies are warranted to characterize the tensile properties of PHU−POSS composites including tensile strength and strain-at-break.

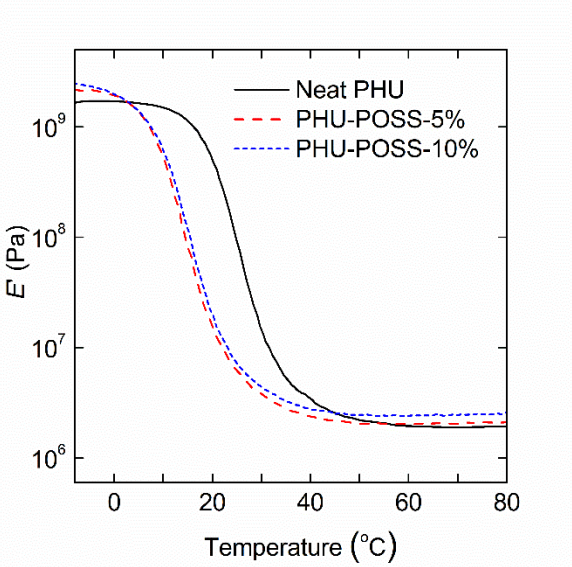

Figure 5-8. Temperature dependence of the storage moduli of 1st molded neat PHU, PHU-POSS-5%, and PHU-POSS-10%.

5.3.5 Effect of POSS incorporation on stress relaxation behavior of PHU networks.

The ability to relax external stress under appropriate conditions is a defining characteristic of dynamic polymer networks. For PHU networks, stress relaxation at elevated temperatures is enabled by simultaneous associative transcarbamoylation exchange reactions and dissociative reversible cyclic carbonate aminolysis reactions. We have characterized the effect of POSS incorporation on stress relaxation of dynamic PHU networks by DMA. Stress relaxation tests at 140−170 °C were conducted under a strain of 5%. Figure 5-9 shows the decay of stress relaxation modulus as a function of relaxation time at different temperatures. Regardless of the loading of POSS, at all tested temperatures, the PHU−POSS composites relax much more slowly than the neat PHU network. It is generally recognized that when non-reactive nanofillers are incorporated into a network matrix, the mobility of the network is typically reduced because of the adsorption of polymer chains onto filler surface at the polymer−filler interfaces. For our PHU−POSS

nanocomposites, the impact on network mobility from chain adhesion is minimized by using POSS that have 8 to 12 reactive carbonate groups, which shield the polymer chains from interacting with and adhering to the POSS surface as reinforcing agent. However, when part of the trifunctional carbonates THPMTC was replaced with POSS molecules possessing 8 to 12 reactive carbonate groups, the resulting networks are much denser and more inflexible compared with the neat PHUs, and therefore the stress relaxation rate is still retarded. Nevertheless, with increasing temperature, the difference in stress relaxation rate between neat PHU networks and PHU−POSS composites is diminished, possibly because at high temperatures, the stress relaxation process of PHU networks is achieved predominantly by dissociative reverse cyclic carbonate aminolysis reaction, so all systems are equally liquid-like and highly flexible.

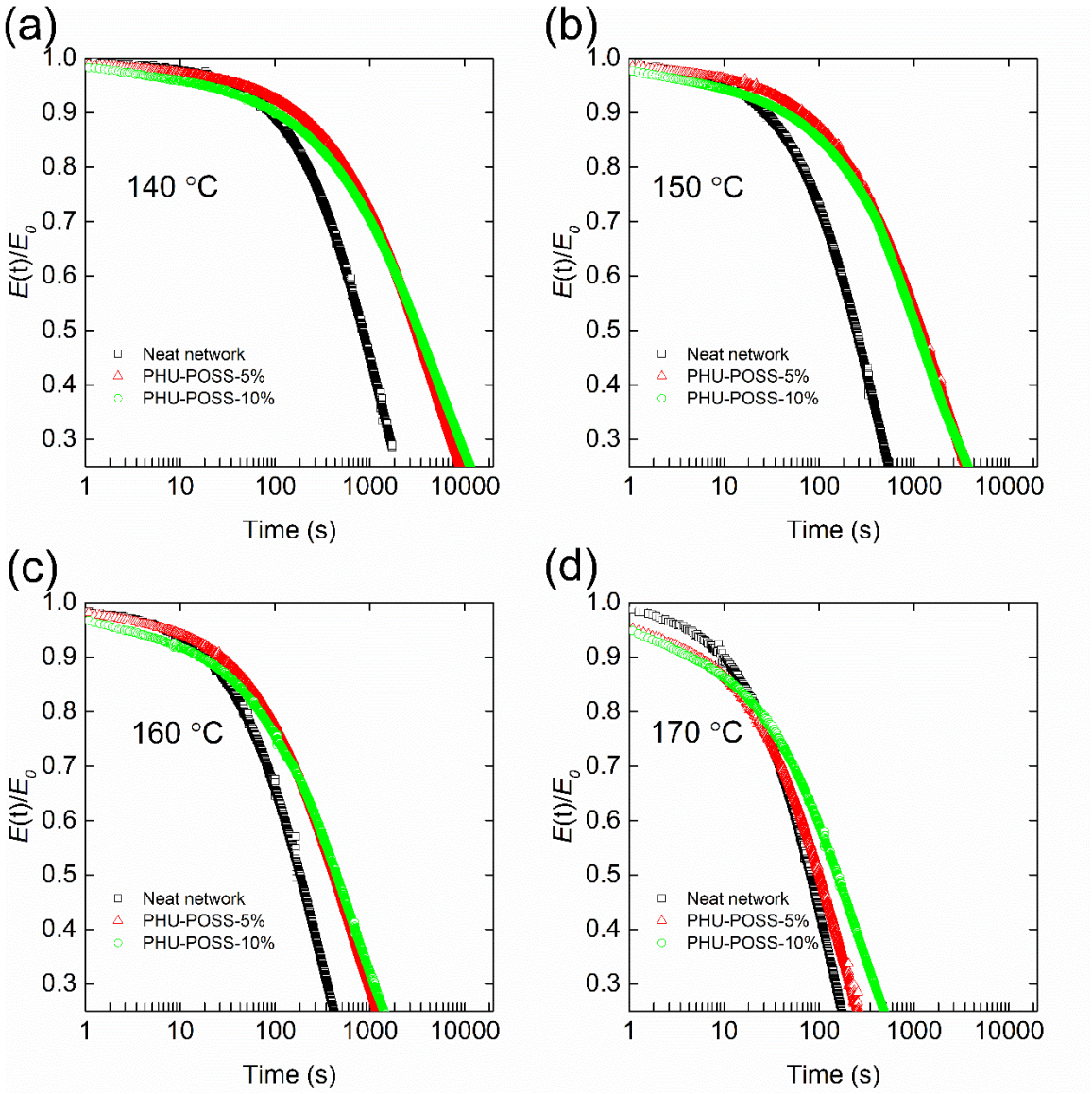

Figure 5-9. Stress relaxation curves of neat PHU networks and PHU-POSS network composites at (a) 140 °C, (b) 150 °C, (c) 160 °C, and (d) 170 °C.

We note that with increasing POSS loading, although the average stress relaxation time is increased significantly, the systems containing more POSS exhibit relatively faster relaxations at the initial stage of the stress relaxation experiments. This observation suggests that the relaxation of PHU−POSS composites comprises a multitude of relaxation modes, and a single Maxwell element is insufficient to model the process. To model the effect of POSS incorporation on the

stress relaxation of PHU networks, we used the Kohlrausch−Williams−Watts (KWW) stretched exponential decay function to fit the stress relaxation data. The KWW stretched exponential decay function is expressed as follows (X. Chen, Li, Wei, Venerus, et al., 2019; Fancey, 2005; Hooker & Torkelson, 1995):

$$\frac{\sigma(t)}{\sigma_0} = \exp\left\{-\left(\frac{t}{\tau^*}\right)^{\beta}\right\} \tag{5-2}$$

where σ(t)/σ_0 is the normalized stress at time t, τ* is the characteristic relaxation time, and β is the exponent that controls the shape of the stretched exponential decay and reflects the breadth of the relaxation distribution. β takes values in the range $0 < \beta \leq 1$, with $\beta = 1$ corresponding to a single-exponential decay response and $\beta \ll 1$ indicating an extremely broad distribution of relaxation times. For a KWW decay, the average relaxation time, $\langle\tau\rangle$, is given by (X. Chen, Li, Wei, Venerus, et al., 2019; Hooker & Torkelson, 1995)

$$\langle\tau\rangle = \frac{\tau^*\Gamma(\frac{1}{\beta})}{\beta} \tag{5-3}$$

where Γ is the Gamma function. Table 5-S4 shows the detailed fitting results obtained from both KWW stretched exponential decay and single-exponential decay analyses for neat PHU networks and PHU−POSS composites. For neat PHU networks, β increases slightly with increasing temperature, and the value becomes very close to 1 at 170 °C, indicating a nearly single-exponential decay response. With increasing POSS content of the materials, β decreases at all tested temperatures, suggesting a broadened distribution of relaxation times and a more complex relaxation mode with higher POSS loading.

Figure 5-10 shows the Arrhenius plot of $\langle\tau\rangle$ over the temperature range of 140 °C ≤ T ≤ 170 °C for determining the apparent activation energy ($E_{a,\tau}$) of stress relaxation; the detailed results are summarized in Table 5-2. The $E_{a,\tau}$ of neat PHU networks was calculated to be 121

kJ/mol, which is in reasonable agreement with values reported by other studies on dynamic PHU networks (X. Chen, Li, Wei, Venerus, et al., 2019; Fortman, Snyder, et al., 2018). When POSS molecules are added to the neat PHU matrix, $E_{a,\tau}$ increases dramatically, indicating a stronger temperature dependence of the relaxation process. As shown in Figure 5-10, at low temperatures, PHU−POSS composites exhibit significantly longer average relaxation times than the neat PHU network. This occurs because when part of the original trifunctional cross-linker THPMTC is replaced with the multifunctional POSS-CC cross-linker with 8–12 functional groups, the composites have a much more restricted network structure and hence substantially reduced flexibility at low temperatures than the neat PHU network. With increasing temperature, the average relaxation times of the three systems become similar. At sufficiently high temperatures, all networks are far above their T_gs, and the reverse cyclic carbonate aminolysis reaction leads to a less cross-linked state. Therefore, the dynamics of the three systems become more alike. These above-mentioned effects result in a stronger temperature dependence of the relaxation process and thus an increase in $E_{a,\tau}$ after POSS incorporation. The secondary effect of POSS incorporation on $E_{a,\tau}$ values is that PHU-POSS-5 exhibits a greater $E_{a,\tau}$ value than PHU-POSS-10. This is because the stress relaxation process of a dynamic polymer network depends on both the activation energies of the dynamic chemistries and the viscoelastic behavior of the materials. The POSS-CC cross-linker has flexible side chains which result in a decrease in overall T_g of the materials with increasing POSS-CC content. Therefore, at the same temperature, PHU-POSS-10 networks are more liquid-like compared to PHU-POSS-5. This subsequently leads to a smaller temperature dependence or a smaller $E_{a,\tau}$ of the stress relaxation process for the PHU-POSS-10 than PHU-POSS-5.

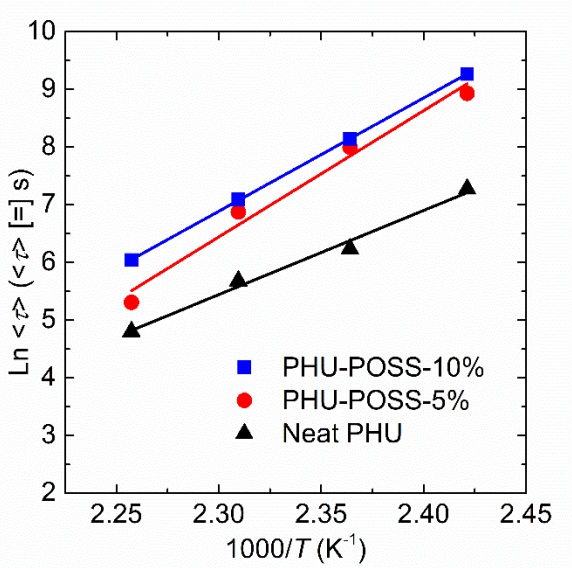

Figure 5-10. Arrhenius apparent activation energy of stress relaxation for the neat PHU networks and PHU-POSS network composites.

Table 5-2. <τ> at 140 °C and apparent activation energy of stress relaxation of the 1st molded neat PHU network and PHU-POSS network composites.

Sample	<τ> at 140 °C (s)	Apparent activation energy (kJ/mol)
Neat PHU	1440	121
PHU-POSS-5%	7530	182
PHU-POSS-10%	10540	163

5.3.6 Creep performance of neat PHU network and PHU-POSS network composites.

Because of their dynamic nature, there is a potential shortcoming of CANs related to creep during use at elevated temperature, which is undesirable for many applications (Denissen et al., 2016). Creep refers to the continuous, time-dependent deformation of materials under constant stress (Sperling, 2006). Conventional thermosets composed of fixed covalent bonds are intrinsically creep-resistant (Nielsen, 1969; Plazek, 1966; Watanabe, 1962) whereas CANs are susceptible to creep especially at elevated temperature but still well below the reprocessing temperature, as demonstrated in numerous studies (Capelot, Unterlass, et al., 2012; Denissen et al.,

2015; W. Liu et al., 2017; Lu & Guan, 2012; Snijkers et al., 2017). To arrest elevated temperature creep of CANs, an effective approach is to employ a dynamic chemistry with high activation energy and strong temperature dependence such that the dynamic mechanism remains relatively inactive and allows for creep resistance at temperatures not too far below the reprocessing temperature (Bin Rusayyis & Torkelson, 2021; Li et al., 2021; Y. Liu et al., 2019).

A previous study involving alkoxyamine dynamic chemistry has indicated that the elevated-temperature creep resistance of CANs should not be affected significantly by network details or by the presence or absence of fillers (Li et al., 2021). To determine the creep response of our dynamic PHU network and the potential impact of POSS incorporation on the response, linear viscoelastic creep tests were performed at 80 °C and 90 °C, some 50−60 °C below the reprocessing temperature, under a constant 3.0 kPa shear stress. At both temperatures, the materials are well above their T_gs and in the rubbery plateau regime. Figure 5-11 shows the creep responses for the neat PHU network and PHU-POSS network composites. For all systems, the time-dependent creep is extremely small after 50000 s (~14 h). Creep strain values ($\Delta\varepsilon$) summarized in Table 5-3 were determined as the difference in strain at t = 50000 s and t = 1800 s (i.e., $\Delta\varepsilon = \varepsilon_{50000} - \varepsilon_{1800}$) such that the values only reflect pure creep, instead of delayed elastic deformation (Plazek, 1966). The creep strain values of neat PHU and PHU−POSS composites are only 0.003 (i.e., 0.3%) at 80 °C and 0.005 (i.e., 0.5%) at 90 °C, which are extremely small and comparable to the response associated with permanently cross-linked static networks (Nielsen, 1969; Plazek, 1966; Watanabe, 1962). These results indicate that the hydroxyurethane dynamic chemistry is very effective in suppressing long-term elevated-temperature creep at 80−90 °C, and this excellent creep-resistant feature is not affected significantly by POSS incorporation in which POSS serves as a fraction of the dynamic covalent crosslinks in the network.

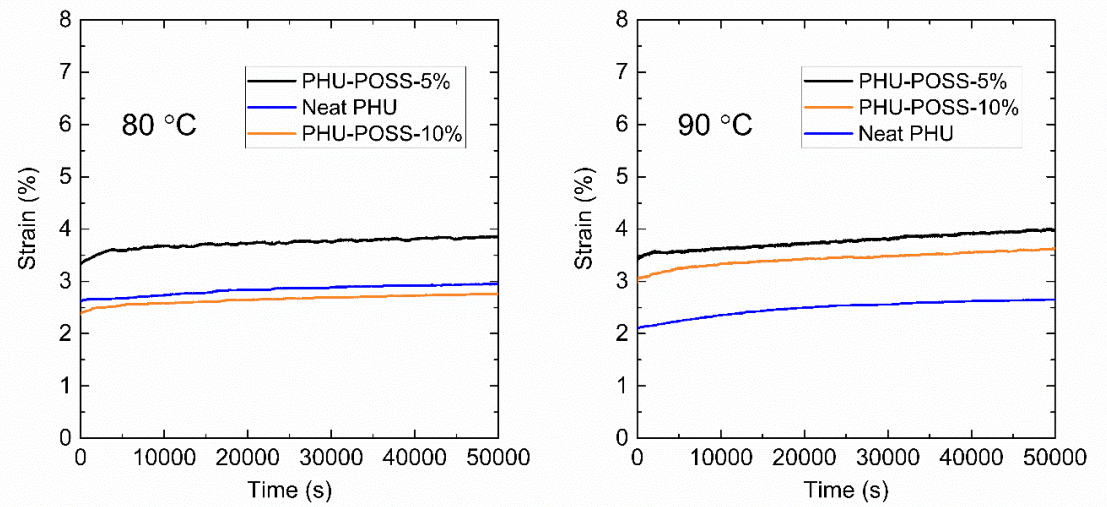

Figure 5-11. Creep responses for the neat PHU network and PHU-POSS network composites at (a) 80 °C and (b) 90 °C.

Table 5-3. Creep strain, $\Delta\varepsilon$, of neat PHU network and PHU-POSS network composites at different temperatures under a constant creep stress of 3.0 kPa.

Sample	$\Delta\varepsilon$ at 80 °C	$\Delta\varepsilon$ at 90 °C
Neat PHU	0.003	0.004
PHU-POSS-5%	0.003	0.004
PHU-POSS-10%	0.003	0.005

Note: Creep strain is taken as $\Delta\varepsilon = \varepsilon_{50000\ s} - \varepsilon_{1800\ s}$.

Finally, we note that in Figure 5-11 the instantaneous strains do not strictly follow a decreasing trend with increasing POSS content. Based on our previous experience with shear creep measurements on solid-state samples using a parallel-plate fixture, the instantaneous strain values are strongly impacted by the surface roughness of the samples. The samples need to be cured into a disk shape using a high-temperature compression molding device before the creep measurements. If the disks have very smooth surfaces after curing, the instantaneous strain usually reflects the trend in modulus very well. However, if the samples have relatively rough surfaces, the normal force acting on the samples needs to be adjusted until a good contact with the parallel plate is

achieved, and this kind of adjustment usually results in impacts on the instantaneous strain values. Nevertheless, creep is a time-dependent response, and the creep strain is determined from the absolute change in strain values over time, so the instantaneous strain value should not have impacts on the time-dependent strain that is associated with creep.

5.4 Conclusions

We have used POSS with cyclic carbonate end groups as covalently attached nanofillers to develop reprocessable PHU−POSS network composites. The incorporation of POSS leads to enhanced thermal stability and significantly enhanced rubbery plateau modulus of the networks relative to the PHU without nanofiller. Because of the inherent dynamic nature of hydroxyurethane linkage, the PHU−POSS network composites can be melt-reprocessed at elevated temperatures. With up to 10 wt% POSS loading, PHU−POSS network composites exhibit excellent reprocessability and can undergo multiple reprocessing cycles with 100% recovery of cross-link density; such excellent property recovery has not been achieved before with dynamic PHU network composites derived from conventional silica nanoparticles. The stress relaxation activation energy $E_{a,\tau}$ associated with the average relaxation time of the networks was determined using the data from the high-temperature stress relaxation tests. It was found that $E_{a,\tau}$ increases when POSS molecules are incorporated into the neat PHU matrix, suggesting an increase in relaxation barrier. Lastly, the linear viscoelastic creep response of the neat PHU network and PHU-POSS network composites was characterized via creep tests under a constant 3.0 kPa shear stress. We found that dynamic PHU networks exhibit nearly no creep over 50000 s at temperatures of 80−90 °C, indicating the hydroxyurethane dynamic chemistry is effective in arresting elevated-temperature creep, regardless of the presence of nanofillers. This study highlights the advantages

and effectiveness of POSS molecules for fabricating high-performance reprocessable network composites.

Acknowledgments

This work was done in collaboration with Xi Chen, Mohammed Bin Rusayyis, and Nathan Purwanto from the Torkelson research group at Northwestern University. This research is now published (S. Hu et al., 2022): *Polymer* 2022, 252, 124971 (DOI: 10.1016/j.polymer.2022.124971).

5.5 Supporting Information

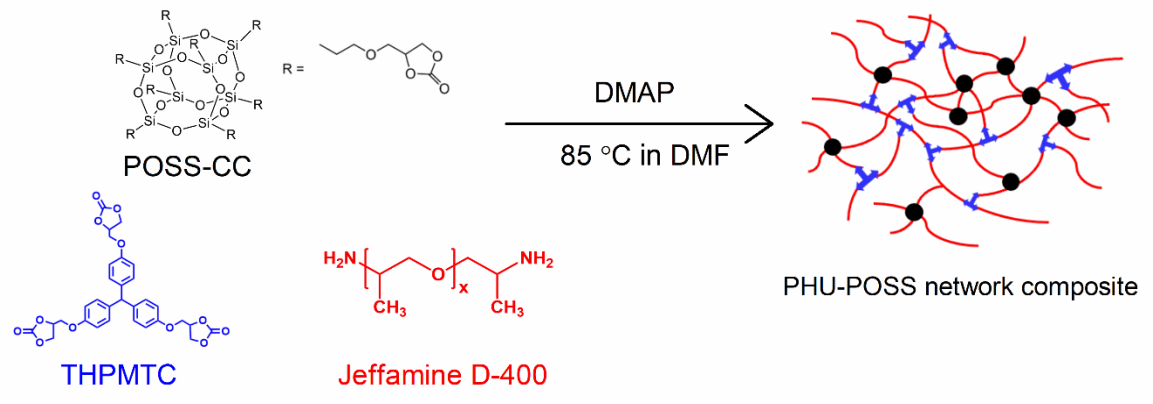

Figure 5-S1. Synthesis route to the PHU−POSS network composites.

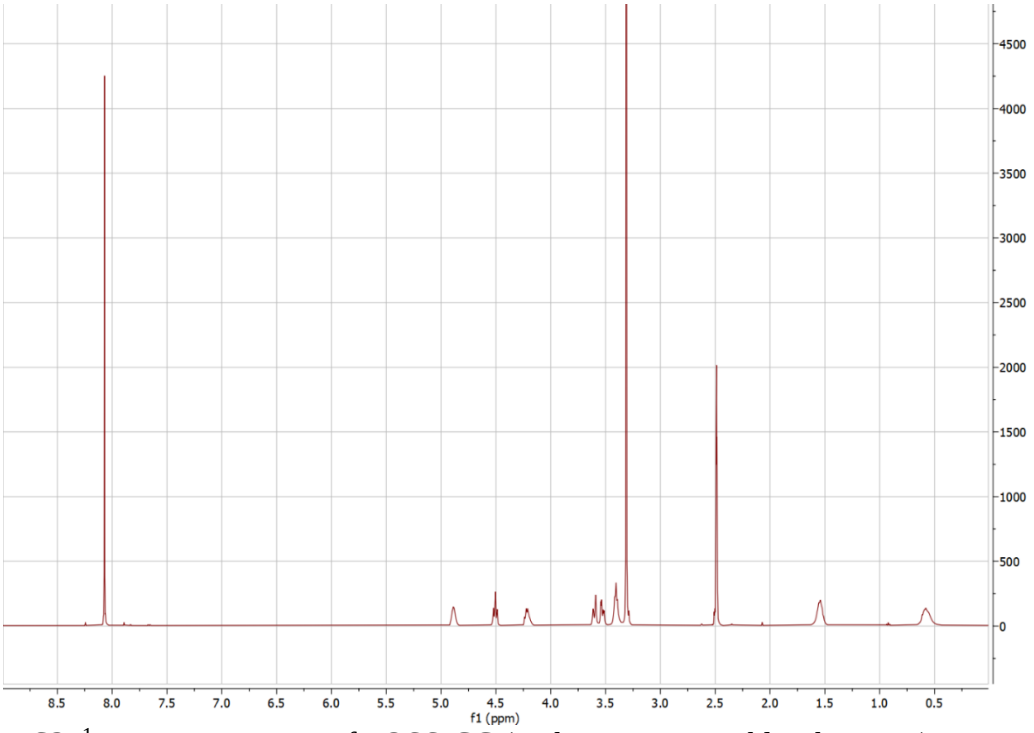

Figure 5-S2. ^{1}H NMR spectrum of POSS-CC (with 1,2,4,5-tetrachlorobenzene).

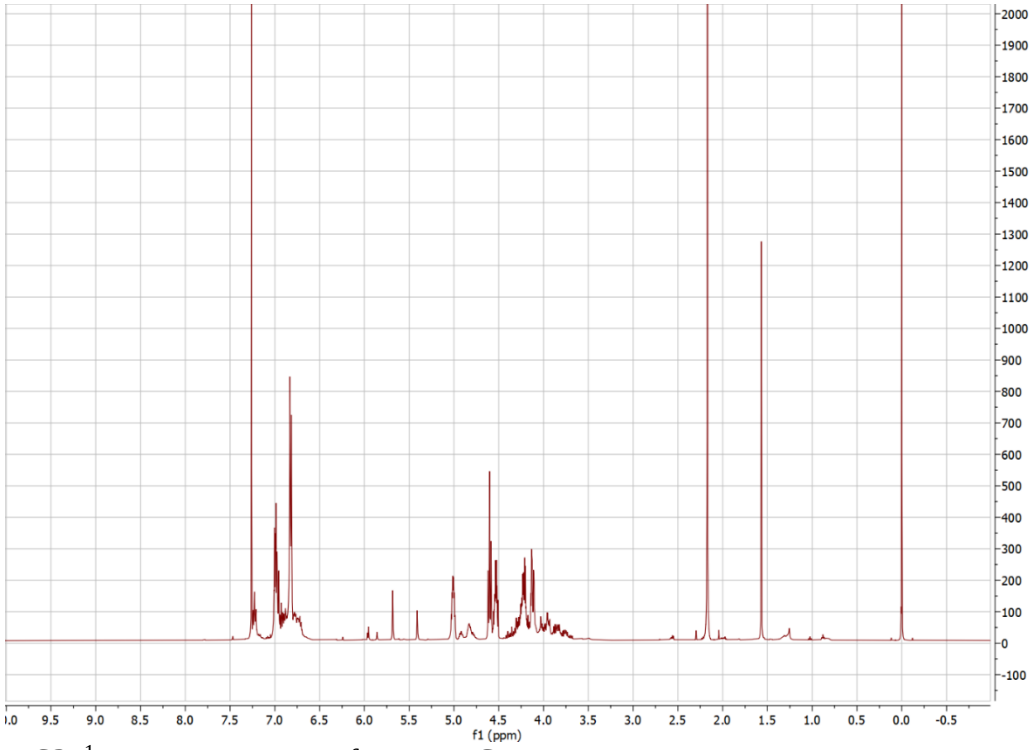

Figure 5-S3. ^{1}H NMR spectrum of THPMTC.

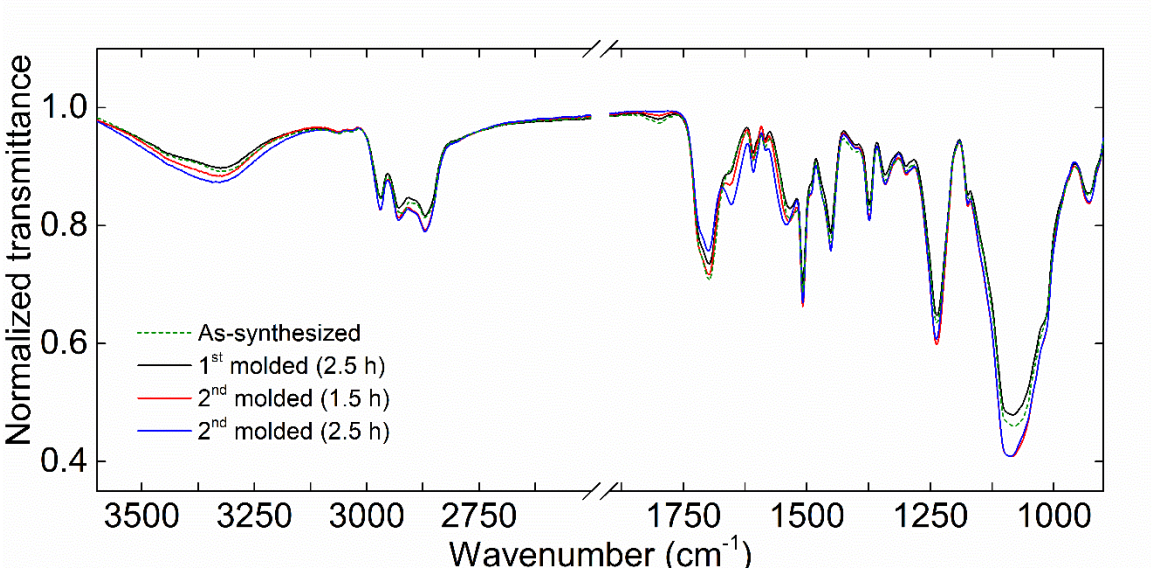

Figure 5-S4. FTIR spectra of as-synthesized and reprocessed PHU-POSS-10% samples.

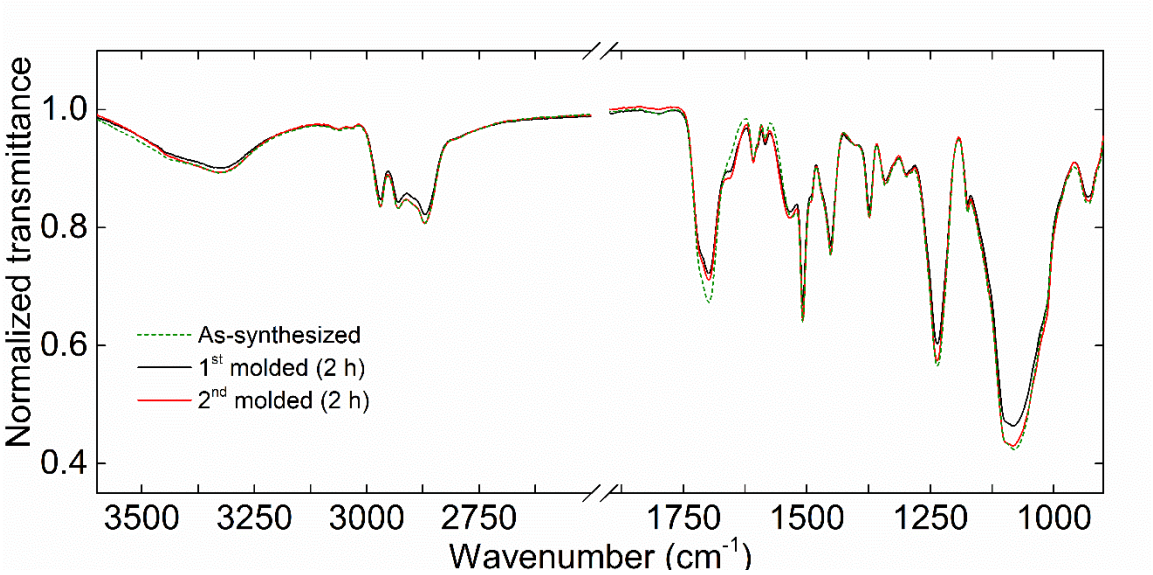

Figure 5-S5. FTIR spectra of as-synthesized and reprocessed PHU-POSS-5% samples.

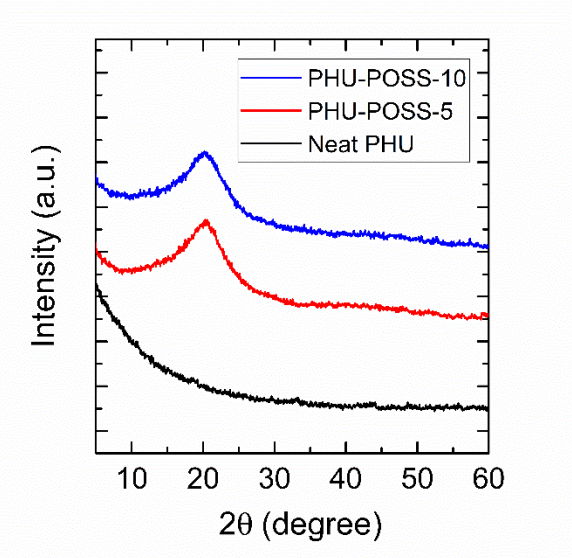

Figure 5-S6. XRD WAXS patterns of 1st molded neat PHU network and PHU−POSS network composites.

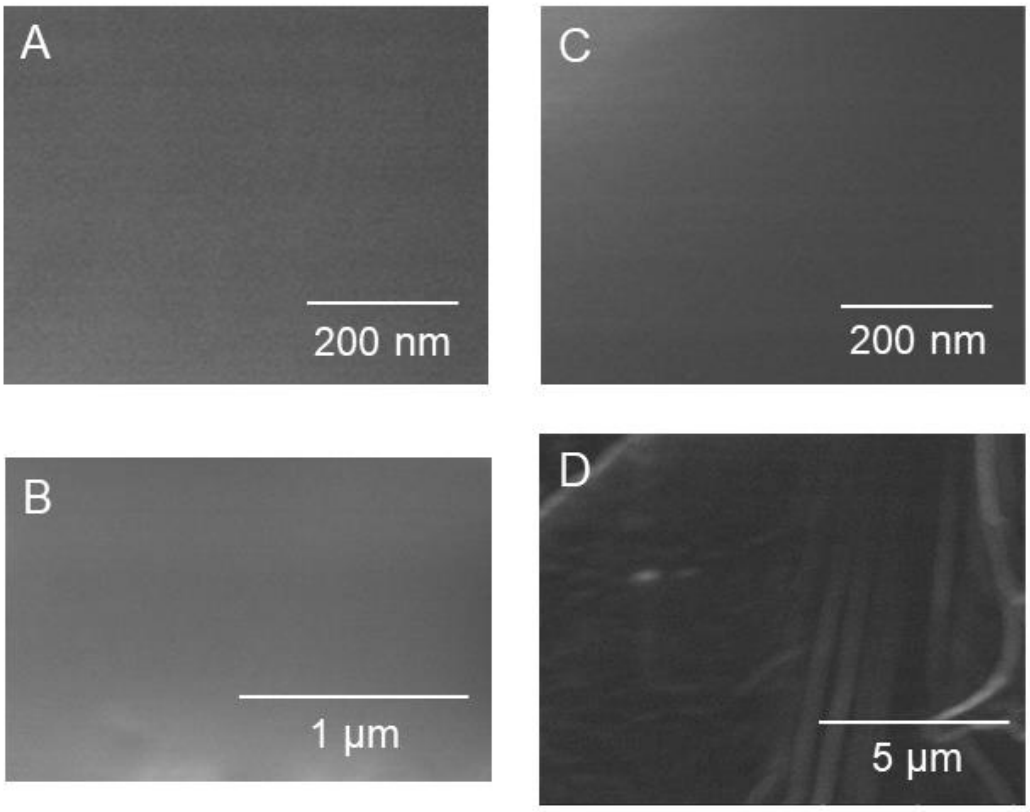

Figure 5-S7. SEM images of 1st molded PHU-POSS-5 (A and B) and 1st molded PHU-POSS-10 (C and D).

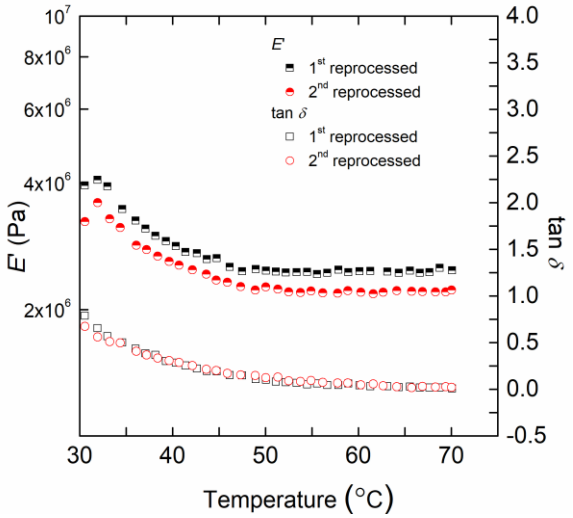

Figure 5-S8. ~10% loss in rubbery plateau *E*' from the 1st molded PHU-POSS-10 to the 2nd molded PHU-POSS-10.

Table 5-S1. Swelling ratio and gel content of as-synthesized and molded neat PHU network and PHU−POSS network composites.

Sample		Swelling ratio (%)	Gel content (%)
Neat PHU	**As-synthesized**	350 ± 9	97 ± 1
	1st molded	364 ± 7	96 ± 1
	2nd molded	378 ± 8	97 ± 2
PHU-POSS-5	**As-synthesized**	284 ± 2	97 ± 1
	1st molded	307 ± 6	96 ± 3
	2nd molded	313 ± 7	94 ± 2
PHU-POSS-10	**As-synthesized**	232 ± 4	97 ± 3
	1st molded	274 ± 8	93 ± 1
	2nd molded	276 ± 5	95 ± 2

Table 5-S2. T_g and T_g breadth of as-synthesized neat PHU network and PHU−POSS network composites.

Sample	T_g by ½ΔC_p method (°C)	T_g breadth (°C)
Neat PHU	21 ± 1	11 ± 1
PHU-POSS-5	14 ± 1	13 ± 1
PHU-POSS-10	10 ± 1	13 ± 1

Table 5-S3. Thermogravimetric analysis of neat PHU networks and PHU−POSS network composites.

Sample	*T* (°C)	
	At 5% weight loss	At 50% weight loss
Neat PHU	288 ± 3	378 ± 1
PHU-POSS-5	296 ± 1	382 ± 3
PHU-POSS-10	305 ± 3	388 ± 4

Table 5-S4. Stress relaxation fitting parameters from single exponential decay and stretched exponential decay for 1st molded neat PHU networks and PHU−POSS network composites.

Sample and temperature		Single exponential decay	Stretched exponential decay		
		τ^* (s)	τ^* (s)	β	$\langle\tau\rangle$ (s)
Neat PHU	**140 °C**	1301	1311	0.84	1437
	150 °C	377	375	0.87	402
	160 °C	283	278	0.90	293
	170 °C	122	119	0.96	121
PHU-POSS-5%	**140 °C**	5431	5509	0.65	7526
	150 °C	2415	2394	0.68	3118
	160 °C	731	739	0.68	962
	170 °C	166	165	0.74	199
PHU-POSS-10%	**140 °C**	6254	6363	0.56	10540
	150 °C	1937	2072	0.56	3432
	160 °C	802	814	0.61	1199
	170 °C	280	284	0.61	418

CHAPTER 6

Background

This chapter introduces core concepts involved in this dissertation regarding residual stress, fluorescence spectroscopy, and stiffness and stiffness-confinement effect.

6.1 Residual Stress in Polymer Films

Residual stress is stress that remains in a material after external forces have been removed (Chung et al., 2009). In polymeric materials, residual stress results from processes that trap polymer chains into non-equilibrium conformations. One example is the spin coating process. Spin coating is a widely used technique to fabricate uniform polymer thin films. The process involves depositing a polymer solution onto a flat substrate then rotating the substrate at high speeds to evenly spread the solution by centrifugal force. During the high-speed spinning process, polymer chains overlap and entangle as solvent is rapidly evaporated (Chandran et al., 2019). As evaporation proceeds, the relaxation time of polymer chains progressively increases and eventually exceeds the time needed to evaporate the remaining solvent (Chandran et al., 2019). As a result, spin coating usually results in non-equilibrium local chain conformations and thereby residual stresses in the as-cast films (Francis et al., 2002; Malzbender & de With, 2000; Reiter & Khanna, 2000). Residual stresses remain in polymer films until sufficient annealing is done to relax the stresses (Askar et al., 2015). Unrelaxed residual stresses in thin polymer films can induce microscopic defects and macroscopic dimensional changes; both are critical considerations and could be detrimental to applications such as thin film coatings and nanoscale polymer devices (Chung et al., 2009).

Approaches to characterize residual stresses in polymer thin films include the curvature method (Croll, 1979; Ree et al., 1993), blister (Guo et al., 2005), surface wrinkling (Chung et al., 2009), cylindrical punch (Ju et al., 2007), cantilever bending method (Thomas & Steiner, 2011), dewetting (Chandran & Reiter, 2019; Chowdhury et al., 2012; Damman et al., 2007; Reiter et al., 2005), fluorescence (Askar et al., 2015; Mundra et al., 2006; Muraki et al., 2002; Shiga et al., 1998), ellipsometry (Askar et al., 2015), etc. Most approaches have their own limitations. Curvature or deflection-based methods relate the deflection of a thick elastic substrate to the average residual stress of a thin film. Because this technique is nondestructive and real-time, it is among the most widely used methods. However, curvature methods are less reliable for ultrathin films when such methods are difficult to resolve small changes in curvature (Chung et al., 2009; Y. J. Tang et al., 2007). Blister, cylindrical punch, and cantilever bending techniques are contact-based methods and could impart external stresses on samples and convolute stress measurements. Surface wrinkling involves compression of a composite comprised of an elastic film and a thick, elastic substrate. The compression results in formation of a periodic wrinkling pattern in the film, and the dimensions and onset of wrinkle formation can be related to the elastic modulus of the polymer film and give information on residual stress (Chung et al., 2009). The surface wrinkling technique does not involve direct contact with samples; however, the characterization process does involve a change in sample geometry, and the impact of which on residual stress remains unknown.

Optical methods are useful for avoiding issues associated with contact and deformation methods. Mundra et al. (Mundra et al., 2006) demonstrated that intrinsic monomer and excimer fluorescence of phenyl rings could be used to characterize stress relaxation process in spin-coated styrene-containing polymer films via changes in the ratio of excimer to monomer fluorescence. It was found that although residual stress can partially relax upon heating in the glassy state, full

relaxation only occurs when polymer films are annealed in the rubbery state for a period of time that is longer than the average cooperative segmental relaxation time (Mundra et al., 2006). Askar et al. (Askar et al., 2015) used ellipsometry and fluorescence to characterize the residual stress relaxation in polystyrene (PS) films. Ellipsometry characterizes residual stress relaxation via sensitivity to time- and temperature-dependent changes in film thickness that occurs during stress relaxation, whereas fluorescence provides sensitivity to stress relaxation via the dependence of a vibronic band intensity ratio (I_1/I_3) of emission spectra of pyrenyl dyes that are covalently attached at trace levels to PS chains. Askar et al. (Askar et al., 2015) hypothesized that the underlying mechanism of residual stress relaxation in polymers is β-relaxation, which involves sub-segmental relaxations such as the reorientation of a side functional group. The temperature dependence of residual stress relaxation timescales for bulk PS films was found to follow an Arrhenius behavior, and the calculated activation energy (E_a) is in reasonable accordance with E_a values reported for the β-relaxation in bulk PS (Askar et al., 2015).

6.2 Stiffness in Bulk and Confined Polymers

Stiffness or modulus is related to short-timescale (~nanosecond), high-frequency vibrations or mobility in materials (Sperling, 2006). Experimental characterizations such as incoherent neutron scattering (sensitive to hydrogen atom density) have demonstrated the connection between the mean-squared displacement (MSD), $\langle u^2 \rangle$, and modulus (Inoue et al., 2005; Soles et al., 2002; Ye et al., 2015). At temperatures well below T_g, $\langle u^2 \rangle$ is inversely proportional to the local spring constant, κ, for harmonic vibration of segments within their neighbors, where κ scales with the high-frequency shear modulus (Ye et al., 2015). $\langle u^2 \rangle$ of glasses is tuned or altered according to a "caging" mechanism. Reductions in $\langle u^2 \rangle$ (or increases in κ) suggest that the atoms

are trapped in deeper potential energy minima, or "caged" by their environment (Soles et al., 2002), i.e., vibrations associated with MSD are suppressed in a "caged" or stiff environment.

When polymers are confined to a nanoscale, many key properties including the glass transition temperature (T_g) (Ellison & Torkelson, 2003; Jin & Torkelson, 2016; Keddie et al., 1994b; Keddie & Jones, 1995; S. Kim et al., 2009; Mundra et al., 2006; Napolitano et al., 2017; Pye & Roth, 2011; T. Wang et al., 2019), fragility (Lan & Torkelson, 2016; Riggleman et al., 2006; L. Zhang et al., 2017), physical aging rate (Ellison et al., 2002; Priestley et al., 2005; Rittigstein & Torkelson, 2006; Shavit & Riggleman, 2014), and stiffness (Askar & Torkelson, 2016; Briscoe et al., 1998; Brune et al., 2016; Cheng et al., 2007; Delcambre et al., 2010; Evans et al., 2012; Forrest et al., 1998; Gomopoulos et al., 2009, 2010; Inoue et al., 2005, 2006; Lee et al., 1996; Y. Liu et al., 2015; Song et al., 2019; Stafford et al., 2004, 2006; Torres et al., 2012; Tweedie et al., 2007; Watcharotone et al., 2011; Xia et al., 2016; Xia & Keten, 2015; Xia & Lan, 2019; S. Xu et al., 2010; M. Zhang et al., 2017, 2018) can deviate from bulk behavior. Among all these properties, T_g-confinement effects are most frequently studied, and the majority of past studies show agreement regarding general trends for particular polymer–substrate pairs. Stiffness-confinement effect has been investigated for nearly as long as T_g-confinement effect. However, various reports are conflicting, and general trends regarding stiffness-confinement behavior are unclear.

It has been hypothesized that stiffness-confinement effect of supported polymer films is related to the rigidity of substrates. Past studies on polymer films supported on rigid substrates have indicated enhancement in stiffness/modulus with decreasing film thickness. For example, using picosecond acoustic techniques, Lee et al. (Lee et al., 1996) measured the change in longitudinal wave speed (the square of which is proportional to through film elastic modulus) in aluminum- and silicon-supported thin PMMA films as a function of film thickness; a pronounced

increase in longitudinal wave speed and hence modulus was observed when the film thickness is below 40 nm. Using inelastic and quasi-elastic neutron scattering, Inoue et al. (Inoue et al., 2006) discovered that the MSD, $\langle u^2 \rangle$, for a 40-nm-thick glass-supported PS film decreased substantially relative to the bulk behavior at temperatures above and below T_g (recall that $\langle u^2 \rangle$ is described in numerous reports to be inversely proportional to local stiffness (Inoue et al., 2005; Soles et al., 2002; Ye et al., 2015)). In 2016, Askar and Torkelson (Askar & Torkelson, 2016) used a novel fluorescence-based approach to characterize the stiffness of PS films supported on rigid glass substrates. They demonstrated that stiffness of PS films is subject to combined perturbations from the substrate and free-surface interfaces; for sufficiently thin films, enhancement effects near the substrate dominate over the reduction effects near the free surface, thus leading to an enhancement of overall stiffness (Askar & Torkelson, 2016).

For polymer films that are free-standing or supported on soft substrates, previous studies mostly reported a reduction in stiffness with confinement. For example, Stafford et al. (Stafford et al., 2004) applied a buckling-based method to measure the elastic properties of polydimethylsiloxane-supported PS and PMMA films with thickness ranging from 200 to 5 nm; both polymers exhibit reduction in modulus with decreasing film thickness at 40 nm and below. Liu et al. (Y. Liu et al., 2015) developed an ultrathin film tensile test method that can directly measure the stress-strain response of thin polymer films floating on water; for PS films, they reported a continuous decrease in Young's modulus with decreasing film thickness down to 15 nm.

6.3 Fluorescence Spectroscopy

6.3.1 Basics of fluorescence

The fluorescence process is often illustrated with the classical Jablonski diagram (Figure 6-1). The process begins with the excitation of electrons of a fluorophore from the ground electronic state (S_0, v_0) to one of the various vibrational levels in the excited electronic state. The excited electrons are in non-equilibrium states and will eventually return to the ground state by dissipating the energy they have gained. After excitation, the electrons will first dissipate energy through vibrational relaxation or internal conversion until they return to the lowest vibrational level of the first excited singlet state (S_1, v_0). Electrons can then further relax to the ground state by various competing pathways including non-radiative relaxation pathways (vibrations, rotations, etc.) and radiative relaxation pathways (fluorescence). From (S_1, v_0), electrons can return to (S_0, v_0) solely through non-radiative pathways or solely through radiative pathways; alternatively, they can first relax to (S_0, $v_{n\,(n>0)}$) through fluorescence and then dissipate the remaining energy through non-radiative pathways and reach (S_0, v_0). The fluorescence absorbance spectra and fluorescence emission spectra are mirror symmetric. Because of the existence of the non-radiative relaxation pathways, the energies of photons emitted during fluorescence are lower than those of the photons absorbed during excitation; for this reason, fluorescence emission spectra are shifted toward lower energy (higher wavelengths) relative to the absorption spectra.

Some organic fluorophores, e.g., phenyl rings in polystyrene, exhibit a broad, rather featureless, monomer fluorescence spectrum, i.e., emission from a single excited-state fluorophore (Mundra et al., 2006). Some fluorophores, e.g., phenyl rings (Wong, Kim, Roth, et al., 2007) and pyrene (S. D. Kim & Torkelson, 2002), also exhibit broad, featureless excimer fluorescence, or fluorescence emission from excited-state dimers in which the two fluorophores are coplanar and

separated by a few Angstroms. Excimer-to-monomer fluorescence intensity ratios are a form of intrinsic fluorescence characterization that has been exploited for more than three decades to characterize behavior in polymer-based systems, including phase separation in blends containing polystyrene (Tsai & Torkelson, 1988), disorder-to-order transitions in block copolymers (Roth & Torkelson, 2007), critical micelle concentrations and temperatures of gradient and block copolymers in homopolymer (Evans et al., 2013; Sandoval et al., 2008; Wong, Kim, & Torkelson, 2007), and nanophase-separation via hard-segment organization in telechelic polydimethylsiloxane (S. D. Kim & Torkelson, 2002).

In contrast to many fluorophores with featureless monomer emission spectra, the fluorescence emission spectrum for pyrene has five distinct peaks, each corresponding to a transition at different energy level. For example, the peak associated with the highest-energy (lowest wavelength) emission, i.e., the first vibronic peak, corresponds to the transition from (S_1, v_0), directly to (S_0, v_0) (Kalyanasundaram & Thomas, 1977; Karpovich & Blanchard, 1995). Notably, as described below, intensity ratios of one pyrene monomer peak to a second pyrene monomer peak can provide intrinsic fluorescence characterization of local response in organic media.

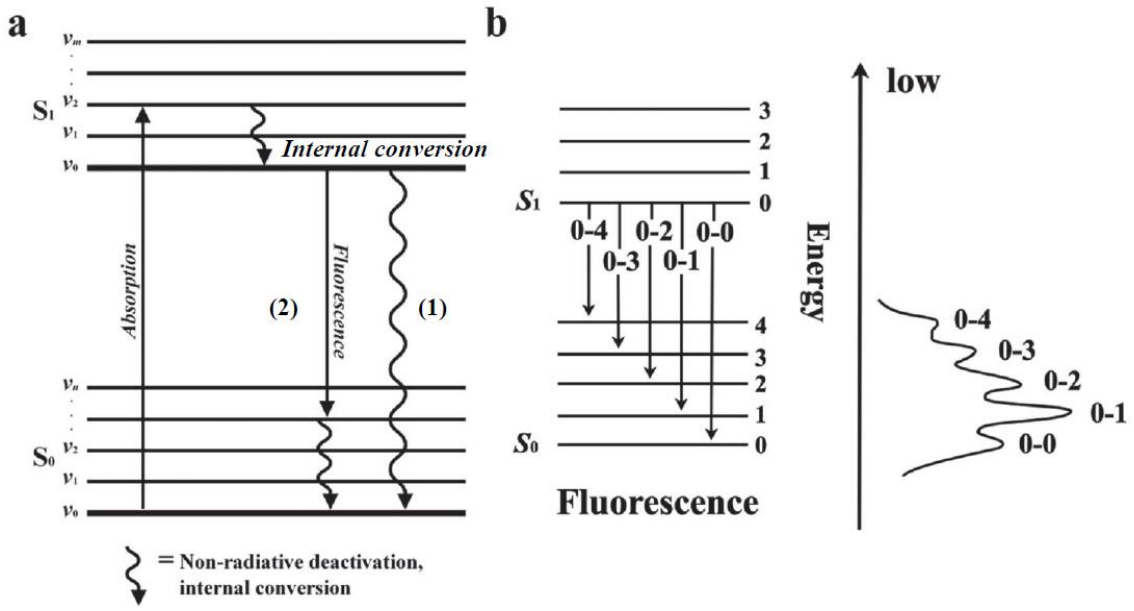

Figure 6-1. (a) Jablonski diagram illustrating fluorescence as a competing decay pathway with internal conversion process (vibrational or rotational motions). (b) Electronic transitions between different energy levels correspond to different vibronic bands in fluorescence emission spectrum. Figure from reference ((Burroughs et al., 2018)).

6.3.2 Sensitivity of pyrene to molecular caging and characterization of stiffness using fluorescence

The monomer fluorescence emission spectrum from pyrenyl dyes has a strong dependence on the local molecular caging state. For example, the intensity ratio of peak I to peak III (I_1/I_3) of pyrene is strongly affected by solvent polarity (Figure 6-2). In 1977, Kalyanasundaram and Thomas (Kalyanasundaram & Thomas, 1977) discovered that I_1/I_3 increases with increasing solvent polarity, which can be explained by a caging mechanism. Upon excitation, electrons in pyrene undergo a transition from a symmetrical distribution to an unsymmetrical distribution, which induces a dipole moment in the excited-state pyrene. In high-polarity solvent, there are greater dipole-dipole couplings between the excited-state pyrene molecules and solvent molecules. This greater molecular caging restricts non-radiative forms of energy decay such as vibrations and

promotes the radiative fluorescence pathway. This ultimately leads to an enhancement of peak I and the expenses of other peaks, with the strongest effect observed relative to peak III (Kalyanasundaram & Thomas, 1977). In 1995, Karpovich and Blanchard S_2 (Karpovich & Blanchard, 1995) demonstrated that the sensitivity of pyrene to solvent polarity originates from the vibronic coupling between the weakly allowed first excited singlet state S_1 and the strongly allowed second excited singlet state. In high-polarity environments, the induced dipole-dipole coupling mediates vibronic coupling and therefore emission band intensities, which leads to the solvent polarity dependent emission response seen for pyrene.

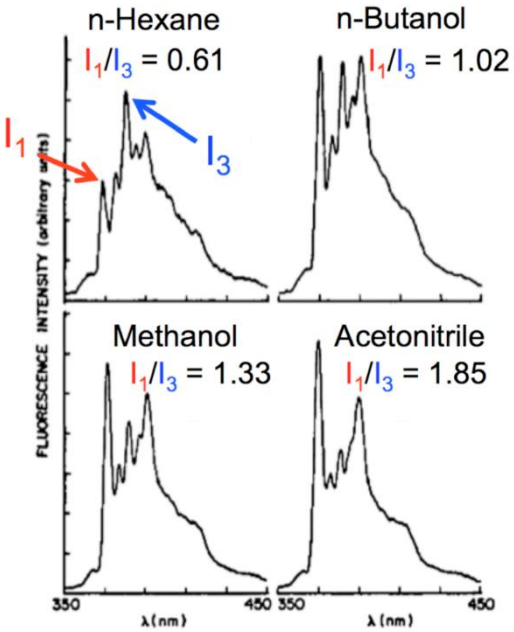

Figure 6-2. Pyrene fluorescence emission spectra in four solvents with increasing polarity from *n*-hexane, *n*-butanol, methanol, and acetonitrile. I_1/I_3 represents the ratio of the first vibronic peak intensity to the third vibronic peak intensity. (Reproduced from reference (Kalyanasundaram & Thomas, 1977))

The sensitivity of the pyrene fluorescence spectrum to molecular caging makes pyrene a useful probe to characterize polymer properties that are related to sub-segmental relaxations or

molecular vibrations. For example, stiffness of polymer films can be characterized by measuring I_1/I_3 of pyrenyl dyes that are covalently attached at trace levels to polymer chains. In more stiff environments, excited-state pyrene is caged to a greater extent, which leads to enhancements in the I_1/I_3 value. The sensitivity of the I_1/I_3 value to local stiffness has been exploited for a number of purposes related to polymer response, including characterization of the T_g-confinement effect and its distribution across the thickness of nanoconfined, free standing polymer films (S. Kim et al., 2008; S. Kim & Torkelson, 2011), the effect of nanoparticles on the local polarity in polymer nanocomposites (Mundra et al., 2007), multiple component T_gs in miscible polymer blends (Evans & Torkelson, 2012), the role of neighboring domains in modifying the T_g-confinement effect in immiscible polymer blends (Evans et al., 2015), and order-to-disorder transitions in block copolymer films (Qiang et al., 2020).

Relevant to this thesis, Askar and Torkelson (Askar & Torkelson, 2016) used the I_1/I_3 method to characterize the average stiffness of PS thin films upon nanoscale confinement and to study the roles of free-surface and substrate interface on stiffness-confinement behavior; they discovered that single-layer PS films stiffen with confinement, and stiffness is enhanced near a substrate and reduced near a free surface. In a later study by Zhang et al. (M. Zhang et al., 2017), the length scales over which stiffness or modulus is modified by the presence of a substrate in a model nanocomposite comprised of a PS film supported on both sides by glass substrates were characterized by both fluorescence and atomic force microscopy (AFM). The two techniques show qualitative and quantitative agreement regarding stiffness gradient length scales, indicating that fluorescence is an effective non-contact tool to characterize stiffness of polymers.

CHAPTER 7

Small Changes in Copolymer Composition Strongly Impact Residual Stress Relaxation in Styrene/Acrylic Random Copolymer Films

7.1 Introduction

Polymers confined to nanoscopic dimensions are found in many applications including photoresists (Vogt et al., 2006; Wieberger et al., 2011), nanocomposites (Paul & Robeson, 2008; Potts et al., 2011), flexible electronics (S. Wang et al., 2018; J. Xu et al., 2017), and membranes (Ismail et al., 2019; Trigg & Winey, 2019). Spin coating is one of the most common techniques to fabricate homogeneous polymer films with thickness down to nanometers (Hall et al., 1998). During spin coating, polymer solution is dispensed onto a substrate surface; then, the substrate is spun at high speeds to spread the solution by centrifugal force. Because the high-speed spinning process results in non-equilibrium local chain formations, many studies have demonstrated that residual stress can present in as-cast polymer films prepared by spin coating (Francis et al., 2002; Malzbender & de With, 2000; Reiter et al., 2005; Reiter & Khanna, 2000). The residual stress gives rise to changes in the ultimate physical properties of polymer films and is detrimental in many applications (Chowdhury et al., 2016; Malzbender & de With, 2000). Understanding the residual stress relaxation process is of great importance in order that failures associated with non-equilibrated physical properties can be prevented.

Many techniques including cylindrical punch (Ju et al., 2007), prism coupling method (Ree et al., 1994), surface wrinkling (Chung et al., 2009, 2011), bending method (Croll, 1978, 1979; Thomas & Steiner, 2011), dewetting (Chandran & Reiter, 2019; Damman et al., 2007; Fan et al., 2020; Reiter, 1994, 2013; Reiter et al., 2005; Richardson et al., 2003; Ziebert & Raphaël, 2009),

fluorescence (Askar et al., 2015; Mundra et al., 2006, 2007), and ellipsometry (Askar et al., 2015) have been employed to characterize the residual stress relaxation process in spin-coated polymer films. Despite extensive past research efforts, the aforementioned studies have been limited to homopolymers, and little research effort has focused on related behavior of random copolymers. Random or statistical copolymers are important both scientifically and industrially because they combine chemical and physical properties of two or more different constituents while not causing phase separation.

Residual stresses remain in polymer films until sufficient annealing is done to relax the stresses. Mundra et al. (Mundra et al., 2006) demonstrated via intrinsic monomer and excimer fluorescence of styrene-containing polymer films that full stress relaxation only occurs when polymer films are annealed at ~15–20 K above the film T_g for a period of time that is longer than the average cooperative segmental relaxation time. Askar et al. (Askar et al., 2015) used ellipsometry and fluorescence to characterize spin-coated polystyrene (PS) films and showed that residual stress relaxation in PS films occurs over periods of hours in the rubbery state, and the relaxation timescale has strong temperature dependence. Here, we study the impact of a slight change in polymer composition on residual stress relaxation in spin-coated polymers films. Specifically, we use ellipsometry and fluorescence to characterize residual stress relaxation in poly(styrene/*n*-butyl acrylate) (P(S/nBA)) random copolymer films, where the nBA molar content is controlled at very low levels, and demonstrate that a small level of nBA units can significantly modify the residual stress relaxation behavior from that of neat PS films.

Residual stress relaxation in polymer films is usually accompanied by small but measurable changes in film thickness (Askar et al., 2015); ellipsometry provides sensitivity to residual stress relaxation via time-dependent and temperature-dependent changes in thickness of polymer films

spin coated onto silica substrates. With fluorescence, stress relaxation is characterized by monitoring the time-dependent and temperature-dependent changes in an intensity ratio associated with the emission spectra of pyrenyl dyes covalently attached at a trace level to the polymer backbones. Studies on pyrene fluorescence have demonstrated that the intensity ratio of the first vibronic band peak to the third vibronic band peak, I_1/I_3, in pyrene emission spectra is strongly affected by local molecular caging state (Askar et al., 2015; Askar & Torkelson, 2016; Evans & Torkelson, 2012; Kalyanasundaram & Thomas, 1977; Karpovich & Blanchard, 1995; S. Kim et al., 2008; M. Zhang et al., 2017). Upon excitation, electrons in pyrene may return to the ground state via both non-radiative and radiative pathways. In a caged or stressed environment, non-radiative pathways, e.g., vibrations and rotations are restricted, and high-energy radiative pathways (fluorescence) are enhanced. For vibronic coupling dyes like pyrene which have overlapping excited-state energy levels, greater molecular caging can mediate the vibronic couplings and ultimately leads to enhancement in I_1 at the expense of other peaks, and the strongest effects was observed relative to I_3. Therefore, as stresses in polymer films are relaxed, reduced caging results in corresponding decrease in the I_1/I_3 values of pyrene fluorescence emission spectrum.

7.2 Experimental Methods

7.2.1 Materials

Styrene (Sigma-Aldrich, 99%) and *n*-butyl acrylate (Sigma-Aldrich, 99%) were deinhibited using *tert*-butylcatechol inhibitor remover (Sigma-Aldrich) and monomethyl ether hydroquinone inhibitor remover (Sigma-Aldrich) and dried over calcium hydride overnight. Pyrenylmethyl methacrylate (MPy) was synthesized by esterification of methacryloyl chloride (Sigma-Aldrich) and 1-pyrenyl methanol (Sigma-Aldrich) following synthesis procedures

previously described by Ellison and Torkelson (Ellison & Torkelson, 2002). Benzoyl peroxide (BPO) was purchased from Sigma-Aldrich. Toluene, methanol, tetrahydrofuran (THF, HPLC grade), sulfuric acid, and hydrogen peroxide were purchased from Fisher Chemical.

7.2.2 Synthesis of polymers

PS and P(S/nBA)s were synthesized by bulk free radical polymerization at 60 °C using BPO (0.5 mg/mL monomer) as initiator. Monomer mixtures with different compositions were used to generate copolymers with various nBA contents. To synthesize MPy-labeled P(S/nBA)s, MPy was copolymerized at a trace level (0.5 mol% with respect to monomers) with other monomers. The as-synthesized random copolymers were washed seven times by dissolving in toluene and precipitating in methanol to remove residual initiators and monomers. The washed polymers were dried at 80 °C in a vacuum oven for three days prior to use.

7.2.3 Characterization of as-synthesized copolymers

The labeling efficiency (moles of pyrene-labeled repeat units relative to moles of total repeat units) of MPy-labeled P(S/nBA)s was determined by UV−vis absorbance spectroscopy (Perkin-Elmer Lambda 35) using 0.1 mg/mL THF solutions of the copolymers. The absorbance spectrum was measured at wavelengths from 280 nm to 380 nm, and the label concentration was determined from the absorbance of the peak at ~335 nm using Beer's law, where $A = \mathcal{E}lc$; $\mathcal{E}$ is 37300 $M^{-1}\cdot cm^{-1}$ for pyrene, and l is 1 cm.

The bulk glass transition temperatures (T_gs) were determined via differential scanning calorimetry (Mettler Toledo DSC822e). Each sample was first annealed at 140 °C for 15 min and then cooled to 60 °C at a rate of 40 °C/min. $T_{g,onset}$ values were obtained from the second heating cycle at a heating rate of 10 °C/min.

Molecular weight and dispersity were determined by gel permeation chromatography

(GPC; Waters Breeze v3.20) coupled with a multiangle laser light-scattering detector (mini-Dawn, Wyatt Technologies). Properties of unlabeled and MPy-labeled PS and P(S/nBA)s are summarized in Table 7-1.

Table 7-1. Summary of properties of PS and P(S/nBA)s used in this study.

P(S/nBA) (mol%/mol%)	M_n (kg/mol)	Dispersity[a]	$T_{g,\,onset}$ (°C) by DSC	Labeling efficiency (mol%)
Blank PS	390	1.42	100	-
Labeled PS	390	1.33	100	1.0
Blank 98/2	500	1.30	98	-
Labeled 98/2	550	1.35	98	1.0
Blank 95/5	390	1.37	85	-
Labeled 95/5	450	1.36	85	1.2

[a] Dispersity is low because low-molecular-weight polymers have been removed during the seven-times dissolution and precipitation purification step.

7.2.4 Sample preparation

Glass and silica substrates were cleaned by submersion in piranha solution (75 vol% sulfuric acid/25 vol% hydrogen peroxide) at 90 °C for 1 h followed by thoroughly rinsing with deionized water. Single-layer films were prepared by spin-coating toluene solutions containing 0.5 to 6.0 wt% polymers onto substrates with spin speeds ranging from 1400 to 2100 rpm. The spin-coated films were annealed at $T_g - 40$ °C overnight to remove residual solvent before residual stress relaxation characterization.

7.2.5 Ellipsometry

To determine the film thickness, polymer solutions were spin-coated onto silicon slides with a native silicon oxide layer and characterized at room temperature using spectroscopic ellipsometry (J. A. Woollam Co. M-2000D over a range of wavelengths from 400 to 1000 nm).

The ellipsometric angles (ψ and Δ) of incident light reflected off silicon-supported films were measured and fitted to a Cauchy layer model to determine the film thickness. The Cauchy layer model includes a polymer layer on top of a silicon substrate containing a 2-nm-thick silicon oxide surface layer. With the same solution concentration and spin speed, the spin-coated films are assumed to have the same thickness on silica and glass.

To determine the time that is required to fully relax the residual stress in bulk polymer films using ellipsometry, the thickness of silica-supported bulk films was monitored during long-period (at least 12 h) isothermal annealing at $T > T_g$.

7.2.6 Fluorescence

Fluorescence was used to characterize the intensity ratio of the first to the third vibronic band peak (I_1/I_3) of MPy emission spectra, which reflects molecular caging and hence the stress state of MPy-labeled polymer films. Emission spectra of MPy-labeled films were collected (Photon Technology International fluorimeter in front-face geometry) at wavelengths from 374 to 392 nm (0.5 nm increment, 0.5 s integration) with excitation at 324 nm. Excitation and emission slit widths were 0.5 mm (1 nm bandpass). I_1 and I_3 were calculated from an average of five data points spanning a 2 nm window: I_1 was an average of five data points between ~375.5 nm and ~377.5 nm, and I_3 was an average of five data points between ~386.5 nm and ~388.5 nm.

To characterize the residual stress relaxation timescales, glass-supported MPy-labeled P(S/nBA) films were placed on a heating stage pre-heated to desired annealing temperatures. Samples were held isothermally at the annealing temperatures for at least 12 h with spectra at wavelengths from 374 nm to 392 nm collected every 15 min. Background noise was measured by acquiring the spectra of the films at wavelengths from ~350 nm to ~352 nm where no emission peak is present and subtracted from the emission spectra.

7.3 Results and Discussion

Spin coating is a common technique to deposit uniform, thin polymer films onto flat substrates. During the spinning process, polymer chains overlap and entangle as solvent is rapidly evaporated. As evaporation proceeds, the relaxation time of polymer chains progressively increases and eventually exceeds the time needed to evaporate the remaining solvent molecules (Chandran et al., 2019). As a result, spin coating usually results in non-equilibrium local chain conformations and thereby residual stresses in the as-cast films. The residual stress can be removed by annealing the films at temperatures above T_g. In this study, we used both ellipsometry and fluorescence techniques to characterize the time that is required to completely remove the residual stress as a function of annealing temperature for spin-coated P(S/nBA) films.

Stress relaxation in polymer films may be accompanied by small but measurable decreases or increases in thickness. We first used spectroscopic ellipsometry to probe the effect of residual stress relaxation on thickness of rubbery-state bulk 98/2 and 95/5 P(S/nBA) films (contains 2 and 5 mol% nBA, respectively). A measurement with a bulk PS film was performed for reference purposes. Prior to measurements, bulk, silica-supported polymer films were annealed under vacuum at T_g – 40 °C for 12 h to remove residual solvent. Since residual stress relaxation only happens in the rubbery state, this annealing temperature does not lead to changes in the stress state of the polymer films. After annealing, the films were transferred onto a heating stage pre-heated to ~30 °C above the respective T_g and held isothermally under nitrogen flow as film thickness was constantly measured via ellipsometry. Figure 7-1(b) and 7-1(c) show the evolution of normalized film thickness as a function of annealing time for bulk, 400-nm-thick 98/2 and 95/5 P(S/nBA) films at T_g^{bulk} + 30 °C. Upon annealing, the thickness of both films constantly decreases. Because residual toluene has been removed from the spin-coated films prior to ellipsometry

characterizations, the decrease in film thickness is unrelated to solvent loss but instead is related to residual stress relaxation. The stress relaxation timescale is determined to be the time after which the change in normalized film thickness is within ± 0.0001. Based on the ellipsometry results, at T_g^{bulk} + 30 °C, the thickness of the bulk, 400-nm-thick 98/2 P(S/nBA) film requires ~7 h to reach steady state values; in contrast, the thickness of the bulk, 400-nm-thick 95/5 P(S/nBA) film did not reach steady state values even after 33 h of isothermal annealing.

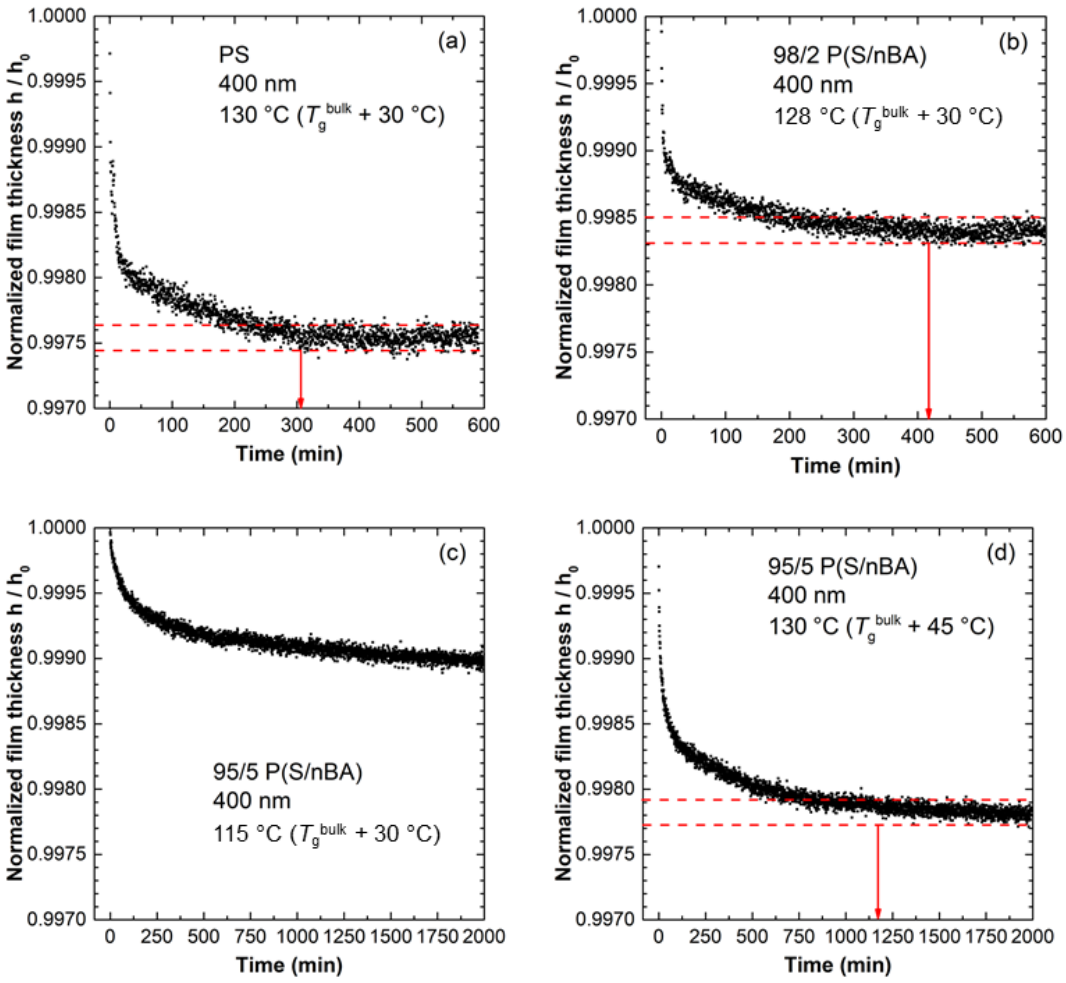

Figure 7-1. Ellipsometry measurement of thickness as a function of anneal time for bulk (400-nm-thick) (a) PS, (b) 98/2 P(S/nBA) and (c) 95/5 P(S/nBA) films at T_g^{bulk} + ~30 °C and for (d) 95/5 P(S/nBA) at T_g^{bulk} + ~45 °C.

For comparison purposes, we performed a similar characterization on a bulk PS film. As shown in Figure 7-1(a), at T_g^{bulk} + 30 °C (130 °C), the thickness of the bulk, 400-nm-thick PS film only needs ~5 h to reach steady state values. Thus, the residual stress relaxation timescale increases by ~40% when 2 mol% nBA is added to neat PS and by more than an order of magnitude when nBA molar content reaches 5 mol%. To eliminate the possible impact of lower thermal energy on the vastly extended residual stress relaxation timescale of bulk 95/5 P(S/nBA), we characterized the thickness change of a 400-nm-thick 95/5 P(S/nBA) film during isothermal annealing at 130 °C, which is the same absolute temperature as that used for annealing the bulk PS film. As shown in Figure 7-1(d), when annealed at 130 °C (T_g^{bulk} + 45 °C), the bulk 95/5 P(S/nBA) film needs ~18 h or a factor of 6 greater than that of neat PS to fully relax, which indicates that the residual stress relaxation timescale of the bulk 95/5 P(S/nBA) film is markedly increased relative to neat PS even when the 95/5 P(S/nBA) film is annealed at a higher temperature relative to T_g^{bulk}. For a 400-nm-thick 95/5 P(S/nBA) film, with only 5 mol% nBA, the attractive hydrogen bonding interactions happening at the polymer−substrate interface are less likely to impact the average relaxation behavior of the entire film. Therefore, the vastly different residual stress relaxation behaviors suggest that P(S/nBA) and PS systems are inherently different, and the molecular dynamics of neat PS films can be substantially or even dramatically modified with a very small amount of nBA.

The effect of isothermal annealing on stress relaxation of bulk P(S/nBA) films was also studied via fluorescence by monitoring the changes in emission spectra of MPy that is covalently attached to P(S/nBA). The fluorescence approach is based on the sensitivity of pyrene spectra to changes in local molecular caging; higher I_1/I_3 values represent a more caged environment and thus a more stressed state. $I1/I3$ is expected to decrease as the stress in polymer films is relaxed. Figure 7-2 shows emission spectra for a 514-nm-thick MPy-labeled 95/5 P(S/nBA) single-layer

film during isothermal annealing at 115 °C (T_g^{bulk} + 30 °C), with spectra were normalized relative to I_1. With increasing annealing time, I_3 progressively increases relative to I_1; hence, the I_1/I_3 value progressively decreases, consistent with reductions in caging and hence residual stress being relaxed in the films.

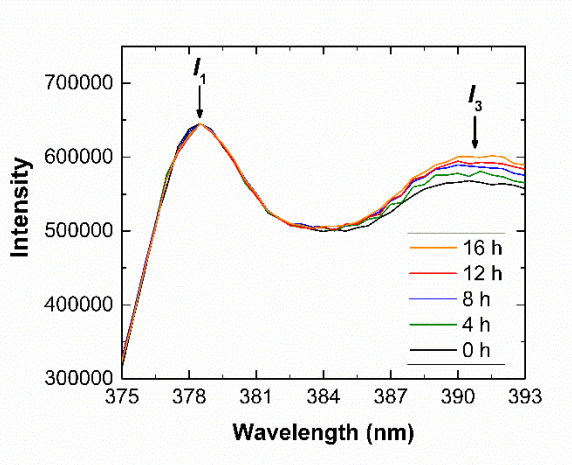

Figure 7-2. Fluorescence emission spectra of a 514-nm, pyrene-labeled, single-layer 400-nm-thick 95/5 P(S/nBA) film during isothermal annealing at 115 °C. Spectra are normalized relative to I_1 at 0 h. The value of I_1/I_3 decreases with increasing annealing time.

Figure 7-3(a) shows the evolution of I_1/I_3 values for a bulk, MPy-labeled PS film supported on glass during isothermal annealing at T_g^{bulk} + 30 °C. Upon annealing, I_1/I_3 decreased with increasing annealing time and then reached apparent steady-state values. Relaxation time was obtained from the intersection of lines corresponding to the deceasing regimes and steady-state regimes. At T_g^{bulk} + 30 °C, I_1/I_3 of the bulk PS film reached steady-state values after ~3 h, indicating that residual stress relaxation occurred over ~3 h. This timescale is in reasonable agreement with the report by Askar et al. (Askar et al., 2015), in which they employed the same fluorescence-based approach to characterize the residual stress relaxation behavior in bulk PS films and discovered that a spin-coated, bulk PS film required ~2 h to fully relax at T_g^{bulk} + 30 °C.

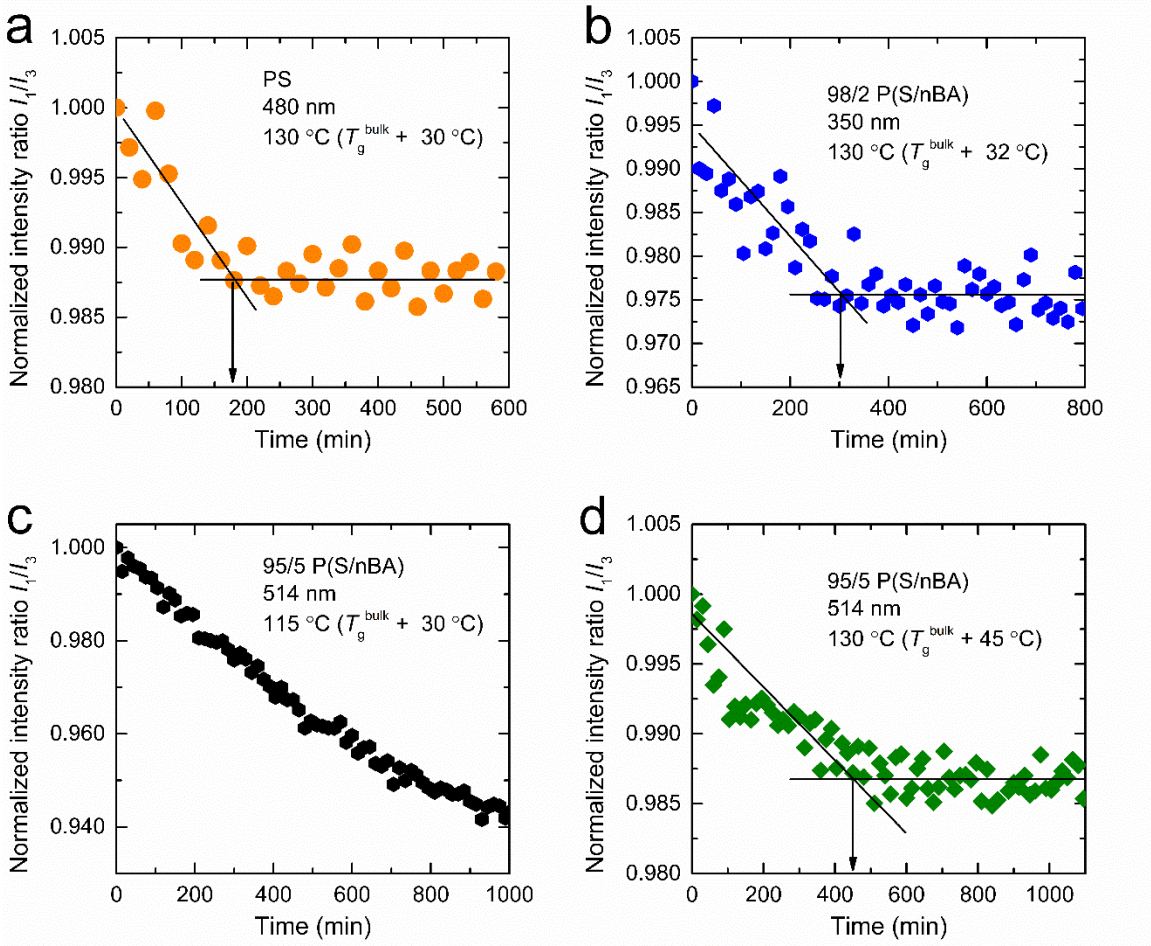

Figure 7-3. Fluorescence characterization of I_1/I_3 values as a function of anneal time for bulk (a) PS, (b) 98/2 P(S/nBA), and (c) 95/5 P(S/nBA) films at T_g^{bulk} + ~30 °C and for (d) 95/5 P(S/nBA) at T_g^{bulk} + ~45 °C.

Figures 7-3(b) and 7-3(c) show the evolution of I_1/I_3 values of a bulk 98/2 P(S/nBA) and a bulk 95/5 P(S/nBA) films supported on glass during isothermal annealing at T_g^{bulk} + ~30 °C. For the bulk 98/2 P(S/nBA) film, I_1/I_3 reached steady state after ~5 h of annealing, indicating that residual stress relaxation occurred over ~5 h. This timescale is increased fractionally compared to that of the neat PS film shown in Figure 7-3(a). For the bulk 95/5 P(S/nBA) film (Figure 7-3(c)), I_1/I_3 continued to decrease and did not reach steady state values even after 16 h of isothermal

annealing at T_g^{bulk} + 30 °C. To eliminate the impact of thermal energy on stress relaxation timescales, we increased the annealing temperature and measured the I_1/I_3 values of another bulk 95/5 P(S/nBA) film during isothermal annealing at 130 °C, which is 45 °C above T_g^{bulk}. At 130 °C, I_1/I_3 of the bulk 95/5 P(S/nBA) film reached steady-state values after ~7 h (Figure 7-3(d)). This relaxation timescale is further extended relative to that of the bulk 98/2 P(S/nBA) film at the same absolute temperature. We note that the relaxation timescales determined via fluorescence are in qualitative but not quantitative agreement with the timescales determined via ellipsometry shown in Figure 7-2 because of the difference in the resolution of the two techniques. Ellipsometry is particularly sensitive to minor changes and provides resolution up to 1 part per 10000, whereas the fluorescence-based I_1/I_3 method only allows detection of changes that are greater than 2 parts per 1000.

Like the observations associated with ellipsometry characterization, fluorescence characterization also indicates that the residual stress relaxation timescales of bulk P(S/nBA) films (where PS can be considered as P(S/nBA) containing 0 mol% nBA) are significantly affected by the presence and the molar content of nBA. With a few mole percent of nBA in the system, the relaxation behavior is vastly changed from neat PS. The relaxation timescale is increasingly extended with increasing molar amount of nBA in the copolymer both at the same relative annealing temperature above T_g^{bulk} and at the same absolute annealing temperature. The dramatic effect of nBA units on extending the residual stress relaxation timescale of spin-coated films is not yet well understood. We hypothesize that such behavior may be caused by dipole–dipole interactions or van der Waals interactions between ester groups in nBA units impacting the overall sub-segmental relaxation process of the entire film.

For P(S/nBA) random copolymers, fluorescence characterizations were also performed on

ultrathin films to determine the effect of nanoscale confinement on residual stress relaxation. Attempts were also made to determine the relaxation timescales using ellipsometry. However, the centrifugal force during spin coating can result in excess polymers to reside on the edge of the substrate; these excess polymers tend to diffuse towards the center and impact the local thickness in the film. Thus, ellipsometry-based characterizations of the residual stress relaxation process which rely on monitoring thickness changes are not feasible for ultrathin films.

Figure 7-4 shows the fluorescence-based characterization for residual stress relaxation in ultrathin, 25-nm-thick 98/2 and 95/5 P(S/nBA) films at 130 °C. The times that are required for 25-nm-thick 98/2 and 95/5 P(S/nBA) films to completely relax the residual stress at 130 °C are ~5 h and ~7 h, respectively, which are nearly the same as those for bulk films. In other words, the 98/2 and 95/5 P(S/nBA) films exhibit little or no effect of nanoscale confinement on stress relaxation.

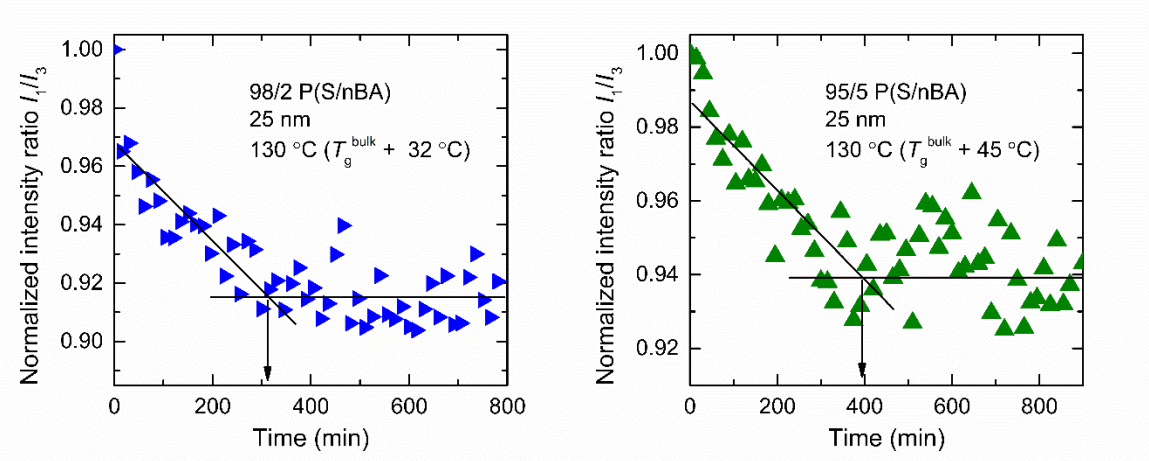

Figure 7-4. Fluorescence characterization of I_1/I_3 values as a function of anneal time for ultrathin 98/2 and 95/5 P(S/nBA) film at 130 °C.

We note that the T_gs of the 25-nm-thick 98/2 and 95/5 P(S/nBA) films are expected to be slightly lower than those of the bulk films. Past research has shown that T_gs of polymer films

exhibit a dependence on thickness when the films are sufficiently thin (Keddie et al., 1994a, 1994b; Forrest et al., 1997; Mundra et al., 2007; Grohens et al., 1998; Kawana & Jones, 2001; J. H. Kim et al., 2001; Tsui et al., 2001; Ellison & Torkelson, 2003; Fakhraai & Forrest, 2005; Roth et al., 2006; Bäumchen et al., 2012; Lan & Torkelson, 2014; Vignaud et al., 2014; Geng & Tsui, 2016; Jin & Torkelson, 2016; L. Zhang et al., 2016; T. Wang et al., 2019; Evans & Torkelson, 2012; S. Kim et al., 2008; Mundra et al., 2006). For polymer films without strong attractive interactions with a substrate, nanoscale confinement will cause T_g to decrease with decreasing film thickness. In contrast, if sufficiently strong attractive interactions such as hydrogen bonding are present in the polymer–substrate interface, an increase in T_g with decreasing film thickness will be observed. Kim et al. reported via ellipsometry-based characterization that the T_g of a 23-nm-thick PS film supported on silicon slide exhibits a ~10 °C decrease compared to that of a bulk film (S. Kim et al., 2009). For the glass-supported P(S/nBA) films characterized in this study, the nBA units can undergo attractive hydrogen bonding interactions with the hydroxyl groups on glass surface. This substrate effect will counteract the free-surface effect and lead to a suppressed overall T_g-confinement effect compared to neat PS.

As determined by ellipsometry, the T_gs of ultrathin, 26-nm-thick 98/2 and 95/5 P(S/nBA) films are 3 ± 1 °C and 4 ± 1 °C lower than the T_g^{bulk} values (Wang et al. 2022). Therefore, although the ultrathin films in Figure 7-4 were annealed at the same absolute temperature of 130 °C as the bulk films in Figure 7-3(b) and (d), the ultrathin films were annealed at slightly higher relative temperatures above the film T_g. Nevertheless, the results indicate that at a specific absolute temperature, the relaxation timescales of 98/2 and 95/5 P(S/nBA) films remain invariant or little changed with nanoscale confinement.

7.4 Conclusions

We used ellipsometry and fluorescence to characterize the residual stress relaxation in spin-coated P(S/nBA) films at low nBA content. The annealing times determined by the two techniques to fully relax the residual stress at a certain annealing temperature agree qualitatively but not quantitively with each other due to the difference in the resolution of the techniques. Nevertheless, both characterization methods show that the residual stress relaxation timescales of spin-coated P(S/nBA) films are significantly, and sometimes dramatically, impacted by the presence and the molar content of nBA in the copolymers. The presence of a few mole percent of nBA can vastly change the relaxation behaviors from those of neat PS films. With 5 mol% nBA, the residual stress relaxation process of bulk 95/5 P(S/nBA) films occurs over a significantly extended period of time compared to neat PS films. This phenomenon has been hypothesized to be related to dipole–dipole interactions between the nBA units. Future studies are needed to test this hypothesis.

Acknowledgements

This work was done in collaboration with Tong Wang and Tong Wei from the Torkelson research group at Northwestern University.

CHAPTER 8

Effects of Attractive Interfacial Interactions on Local, Nanoscale Stiffness of Supported Copolymer Adhesive Films

8.1 Introduction

Pressure-sensitive adhesives are an important class of materials that can adhere to various heterogeneous substrates by applying light pressure (Creton, 2003; Moon et al., 2018; Pocius, 2012; Tiu et al., 2019). They are widely used in a broad range of industries including electronics, biomedical devices, office supplies, and displays. Commercial pressure-sensitive adhesives are mixtures of viscoelastic polymers, tackifiers, stabilizers, etc. (Abbott, 2015) The bonding process of pressure-sensitive adhesives is physical in nature (Creton, 2003). The viscous characteristics of pressure-sensitive adhesives allow them to quickly wet and bond to a surface upon application onto substrates, whereas the elastic characteristics resist deformation once adhered (Dobson et al., 2020; Feldstein & Siegel, 2012; Fuensanta & Martín-Martínez, 2020). Significant research effort in the adhesion community has been devoted to understanding the correlations between the bulk viscoelastic behaviors and adhesion of pressure-sensitive adhesives (Chang, 1997; S. Kim et al., 2021; Marin & Derail, 2006; Sun et al., 2013; H. W. H. Yang & Chang, 1997; Yarusso, 1999). Although some general trends exist with respect to bulk rheology versus pressure-sensitive adhesive performance, such correlations often break down especially for systems with complex compositions or formulations.

It is well-known that adhesion depends strongly on the substrate, implying that besides bulk viscoelasticity, interfacial properties at the adhesive–substrate interface may also affect the performance of pressure-sensitive adhesives. Past studies have demonstrated the important role of

interfaces and interfacial effects on key properties of polymer thin films (Ellison & Torkelson, 2002, 2003; Jin & Torkelson, 2016; Keddie et al., 1994b; Keddie & Jones, 1995; S. Kim et al., 2009; Mundra et al., 2006; Napolitano et al., 2017; Priestley et al., 2005; Pye & Roth, 2011; Shavit & Riggleman, 2014; T. Wang et al., 2019; Watcharotone et al., 2011). For example, the glass transition temperatures (T_gs) of polymer films exhibit a dependence on thickness when the films are sufficiently thin (Ellison & Torkelson, 2003; Keddie et al., 1994b; Keddie & Jones, 1995; S. Kim et al., 2009; Mundra et al., 2006; Napolitano et al., 2017; Pye & Roth, 2011; T. Wang et al., 2019). Keddie *et al.* (Keddie et al., 1994b) studied poly(methyl methacrylate) (PMMA) films supported on silica and observed an increase in T_g with decreasing film thickness. They proposed that the attractive hydrogen bonding interactions between PMMA and the substrate, which reduce cooperative segmental mobility at the polymer–substrate interface and increase T_g, were dominant over free surface effects that enhance cooperative segmental mobility and reduce T_g, causing an increase in overall T_g of the film upon nanoscale confinement (Keddie et al., 1994b). Interfacial effects on polymer properties have also been demonstrated through stiffness-confinement effects (Askar & Torkelson, 2016; Briscoe et al., 1998; Brune et al., 2016; Cheng et al., 2007; Delcambre et al., 2010; Evans et al., 2012; Forrest et al., 1998; Gomopoulos et al., 2009, 2010; Inoue et al., 2005, 2006; Lee et al., 1996; Y. Liu et al., 2015; Song et al., 2019; Stafford et al., 2004, 2006; Torres et al., 2012; Tweedie et al., 2007; Watcharotone et al., 2011; Xia et al., 2016; Xia & Keten, 2015; Xia & Lan, 2019; S. Xu et al., 2010; M. Zhang et al., 2017, 2018). Askar and Torkelson (Askar & Torkelson, 2016) used a novel fluorescence-based approach to characterize the stiffness of polystyrene (PS) films supported on glass and found that the stiffness of PS film is subjected to combined perturbations from the substrate and free-surface interfaces; for sufficiently thin PS

films, enhancement effects near the substrate dominate over the reduction effects near the free surface, leading to an enhancement of overall stiffness.

Inspired by these past studies, in the current study, we investigate the influence of attractive polymer–substrate interactions on modulus/stiffness of supported polymer films near the substrate interface. The investigation was performed on poly(styrene/*n*-butyl acrylate) (P(S/nBA)) random copolymer films, where P(S/nBA) is a model pressure-sensitive adhesive system given that both styrene and *n*-butyl acrylate are commonly employed monomers in pressure-sensitive adhesive formulations. Modulus/stiffness-confinement effects have been studied for nearly as long as T_g-confinement effects; however, various past studies are conflicting, and general trends regarding stiffness-confinement behavior still remain unclear. Inoue et al. (Inoue et al., 2006) used incoherent neutron scattering to measure changes in mean-squared displacement $\langle u^2 \rangle$, which is inversely proportional to glassy-state modulus, of PS films supported on glass. It was found that $\langle u^2 \rangle$ decreases significantly in 40-nm-thick films relative to bulk response, indicating an increase in modulus with nanoconfinement. In contrast, Stafford et al. (Stafford et al., 2004) used a buckling-based metrology to measure the elastic properties of polydimethylsiloxane-supported PS films and showed that the apparent modulus of the films decreases with decreasing film thickness at ~40 nm and below. One explanation for such conflicting results is that stiffness-confinement effects in supported polymer films originate from the disparity between the rigidity of polymers and substrates. The majority of past studies have shown that stiffness of supported polymer films is enhanced near a rigid substrate and reduced near a soft substrate. However, besides rigidity, what are the effects of interfacial interactions on stiffness-confinement effects?

Here, we provide the first investigation of the impact of attractive hydrogen bonding interactions on local stiffness and stiffness gradient length scales in supported polymer films. We

isolated the effect of interfacial interactions from substrate rigidity on stiffness of supported P(S/nBA) films by using the same substrate species (glass) throughout the study and tuning the attractive hydrogen bonding interactions between the films and the substrates by varying the copolymer composition and the substrate surface hydrophilicity. Stiffness characterization was achieved by a self-referencing fluorescence-based method developed by Torkelson and coworkers (Askar et al., 2015; Askar & Torkelson, 2016; M. Zhang et al., 2017). This technique relies on the environmental sensitivity of a pyrenyl label covalently attached at trace levels to polymer chains, from the fluorescence emission spectrum of which qualitative characterizations of local molecular caging state and hence stiffness can be achieved. Details regarding principles of fluorescence spectroscopy and its use to characterize stiffness are provided in Chapter 6.

We discovered that attractive polymer–substrate hydrogen bonding interactions have an enhancement effect on the stiffness of P(S/nBA) films, and the length scale over which substrate perturbations modify the average stiffness depends significantly on the strength of the attractive interactions. When the hydroxyl groups on a glass surface are removed to prevent the formation of hydrogen bonds, the perturbation length scale of substrate effects on stiffness decreases accordingly. Thus, in addition to the substrate rigidity effect, our study shows for the first time that interfacial effects are an important contributor to stiffness-confinement effects of supported polymer films. This work can help to establish the correlation between interfacial properties and pressure-sensitive adhesive performance and have the potential to contribute to a better pressure-sensitive adhesive design.

8.2 Experimental Methods

8.2.1 Materials

Styrene (Sigma-Aldrich, 99%) and *n*-butyl acrylate (nBA, Sigma-Aldrich, 99%) were deinhibited using *tert*-butylcatechol inhibitor remover (Sigma-Aldrich) and monomethyl ether hydroquinone inhibitor remover (Sigma-Aldrich) and dried over calcium hydride overnight. Pyrenylmethyl methacrylate (MPy) was synthesized by esterification of methacryloyl chloride (Sigma-Aldrich) and 1-pyrenyl methanol (Sigma-Aldrich) following synthesis procedures previously described by Ellison and Torkelson (Ellison & Torkelson, 2002). Benzoyl peroxide (BPO) was purchased from Sigma-Aldrich. Toluene, methanol, tetrahydrofuran (THF, HPLC grade), sulfuric acid, and hydrogen peroxide were purchased from Fisher Chemical.

8.2.2 Synthesis of P(S/nBA) random copolymers

Poly(styrene/*n*-butyl acrylate) random copolymers were synthesized by bulk free radical polymerization at 60 °C using BPO (0.5 mg/mL monomer) as initiator. Monomer mixtures with different compositions were used to generate copolymers with various nBA contents. To synthesize MPy-labeled P(S/nBA)s, MPy was copolymerized at a trace level (0.5 mol% with respect to monomers) with other monomers. The as-synthesized random copolymers were washed seven times by dissolving in toluene and precipitating in methanol to remove residual initiators and monomers. The washed polymers were dried at 80 °C in a vacuum oven for three days prior to use.

8.2.3 Characterization of as-synthesized P(S/nBA) random copolymers

The labeling efficiency (moles of pyrene-labeled repeat units relative to moles of total repeat units) of MPy-labeled P(S/nBA)s was determined by UV−vis absorbance spectroscopy (Perkin-Elmer Lambda 35) using 0.1 mg/mL THF solutions of the copolymers. The absorbance

spectrum was measured at wavelengths from 280 nm to 380 nm, and the label concentration was determined from the absorbance of the peak at ~335 nm using Beer's law, where $A = \mathcal{E}lc$; $\mathcal{E}$ is 37300 $M^{-1} \cdot cm^{-1}$ for pyrene, and l is 1 cm.

The bulk glass transition temperatures (T_gs) were determined via differential scanning calorimetry (DSC, Mettler Toledo DSC822e). Each sample was first annealed at a temperature that is ~40 °C above the expected T_g for 15 min and cooled to ~40 °C below the expected T_g at a rate of 40 °C/min. For 5/95 P(S/nBA; the expected T_g is far below 0 °C. To determine the exact T_g value, the sample was cooled to −70 °C, which is the lowest temperature that the DSC cooler can reach. $T_{g,onset}$ values were obtained from the second heating cycle at a heating rate of 10 °C/min.

Molecular weight and dispersity were determined by gel permeation chromatography (GPC; Waters Breeze v3.20) coupled with a multiangle laser light-scattering detector (mini-Dawn, Wyatt Technologies). Properties of as-synthesized, unlabeled and MPy-labeled P(S/nBA)s are summarized in Table 8-1.

Table 8-1. Summary of properties for P(S/nBA)s used in this study.

P(S/nBA) (mol%/mol%)	M_n (kg/mol)	Dispersity[a]	$T_{g,\,onset}$ (°C) by DSC	Labeling efficiency (mol%)
Blank 5/95	2000	1.16	−43	-
Labeled 5/95	1800	1.29	−43	1.2
Blank 33/67	1200	1.22	−13	-
Labeled 33/67	1400	1.35	−13	1.3
Blank 59/41	520	1.23	29	-
Labeled 59/41	670	1.26	30	1.0
Blank 95/5	390	1.37	85	-
Labeled 95/5	450	1.36	85	1.2

[a]Dispersity is low because low-molecular-weight polymers have been removed during the seven-times dissolution and precipitation purification step.

8.2.4 Substrate preparation

Hydrophilic glass substrates were prepared by submerging glass slides in piranha solution (75 vol% sulfuric acid/25% hydrogen peroxide) at 90 °C for 1 h. Then, substrates were thoroughly rinsed with deionized water and dried under rapid nitrogen flow. Water contact angles on substrates were measured using a Kruss DSA100 drop shape analyzer. Static contact angles of deionized water were measured at ambient temperature using the sessile drop method with a drop volume of 3 μL. The measured water contact angle on hydrophilic glass is ~15°. Hydrophobic glass substrates were prepared by surface modification of the hydrophilic glass with toluene solution of dichlorodimethylsilane. Glass slides that were pre-cleaned with piranha solution were submerged in a toluene solution of dichlorodimethylsilane (5 vol% dichlorodimethylsilane/95 vol% toluene) for 2 h. Then, the slides were rinsed with pure toluene, placed in methanol for 15 min, and dried under rapid nitrogen flow. After modification, the hydroxyl groups on hydrophilic glass surface were replaced with methyl groups. The measured water contact angle on hydrophobic glass substrates is ~105°. A schematic representation of the hydrophilic and hydrophobic glass substrates is shown in Scheme 8-1.

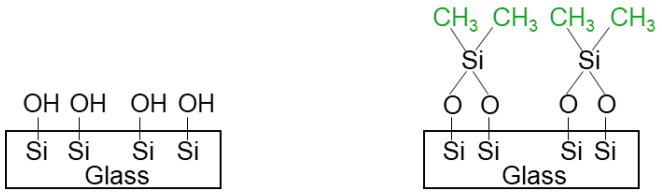

Scheme 8-1. Representative figures of hydrophilic glass substrates (left) and hydrophobic glass substrates (right).

8.2.5 Film preparation

To prepare bilayer films, toluene solutions of blank and MPy-labeled P(S/nBA)s (containing 0.5 wt% to 6.0 wt% polymers) were spin-coated onto sodium chloride (NaCl) disks and glass substrates, respectively, with spin speeds ranging from 1400 to 2100 rpm to yield single-layer, NaCl-supported, bulk, unlabeled P(S/nBA) films and single-layer, glass-supported, MPy-labeled P(S/nBA) films of various thickness. After spin coating, single-layer films were annealed at elevated temperatures under vacuum to remove the residual stress and solvent. Annealing temperatures and time were different for each copolymer species and were determined based on residual stress relaxation characterization results obtained by fluorescence. The procedures for characterizing residual stress relaxation timescales using fluorescence were discussed in Chapter 7.

After annealing, NaCl-supported, bulk, unlabeled P(S/nBA) films were transferred at room temperature to the top of glass-supported, MPy-labeled P(S/nBA) films by a water transfer technique to yield bilayer films. The water transfer technique has been extensively used by Torkelson and coworkers to prepare bilayer films and study the interfacial effects on polymer properties (Askar & Torkelson, 2016; Ellison & Torkelson, 2003; Evans et al., 2012; Priestley et al., 2005; Roth et al., 2007; Roth & Torkelson, 2007). Residual water in the bilayer films was evaporated overnight under vacuum at the room temperature. For P(S/nBA)s with T_gs higher than the room temperature, bilayer films were further annealed at T_g + 20 °C for 2 h to heal the two layers together prior to fluorescence characterization. A schematic representation of the bilayer films is shown in Scheme 8-2.

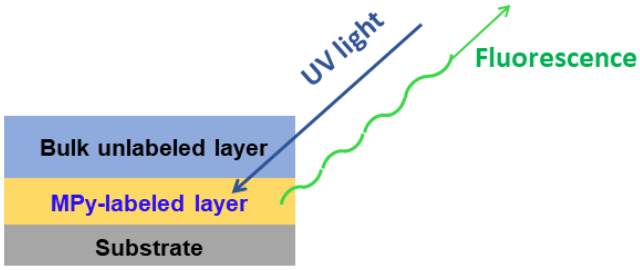

Scheme 8-2. Representative figure of the bilayer film. A MPy-labeled layer is spin-coated directly onto the substrate and covered with a bulk, 600-nm-thick, unlabeled layer to block any potential perturbations from the free-surface interface.

8.2.6 Ellipsometry

The thickness of a spin-coated polymer film is proportional to the solution concentration and inversely proportional to the spin speed (Emslie et al., 1958; Mouhamad et al., 2014). Different combinations of solution concentration and spin speed yield a wide range of thicknesses. To determine the film thickness for a specific combination of solution concentration and spin speed, polymer solutions were first spin-coated onto silica wafers and characterized at room temperature using spectroscopic ellipsometry (J. A. Woollam Co. M-2000D over a range of wavelengths from 400 to 1000 nm). The ellipsometric angles of incident light reflected off silica-supported films were measured and fitted to a Cauchy layer model to determine the thickness. The Cauchy layer model included a polymer layer atop a silicon substrate containing a 2-nm-thick silicon oxide surface layer. Once the exact thickness of the silica-supported films was known, polymer solutions were spin-coated onto desired substrates from the same solutions with the same spin speeds. With the same solution concentration and spin speed, the spin-coated films of a particular copolymer species were assumed to have the same thickness on all types of substrates.

8.2.7 Fluorescence spectroscopy

Fluorescence spectroscopy was used to characterize the intensity ratio of the first vibronic band peak to the third vibronic band peak (I_1/I_3) of MPy emission spectra, which reflects molecular caging and stiffness of MPy-labeled P(S/nBA) films. Emission spectra were collected (Photon Technology International fluorimeter in front-face geometry) at wavelengths from 374 nm to 392 nm (0.5 nm increment, 0.5 s integration) with excitation at 324 nm. Excitation and emission slit widths were 0.5 mm (1 nm bandpass). Typical fluorescence emission spectra of MPy covalently attached to P(S/nBA) backbones are shown in Figure 8-1. I_1/I_3 values were calculated from an average of five data points spanning a 2 nm window: I_1 was an average of data points between ~375.5 nm and ~377.5 nm, and I_3 was an average of data points between ~386.5 nm and ~388.5 nm. Emission spectra were collected from T_g + 40 °C to T_g – 40 °C, or from 80 °C to 0 °C for systems with T_gs lower than the ambient temperature, in 5 °C decrements. Before collecting a spectrum, films were held for 5 min at each temperature to enable thermal equilibration. Once spectra were collected, background noise was measured from the same film and was taken as the average emission intensity values between 350 nm and 352 nm where no emission peak is present and subtracted from the emission spectra.

8.3 Results and Discussion

The fluorescence-based, intensity ratio method for stiffness characterizations is based on the sensitivity of pyrene to changes in local molecular caging. Stiffness is related to high-frequency, short-time-scale molecular vibrations in materials; higher stiffness corresponds to a more caged environment in which such vibrations are suppressed. Pyrene belongs to a class of fluorophores known as vibronic coupling dyes which exhibit overlapping excited-state energy levels. Caged

environments can mediate or separate the overlapping energy levels and cause changes in the spectral shape of pyrene fluorescence emission, with enhancements in high-energy (low-wavelength) emissions at the expenses of low-energy (high-wavelength) emissions. As such, in stiffer environments, I_1/I_3 of pyrene fluorescence emission spectrum increases as a result of greater caging.

As illustrated in Scheme 8-2, a bilayer film geometry was employed for stiffness characterizations. MPy-labeled P(S/nBA) substrate layers were placed adjacent to the substrate to provide direct characterizations of the stiffness response near the substrate interface. The thickness of the MPy-labeled underlayer is varied to determine the stiffness gradient length scales over which the stiffness of a supported film is impacted by the presence of a substrate. A bulk, unlabeled P(S/nBA) layer is placed atop the MPy-labeled substrate layer to block any potential perturbations from the free surface interface.

Attractive hydrogen bonding interactions between P(S/nBA) films and glass substrates were first tuned by varying the copolymer composition. The ester groups in nBA units act as hydrogen bond acceptors and can hydrogen-bond to hydroxyl groups on the piranha-treated, hydrophilic glass surface. With increasing nBA molar content, the hydrogen bonding interactions are expected to be stronger due to a higher number of moieties that can participate the interactions. We synthesized a series of P(S/nBA)s with nBA molar content ranging from 41 mol% to 95 mol% and characterized the stiffness of the substrate-adjacent layer by fluorescence. Figure 8-1 shows representative spectra of MPy-labeled P(S/nBA) substrate layers within bilayer films collected with the 59/41 P(S/nBA) at 80 °C. Locations of the first and third vibronic peaks are indicated with arrows, and spectra are normalized relative to I_1. It can be seen clearly from Figure 8-1 that I_1/I_3 progressively increases with decreasing thickness of the MPy-labeled substrate layer,

indicating greater molecular caging and hence higher stiffness in regions closer to the substrate interface.

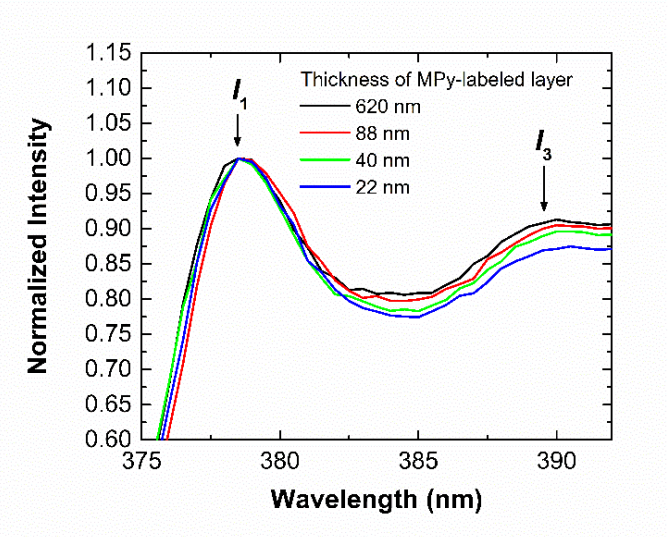

Figure 8-1. Fluorescence emission spectra at 80 °C for MPy-labeled 59/41 P(S/nBA) layers placed directly adjacent to the substrate within bilayer films. Locations of the first and third vibronic peaks are indicated. Intensities are normalized relative to I_1.

Figure 8-2 summarizes I_1/I_3 values of MPy-labeled substrate layers within bilayer 95/5, 59/41, 33/67, and 5/95 P(S/nBA) films supported on hydrophilic glass substrates measured at different temperatures. For 95/5 and 59/41 P(S/nBA)s, measurements were taken at temperatures both above and below T_g; for 33/67 and 5/95 P(S/nBA)s, measurements were only taken at temperatures above T_g given that the T_gs of 33/67 and 5/95 P(S/nBA)s are too low, and the temperature controller coupled with the fluorimeter is incapable to reach temperatures below their T_gs. Figure 8-2(a) shows the results associated with 95/5 P(S/nBA) films. At all tested temperatures, I_1/I_3 of the MPy-labeled 95/5 P(S/nBA) substrate layers remains invariant (within experimental error) with decreasing substrate-layer thickness down to 88 nm, which suggests an unchanged molecular caging state and hence stiffness across a broad film thickness range. I_1/I_3 starts to exhibit

increasing values at 65 nm and below, indicating that the film stiffens when approaching the substrate, and the perturbations from the substrate interface extend far enough to perturb the overall stiffness response of a 65-nm-thick layer. The enhancement effects on stiffness from the substrate interface can be attributed to two factors: first, as reported by Askar et al. (Askar & Torkelson, 2016) as well as the majority of other studies on stiffness/modulus-confinement effects, rigid substrates have inherent stiffening effects on supported polymer films in the polymer–substrate interfacial region as a result of greater caging near the substrates; second, the hydrogen bonding interactions between the film and the substrate may also contribute to the stiffening effects, though this is less likely to be the case for 95/5 P(S/nBA) since there is only 5 mol% nBA present.

Figures 8-2(b), 8-2(c), and 8-2(d) show I_1/I_3 values of P(S/nBA) films as nBA molar content in the copolymers is gradually increased. Similar to the observations in Figure 8-2(a), at all tested temperatures, I_1/I_3 of the MPy-labeled substrate layer first remains invariant (within experimental error) with decreasing substrate-layer thickness and then exhibits increasing values starting at a particular thickness. The thickness below which I_1/I_3 was observed to exceed the bulk values for each copolymer species, which is considered as the perturbation length scale associated with substrate effects on film stiffness, is summarized in Table 8-2. Overall, on hydrophilic glass, the substrate effects perturb the average stiffness of a supported film over a greater length scale with increasing nBA molar content. A higher nBA content corresponds to a stronger hydrogen bonding interactions between the films and the hydrophilic substrates due to a higher number of moieties that can participate the hydrogen bonding. Therefore, these results indicate that besides substrate rigidity, stiffness of supported polymer films near the substrate is also impacted by interfacial interactions. Attractive hydrogen bonding interactions restrict the molecular vibrations immediately next to the substrate. With increasing nBA content, the stronger interfacial

interactions restrict the vibrations to a greater extent; the restricted segments further impact the vibrations within their neighbors and lead to an increased perturbation length scale over which the stiffness of the film is impacted or modified.

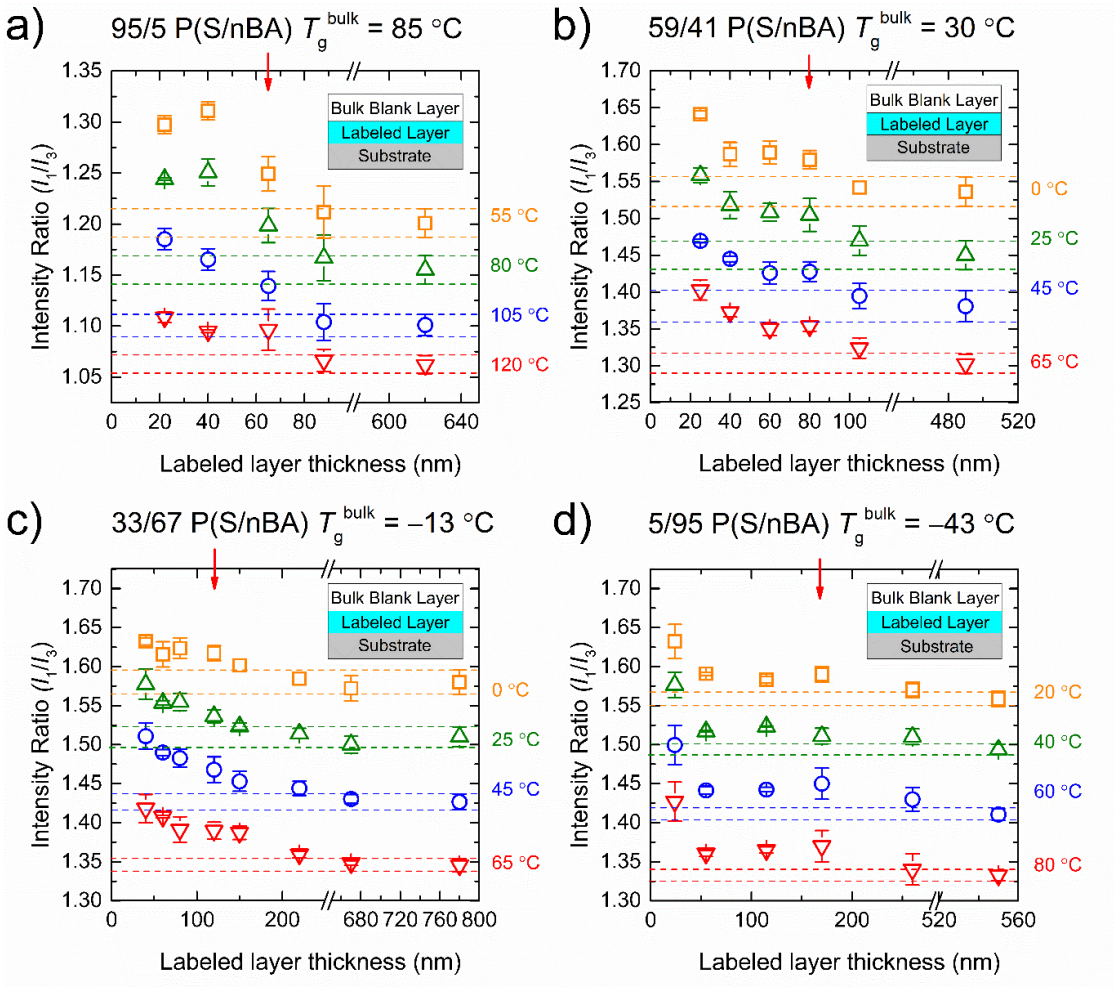

Figure 8-2. Fluorescence I_1/I_3 values as a function of MPy-labeled substrate-layer thickness within bilayer films of (a) 95/5 P(S/nBA), (b) 59/41 P(S/nBA), (c) 33/67 P(S/nBA), and (d) 5/95 P(S/nBA) films supported on hydrophilic glass substrates. Measurements were taken in both the rubbery and the glassy state for 95/5 and 59/41 P(S/nBA)s and only in the rubbery state for 33/67 and 5/95 P(S/nBA)s. Error bars are associated with three measurements on three separate samples. Dashed lines indicate the *I*1/*I*3 values for the thickest films in each data set.

Table 8-2. Summary of length scales over which substrate perturbations modify the stiffness response of P(S/nBA)s extending from the polymer–substrate interface on hydrophilic and hydrophobic glass substrates.

P(S/nBA) (mol%/mol%)	Perturbation length scale on hydrophilic glass (nm)	Perturbation length scale on hydrophobic glass (nm)
95/5	~65	-
59/41	~80	~60
33/67	~120	~60
5/95	~170	~60

To confirm our findings, we performed substrate modifications to change the hydrophilicity of the glass substrates. We treated the hydrophilic glass substates by silanization using a toluene solution of dichlorodimethylsilane to replace the hydroxyl groups on the substrate surface with methyl groups. After the surface modification, the water contact angle of the substrates increases from ~15° to ~105°, representing a significant decrease in surface hydrophilicity. Figure 8-3 summarizes I_1/I_3 values of MPy-labeled substrate layers within bilayer 59/41, 33/67, and 5/95 P(S/nBA) films supported on hydrophobic glass substrates measured at different temperatures. Measurements were not performed on 95/5 P(S/nBA) films given that this system contains only 5 mol% nBA, and substrate modification would likely not yield observable changes to the fluorescence results. Similar to the characterizations associated with films supported on hydrophilic glass, measurements for hydrophobic-glass-supported films were taken at temperatures both above and below T_g for 95/5 and 59/41 P(S/nBA)s and only at temperatures above T_g for 33/67 and 5/95 P(S/nBA)s.

Figure 8-3 shows that on hydrophobic glass, with decreasing labeled-layer thickness, I_1/I_3 exceeds the bulk values and further increases at a particular thickness and below at all tested temperatures, indicating that the stiffness of P(S/nBA) films is enhanced near the substrate interface despite the absence of attractive interfacial interactions. A summary of the perturbation

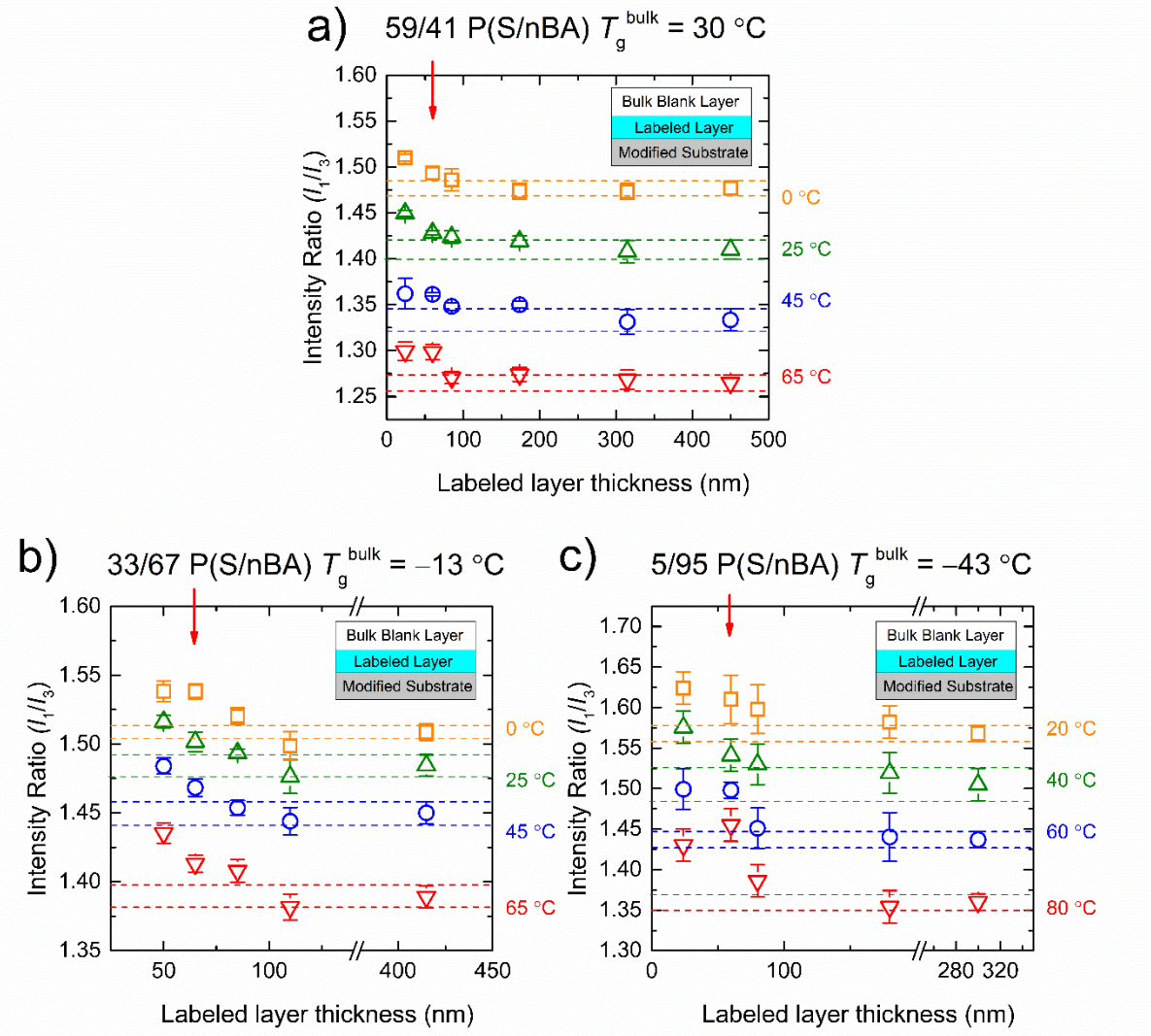

Figure 8-3. Fluorescence I_1/I_3 values as a function of MPy-labeled-layer thickness within bilayer films of (a) 59/41 P(S/nBA), (b) 33/67 P(S/nBA), and (c) 5/95 P(S/nBA) films supported on hydrophobic glass. Measurements were taken in both the rubbery and glassy state for 59/41 P(S/nBA) and only in the rubbery state for 33/67 and 5/95 P(S/nBA). Error bars are associated with three measurements on three separate samples. Dashed lines indicate the $I1/I3$ values for the thickest films in each data set.

length scales associated with substrate effects on hydrophobic glass for each P(S/nBA) system is shown in Table 8-2. For a particular P(S/nBA) species, the substrate-perturbation length scale decreases after the hydroxyl groups on glass surface were removed. The reduction in perturbation

length scale is more significant for P(S/nBA)s with higher nBA content: for 5/95 P(S/nBA), the length scale decreases by ~110 nm, whereas for 59/41 P(S/nBA), the length scale only decreases by ~20 nm. In addition, regardless of the copolymer composition, the substrate-perturbation length scales for all three P(S/nBA) systems are within error the same on hydrophobic glass, which is ~60 nm. On hydrophobic glass, P(S/nBA) films are no longer able to undergo attractive hydrogen bonding interactions with the substrate due to the absence of hydrogen bond donors. In this case, the enhancement in stiffness mainly originates from the inherent stiffening effects of a rigid substrate, which are comparable for all three P(S/nBA) systems studied, thus leading to a uniform substrate-perturbation length scale.

The uniform, ~60-nm perturbation length scale associated with hydrophobic glass is very close to the length scale for 95/5 P(S/nBA) films supported on hydrophilic glass (~66 nm); in the latter case, although hydrogen bond donors exist on substrate surface, hydrogen bonding interactions are weak due to the very low nBA molar content. We note that the substrate-perturbation length scales for all P(S/nBA) films supported on hydrophobic glass are shorter compared to that of PS films supported on hydrophilic glass reported by Askar and Torkelson (Askar & Torkelson, 2016). In PS films, there are no functional groups that can form attractive interactions with the hydrophilic substrate surface, so the substrate perturbations to stiffness should solely originate from the inherent stiffening effect of a rigid substrate material. However, for hydrophilic-glass-supported PS films, the substrate perturbations extend over at least 200 nm from the substrate interface as reported by Askar and Torkelson (Askar & Torkelson, 2016), which is substantially longer compared to the ~60-nm length scale associated with P(S/nBA) films supported on hydrophobic glass. The substrate-perturbation length scale for PS films is even longer than those associated with all four P(S/nBA) systems supported on hydrophilic glass characterized

in this study, although the P(S/nBA) films contain various amount of nBA units that can form attractive hydrogen bonding interactions with the hydrophilic substrate surface. A possible explanation is that P(S/nBA) and PS are inherently different materials, so the perturbation length scales for the two polymers cannot be directly compared. Chapter 7 discussed about the ability of a very small amount of nBA units to significantly modify the residual stress relaxation behavior of P(S/nBA) relative to PS films, so it is possible that the presence of nBA units in P(S/nBA) films also significantly changed the short-time-scale molecular vibrations related to the stiffness of materials relative to neat PS.

Based on the fluorescence characterization results of P(S/nBA) films supported on hydrophilic and hydrophobic glass, we can conclude that the stiffness of supported P(S/nBA) films can be substantially enhanced near the substrate interface by attractive hydrogen bonding interactions. The length scale over which substrate perturbations modify the average stiffness of supported P(S/nBA) films depends strongly on the number of moieties that can participate in the hydrogen bonding. On hydrophilic glass where the total number of hydroxyl groups on the substrate surface is maximized by treatment with Piranha solution, the length scale of substrate perturbations to stiffness increases with increasing nBA molar content. This effect is due to the ability of ester groups in nBA units to hydrogen-bond to the surface hydroxyl groups. On hydrophobic glass where all hydroxyl groups on glass surface are replaced with methyl groups, the length scale of substrate perturbations to stiffness becomes independent of nBA molar content, and all P(S/nBA)s exhibit the same length scale because no hydrogen bonding interaction is allowed to form in the interfacial region.

8.4 Conclusions

We investigated the effect of attractive hydrogen bonding interactions on stiffness of supported P(S/nBA) films in the polymer–substrate interfacial region. The hydrogen bonding interactions between P(S/nBA) films and glass substrates were tuned by two methods. In the first method, nBA molar content in P(S/nBA)s is gradually increased to yield stronger hydrogen bonding interactions between the films and the hydrophilic substrate surface. In the second method, hydroxyl groups on hydrophilic glass were removed by substrate modifications to yield hydrophobic substrate surface that prevents the formation of hydrogen bonds. Fluorescence characterizations show that both hydrophilic and hydrophobic glass substrates enhance the stiffness of supported P(S/nBA) films in the interfacial region. On hydrophilic glass, the length scale over which substrate perturbations propagate into the films and modify the average stiffness response near the substrate increases from 66 to 180 nm when nBA molar content is increased from 5 to 95 mol%. On hydrophobic glass, the length scale of substrate perturbations to stiffness of P(S/nBA)s is independent of nBA content, with all P(S/nBA)s exhibit a same length scale of ~60 nm. Thus, this study shows that in addition to substrate rigidity, attractive interfacial interactions can also modify the stiffness of supported polymer films near the substrate. Future comparisons of the findings from this study with adhesion test results on the same model pressure-sensitive adhesives systems has the potential to help better understand pressure-sensitive adhesives performance.

Acknowledgements

This work was done in collaboration with Tong Wang and Tong Wei from the Torkelson research group at Northwestern University.

CHAPTER 9

Interfacial Stiffness and Stiffness Gradient Length Scales Near Substrates in Supported Poly(Styrene/2-Ethylhexyl acrylate) Films

9.1 Introduction

Modulus/stiffness-confinement effects in polymer films have been studied using a range of techniques for a variety of polymer/substrate pairs (Askar & Torkelson, 2016; Briscoe et al., 1998; Brune et al., 2016; Cheng et al., 2007; Delcambre et al., 2010; Evans et al., 2012; Forrest et al., 1998; Gomopoulos et al., 2009, 2010; Inoue et al., 2005, 2006; Lee et al., 1996; Y. Liu et al., 2015; Song et al., 2019; Stafford et al., 2004, 2006; Torres et al., 2012; Tweedie et al., 2007; Watcharotone et al., 2011; Xia et al., 2016; Xia & Keten, 2015; Xia & Lan, 2019; S. Xu et al., 2010; M. Zhang et al., 2017, 2018). Most investigations are performed on homopolymers, and little research effort has focused on behaviors of random copolymers. Random or statistical copolymers are important both scientifically and industrially because they combine chemical and physical properties of two or more different monomers while not causing phase separation. Chapter 8 investigated the perturbations originating at the substrate interface to stiffness of supported poly(styrene/*n*-butyl acrylate) (P(S/nBA)) films, where P(S/nBA)s are model pressure-sensitive adhesives given that styrene and *n*-butyl acrylate (nBA) are both common monomers used in pressure-sensitive adhesive formulations. The stiffness characterization was achieved via a self-referencing fluorescence technique which relies on a measurable intensity ratio $I1/I3$ of a pyrenyl dye covalently attached to polymer backbones that increases in caged and hence stiff environments (Kalyanasundaram & Thomas, 1977). Details regarding principles of fluorescence spectroscopy and its use to characterize stiffness are discussed in Chapter 6.

In Chapter 8, attractive hydrogen bonding interactions between ester groups in P(S/nBA) and hydroxyl groups on a glass substrate surface were found to lead to enhancement in stiffness of P(S/nBA) films in the polymer–substrate interfacial region. With increasing nBA molar content in the copolymer, the length scale associated with the enhancement in average stiffness near the substrate interface increases because of the increasing number of moieties that can participate in the formation of hydrogen bonds. A better understanding of interfacial stiffness in supported copolymer adhesives is potentially helpful for better pressure-sensitive adhesive designs because stiffness is related to glassy-state modulus and hence adhesion of pressure-sensitive adhesives. Here, we use the same fluorescence-based characterization approach to investigate the interfacial stiffness in another acrylic-based random copolymer, poly(styrene/2-ethylhexyl acrylate) (P(S/EHA)). 2-ethylhexyl acrylate (EHA) is an acrylic monomer that is commonly employed in pressure-sensitive adhesive formulations. 2-ethylhexyl acrylate has been found beneficial to pressure-sensitive adhesive performance because of its ability to lead to copolymers with low T_gs and hence good wetting with substrates. To understand the effect of a slight change in monomer structure from nBA to EHA on interfacial stiffness and substrate effects in supported acrylic-based random copolymer films, we synthesized a series of P(S/EHA)s with bulk T_gs similar to some of the P(S/nBA)s studied in Chapter 8 and used fluorescence to characterize stiffness in the interfacial region of films supported on hydrophilic and hydrophobic glass substrates. We discovered that P(S/EHA)s exhibit dramatically different substrate effects and stiffness gradient length scale from those of P(S/nBA)s with similar bulk T_gs.

9.2 Experimental Methods

9.2.1 Materials

Styrene (Sigma-Aldrich, 99%) and 2-ethylhexyl acrylate (EHA, Sigma-Aldrich, 98%) were deinhabited using tert-butylcatechol inhibitor remover (Sigma-Aldrich) and monomethyl ether hydroquinone inhibitor remover (Sigma-Aldrich), respectively, and dried over calcium hydride overnight. Pyrenylmethyl methacrylate (MPy) was synthesized by esterification of methacryloyl chloride (Sigma-Aldrich) and 1-pyrenyl methanol (Sigma-Aldrich) following synthesis procedures previously described by Ellison and Torkelson (Ellison & Torkelson, 2002). Benzoyl peroxide (BPO) was purchased from Sigma-Aldrich. Toluene, methanol, tetrahydrofuran (THF, HPLC grade), sulfuric acid, and hydrogen peroxide were purchased from Fisher Chemical.

9.2.2 Synthesis of P(S/EHA) random copolymers

Poly(styrene/2-ethylhexyl acrylate) random copolymers with various EHA molar content were synthesized via bulk free radical polymerization at 60 °C using BPO (0.5 mg/mL monomer) as initiator. To synthesize MPy-labeled P(S/EHA)s, MPy was copolymerized at trace levels with the monomers. The as-synthesized random copolymers were washed for seven times by dissolving in toluene and precipitating in methanol to remove residual initiators and monomers. The washed polymers were dried at 80 ℃ in a vacuum oven for 3 days prior to use.

9.2.3 Characterization of as-synthesized P(S/EHA) random copolymers

The labeling efficiency (moles of pyrene-labeled repeat units relative to moles of total repeat units) of MPy-labeled P(S/EHA)s was determined by UV−vis absorbance spectroscopy (Perkin-Elmer Lambda 35) using 0.1 mg/mL THF solutions of the copolymers. The absorbance spectrum was measured at wavelengths from 280 nm to 380 nm, and the label concentration was determined from the absorbance of the peak at ~335 nm using Beer's law, where $A = \mathcal{E}lc$; $\mathcal{E}$ is

37300 $M^{-1} \cdot cm^{-1}$ for pyrene, and l is 1 cm.

The bulk glass transition temperatures (T_gs) were determined via differential scanning calorimetry (DSC, Mettler Toledo DSC822e). Each sample was first annealed at a temperature that is ~40 °C above the expected T_g^{bulk} for 15 min and cooled to ~40 °C below the expected T_g^{bulk} at a rate of 40 °C/min (for 27/73 P(S/EHA), the expected T_g^{bulk} is far below 0 °C. To determine the exact T_g^{bulk} value, the sample was cooled to −70 °C, which is the lowest temperature that the DSC cooler can reach). $T_{g,onset}$ values were obtained from the second heating cycle at a heating rate of 10 °C/min.

Molecular weight and dispersity were determined by gel permeation chromatography (GPC; Waters Breeze v3.20) coupled with a multiangle laser light-scattering detector (mini-Dawn, Wyatt Technologies). Properties of as-synthesized, unlabeled and MPy-labeled P(S/EHA)s are summarized in Table 9-1.

Table 9-1. Summary of properties for P(S/EHA)s used in this study.

P(S/EHA) (mol%/mol%)	M_n (kg/mol)	Dispersity[a]	$T_{g,\ onset}$ (°C) by DSC	Labeling efficiency (mol%)
Blank 94/6	400	1.39	85	-
Labeled 94/6	460	1.32	85	1.3
Blank 75/25	600	1.23	28	-
Labeled 75/25	630	1.25	28	1.3
Blank 27/73	710	1.27	−43	-
Labeled 27/73	590	1.37	−43	1.0

[a]Dispersity is low because low-molecular-weight polymers have been removed during the seven-times dissolution and precipitation purification step.

9.2.4 Substrate preparation

Hydrophilic glass substrates were prepared by submerging glass slides in piranha solution (75 vol% sulfuric acid/25% hydrogen peroxide) at 90 °C for 1 h. Then, substrates were thoroughly rinsed with deionized water and dried under rapid nitrogen flow. Water contact angles on substrates were measured using a Kruss DSA100 drop shape analyzer. Static contact angles of deionized water were measured at ambient temperature using the sessile drop method with a drop volume of 3 μL. The measured water contact angle on hydrophilic glass is ~15°. Hydrophobic glass substrates were prepared by surface modification of the hydrophilic glass with toluene solution of dichlorodimethylsilane. Glass slides that were pre-cleaned with piranha solution were submerged in a toluene solution of dichlorodimethylsilane (5 vol% dichlorodimethylsilane/95 vol% toluene) for 2 h. Then, the slides were rinsed with pure toluene, placed in methanol for 15 min, and dried under rapid nitrogen flow. After modification, the hydroxyl groups on hydrophilic glass surface were replaced with methyl groups. The measured water contact angle on hydrophobic glass substrates is ~105°. A schematic representation of the hydrophilic and hydrophobic glass substrates is shown in Scheme 9-1.

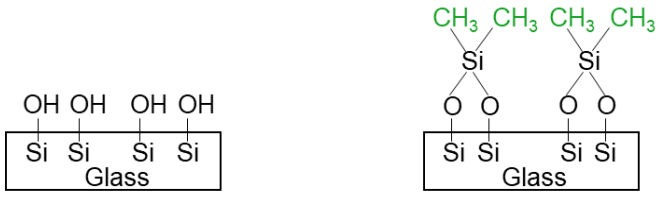

Scheme 9-1. Representative figures of hydrophilic glass substrates (left) and hydrophobic glass substrates (right).

9.2.5 Film preparation

Bilayer films were prepared as follows. Toluene solutions of neat and MPy-labeled P(S/EHA)s (containing 0.5 wt% to 6.0 wt% polymers) were spin-coated onto sodium chloride (NaCl) disks and glass substrates, respectively with spin speeds ranging from 1400 to 2100 rpm to yield NaCl-supported, single-layer, 600-nm-thick, unlabeled P(S/EHA) films and glass-supported, single-layer, MPy-labeled P(S/EHA) films with various thickness. After spin coating, single-layer films were annealed at elevated temperatures under vacuum to remove the residual stress and solvent. Annealing temperatures and time were determined based on residual stress relaxation characterization results obtained by fluorescence and were 130 °C for 8 h, 90 °C for 9 h, 25 °C for 12 h for 94/6, 75/25, and 27/73 P(S/EHA), respectively. The procedures for characterizing residual stress relaxation timescales using fluorescence were discussed in Chapter 7.

After annealing, NaCl-supported, bulk, unlabeled P(S/EHA) films were transferred at room temperature to the top of glass-supported, MPy-labeled P(S/EHA) films by a water transfer technique to yield bilayer films. The water transfer technique has been extensively used by Torkelson and coworkers to prepare bilayer films and study the interfacial effects on polymer properties (Askar & Torkelson, 2016; Ellison & Torkelson, 2003; Evans et al., 2012; Priestley et al., 2005; Roth et al., 2007; Roth & Torkelson, 2007). Residual water in the bilayer films was evaporated overnight under vacuum at the room temperature. For P(S/EHA)s with T_gs higher than the room temperature, bilayer films were further annealed at T_g + 20 °C for 2 h to heal the two layers together prior to fluorescence characterization. A schematic representation of the bilayer films is shown in Scheme 9-2.

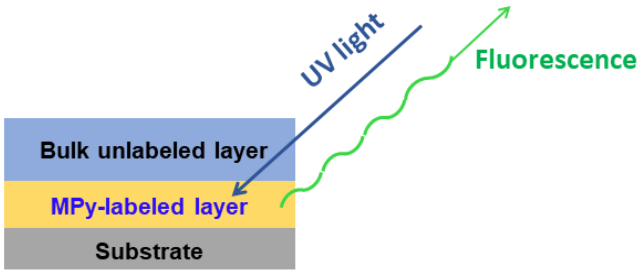

Scheme 9-2. Representative figure of the bilayer film. A MPy-labeled layer is spin coated directly onto the substrate. The MPy-labeled layer is covered with a bulk, 600-nm-thick, unlabeled layer to block any potential perturbations from the free-surface interface.

9.2.6 Ellipsometry

The thickness of a spin-coated polymer film is proportional to the polymer solution concentration and inversely proportional to the spin speed (Emslie et al., 1958; Mouhamad et al., 2014). Different combinations of solution concentration and spin speed yield a wide range of thickness. To determine the film thickness for a specific combination of solution concentration and spin speed, polymers were first spin-coated onto silica wafers and characterized at room temperature using spectroscopic ellipsometry (J. A. Woollam Co. M-2000D over a range of wavelengths from 400 to 1000 nm). The ellipsometric angles of incident light reflected off silica-supported films were measured and fitted to a Cauchy layer model to determine the thickness. The Cauchy layer model included a P(S/EHA) layer atop a silicon substrate containing a 2-nm-thick silicon oxide surface layer. Once the exact thickness of the silica-supported films was known, polymer solutions were spin coated onto desired substrates from the same solutions with the same spin speeds. With the same solution concentration and spin speed, the spin-coated films were assumed to have the same thickness on any types of substrates.

9.2.7 Fluorescence spectroscopy

Fluorescence spectroscopy was used to characterize the intensity ratio of the first vibronic band peak to the third vibronic band peak (I_1/I_3) of MPy emission spectra, which reflects the molecular caging state and hence stiffness of MPy-labeled films. Emission spectra were collected (Photon Technology International fluorimeter in front-face geometry) at wavelengths from 374 nm to 392 nm (0.5 nm increment, 0.5 s integration), with excitation at 324 nm. Excitation and emission slit widths were 0.5 mm (1 nm bandpass). Typical fluorescence emission spectra of MPy covalently attached to P(S/EHA) backbones are shown in Figure 9-1. I_1/I_3 values were calculated from an average of five data points spanning a 2 nm window: I_1 was an average of data points between ~375.5 nm and ~377.5 nm, and I_3 was an average of data points between ~386.5 nm and ~388.5 nm. Emission spectra were collected from T_g + 40 °C to T_g – 40 °C, or from 80 °C to 0 °C for systems with T_gs lower than the ambient temperature, in 5 °C decrements. Before collecting a spectrum, films were held for 5 min at each temperature to enable thermal equilibration. Once spectra were collected, background noise was measured from the emission intensity between 350 nm and 352 nm of the same film where no emission peak is present as subtracted from the emission spectra.

9.3 Results and Discussion

As illustrated in Scheme 9-2, a bilayer film geometry was employed for stiffness characterizations. MPy-labeled P(S/EHA) substrate layers were placed adjacent to the substrate to provide direct characterizations of the stiffness response near the substrate interface. The thickness of the MPy-labeled underlayer is varied to determine the stiffness gradient length scales over which the stiffness of a supported film is impacted by the presence of a substrate. A bulk, unlabeled

P(S/EHA) layer is placed atop the MPy-labeled substrate layer to block any potential perturbations from the free surface interface. Figure 9-1 shows representative spectra of MPy-labeled P(S/EHA) substrate layers within bilayer films collected with the 75/25 P(S/EHA) at 70 °C. Locations of the first and third vibronic peaks are indicated with arrows, and spectra are normalized relative to I_1. It can be seen clearly from Figure 9-1 that I_1/I_3 progressively increases with decreasing thickness of the MPy-labeled substrate layer, indicating greater molecular caging and hence higher stiffness in regions closer to the substrate interface.

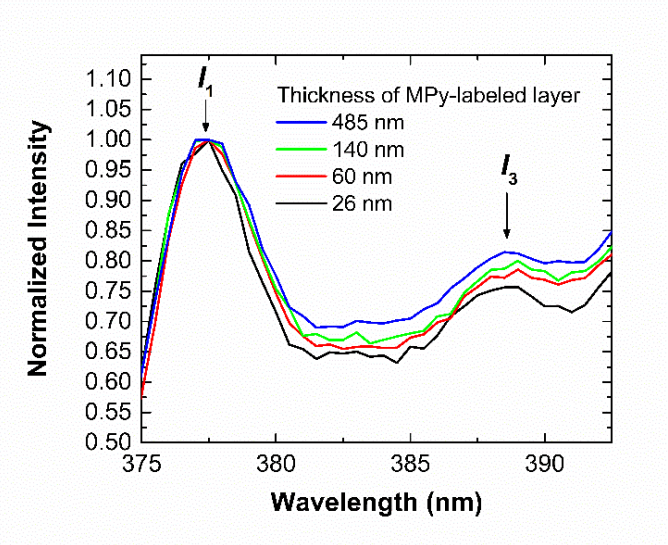

Figure 9-1. Fluorescence emission spectra at 70 °C for MPy-labeled 75/25 P(S/EHA) layers placed directly adjacent to the substrate within bilayer films. Locations of the first and third vibronic peaks are indicated. Intensities are normalized relative to I_1.

To understand the effect of a slight change in monomer structure from nBA to EHA on interfacial stiffness and stiffness gradient length scales of supported acrylic-based random copolymer films, we synthesized three P(S/EHA)s with various S/EHA molar ratios, i.e., 94/6, 75/25, and 27/73 P(S/EHA)s, which exhibit bulk T_g values of 85 °C, 28 °C, and −43 °C,

respectively. The copolymer compositions are carefully chosen such that the bulk T_gs are the same, within experimental error, as those of 95/5, 59/41, and 5/95 P(S/nBA)s discussed in Chapter 8.

To characterize the stiffness of P(S/EHA) films near the substrate interface, a bilayer film geometry is employed in which a MPy-labeled substrate layer that is responsive to UV light excitation is directly spin-coated on glass substrates, and a 600-nm-thick, unlabeled layer is placed atop the MPy-labeled layer to block any potential interferences from the free-surface interface. Figure 9-2 shows I_1/I_3 values as a function of MPy-labeled-layer thickness for 94/6, 75/25, and 27/73 P(S/EHA) films supported on hydrophilic glass. For 94/6 and 75/25 P(S/EHA)s, measurements were taken at temperatures both above and below T_g; for 27/73 P(S/EHA), measurements were only taken at temperatures above T_g because the T_g of 27/73 P(S/EHA) is too low, and the temperature controller coupled with the fluorimeter is incapable to reach temperatures below its T_g.

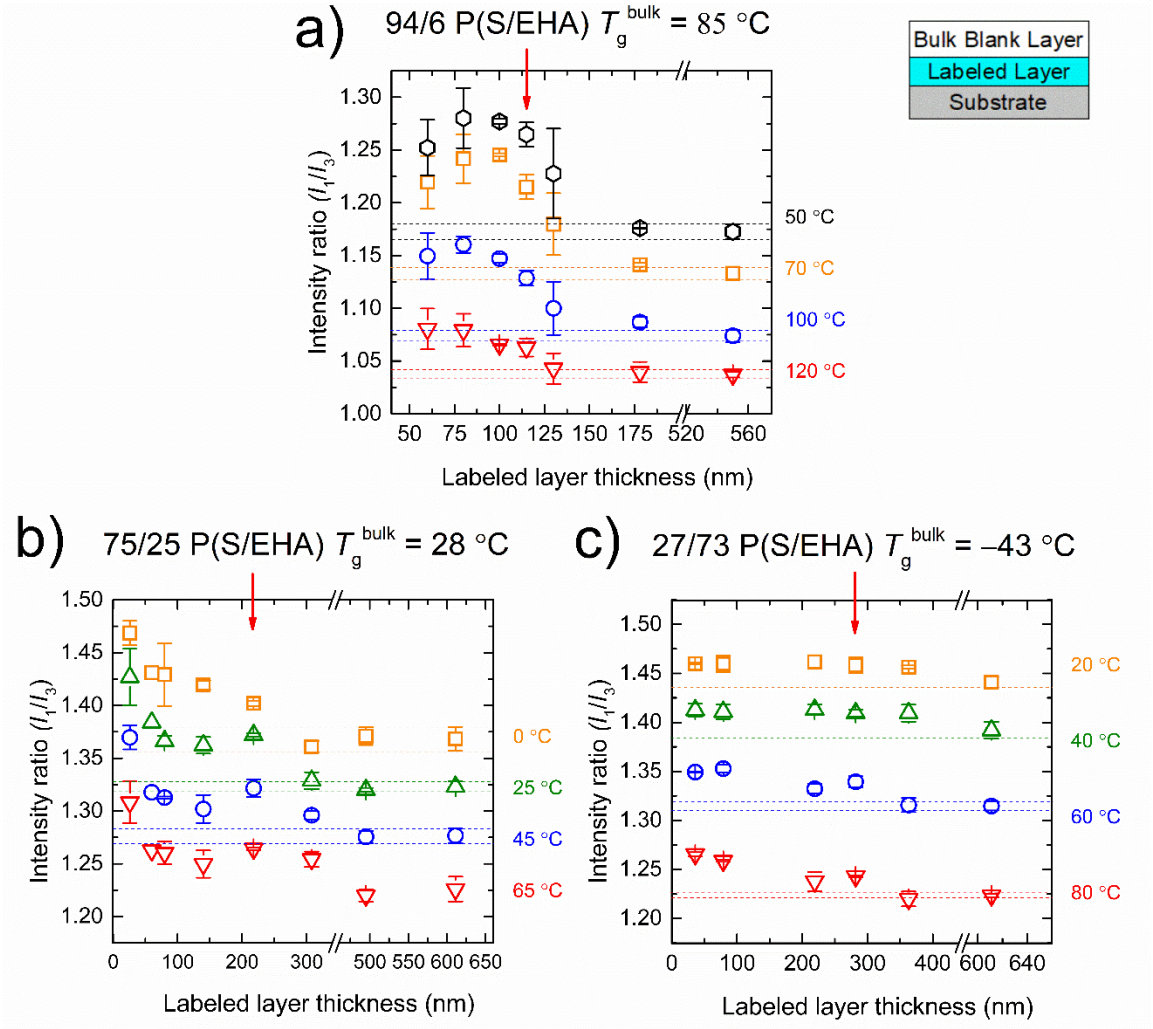

Figure 9-2. Fluorescence I_1/I_3 values as a function of MPy-labeled substrate-layer thickness within bilayer films of a) 94/6 P(S/EHA), b) 75/25 P(S/EHA), and c) 27/73 P(S/EHA) films supported on hydrophilic glass substrates. Error bars are associated with three measurements on three separate samples. Dashed lines indicate the *I*1/*I*3 values for the thickest films in each data set.

At all tested temperatures, P(S/EHA) with 6 mol% EHA exhibits an invariance in *I*1/*I*3 and hence stiffness down to a substrate-layer thickness of 130 nm and stiffening for thicknesses at or below 115 nm; P(S/EHA) with 25 mol% EHA exhibits an invariance in stiffness down to a substrate-layer thickness of 308 nm and stiffening for thicknesses at or below 220 nm; P(S/EHA) with 73 mol% EHA exhibits an invariance in stiffness down to a thickness of 363 nm and stiffening for thicknesses at or below 280 nm. The stiffness gradient length scales over which the hydrophilic

substrate interface perturbs the stiffness responses of the three P(S/EHA)s are summarized in Table 9-2. The greater $I1/I3$ values in regions closer to the substrate indicate an enhancement in stiffness originating from the substrate interface. As shown in Table 9-2, the length scale associated with substrate perturbations increases with increasing EHA molar content. Similar trends were observed for P(S/nBA) films supported on hydrophilic glass in which the length scale of substrate perturbations to stiffness also increases with increasing nBA molar content (see Chapter 8). However, for P(S/EHA)s and P(S/nBA)s with similar bulk T_gs, the stiffness gradient length scales for P(S/EHA)s are significantly longer compared to those of P(S/nBA)s. For example, the length scale is ~115 nm for 94/6 P(S/EHA) and only ~65 nm for 95/5 P(S/nBA); the length scale is ~280 nm for 27/73 P(S/EHA) and only ~170 nm for 5/95 P(S/nBA). One hypothesis that could explain the substantially stronger substrate perturbations to stiffness in P(S/EHA) films is that the molecular structure of EHA allows the polymer chain segments to more effectively hydrogen-bond to the hydroxyl groups on hydrophilic glass surface.

We note that the substrate-perturbation length scale for 94/6 P(S/EHA) films supported on hydrophilic glass is shorter compared to that of polystyrene (PS) films supported on hydrophilic glass reported by Askar and Torkelson (Askar & Torkelson, 2016), although the 94/6 P(S/EHA) system contains only 6 mol% EHA units that can form attractive hydrogen bonding interactions with the hydrophilic glass substrate surface. For PS films, the substrate perturbations extend over at least 200 nm from the substrate interface as reported by Askar and Torkelson (Askar & Torkelson, 2016), which is substantially longer compared to the ~115-nm perturbation length scale associated with 94/6 P(S/EHA) films. A possible explanation, which is similar to that provided in Chapter 8 for the shorter perturbation length scales associated with P(S/nBA) films compared to that of neat PS films, is that P(S/EHA) and PS are inherently different materials, so the perturbation

length scales for the two polymers might not be able to be compared directly. It is possible that the presence of EHA units significantly changed the short-time-scale molecular vibrations related to the stiffness of materials relative to neat PS.

Table 9-2. Summary of length scales over which substrate perturbations modify the stiffness response of P(S/EHA) and P(S/nBA)s extending from the polymer–substrate interface on hydrophilic and hydrophobic glass substrates. Results for P(S/nBA) are re-tabulated from Chapter 8.

P(S/EHA) (mol%/mol%)	**$T_{g,\,onset}$ (°C) by DSC**	**Perturbation length scale on hydrophilic glass (nm)**	**Perturbation length scale on hydrophobic glass (nm)**
94/6	85	~115	~115
75/25	28	~220	~220
27/73	−43	~280	-
P(S/nBA) (mol%/mol%)	**$T_{g,\,onset}$ (°C) by DSC**	**Perturbation length scale on hydrophilic glass (nm)**	**Perturbation length scale on hydrophobic glass (nm)**
95/5	85	~65	-
59/41	30	~80	~60
33/67	−13	~120	~60
5/95	−43	~170	~60

Following the characterizations of P(S/EHA) films supported on hydrophilic glass, we treated the hydrophilic glass substates with dichlorodimethylsilane to replace the hydroxyl groups on substrate surface with methyl groups. After modification, the substrate water contact angle increases from ~15° to ~105°, representing a significant decrease in the number of surface hydroxyl groups. Figure 9-3 summarizes I_1/I_3 values of MPy-labeled substrate layers within bilayer 94/6 and 75/25 P(S/EHA) films supported on hydrophobic glass measured at different temperatures. For both systems, I_1/I_3 values still exhibit an increasing trend with decreasing

substrate-layer thickness at a specific thickness and below, indicating that stiffness of 94/6 and 75/25 P(S/EHA) films is enhanced near the hydrophobic substrate interface.

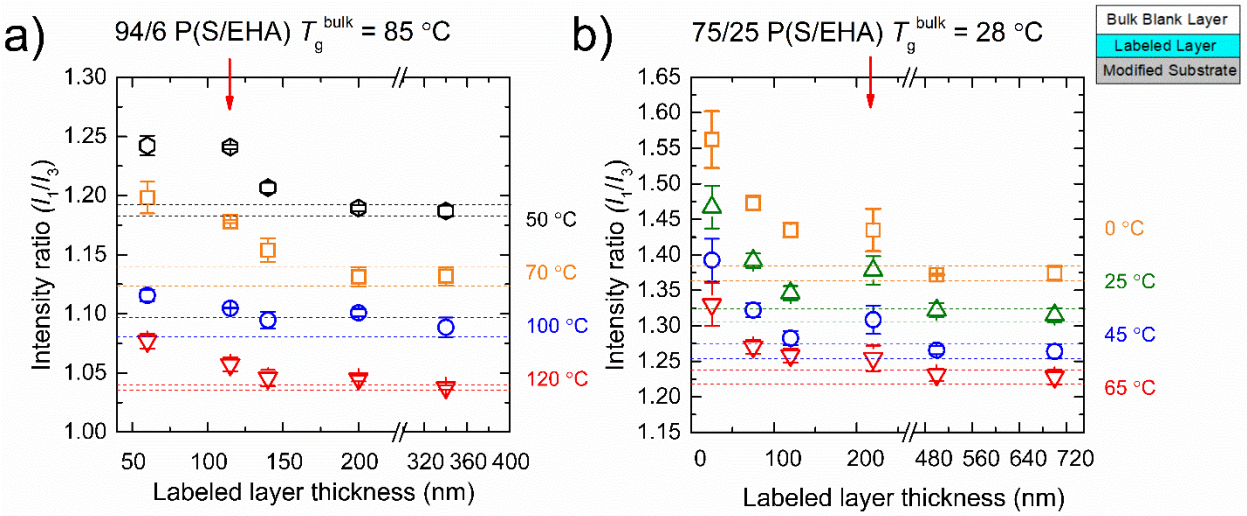

Figure 9-3. Fluorescence I_1/I_3 values as a function of MPy-labeled substrate-layer thickness within bilayer films of a) 94/6 and b) 75/25 P(S/EHA) films supported on hydrophobic glass substrates. Error bars are associated with three measurements on three separate samples. Dashed lines indicate the $I1/I3$ values for the thickest films in each data set.

Surprisingly, comparing the perturbation length scales on hydrophilic and hydrophobic glass substrates, we discovered that the perturbation length scales for both 94/6 and 75/25 P(S/EHA) systems are independent of substrate hydrophilicity, i.e., the length scales remain constant upon removal of the interfacial hydrogen bonding interactions (see Table 9-2). For supported P(S/nBA) films characterized in Chapter 8, significant reductions in stiffness gradient length scales were observed when hydroxyl groups on glass surface were removed, suggesting that hydrogen bonding interactions are one of the major contributors of stiffening of P(S/nBA) films in the interfacial region. However, in P(S/EHA)s, the stiffness gradient length scale appears to be unaffected by hydrogen bonding interactions. Nevertheless, in P(S/EHA)s, the stiffness gradient length scales on hydrophilic glass substrates still show dependence on EHA content, indicating

that the underlying cause for substrate perturbations to stiffness is still related to some interactions associated with the EHA units. One possible explanation is that since EHA has a more flexible structure than nBA, EHA units can potentially give rise to more enhanced high-frequency vibrations or mobility, i.e., the P(S/EHA) films might have lower inherent stiffness than P(S/nBA) films. Thus, a rigid glass substrate would have a greater restriction effect on the vibrations of P(S/EHA) films and lead to greater stiffness gradient length scales compared with P(S/nBA) films. Another possible explanation is that EHA units in P(S/EHA) films may result in strong attractive van der Waals forces being generated between the films and the substrate surface. Because van der Waals interactions are only weakly dependent on the hydrophilicity/hydrophobicity nature of the interacting surfaces (Autumn et al., 2002), this effect may explain the constant stiffness gradient length scales in P(S/EHA) films upon hydrophobic modification of the substrate surface.

9.4 Conclusions

We investigated the interfacial stiffness and stiffness gradient length scales of P(S/EHA) random copolymer films near the substrate interface using a fluorescence approach, which qualitatively measures the average stiffness across a MPy-labeled substrate layer via the sensitivity of a measurable intensity ratio of pyrene, I_1/I_3, to molecular caging. Comparisons were made with the study on supported P(S/nBA) films described in Chapter 8 to understand the role of different acrylic monomers on the substrate perturbations to stiffness of acrylic-based random copolymer films. The stiffness of P(S/EHA) films is substantially enhanced relative to bulk behavior near both hydrophilic and hydrophobic glass substrates. The stiffness gradient length scale over which the average stiffness of P(S/EHA) films is modified by the presence of a substrate interface

increases with increasing EHA molar content, and the length scale is independent of the hydrophilic/hydrophobic nature of the substrate.

On hydrophilic glass, the stiffness gradient length scales are ~115 nm, ~220 nm, and ~280 nm in 94/6, 75/25, and 27/73 P(S/EHA) films, respectively. These values are ~80–180% greater than those associated with P(S/nBA)s with similar bulk T_gs characterized in Chapter 8. Upon removal of hydroxyl groups on the substrate surface, the stiffness gradient length scales in P(S/EHA) films remain unchanged but increase with increasing EHA molar content, whereas in P(S/nBA) films, the stiffness gradient length scale decreases substantially after the substrate is hydrophobically modified and exhibits a uniform, ~60-nm value for all compositions. These results indicate that in sharp contrast to supported P(S/nBA) films in which the stiffness gradient length scales near the substrate surface depend significantly on attractive hydrogen bonding interactions, the stiffness of P(S/EHA) films exhibits little or no effect to such perturbations. The current hypothesis is that for P(S/EHA) systems the effect of attractive interfacial interactions on stiffness is negligible compared to the strong inherent stiffening effect of a rigid glass substrate or to the strong attractive van der Waals forces generated between the P(S/EHA) films and the substrate surface by EHA units.

Acknowledgements

This work was done in collaboration with Tong Wang from the Torkelson research group at Northwestern University.

CHAPTER 10

Conclusions and Recommendations for Future Work

This dissertation describes the development of simple, efficient approaches that enhance the reprocessability, sustainability, and material properties of polyurethane (PU) and PU-like network materials. Additionally, this dissertation focuses on understanding the stress relaxation and stiffness of supported acrylic random copolymer films. The key findings of each chapter as well as recommendations for future research are summarized and offered below.

Section I

In Chapter 3, we investigated factors that affect the reprocessability of conventional PU networks and developed two simple methods to enhance the property recovery of PU networks after reprocessing. We showed that the reprocessability and thermal stability of dynamic PU networks can be enhanced by incorporating excess free hydroxyl groups and/or increasing the cross-linker functionality from three to four. Using these two strategies, we demonstrated via a model PU network that the inherent dynamic nature of urethane linkages can lead to full recovery of cross-link density and tensile properties after multiple reprocessing steps. Although excess hydroxyl groups are beneficial for property recovery after reprocessing, the unbalanced stoichiometry can lead to reductions in tensile properties such as Young's modulus and tensile strength of the as-synthesized materials. Future studies should further increase the functionality of the cross-linker from four to five to determine whether full property recovery after reprocessing could be achieved with a lower level of excess free hydroxyl groups. In this work, we also showed via a proof-of-principle demonstration that the dynamic nature of urethane linkages can potentially be used to depolymerize the PU networks and achieve monomer recovery. Future studies should

optimize the depolymerization conditions by exploring different catalysts, quantifying the monomer yields, and correlating the depolymerization efficiency with monomer structures. Future studies should also separate and purify the depolymerized products to obtain pure monomers that can be repolymerized back into the same PU networks such that a closed-loop recycling can be achieved.

Chapter 4 describes the syntheses of PHU networks from bio-based precursors. Two bio-based cyclic carbonate cross-linkers, carbonated soybean oil (CSBO) and sorbitol ether carbonate (SEC), were studied. Both cross-linkers were obtained by sequestering CO_2 into their epoxy precursors. CSBO leads to PHU networks with excellent reprocessability. Within experimental error, CSBO-based PHU networks can undergo three reprocessing cycles with full recovery of cross-link density and tensile properties. The reprocessing was achieved via three concurrent dynamic chemistries: reversible cyclic carbonate aminolysis, transesterification between the urethane linkages and the pendent hydroxyl groups, and transesterification between the ester groups in CSBO and the pendent hydroxyl groups. In contrast, SEC-based PHU networks exhibit poor reprocessability even with high reprocessing temperatures and catalyst loading. Although the hydroxyurethane linkages in SEC-based PHU networks can undergo dynamic reactions during reprocessing, the presence of multiple cyclic carbonate groups on adjacent carbon atoms in the SEC backbone leads to steric effects and reduced mobility of the networks, which makes it difficult for the network chains to undergo topological rearrangements that are necessary to achieve reprocessing. This chapter highlights the effectiveness of CSBO as a green, renewable precursor for reprocessable PHU networks and demonstrates the importance of monomer choice for the design of reprocessability networks. Future studies should explore more bio-based materials with various molecular structures such that different material properties can be achieved. In addition,

monomer choice in this chapter was mainly based on commercial availability; in the future, it would be worthwhile to take advantage of simulation tools that can help to find available bio-based monomers or to identify chemicals that can be transferred via simple synthesis steps into required monomers such that more choices of bio-based monomers are available.

Chapter 5 describes the syntheses of dynamic PHU network composites using cyclic-carbonate-terminated POSS as reinforcing fillers. POSS was reacted into the network matrix serving as both nanofillers and a fraction of cross-linkers. The incorporation of POSS substantially enhanced the mechanical properties and thermal stability of the networks relative to the neat PHUs synthesized without nanofillers. Because of the inherent dynamic nature of hydroxyurethane linkages, PHU−POSS network composites can be melt-reprocessed at elevated temperatures. With up to 10 wt% POSS loading, PHU−POSS network composites can undergo multiple reprocessing cycles with 100% recovery of cross-link density. Such excellent property recovery after reprocessing has not been achieved before with PHU network composites reinforced with conventional silica nanoparticles. We also show in this study that hydroxyurethane dynamic chemistry leads to excellent creep resistance at elevated temperatures up to 90 °C. Many opportunities are worth investigating further. For example, the maximum POSS loading in this study is 10 wt% of the total weight of the network; future studies could further increase the POSS loading to see how reprocessability and other properties of the composites are impacted by an elevated filler loading. In addition, it is possible that a higher POSS loading would lead to nano- or microscale phase separation. Future studies should examine the morphology change of the PHU−POSS composites with increasing POSS loading and investigate whether the phase separation have an impact on the property recovery of the composites after reprocessing. Finally,

other types of nanofillers should also be explored for the development of dynamic PHU network composites such that a variety of material properties could be achieved for different applications.

Section II

Chapter 7 is concerned with the residual stress relaxation behavior of spin-coated P(S/nBA) films with low nBA molar content. This chapter could be considered as a preliminary study for Chapter 8 which focuses on the substrate effects on stiffness of P(S/nBA) films. Because stiffness and residual stress are both related to molecular caging and both can impact the I_1/I_3 values of the pyrene fluorescence emission spectrum, residual stress needs to be completely removed from the films before stiffness characterizations such that the measured I_1/I_3 values depend only on stiffness. In Chapter 7, the residual stress relaxation process in P(S/nBA) films were characterized by ellipsometry and fluorescence. Both techniques show that residual stress relaxation occurs over a period of hours in the rubbery state of the films. By comparing the residual stress relaxation timescales of neat PS films and P(S/nBA) films with very low nBA molar content ($\leq$ 5 mol%) at the same absolute temperature or the same relative temperature above the bulk T_g, we discovered that the presence of a very small amount of nBA can vastly change the relaxation behaviors from neat PS films. With 2 or 5 mol% nBA, the residual stress relaxation process of bulk P(S/nBA) films occurs over significantly extended periods of time than that of neat PS films. Future studies should investigate the residual stress relaxation behavior of P(S/nBA) films more comprehensively. For example, for a particular P(S/nBA) composition, residual stress relaxation timescale should be characterized as a function of annealing temperatures over a greater range to see whether the timescale follows an Arrhenius temperature dependence and to determine the associated activation energy.

Chapter 8 discusses about the substrate effects on stiffness of supported P(S/nBA) films. We discovered that the interfacial stiffness of glass-supported P(S/nBA) films is enhanced by attractive hydrogen bonding interactions. When the nBA molar content in P(S/nBA)s is gradually increased from 5 mol% to 95 mol% to yield stronger hydrogen bonding interactions between the films and the hydrophilic substrate surface, the length scale over which substrate perturbations modify the average stiffness of the film near the substrate interface increases from 60–70 nm to 180 nm. When the hydroxyl groups on a hydrophilic glass surface are substituted by methyl groups to yield a hydrophobic substrate surface that prevents the formation of interfacial hydrogen bonds, the stiffness of P(S/nBA) films is still enhanced near the substrate interface, but the length scale of substrate perturbations becomes independent of nBA content, with all P(S/nBA) films exhibit the same length scale of ~60 nm. This study shows that attractive interfacial interactions are one of the major contributors to substrate perturbations on stiffness of supported P(S/nBA)s films. Because P(S/nBA) is a model pressure-sensitive adhesive system, future studies should add tackifiers or additives that are commonly employed in pressure-sensitive adhesive formulations into P(S/nBA)s to investigate the impact of these compounds on the substrate effects and stiffness gradient length scales in supported P(S/nBA)s. In addition, Chapter 8 only focuses on the substrate effects on stiffness; future studies should also investigate the interfacial stiffness and stiffness gradient length scales in supported P(S/nBA) films near the free-surface interface. Stiffness of single-layer films should also be characterized to understand whether single-layer films are subject to combined perturbations from both the substrate interface and the free-surface interface. More substrate species including stainless steel and high-density polyethylene could also be tested.

Finally, Chapter 9 investigates the substrate effects on stiffness of supported P(S/EHA) films containing 6 to 73 mol% EHA, and the results were compared with those from Chapter 8 to

understand the role of different acrylic monomers in affecting the substrate perturbations on stiffness of acrylic-based random copolymer films. We discovered that the stiffness of P(S/EHA) films is enhanced near both hydrophilic and hydrophobic substrate interfaces and that the stiffness gradient length scale over which the average film stiffness is modified by the presence of a substrate interface increases with increasing EHA molar content. On hydrophilic glass and for P(S/EHA)s and P(S/nBA)s with similar bulk T_gs, the stiffness gradient length scales associated with P(S/EHA) films are substantially longer than those of P(S/nBA) films. The stiffness gradient length scales in supported P(S/EHA)s are unaffected by hydrophobic modification of the substrate surface, indicating that attractive hydrogen bonding interactions are not a major cause of the stiffness deviation of P(S/EHA) films near a substrate. Many further opportunities are worth investigating. For example, future studies could increase the EHA molar content to above 90 mol% and examine whether hydrogen bonding interactions have a greater impact on stiffness and stiffness gradient length scales in P(S/EHA) films when more moieties that can participate in hydrogen bonding formation are present. Finally, it would also be worthwhile to explore copolymers derived from other acrylic monomers to determine how the stiffness behaviors further change relative to P(S/nBA) and P(S/EHA) films.

REFERENCES

Abbott, S. (2015). *Adhesion Science: Principles and Practice Steven Abbott*. DEStech Publications, Inc.

Adzima, B. J., Aguirre, H. A., Kloxin, C. J., Scott, T. F., & Bowman, C. N. (2008). Rheological and chemical analysis of reverse gelation in a covalently cross-linked Diels−Alder polymer network. *Macromolecules*, *41*(23), 9112–9117.

Akindoyo, J. O., Beg, M. D. H., Ghazali, S., Islam, M. R., Jeyaratnam, N., & Yuvaraj, A. R. (2016). Polyurethane types, synthesis and applications – a review. *RSC Advances*, *6*(115), 114453–114482.

Anaya, O., Jourdain, A., Antoniuk, I., Romdhane, H. B., Montarnal, D., & Drockenmuller, E. (2021). Tuning the viscosity profiles of high-Tg poly(1,2,3-triazolium) covalent adaptable networks by the chemical structure of the N-substituents. *Macromolecules*, *54*(7), 3281–3292.

Askar, S., Evans, C. M., & Torkelson, J. M. (2015). Residual stress relaxation and stiffness in spin-coated polymer films: Characterization by ellipsometry and fluorescence. *Polymer*, *76*, 113–122.

Askar, S., & Torkelson, J. M. (2016). Stiffness of thin, supported polystyrene films: Free-surface, substrate, and confinement effects characterized via self-referencing fluorescence. *Polymer*, *99*, 417–426.

Autumn, K., Sitti, M., Liang, Y. A., Peattie, A. M., Hansen, W. R., Sponberg, S., Kenny, T. W., Fearing, R., Israelachvili, J. N., & Full, R. J. (2002). Evidence for van der Waals adhesion in gecko setae. *Proceedings of the National Academy of Sciences of the United States of America*, *99*(19), 12252–12256.

Bähr, M., Bitto, A., & Mülhaupt, R. (2012). Cyclic limonene dicarbonate as a new monomer for non-isocyanate oligo- and polyurethanes (NIPU) based upon terpenes. *Green Chemistry*, *14*(5), 1447–1454.

Bähr, M., & Mülhaupt, R. (2012). Linseed and soybean oil-based polyurethanes prepared via the non-isocyanate route and catalytic carbon dioxide conversion. *Green Chemistry*, *14*(2), 483–489.

Bai, J., Li, H., Shi, Z., & Yin, J. (2015). An eco-friendly scheme for the cross-linked polybutadiene elastomer via thiol–ene and Diels–Alder click chemistry. *Macromolecules*, *48*(11), 3539–3546.

Bäumchen, O., McGraw, J. D., Forrest, J. A., & Dalnoki-Veress, K. (2012). Reduced glass transition temperatures in thin polymer films: Surface effect or artifact? *Physical Review Letters*, *109*(5), 055701.

Bayer, O. (1947). Das di-isocyanat-polyadditionsverfahren (polyurethane). *Angewandte Chemie*, *59*(9), 257–272.

Beniah, G., Chen, X., Uno, B. E., Liu, K., Leitsch, E. K., Jeon, J., Heath, W. H., Scheidt, K. A., & Torkelson, J. M. (2017). Combined effects of carbonate and soft-segment molecular structures on the nanophase separation and properties of segmented polyhydroxyurethane. *Macromolecules*, *50*(8), 3193–3203.

Beniah, G., Fortman, D. J., Heath, W. H., Dichtel, W. R., & Torkelson, J. M. (2017). Non-isocyanate polyurethane thermoplastic elastomer: Amide-based chain extender yields enhanced nanophase separation and properties in polyhydroxyurethane. *Macromolecules*, *50*(11), 4425–4434.

Beniah, G., Heath, W. H., Jeon, J., & Torkelson, J. M. (2017). Tuning the properties of segmented polyhydroxyurethanes via chain extender structure. *Journal of Applied Polymer Science*, *134*(45), 44942.

Beniah, G., Liu, K., Heath, W. H., Miller, M. D., Scheidt, K. A., & Torkelson, J. M. (2016). Novel thermoplastic polyhydroxyurethane elastomers as effective damping materials over broad temperature ranges. *European Polymer Journal*, *84*, 770–783.

Beniah, G., Uno, B. E., Lan, T., Jeon, J., Heath, W. H., Scheidt, K. A., & Torkelson, J. M. (2017). Tuning nanophase separation behavior in segmented polyhydroxyurethane via judicious choice of soft segment. *Polymer*, *110*, 218–227.

Bin Rusayyis, M. A., & Torkelson, J. M. (2020). Recyclable polymethacrylate networks containing dynamic dialkylamino disulfide linkages and exhibiting full property recovery. *Macromolecules*, *53*(19), 8367–8373.

Bin Rusayyis, M. A., & Torkelson, J. M. (2021). Reprocessable covalent adaptable networks with excellent elevated-temperature creep resistance: Facilitation by dynamic, dissociative bis(hindered amino) disulfide bonds. *Polymer Chemistry*, *12*(18), 2760–2771.

Bin Rusayyis, M. A., & Torkelson, J. M. (2022). Reprocessable and recyclable chain-growth polymer networks based on dynamic hindered urea bonds. *ACS Macro Letters*, *11*(4), 568–574.

Blattmann, H., Fleischer, M., Bähr, M., & Mülhaupt, R. (2014). Isocyanate- and phosgene-free routes to polyfunctional cyclic carbonates and green polyurethanes by fixation of carbon dioxide. *Macromolecular Rapid Communications*, *35*(14), 1238–1254.

Blattmann, H., & Mülhaupt, R. (2016). Multifunctional POSS cyclic carbonates and non-isocyanate polyhydroxyurethane hybrid materials. *Macromolecules*, *49*(3), 742–751.

Bossion, A., Aguirresarobe, R. H., Irusta, L., Taton, D., Cramail, H., Grau, E., Mecerreyes, D., Su, C., Liu, G., Müller, A. J., & Sardon, H. (2018). Unexpected synthesis of segmented poly(hydroxyurea–urethane)s from dicyclic carbonates and diamines by organocatalysis. *Macromolecules*, *51*(15), 5556–5566.

Brandt, J., Oehlenschlaeger, K. K., Schmidt, F. G., Barner-Kowollik, C., & Lederer, A. (2014). State-of-the-art analytical methods for assessing dynamic bonding soft matter materials. *Advanced Materials*, *26*(33), 5758–5785.

Brazel, C. S., & Rosen, S. L. (2012). *Fundamental Principles of Polymeric Materials, 3rd Edition*. Wiley.

Briscoe, B. J., Fiori, L., & Pelillo, E. (1998). Nano-indentation of polymeric surfaces. *Journal of Physics D: Applied Physics*, *31*(19), 2395–2405.

Brune, P. F., Blackman, G. S., Diehl, T., Meth, J. S., Brill, D., Tao, Y., & Thornton, J. (2016). Direct measurement of rubber interphase stiffness. *Macromolecules*, *49*(13), 4909–4922.

Burroughs, M. J., Christie, D., Gray, L. A. G., Chowdhury, M., & Priestley, R. D. (2018). 21st century advances in fluorescence techniques to characterize glass-forming polymers at the nanoscale. *Macromolecular Chemistry and Physics*, *219*(3), 1700368.

Capelot, M., Montarnal, D., Tournilhac, F., & Leibler, L. (2012). Metal-catalyzed transesterification for healing and assembling of thermosets. *Journal of the American Chemical Society*, *134*(18), 7664–7667.

Capelot, M., Unterlass, M. M., Tournilhac, F., & Leibler, L. (2012). Catalytic control of the vitrimer glass transition. *ACS Macro Letters*, *1*(7), 789–792.

Chakma, P., & Konkolewicz, D. (2019). Dynamic covalent bonds in polymeric materials. *Angewandte Chemie International Edition*, *58*(29), 9682–9695.

Chanda, M. (2013). *Introduction to Polymer Science and Chemistry: A Problem-Solving Approach, 2nd Edition*. CRC Press.

Chandran, S., Baschnagel, J., Cangialosi, D., Fukao, K., Glynos, E., Janssen, L. M. C., Müller, M., Muthukumar, M., Steiner, U., Xu, J., Napolitano, S., & Reiter, G. (2019). Processing pathways decide polymer properties at the molecular level. *Macromolecules*, *52*(19), 7146–7156.

Chandran, S., & Reiter, G. (2019). Segmental rearrangements relax stresses in nonequilibrated polymer films. *ACS Macro Letters*, *8*(6), 646–650.

Chang, E. P. (1997). Viscoelastic properties of pressure-sensitive adhesives. *The Journal of Adhesion*, *60*(1–4), 233–248.

Chao, A., & Zhang, D. (2019). Investigation of secondary amine-derived aminal bond exchange toward the development of covalent adaptable networks. *Macromolecules*, *52*(2), 495–503.

Chattopadhyay, D. K., & Raju, K. V. S. N. (2007). Structural engineering of polyurethane coatings for high performance applications. *Progress in Polymer Science*, *32*(3), 352–418.

Chen, J.-H., Hu, D.-D., Li, Y.-D., Meng, F., Zhu, J., & Zeng, J.-B. (2018). Castor oil derived poly(urethane urea) networks with reprocessability and enhanced mechanical properties. *Polymer*, *143*, 79–86.

Chen, J.-H., Hu, D.-D., Li, Y.-D., Zhu, J., Du, A.-K., & Zeng, J.-B. (2018). Castor oil-based high performance and reprocessable poly(urethane urea) network. *Polymer Testing*, *70*, 174–179.

Chen, L., Zhang, L., Griffin, P. J., & Rowan, S. J. (2020). Impact of dynamic bond concentration on the viscoelastic and mechanical properties of dynamic poly(alkylurea-co-urethane) networks. *Macromolecular Chemistry and Physics*, *221*(1), 1900440.

Chen, X., Dam, M. A., Ono, K., Mal, A., Shen, H., Nutt, S. R., Sheran, K., & Wudl, F. (2002). A thermally re-mendable cross-linked polymeric material. *Science*, *295*(5560), 1698–1702.

Chen, X., Hu, S., Li, L., & Torkelson, J. M. (2020). Dynamic covalent polyurethane networks with excellent property and cross-link density recovery after recycling and potential for monomer recovery. *ACS Applied Polymer Materials*, *2*(5), 2093–2101.

Chen, X., Li, L., Jin, K., & Torkelson, J. M. (2017). Reprocessable polyhydroxyurethane networks exhibiting full property recovery and concurrent associative and dissociative dynamic chemistry via transcarbamoylation and reversible cyclic carbonate aminolysis. *Polymer Chemistry*, *8*(41), 6349–6355.

Chen, X., Li, L., & Torkelson, J. M. (2019). Recyclable polymer networks containing hydroxyurethane dynamic cross-links: Tuning morphology, cross-link density, and associated properties with chain extenders. *Polymer*, *178*, 121604.

Chen, X., Li, L., Wei, T., & Torkelson, J. M. (2019). Reprocessable polymer networks designed with hydroxyurethane dynamic cross-links: effect of backbone structure on network morphology, phase segregation, and property recovery. *Macromolecular Chemistry and Physics*, *220*(13), 1900083.

Chen, X., Li, L., Wei, T., Venerus, D. C., & Torkelson, J. M. (2019). Reprocessable polyhydroxyurethane network composites: Effect of filler surface functionality on cross-link density recovery and stress relaxation. *ACS Applied Materials & Interfaces*, *11*(2), 2398–2407.

Chen, Y., Tang, Z., Zhang, X., Liu, Y., Wu, S., & Guo, B. (2018). Covalently cross-linked elastomers with self-healing and malleable abilities enabled by boronic ester bonds. *ACS Applied Materials & Interfaces*, *10*(28), 24224–24231.

Cheng, W., Sainidou, R., Burgardt, P., Stefanou, N., Kiyanova, A., Efremov, M., Fytas, G., & Nealey, P. F. (2007). Elastic properties and glass transition of supported polymer thin films. *Macromolecules*, *40*(20), 7283–7290.

Chowdhury, M., Freyberg, P., Ziebert, F., Yang, A. C.-M., Steiner, U., & Reiter, G. (2012). Segmental relaxations have macroscopic consequences in glassy polymer films. *Physical Review Letters*, *109*(13), 136102.

Chowdhury, M., Sheng, X., Ziebert, F., Yang, A. C.-M., Sepe, A., Steiner, U., & Reiter, G. (2016). Intrinsic stresses in thin glassy polymer films revealed by crack formation. *Macromolecules*, *49*(23), 9060–9067.

Chung, J. Y., Chastek, T. Q., Fasolka, M. J., Ro, H. W., & Stafford, C. M. (2009). Quantifying residual stress in nanoscale thin polymer films via surface wrinkling. *ACS Nano*, *3*(4), 844–852.

Chung, J. Y., Nolte, A. J., & Stafford, C. M. (2011). Surface wrinkling: A versatile platform for measuring thin-film properties. *Advanced Materials*, *23*(3), 349–368.

Colodny, P. C., & Tobolsky, A. V. (1957). Chemorheological study of polyurethan elastomers 1. *Journal of the American Chemical Society, 79*(16), 4320–4323.

Coran, A. Y. (2003). Chemistry of the vulcanization and protection of elastomers: A review of the achievements. *Journal of Applied Polymer Science*, *87*(1), 24–30.

Cordes, D. B., Lickiss, P. D., & Rataboul, F. (2010). Recent developments in the chemistry of cubic polyhedral oligosilsesquioxanes. *Chemical Reviews, 110*(4), 2081–2173.

Cornille, A., Auvergne, R., Figovsky, O., Boutevin, B., & Caillol, S. (2017). A perspective approach to sustainable routes for non-isocyanate polyurethanes. *European Polymer Journal*, *87*, 535–552.

Cornille, A., Blain, M., Auvergne, R., Andrioletti, B., Boutevin, B., & Caillol, S. (2017). A study of cyclic carbonate aminolysis at room temperature: Effect of cyclic carbonate structures and solvents on polyhydroxyurethane synthesis. *Polymer Chemistry*, *8*(3), 592–604.

Creton, C. (2003). Pressure-sensitive adhesives: An introductory course. *MRS Bulletin*, *28*(6), 434–439.

Croll, S. G. (1978). Internal stress in a solvent-cast thermoplastic coating. *Journal of Coatings Technology*, *50*.

Croll, S. G. (1979). The origin of residual internal stress in solvent-cast thermoplastic coatings. *Journal of Applied Polymer Science*, *23*(3), 847–858.

Damman, P., Gabriele, S., Coppée, S., Desprez, S., Villers, D., Vilmin, T., Raphaël, E., Hamieh, M., Akhrass, S. A., & Reiter, G. (2007). Relaxation of residual stress and reentanglement of polymers in spin-coated films. *Physical Review Letters*, *99*(3), 036101.

Darensbourg, D. J., & Holtcamp, M. W. (1996). Catalysts for the reactions of epoxides and carbon dioxide. *Coordination Chemistry Reviews*, *153*, 155–174.

de Luzuriaga, A. R., Martin, R., Markaide, N., Rekondo, A., Cabañero, G., Rodríguez, J., & Odriozola, I. (2016). Epoxy resin with exchangeable disulfide crosslinks to obtain reprocessable, repairable and recyclable fiber-reinforced thermoset composites. *Materials Horizons*, *3*(3), 241–247.

Delcambre, S. P., Riggleman, R. A., de Pablo, J. J. & Nealey, P. F. (2010). Mechanical properties of antiplasticized polymer nanostructures. *Soft Matter*, *6*(11), 2475–2483.

Delebecq, E., Pascault, J.-P., Boutevin, B., & Ganachaud, F. (2013). On the versatility of urethane/urea bonds: Reversibility, blocked isocyanate, and non-isocyanate polyurethane. *Chemical Reviews*, *113*(1), 80–118.

Deng, Y., Li, S., Zhao, J., Zhang, Z., Zhang, J., & Yang, W. (2014). Crystallizable and tough aliphatic thermoplastic poly(ether urethane)s synthesized through a non-isocyanate route. *RSC Advances*, *4*(82), 43406–43414.

Denissen, W., Droesbeke, M., Nicolaÿ, R., Leibler, L., Winne, J. M., & Du Prez, F. E. (2017). Chemical control of the viscoelastic properties of vinylogous urethane vitrimers. *Nature Communications*, *8*(1), 14857.

Denissen, W., M. Winne, J., & Du Prez, F. E. (2016). Vitrimers: Permanent organic networks with glass-like fluidity. *Chemical Science*, *7*(1), 30–38.

Denissen, W., Rivero, G., Nicolaÿ, R., Leibler, L., Winne, J. M., & Du Prez, F. E. (2015). Vinylogous urethane vitrimers. *Advanced Functional Materials*, *25*(16), 2451–2457.

Dobson, A. L., Bongiardina, N. J., & Bowman, C. N. (2020). Combined dynamic network and filler interface approach for improved adhesion and toughness in pressure-sensitive adhesives. *ACS Applied Polymer Materials*, *2*(3), 1053–1060.

Duval, C., Kébir, N., Jauseau, R., & Burel, F. (2016). Organocatalytic synthesis of novel renewable non-isocyanate polyhydroxyurethanes. *Journal of Polymer Science Part A: Polymer Chemistry*, *54*(6), 758–764.

Elling, B. R., & Dichtel, W. R. (2020). Reprocessable cross-linked polymer networks: Are associative exchange mechanisms desirable? *ACS Central Science*, *6*(9), 1488–1496.

Ellison, C. J., Kim, S. D., Hall, D. B., & Torkelson, J. M. (2002). Confinement and processing effects on glass transition temperature and physical aging in ultrathin polymer films: Novel fluorescence measurements. *The European Physical Journal. E, Soft Matter*, *8*(2), 155–166.

Ellison, C. J., & Torkelson, J. M. (2002). Sensing the glass transition in thin and ultrathin polymer films via fluorescence probes and labels. *Journal of Polymer Science Part B: Polymer Physics*, *40*(24), 2745–2758.

Ellison, C. J., & Torkelson, J. M. (2003). The distribution of glass-transition temperatures in nanoscopically confined glass formers. *Nature Materials*, *2*(10), 695–700.

Elms, J., Beckett, P. N., Griffin, P., & Curran, A. D. (2001). Mechanisms of isocyanate sensitisation. An in vitro approach. *Toxicology in Vitro*, *15*(6), 631–634.

Emslie, A. G., Bonner, F. T., & Peck, L. G. (1958). Flow of a viscous liquid on a rotating disk. *Journal of Applied Physics*, *29*(5), 858–862.

Engels, H.-W., Pirkl, H.-G., Albers, R., Albach, R. W., Krause, J., Hoffmann, A., Casselmann, H., & Dormish, J. (2013). Polyurethanes: Versatile materials and sustainable problem solvers for today's challenges. *Angewandte Chemie International Edition*, *52*(36), 9422–9441.

Evans, C. M., Henderson, K. J., Saathoff, J. D., Shull, K. R., & Torkelson, J. M. (2013). Simultaneous determination of critical micelle temperature and micelle core glass transition temperature of block copolymer–solvent systems via pyrene-label fluorescence. *Macromolecules*, *46*(10), 4131–4140.

Evans, C. M., Kim, S., Roth, C. B., Priestley, R. D., Broadbelt, L. J., & Torkelson, J. M. (2015). Role of neighboring domains in determining the magnitude and direction of Tg-confinement effects in binary, immiscible polymer systems. *Polymer*, *80*, 180–187.

Evans, C. M., Narayanan, S., Jiang, Z., & Torkelson, J. M. (2012). Modulus, confinement, and temperature effects on surface capillary wave dynamics in bilayer polymer films near the glass transition. *Physical Review Letters*, *109*(3), 038302.

Evans, C. M., & Torkelson, J. M. (2012). Determining multiple component glass transition temperatures in miscible polymer blends: Comparison of fluorescence spectroscopy and differential scanning calorimetry. *Polymer*, *53*(26), 6118–6124.

Fakhraai, Z., & Forrest, J. A. (2005). Probing slow dynamics in supported thin polymer films. *Physical Review Letters*, *95*(2), 025701.

Fan, X., Xu, J., Chen, L., Hong, N., Wang, C., Ma, J., & Ma, Y. (2020). Processing induced nonequilibrium behavior of polyvinylpyrrolidone nanofilms revealed by dewetting. *Langmuir*, *36*(50), 15430–15441.

Fancey, K. (2005). A mechanical model for creep, recovery and stress relaxation in polymeric materials. *Journal of Materials Science*, *40*, 4827–4831.

Fang, Y., Du, X., Jiang, Y., Du, Z., Pan, P., Cheng, X., & Wang, H. (2018). Thermal-driven self-healing and recyclable waterborne polyurethane films based on reversible covalent interaction. *ACS Sustainable Chemistry & Engineering*, *6*(11), 14490–14500.

Feldstein, M. M., & Siegel, R. A. (2012). Molecular and nanoscale factors governing pressure-sensitive adhesion strength of viscoelastic polymers. *Journal of Polymer Science Part B: Polymer Physics*, *50*(11), 739–772.

Fisseler-Eckhoff, A., Bartsch, H., Zinsky, R., & Schirren, J. (2011). Environmental isocyanate-induced asthma: Morphologic and pathogenetic aspects of an increasing occupational disease. *International Journal of Environmental Research and Public Health*, *8*(9), 3672–3687.

Flory, P. J. (1953). *Principles of Polymer Chemistry*. Cornell University Press.

Foltran, S., Alsarraf, J., Robert, F., Landais, Y., Cloutet, E., Cramail, H., & Tassaing, T. (2013). On the chemical fixation of supercritical carbon dioxide with epoxides catalyzed by ionic salts: An in situ FTIR and Raman study. *Catalysis Science & Technology*, *3*(4), 1046–1055.

Foltran, S., Maisonneuve, L., Cloutet, E., Gadenne, B., Alfos, C., Tassaing, T., & Cramail, H. (2012). Solubility in CO2 and swelling studies by in situ IR spectroscopy of vegetable-based epoxidized oils as polyurethane precursors. *Polymer Chemistry*, *3*(2), 525–532.

Forrest, J. A., Dalnoki-Veress, K., & Dutcher, J. R. (1997). Interface and chain confinement effects on the glass transition temperature of thin polymer films. *Physical Review E*, *56*(5), 5705–5716.

Forrest, J. A., Dalnoki-Veress, K., & Dutcher, J. R. (1998). Brillouin light scattering studies of the mechanical properties of thin freely standing polystyrene films. *Physical Review E*, *58*(5), 6109–6114.

Fortman, D. J., Brutman, J. P., Cramer, C. J., Hillmyer, M. A., & Dichtel, W. R. (2015). Mechanically activated, catalyst-free polyhydroxyurethane vitrimers. *Journal of the American Chemical Society*, *137*(44), 14019–14022.

Fortman, D. J., Brutman, J. P., De Hoe, G. X., Snyder, R. L., Dichtel, W. R., & Hillmyer, M. A. (2018). Approaches to sustainable and continually recyclable cross-linked polymers. *ACS Sustainable Chemistry & Engineering*, *6*(9), 11145–11159.

Fortman, D. J., Brutman, J. P., Hillmyer, M. A., & Dichtel, W. R. (2017). Structural effects on the reprocessability and stress relaxation of crosslinked polyhydroxyurethanes. *Journal of Applied Polymer Science*, *134*(45), 44984.

Fortman, D. J., Sheppard, D. T., & Dichtel, W. R. (2019). Reprocessing cross-linked polyurethanes by catalyzing carbamate exchange. *Macromolecules*, *52*(16), 6330–6335.

Fortman, D. J., Snyder, R. L., Sheppard, D. T., & Dichtel, W. R. (2018). Rapidly reprocessable cross-linked polyhydroxyurethanes based on disulfide exchange. *ACS Macro Letters*, *7*(10), 1226–1231.

Francis, L. F., Mccormick, A. V., Vaessen, D. M., & Payne, J. A. (2002). Development and measurement of stress in polymer coatings. *Journal of Materials Science*, *37*(22), 4717–4731.

Fu, D., Pu, W., Wang, Z., Lu, X., Sun, S., Yu, C., & Xia, H. (2018). A facile dynamic crosslinked healable poly(oxime-urethane) elastomer with high elastic recovery and recyclability. *Journal of Materials Chemistry A*, *6*(37), 18154–18164.

Fuensanta, M., & Martín-Martínez, J. M. (2020). Viscoelastic and adhesion properties of new poly(ether-urethane) pressure-sensitive adhesives. *Frontiers in Mechanical Engineering*, *6*.

Furtwengler, P., & Avérous, L. (2018). From D-sorbitol to five-membered bis(cyclo-carbonate) as a platform molecule for the synthesis of different original biobased chemicals and polymers. *Scientific Reports*, *8*(1), 9134.

Gama, N. V., Ferreira, A., & Barros-Timmons, A. (2018). Polyurethane foams: Past, present, and future. *Materials*, *11*(10), 1841.

Gao, W., Bie, M., Quan, Y., Zhu, J., & Zhang, W. (2018). Self-healing, reprocessing and sealing abilities of polysulfide-based polyurethane. *Polymer*, *151*, 27–33.

Geng, K., & Tsui, O. K. C. (2016). Effects of polymer tacticity and molecular weight on the glass transition temperature of poly(methyl methacrylate) films on silica. *Macromolecules*, *49*(7), 2671–2678.

Gomez-Lopez, A., Ayensa, N., Grignard, B., Irusta, L., Calvo, I., Müller, A. J., Detrembleur, C., & Sardon, H. (2022). Enhanced and reusable poly(hydroxy urethane)-based low temperature hot-melt adhesives. *ACS Polymers Au*.

Gomez-Lopez, A., Elizalde, F., Calvo, I., & Sardon, H. (2021). Trends in non-isocyanate polyurethane (NIPU) development. *Chemical Communications*, *57*(92), 12254–12265.

Gomopoulos, N., Cheng, W., Efremov, M., Nealey, P. F., & Fytas, G. (2009). Out-of-plane longitudinal elastic modulus of supported polymer thin films. *Macromolecules*, *42*(18), 7164–7167.

Gomopoulos, N., Saini, G., Efremov, M., Nealey, P. F., Nelson, K., & Fytas, G. (2010). Nondestructive probing of mechanical anisotropy in polyimide films on nanoscale. *Macromolecules*, *43*(3), 1551–1555.

Grohens, Y., Brogly, M., Labbe, C., David, M.-O., & Schultz, J. (1998). Glass transition of stereoregular poly(methyl methacrylate) at interfaces. *Langmuir*, *14*(11), 2929–2932.

Guan, J., Song, Y., Lin, Y., Yin, X., Zuo, M., Zhao, Y., Tao, X., & Zheng, Q. (2011). Progress in study of non-isocyanate polyurethane. *Industrial & Engineering Chemistry Research*, *50*(11), 6517–6527.

Guo, S., Wan, K.-T., & Dillard, D. A. (2005). A bending-to-stretching analysis of the blister test in the presence of tensile residual stress. *International Journal of Solids and Structures*, *42*(9), 2771–2784.

Hajiali, F., Tajbakhsh, S., & Marić, M. (2021). Thermally reprocessable bio-based polymethacrylate vitrimers and nanocomposites. *Polymer*, *212*, 123126.

Hall, D. B., Underhill, P., & Torkelson, J. M. (1998). Spin coating of thin and ultrathin polymer films. *Polymer Engineering & Science*, *38*(12), 2039–2045.

Hayashi, M. (2021). Versatile functionalization of polymeric soft materials by implanting various types of dynamic cross-links. *Polymer Journal*, *53*(7), 779–788.

Hicks, D., & Austin, A. (2017). A review of the global PU industry in 2016 and outlook for 2017. *PU Magazine Gupta Verlag, Vol 14*.

Hooker, J. C., & Torkelson, J. M. (1995). Coupling of probe reorientation dynamics and rotor motions to polymer relaxation as sensed by second harmonic generation and fluorescence. *Macromolecules*, *28*(23), 7683–7692.

Hu, S., Chen, X., Bin Rusayyis, M. A., Purwanto, N. S., & Torkelson, J. M. (2022). Reprocessable polyhydroxyurethane networks reinforced with reactive polyhedral oligomeric silsesquioxanes (POSS) and exhibiting excellent elevated temperature creep resistance. *Polymer*, *252*, 124971.

Hu, S., Chen, X., & Torkelson, J. M. (2019). Biobased reprocessable polyhydroxyurethane networks: Full recovery of crosslink density with three concurrent dynamic chemistries. *ACS Sustainable Chemistry & Engineering*, *7*(11), 10025–10034.

Hu, Y., Tang, G., Luo, Y., Chi, S., & Li, X. (2021). Glycidyl azide polymer-based polyurethane vitrimers with disulfide chain extenders. *Polymer Chemistry*, *12*(28), 4072–4082.

Huang, Z., Wang, Y., Zhu, J., Yu, J., & Hu, Z. (2018). Surface engineering of nanosilica for vitrimer composites. *Composites Science and Technology*, *154*, 18–27.

Inoue, R., Kanaya, T., Nishida, K., Tsukushi, I., & Shibata, K. (2005). Inelastic neutron scattering study of low energy excitations in polymer thin films. *Physical Review Letters*, *95*(5), 056102.

Inoue, R., Kanaya, T., Nishida, K., Tsukushi, I., & Shibata, K. (2006). Low-energy excitations and the fast process of polystyrene thin supported films studied by inelastic and quasielastic neutron scattering. *Physical Review E*, *74*(2), 021801.

Ishibashi, J. S. A., & Kalow, J. A. (2018). Vitrimeric silicone elastomers enabled by dynamic meldrum's acid-derived cross-links. *ACS Macro Letters*, *7*(4), 482–486.

Ismail, M. F., Khorshidi, B., & Sadrzadeh, M. (2019). New insights into the impact of nanoscale surface heterogeneity on the wettability of polymeric membranes. *Journal of Membrane Science*, *590*, 117270.

Iyer, K. A., Schueneman, G. T., & Torkelson, J. M. (2015). Cellulose nanocrystal/polyolefin biocomposites prepared by solid-state shear pulverization: Superior dispersion leading to synergistic property enhancements. *Polymer*, *56*, 464–475.

Iyer, K. A., & Torkelson, J. M. (2015). Importance of superior dispersion versus filler surface modification in producing robust polymer nanocomposites: The example of polypropylene/nanosilica hybrids. *Polymer*, *68*, 147–157.

Javni, I., Hong, D. P., & Petrović, Z. S. (2013). Polyurethanes from soybean oil, aromatic, and cycloaliphatic diamines by nonisocyanate route. *Journal of Applied Polymer Science*, *128*(1), 566–571.

Jin, K., Li, L., & Torkelson, J. M. (2016). Recyclable crosslinked polymer networks via one-step controlled radical polymerization. *Advanced Materials*, *28*(31), 6746–6750.

Jin, K., & Torkelson, J. M. (2016). Enhanced Tg-confinement effect in cross-linked polystyrene compared to its linear precursor: Roles of fragility and chain architecture. *Macromolecules*, *49*(14), 5092–5103.

Kloxin, C. J., & Bowman, C. N. (2013). Covalent adaptable networks: Smart, reconfigurable and responsive network systems. *Chemical Society Reviews*, *42*(17), 7161–7173.

Ju, B.-F., Liu, K.-K., Wong, M.-F., & Wan, K.-T. (2007). A novel cylindrical punch method to characterize interfacial adhesion and residual stress of a thin polymer film. *Engineering Fracture Mechanics*, *74*(7), 1101–1106.

Kalyanasundaram, K., & Thomas, J. K. (1977). Environmental effects on vibronic band intensities in pyrene monomer fluorescence and their application in studies of micellar systems. *Journal of the American Chemical Society*, *99*(7), 2039–2044.

Karpovich, D. S., & Blanchard, G. J. (1995). Relating the polarity-dependent fluorescence response of pyrene to vibronic coupling. Achieving a fundamental understanding of the py polarity scale. *The Journal of Physical Chemistry*, *99*(12), 3951–3958.

Kathalewar, M. S., Joshi, P. B., Sabnis, A. S., & Malshe, V. C. (2013). Non-isocyanate polyurethanes: From chemistry to applications. *RSC Advances*, *3*(13), 4110–4129.

Kathalewar, M. S., Sabnis, A., & D'Mello, D. (2014). Isocyanate free polyurethanes from new CNSL based bis-cyclic carbonate and its application in coatings. *European Polymer Journal*, *57*, 99–108.

Kawana, S., & Jones, R. A. L. (2001). Character of the glass transition in thin supported polymer films. *Physical Review E*, *63*(2), 021501.

Keddie, J. L., & Jones, R. A. L. (1995). Glass transition behavior in ultra-thin polystyrene films. *Israel Journal of Chemistry*, *35*(1), 21–26.

Keddie, J. L., Jones, R. A. L., & Cory, R. A. (1994a). Interface and surface effects on the glass-transition temperature in thin polymer films. *Faraday Discussions*, *98*(0), 219–230.

Keddie, J. L., Jones, R. A. L., & Cory, R. A. (1994b). Size-dependent depression of the glass transition temperature in polymer films. *Europhysics Letters (EPL)*, *27*(1), 59–64.

Kim, J. H., Jang, J., & Zin, W.-C. (2001). Thickness dependence of the glass transition temperature in thin polymer films. *Langmuir*, *17*(9), 2703–2710.

Kim, S. D., & Torkelson, J. M. (2002). Nanoscale confinement and temperature effects on associative polymers in thin films: Fluorescence study of a telechelic, pyrene-labeled poly(dimethylsiloxane). *Macromolecules*, *35*(15), 5943–5952.

Kim, S., Hewlett, S. A., Roth, C. B., & Torkelson, J. M. (2009). Confinement effects on glass transition temperature, transition breadth, and expansivity: Comparison of ellipsometry and fluorescence measurements on polystyrene films. *The European Physical Journal E*, *30*(1), 83.

Kim, S., Lee, S. H., Choi, S., Ahn, S., Jang, G.-D., Park, J. S., & Seong, D. G. (2021). Overcoming the trade-off relationship between mechanical and adhesive properties of acrylic pressure sensitive adhesive thin-film by reinforcing polydopamine-coated silica nanoparticles. *Polymer*, *228*, 123937.

Kim, S., Roth, C. B., & Torkelson, J. M. (2008). Effect of nanoscale confinement on the glass transition temperature of free-standing polymer films: Novel, self-referencing fluorescence method. *Journal of Polymer Science Part B: Polymer Physics*, *46*(24), 2754–2764.

Kim, S., & Torkelson, J. M. (2011). Distribution of glass transition temperatures in free-standing, nanoconfined polystyrene films: A test of de Gennes' sliding motion mechanism. *Macromolecules*, *44*(11), 4546–4553.

Kloxin, C. J., & Bowman, C. N. (2013). Covalent adaptable networks: Smart, reconfigurable and responsive network systems. *Chemical Society Reviews*, *42*(17), 7161–7173.

Kloxin, C. J., Scott, T. F., Adzima, B. J., & Bowman, C. N. (2010). Covalent adaptable networks (CANs): A unique paradigm in cross-linked polymers. *Macromolecules*, *43*(6), 2643–2653.

Kuang, X., Zhou, Y., Shi, Q., Wang, T., & Qi, H. J. (2018). Recycling of epoxy thermoset and composites via good solvent assisted and small molecules participated exchange reactions. *ACS Sustainable Chemistry & Engineering*, *6*(7), 9189–9197.

Kuhl, N., Abend, M., Geitner, R., Vitz, J., Zechel, S., Schmitt, M., Popp, J., Schubert, U. S., & Hager, M. D. (2018). Urethanes as reversible covalent moieties in self-healing polymers. *European Polymer Journal*, *104*, 45–50.

Lambeth, R. H., & Henderson, T. J. (2013). Organocatalytic synthesis of (poly)hydroxyurethanes from cyclic carbonates and amines. *Polymer*, *54*(21), 5568–5573.

Lan, T., & Torkelson, J. M. (2014). Methacrylate-based polymer films useful in lithographic applications exhibit different glass transition temperature-confinement effects at high and low molecular weight. *Polymer*, *55*(5), 1249–1258.

Lan, T., & Torkelson, J. M. (2016). Fragility-confinement effects: Apparent universality as a function of scaled thickness in films of freely deposited, linear polymer and its absence in densely grafted brushes. *Macromolecules*, *49*(4), 1331–1343.

Lee, Y., Bretz, K. C., Wise, F. W., & Sachse, W. (1996). Picosecond acoustic measurements of longitudinal wave velocity of submicron polymer films. *Applied Physics Letters*, *69*(12), 1692–1694.

Legrand, A., & Soulié-Ziakovic, C. (2016). Silica–epoxy vitrimer nanocomposites. *Macromolecules*, *49*(16), 5893–5902.

Leitsch, E. K., Beniah, G., Liu, K., Lan, T., Heath, W. H., Scheidt, K. A., & Torkelson, J. M. (2016). Nonisocyanate thermoplastic polyhydroxyurethane elastomers via cyclic carbonate

aminolysis: Critical role of hydroxyl groups in controlling nanophase separation. *ACS Macro Letters*, *5*(4), 424–429.

Lessard, J. J., Garcia, L. F., Easterling, C. P., Sims, M. B., Bentz, K. C., Arencibia, S., Savin, D. A., & Sumerlin, B. S. (2019). Catalyst-free vitrimers from vinyl polymers. *Macromolecules*, *52*(5), 2105–2111.

Li, L., Chen, X., Jin, K., Bin Rusayyis, M. A., & Torkelson, J. M. (2021). Arresting elevated-temperature creep and achieving full cross-link density recovery in reprocessable polymer networks and network composites via nitroxide-mediated dynamic chemistry. *Macromolecules*, *54*(3), 1452–1464.

Li, L., Chen, X., Jin, K., & Torkelson, J. M. (2018). Vitrimers designed both to strongly suppress creep and to recover original cross-link density after reprocessing: quantitative theory and experiments. *Macromolecules*, *51*(15), 5537–5546.

Li, L., Chen, X., & Torkelson, J. M. (2019). Reprocessable polymer networks via thiourethane dynamic chemistry: Recovery of cross-link density after recycling and proof-of-principle solvolysis leading to monomer recovery. *Macromolecules*, *52*(21), 8207–8216.

Li, L., Chen, X., & Torkelson, J. M. (2020). Covalent adaptive networks for enhanced adhesion: Exploiting disulfide dynamic chemistry and annealing during application. *ACS Applied Polymer Materials*, *2*(11), 4658–4665.

Liu, W., Fang, C., Wang, S., Huang, J., & Qiu, X. (2019). High-performance lignin-containing polyurethane elastomers with dynamic covalent polymer networks. *Macromolecules*, *52*(17), 6474–6484.

Liu, W., Hang, G., Mei, H., Li, L., & Zheng, S. (2022). Nanocomposites of polyhydroxyurethane with poss microdomains: Synthesis via non-isocyanate approach, morphologies and reprocessing properties. *Polymers*, *14*(7), 1331.

Liu, W., Schmidt, D. F., & Reynaud, E. (2017). Catalyst selection, creep, and stress relaxation in high-performance epoxy vitrimers. *Industrial & Engineering Chemistry Research*, *56*(10), 2667–2672.

Liu, W.-X., Zhang, C., Zhang, H., Zhao, N., Yu, Z.-X., & Xu, J. (2017). Oxime-based and catalyst-free dynamic covalent polyurethanes. *Journal of the American Chemical Society*, *139*(25), 8678–8684.

Liu, Y., Chen, Y.-C., Hutchens, S., Lawrence, J., Emrick, T., & Crosby, A. J. (2015). Directly measuring the complete stress–strain response of ultrathin polymer films. *Macromolecules*, *48*(18), 6534–6540.

Liu, Y., Tang, Z., Chen, Y., Zhang, C., & Guo, B. (2018). Engineering of β-hydroxyl esters into elastomer–nanoparticle interface toward malleable, robust, and reprocessable vitrimer composites. *ACS Applied Materials & Interfaces*, *10*(3), 2992–3001.

Liu, Y., Tang, Z., Wang, D., Wu, S., & Guo, B. (2019). Biomimetic design of elastomeric vitrimers with unparalleled mechanical properties, improved creep resistance and retained malleability by metal–ligand coordination. *Journal of Materials Chemistry A*, *7*(47), 26867–26876.

Lodge, T. P., & Hiemenz, P. C. (2020). *Polymer Chemistry* (3rd ed.). CRC Press.

Lombardo, V. M., Dhulst, E. A., Leitsch, E. K., Wilmot, N., Heath, W. H., Gies, A. P., Miller, M. D., Torkelson, J. M., & Scheidt, K. A. (2015). Cooperative catalysis of cyclic carbonate

ring opening: Application towards non-isocyanate polyurethane materials. *European Journal of Organic Chemistry*, *2015*(13), 2791–2795.

Lossada, F., Jiao, D., Yao, X., & Walther, A. (2020). Waterborne methacrylate-based vitrimers. *ACS Macro Letters*, *9*(1), 70–76.

Lu, Y.-X., & Guan, Z. (2012). Olefin metathesis for effective polymer healing via dynamic exchange of strong carbon–carbon double bonds. *Journal of the American Chemical Society*, *134*(34), 14226–14231.

Lu, Y.-X., Tournilhac, F., Leibler, L., & Guan, Z. (2012). Making insoluble polymer networks malleable via olefin metathesis. *Journal of the American Chemical Society*, *134*(20), 8424–8427.

Maisonneuve, L., Lamarzelle, O., Rix, E., Grau, E., & Cramail, H. (2015). Isocyanate-free routes to polyurethanes and poly(hydroxy urethane)s. *Chemical Reviews*, *115*(22), 12407–12439.

Malzbender, J., & de With, G. (2000). Cracking and residual stress in hybrid coatings on float glass. *Thin Solid Films*, *359*(2), 210–214.

Marin, G., & Derail, C. (2006). Rheology and adherence of pressure-sensitive adhesives. *The Journal of Adhesion*, *82*(5), 469–485.

McBride, M. K., Worrell, B. T., Brown, T., Cox, L. M., Sowan, N., Wang, C., Podgorski, M., Martinez, A. M., & Bowman, C. N. (2019). Enabling applications of covalent adaptable networks. *Annual Review of Chemical and Biomolecular Engineering*, *10*(1), 175–198.

Montarnal, D., Capelot, M., Tournilhac, F., & Leibler, L. (2011). Silica-like malleable materials from permanent organic networks. *Science*, *334*(6058), 965–968.

Moon, H., Jeong, K., Kwak, M. J., Choi, S. Q., & Im, S. G. (2018). Solvent-free deposition of ultrathin copolymer films with tunable viscoelasticity for application to pressure-sensitive adhesives. *ACS Applied Materials & Interfaces*, *10*(38), 32668–32677.

Mouhamad, Y., Mokarian-Tabari, P., Clarke, N., Jones, R. A. L., & Geoghegan, M. (2014). Dynamics of polymer film formation during spin coating. *Journal of Applied Physics*, *116*(12), 123513.

Mundra, M. K., Ellison, C. J., Behling, R. E., & Torkelson, J. M. (2006). Confinement, composition, and spin-coating effects on the glass transition and stress relaxation of thin films of polystyrene and styrene-containing random copolymers: Sensing by intrinsic fluorescence. *Polymer*, *47*(22), 7747–7759.

Mundra, M. K., Ellison, C. J., Rittigstein, P., & Torkelson, J. M. (2007). Fluorescence studies of confinement in polymer films and nanocomposites: Glass transition temperature, plasticizer effects, and sensitivity to stress relaxation and local polarity. *The European Physical Journal Special Topics*, *141*(1), 143.

Muraki, N., Matoba, N., Hirano, T., & Yoshikawa, M. (2002). Determination of thermal stress distribution in a model microelectronic device encapsulated with alumina filled epoxy resin using fluorescence spectroscopy. *Polymer*, *43*(4), 1277–1285.

Napolitano, S., Glynos, E., & Tito, N. B. (2017). Glass transition of polymers in bulk, confined geometries, and near interfaces. *Reports on Progress in Physics. Physical Society (Great Britain)*, *80*(3), 036602.

Nielsen, L. E. (1969). Cross-linking–effect on physical properties of polymers. *Journal of Macromolecular Science, Part C*, *3*(1), 69–103.

Nohra, B., Candy, L., Blanco, J.-F., Guerin, C., Raoul, Y., & Mouloungui, Z. (2013). From petrochemical polyurethanes to biobased polyhydroxyurethanes. *Macromolecules*, *46*(10), 3771–3792.

North, M., Pasquale, R., & Young, C. (2010). Synthesis of cyclic carbonates from epoxides and CO2. *Green Chemistry*, *12*(9), 1514–1539.

Ochiai, B., & Utsuno, T. (2013). Non-isocyanate synthesis and application of telechelic polyurethanes via polycondensation of diurethanes obtained from ethylene carbonate and diamines. *Journal of Polymer Science Part A: Polymer Chemistry*, *51*(3), 525–533.

Oehlenschlaeger, K. K., Mueller, J. O., Brandt, J., Hilf, S., Lederer, A., Wilhelm, M., Graf, R., Coote, M. L., Schmidt, F. G., & Barner-Kowollik, C. (2014). Adaptable hetero Diels–Alder networks for fast self-healing under mild conditions. *Advanced Materials*, *26*(21), 3561–3566.

Offenbach, J. A., & Tobolsky, A. V. (1956). Chemical relaxation of stress in polyurethane elastomers. *Journal of Colloid Science*, *11*(1), 39–47.

Otsuka, H. (2013). Reorganization of polymer structures based on dynamic covalent chemistry: Polymer reactions by dynamic covalent exchanges of alkoxyamine units. *Polymer Journal*, *45*(9), 879–891.

Paul, D. R., & Robeson, L. M. (2008). Polymer nanotechnology: Nanocomposites. *Polymer*, *49*(15), 3187–3204.

Plazek, D. J. (1966). Effect of crosslink density on the creep behavior of natural rubber vulcanizates. *Journal of Polymer Science Part A-2: Polymer Physics*, *4*(5), 745–763.

Pocius, A. V. (2012). *Adhesion and Adhesives Technology: An Introduction* (3rd edition). Hanser Publications.

Podgórski, M., Fairbanks, B. D., Kirkpatrick, B. E., McBride, M., Martinez, A., Dobson, A., Bongiardina, N. J., & Bowman, C. N. (2020). Toward stimuli-responsive dynamic thermosets through continuous development and improvements in covalent adaptable networks (CANs). *Advanced Materials*, *32*(20), 1906876.

Polgar, L. M., van Duin, M., Broekhuis, A. A., & Picchioni, F. (2015). Use of Diels–Alder chemistry for thermoreversible cross-linking of rubbers: the next step toward recycling of rubber products? *Macromolecules*, *48*(19), 7096–7105.

Potts, J. R., Dreyer, D. R., Bielawski, C. W., & Ruoff, R. S. (2011). Graphene-based polymer nanocomposites. *Polymer*, *52*(1), 5–25.

Poussard, L., Mariage, J., Grignard, B., Detrembleur, C., Jérôme, C., Calberg, C., Heinrichs, B., De Winter, J., Gerbaux, P., Raquez, J.-M., Bonnaud, L., & Dubois, Ph. (2016). Non-isocyanate polyurethanes from carbonated soybean oil using monomeric or oligomeric diamines to achieve thermosets or thermoplastics. *Macromolecules*, *49*(6), 2162–2171.

Priestley, R. D., Broadbelt, L. J., & Torkelson, J. M. (2005). Physical aging of ultrathin polymer films above and below the bulk glass transition temperature: Effects of attractive vs neutral polymer−substrate interactions measured by fluorescence. *Macromolecules*, *38*(3), 654–657.

Pye, J. E., & Roth, C. B. (2011). Two simultaneous mechanisms causing glass transition temperature reductions in high molecular weight freestanding polymer films as measured by transmission ellipsometry. *Physical Review Letters*, *107*(23), 235701.

Qiang, Z., Li, L., Torkelson, J. M., & Wang, M. (2020). Determining order-to-disorder transitions in block copolymer thin films using a self-referencing fluorescent probe. *Molecular Systems Design & Engineering*, *5*(1), 330–338.

Qiu, M., Wu, S., Tang, Z., & Guo, B. (2018). Exchangeable interfacial crosslinks towards mechanically robust elastomer/carbon nanotubes vitrimers. *Composites Science and Technology*, *165*, 24–30.

Ree, M., Chu, C., & Goldberg, M. J. (1994). Influences of chain rigidity, in-plane orientation, and thickness on residual stress of polymer films. *Journal of Applied Physics*, *75*(3), 1410–1419.

Ree, M., Swanson, S., & Volksen, W. (1993). Effect of precursor history on residual stress and relaxation behaviour of high temperature polyimides. *Polymer*, *34*(7), 1423–1430.

Reiter, G. (1994). Dewetting as a probe of polymer mobility in thin films. *Macromolecules*, *27*(11), 3046–3052.

Reiter, G. (2013). Probing properties of polymers in thin films via dewetting. *Glass Transition, Dynamics and Heterogeneity of Polymer Thin Films*, 29–63.

Reiter, G., Hamieh, M., Damman, P., Sclavons, S., Gabriele, S., Vilmin, T., & Raphaël, E. (2005). Residual stresses in thin polymer films cause rupture and dominate early stages of dewetting. *Nature Materials*, *4*(10), 754–758.

Reiter, G., & Khanna, R. (2000). Kinetics of autophobic dewetting of polymer films. *Langmuir*, *16*(15), 6351–6357.

Rekondo, A., Martin, R., de Luzuriaga, A. R., Cabañero, G., Grande, H. J., & Odriozola, I. (2014). Catalyst-free room-temperature self-healing elastomers based on aromatic disulfide metathesis. *Materials Horizons*, *1*(2), 237–240.

Reutenauer, P., Buhler, E., Boul, P. J., Candau, S. J., & Lehn, J.-M. (2009). Room temperature dynamic polymers based on Diels–Alder chemistry. *Chemistry – A European Journal*, *15*(8), 1893–1900.

Richardson, H., Carelli, C., Keddie, J. L., & Sferrazza, M. (2003). Structural relaxation of spin-cast glassy polymer thin films as a possible factor in dewetting. *The European Physical Journal. E, Soft Matter*, *12*(3), 437–440; discussion 440-441.

Riggleman, R. A., Yoshimoto, K., Douglas, J. F., & de Pablo, J. J. (2006). Influence of confinement on the fragility of antiplasticized and pure polymer films. *Physical Review Letters*, *97*(4), 045502.

Rittigstein, P., & Torkelson, J. M. (2006). Polymer–nanoparticle interfacial interactions in polymer nanocomposites: Confinement effects on glass transition temperature and suppression of physical aging. *Journal of Polymer Science Part B: Polymer Physics*, *44*(20), 2935–2943.

Romo-Uribe, A. (2018). Viscoelasticity and microstructure of POSS-methyl methacrylate nanocomposites. Dynamics and entanglement dilution. *Polymer*, *148*, 27–38.

Romo-Uribe, A., & Lichtenhan, J. D. (2021). Melt extrusion and blow molding parts-per-million POSS interspersed the macromolecular network and simultaneously enhanced thermomechanical and barrier properties of polyolefin films. *Polymer Engineering & Science*, *61*(1), 245–257.

Roth, C. B., McNerny, K. L., Jager, W. F., & Torkelson, J. M. (2007). Eliminating the enhanced mobility at the free surface of polystyrene: Fluorescence studies of the glass transition temperature in thin bilayer films of immiscible polymers. *Macromolecules*, *40*(7), 2568–2574.

Roth, C. B., Pound, A., Kamp, S. W., Murray, C. A., & Dutcher, J. R. (2006). Molecular-weight dependence of the glass transition temperature of freely-standing poly(methyl methacrylate) films. *The European Physical Journal E*, *20*(4), 441–448.

Roth, C. B., & Torkelson, J. M. (2007). Selectively probing the glass transition temperature in multilayer polymer films: Equivalence of block copolymers and multilayer films of different homopolymers. *Macromolecules*, *40*(9), 3328–3336.

Röttger, M., Domenech, T., van der Weegen, R., Breuillac, A., Nicolaÿ, R., & Leibler, L. (2017). High-performance vitrimers from commodity thermoplastics through dioxaborolane metathesis. *Science*, *356*(6333), 62–65.

Rubinstein, M., & Colby, R. H. (2003). *Polymer Physics*. Oxford University Press.

Samanta, S., Kim, S., Saito, T., & Sokolov, A. P. (2021). Polymers with dynamic bonds: adaptive functional materials for a sustainable future. *The Journal of Physical Chemistry B*, *125*(33), 9389–9401.

Sandoval, R. W., Williams, D. E., Kim, J., Roth, C. B., & Torkelson, J. M. (2008). Critical micelle concentrations of block and gradient copolymers in homopolymer: Effects of sequence distribution, composition, and molecular weight. *Journal of Polymer Science Part B: Polymer Physics*, *46*(24), 2672–2682.

Scheutz, G. M., Lessard, J. J., Sims, M. B., & Sumerlin, B. S. (2019). Adaptable crosslinks in polymeric materials: Resolving the intersection of thermoplastics and thermosets. *Journal of the American Chemical Society*, *141*(41), 16181–16196.

Schmidt, S., Göppert, N. E., Bruchmann, B., & Mülhaupt, R. (2017). Liquid sorbitol ether carbonate as intermediate for rigid and segmented non-isocyanate polyhydroxyurethane thermosets. *European Polymer Journal*, *94*, 136–142.

Schneiderman, D. K., & Hillmyer, M. A. (2017). 50th anniversary perspective: There is a great future in sustainable polymers. *Macromolecules*, *50*(10), 3733–3749.

Self, J. L., Dolinski, N. D., Zayas, M. S., de Alaniz, J. R., & Bates, C. M. (2018). Brønsted-acid-catalyzed exchange in polyester dynamic covalent networks. *ACS Macro Letters*, *7*(7), 817–821.

Shao, C., Wang, M., Chang, H., Xu, F., & Yang, J. (2017). A self-healing cellulose nanocrystal-poly(ethylene glycol) nanocomposite hydrogel via Diels–Alder click reaction. *ACS Sustainable Chemistry & Engineering*, *5*(7), 6167–6174.

Shavit, A., & Riggleman, R. A. (2014). Physical aging, the local dynamics of glass-forming polymers under nanoscale confinement. *The Journal of Physical Chemistry. B*, *118*(30), 9096–9103.

Shen, W., Du, B., Zhuo, H., & Chen, S. (2022). Recyclable and reprocessable epoxy-polyhedral oligomeric silsesquioxane (POSS)/mesogenic azobenzene/poly (ethylene-co-vinyl acetate) composites with thermal- and light-responsive programmable shape-memory performance. *Chemical Engineering Journal*, *428*, 132609.

Shi, J., Zheng, T., Guo, B., & Xu, J. (2019). Solvent-free thermo-reversible and self-healable crosslinked polyurethane with dynamic covalent networks based on phenol-carbamate bonds. *Polymer*, *181*, 121788.

Shi, J., Zheng, T., Zhang, Y., Guo, B., & Xu, J. (2020). Reprocessable cross-linked polyurethane with dynamic and tunable phenol–carbamate network. *ACS Sustainable Chemistry & Engineering*, *8*(2), 1207–1218.

Shiga, T., Narita, T., Ikawa, T., & Okada, A. (1998). Stress monitoring in thin polymer coatings using time resolved fluorescence. *Polymer Engineering & Science*, *38*(4), 693–698.

Simón, D., Borreguero, A. M., de Lucas, A., & Rodríguez, J. F. (2018). Recycling of polyurethanes from laboratory to industry, a journey towards the sustainability. *Waste Management*, *76*, 147–171.

Snijkers, F., Pasquino, R., & Maffezzoli, A. (2017). Curing and viscoelasticity of vitrimers. *Soft Matter*, *13*(1), 258–268.

Snyder, R. L., Fortman, D. J., De Hoe, G. X., Hillmyer, M. A., & Dichtel, W. R. (2018). Reprocessable acid-degradable polycarbonate vitrimers. *Macromolecules*, *51*(2), 389–397.

Soles, C. L., Douglas, J. F., Wu, W. -l., & Dimeo, R. M. (2002). Incoherent neutron scattering and the dynamics of confined polycarbonate films. *Physical Review Letters*, *88*(3), 037401.

Bonab, V. S., Karimkhani, V., & Manas-Zloczower, I. (2019). Ultra-fast microwave assisted self-healing of covalent adaptive polyurethane networks with carbon nanotubes. *Macromolecular Materials and Engineering*, *304*(1), 1800405.

Soman, B., & Evans, C. M. (2021). Effect of precise linker length, bond density, and broad temperature window on the rheological properties of ethylene vitrimers. *Soft Matter*, *17*(13), 3569–3577.

Song, J., Kahraman, R., Collinson, D. W., Xia, W., Brinson, L. C., & Keten, S. (2019). Temperature effects on the nanoindentation characterization of stiffness gradients in confined polymers. *Soft Matter*, *15*(3), 359–370.

Sperling, L. H. (2006). *Introduction to Physical Polymer Science, 4th Edition*. John Wiley & Sons, Ltd.

Stafford, C. M., Harrison, C., Beers, K. L., Karim, A., Amis, E. J., VanLandingham, M. R., Kim, H.-C., Volksen, W., Miller, R. D., & Simonyi, E. E. (2004). A buckling-based metrology for measuring the elastic moduli of polymeric thin films. *Nature Materials*, *3*(8), 545–550.

Stafford, C. M., Vogt, B. D., Harrison, C., Julthongpiput, D., & Huang, R. (2006). Elastic moduli of ultrathin amorphous polymer films. *Macromolecules*, *39*(15), 5095–5099.

Steblyanko, A., Choi, W., Sanda, F., & Endo, T. (2000). Addition of five-membered cyclic carbonate with amine and its application to polymer synthesis. *Journal of Polymer Science Part A: Polymer Chemistry*, *38*(13), 2375–2380.

Sun, S., Li, M., & Liu, A. (2013). A review on mechanical properties of pressure sensitive adhesives. *International Journal of Adhesion and Adhesives*, *41*, 98–106.

Tajbakhsh, S., Hajiali, F., & Marić, M. (2021). Recyclable polymers with boronic ester dynamic bonds prepared by miniemulsion polymerization. *ACS Applied Polymer Materials*, *3*(7), 3402–3415.

Takahashi, A., Goseki, R., Ito, K., & Otsuka, H. (2017). Thermally healable and reprocessable bis(hindered amino)disulfide-cross-linked polymethacrylate networks. *ACS Macro Letters*, *6*(11), 1280–1284.

Tamami, B., Sohn, S., & Wilkes, G. L. (2004). Incorporation of carbon dioxide into soybean oil and subsequent preparation and studies of nonisocyanate polyurethane networks. *Journal of Applied Polymer Science*, *92*(2), 883–891.

Tanasi, P., Hernández Santana, M., Carretero-González, J., Verdejo, R., & López-Manchado, M. A. (2019). Thermo-reversible crosslinked natural rubber: A Diels-Alder route for reuse and self-healing properties in elastomers. *Polymer*, *175*, 15–24.

Tang, Y. J., Chen, J., Huang, Y. B., Li, D. C., Wang, S. S., Li, Z. H., & Zhang, W. D. (2007). Ultra-sensitive, highly reproducible film stress characterization using flexible suspended thin silicon plates and local curvature measurements. *Journal of Micromechanics and Microengineering*, *17*(10), 1923–1930.

Tang, Z., Zhang, L., Feng, W., Guo, B., Liu, F., & Jia, D. (2014). Rational design of graphene surface chemistry for high-performance rubber/graphene composites. *Macromolecules*, *47*(24), 8663–8673.

Thomas, K. R., & Steiner, U. (2011). Direct stress measurements in thin polymer films. *Soft Matter*, *7*(17), 7839–7842.

Tiu, B. D. B., Delparastan, P., Ney, M. R., Gerst, M., & Messersmith, P. B. (2019). Enhanced adhesion and cohesion of bioinspired dry/wet pressure-sensitive adhesives. *ACS Applied Materials & Interfaces*, *11*(31), 28296–28306.

Tomita, H., Sanda, F., & Endo, T. (2001). Polyaddition of bis(cyclic thiocarbonate) with diamines. novel efficient synthetic method of polyhydroxythiourethanes. *Macromolecules*, *34*(4), 727–733.

Toncelli, C., De Reus, D. C., Picchioni, F., & Broekhuis, A. A. (2012). Properties of reversible diels–alder furan/maleimide polymer networks as function of crosslink density. *Macromolecular Chemistry and Physics*, *213*(2), 157–165.

Torres, J. M., Stafford, C. M., Uhrig, D., & Vogt, B. D. (2012). Impact of chain architecture (branching) on the thermal and mechanical behavior of polystyrene thin films. *Journal of Polymer Science Part B: Polymer Physics*, *50*(5), 370–377.

Trigg, E. B., & Winey, K. I. (2019). Nanoscale layers in polymers to promote ion transport. *Molecular Systems Design & Engineering*, *4*(2), 252–262.

Trovatti, E., Lacerda, T. M., Carvalho, A. J. F., & Gandini, A. (2015). Recycling tires? Reversible crosslinking of poly(butadiene). *Advanced Materials*, *27*(13), 2242–2245.

Truong, T. T., Thai, S. H., Nguyen, H. T., Phung, D. T. T., Nguyen, L. T., Pham, H. Q., & Nguyen, L.-T. T. (2019). Tailoring the hard–soft interface with dynamic Diels–Alder linkages in

polyurethanes: Toward superior mechanical properties and healability at mild temperature. *Chemistry of Materials*, *31*(7), 2347–2357.

Tsai, F. J., & Torkelson, J. M. (1988). Phase separation of oligomeric polystyrene-polybutadiene blends as studied by excimer fluorescence. *Macromolecules*, *21*(4), 1026–1033.

Tsui, O. K. C., Russell, T. P., & Hawker, C. J. (2001). Effect of interfacial interactions on the glass transition of polymer thin films. *Macromolecules*, *34*(16), 5535–5539.

Tweedie, C. A., Constantinides, G., Lehman, K. E., Brill, D. J., Blackman, G. S., & Van Vliet, K. J. (2007). Enhanced stiffness of amorphous polymer surfaces under confinement of localized contact loads. *Advanced Materials*, *19*(18), 2540–2546.

Valentín, J. L., Mora-Barrantes, I., Carretero-González, J., López-Manchado, M. A., Sotta, P., Long, D. R., & Saalwächter, K. (2010). Novel experimental approach to evaluate filler−elastomer interactions. *Macromolecules*, *43*(1), 334–346.

Vignaud, G., S. Chebil, M., Bal, J. K., Delorme, N., Beuvier, T., Grohens, Y., & Gibaud, A. (2014). Densification and depression in glass transition temperature in polystyrene thin films. *Langmuir*, *30*(39), 11599–11608.

Vogt, B. D., Kang, S., Prabhu, V. M., Lin, E. K., Satija, S. K., Turnquest, K., & Wu, W. (2006). Measurements of the reaction−diffusion front of model chemically amplified photoresists with varying photoacid size. *Macromolecules*, *39*(24), 8311–8317.

Wang, J., Du, W., Zhang, Z., Gao, W., & Li, Z. (2021). Biomass/polyhedral oligomeric silsesquioxane nanocomposites: Advances in preparation strategies and performances. *Journal of Applied Polymer Science*, *138*(2), 49641.

Wang, S., Xu, J., Wang, W., Wang, G.-J. N., Rastak, R., Molina-Lopez, F., Chung, J. W., Niu, S., Feig, V. R., Lopez, J., Lei, T., Kwon, S.-K., Kim, Y., Foudeh, A. M., Ehrlich, A., Gasperini,

A., Yun, Y., Murmann, B., Tok, J. B.-H., & Bao, Z. (2018). Skin electronics from scalable fabrication of an intrinsically stretchable transistor array. *Nature*, *555*(7694), 83–88.

Wang, T., Yan, J., Yuan, H., Xu, J., Lam, H. Y., Yu, X., Lv, C., Du, B., & Tsui, O. K. C. (2019). Tg confinement effect of random copolymers of 4-tert-butylstyrene and 4-acetoxystyrene with different compositions. *ACS Macro Letters*, *8*(10), 1280–1284.

Wang, Y., Pan, Y., Zheng, Z., & Ding, X. (2019). Reprocessable and multiple shape memory thermosets with reconfigurability. *Macromolecular Rapid Communications*, *40*(11), 1900001.

Wang, Z., Zhang, X., Zhang, L., Tan, T., & Fong, H. (2016). Nonisocyanate biobased poly(ester urethanes) with tunable properties synthesized via an environment-friendly route. *ACS Sustainable Chemistry & Engineering*, *4*(5), 2762–2770.

Watanabe, K. (1962). Stress relaxation and creep of several vulcanized elastomers. *Rubber Chemistry and Technology*, *35*(1), 182–199.

Watcharotone, S., Wood, C. D., Friedrich, R., Chen, X., Qiao, R., Putz, K., & Brinson, L. C. (2011). Interfacial and substrate effects on local elastic properties of polymers using coupled experiments and modeling of nanoindentation. *Advanced Engineering Materials*, *13*(5), 400–404.

Watuthanthrige, N. D. A, Chakma, P., & Konkolewicz, D. (2021). Designing dynamic materials from dynamic bonds to macromolecular architecture. *Trends in Chemistry*, *3*(3), 231–247.

Wei, T., Jin, K., & Torkelson, J. M. (2019). Isolating the effect of polymer-grafted nanoparticle interactions with matrix polymer from dispersion on composite property enhancement: The example of polypropylene/halloysite nanocomposites. *Polymer*, *176*, 38–50.

Wemyss, A. M., Ellingford, C., Morishita, Y., Bowen, C., & Wan, C. (2021). Dynamic polymer networks: a new avenue towards sustainable and advanced soft machines. *Angewandte Chemie*, *133*(25), 13841–13852.

Wen, Z., Han, X., Fairbanks, B. D., Yang, K., & Bowman, C. N. (2020). Development of thiourethanes as robust, reprocessable networks. *Polymer*, *202*, 122715.

Wen, Z., McBride, M. K., Zhang, X., Han, X., Martinez, A. M., Shao, R., Zhu, C., Visvanathan, R., Clark, N. A., Wang, Y., Yang, K., & Bowman, C. N. (2018). Reconfigurable LC elastomers: Using a thermally programmable monodomain to access two-way free-standing multiple shape memory polymers. *Macromolecules*, *51*(15), 5812–5819.

Wieberger, F., Forman, D. C., Neuber, C., Gröschel, A. H., Böhm, M., Müller, A. H. E., Schmidt, H.-W., & Ober, C. K. (2011). Tailored star-shaped statistical teroligomers viaATRP for lithographic applications. *Journal of Materials Chemistry*, *22*(1), 73–79.

Wojtecki, R. J., Meador, M. A., & Rowan, S. J. (2011). Using the dynamic bond to access macroscopically responsive structurally dynamic polymers. *Nature Materials*, *10*(1), 14–27.

Wong, C. L. H., Kim, J., & Torkelson, J. M. (2007). Breadth of glass transition temperature in styrene/acrylic acid block, random, and gradient copolymers: Unusual sequence distribution effects. *Journal of Polymer Science Part B: Polymer Physics*, *45*(20), 2842–2849.

Wong, C. L. H., Kim, J., Roth, C. B., & Torkelson, J. M. (2007). Comparison of critical micelle concentrations of gradient copolymer and block copolymer in homopolymer: Novel characterization by intrinsic fluorescence. *Macromolecules*, *40*(16), 5631–5633.

Wu, S., Yang, H., Huang, S., & Chen, Q. (2020). Relationship between reaction kinetics and chain dynamics of vitrimers based on dioxaborolane metathesis. *Macromolecules*, *53*(4), 1180–1190.

Xia, W., & Keten, S. (2015). Interfacial stiffening of polymer thin films under nanoconfinement. *Extreme Mechanics Letters*, *4*, 89–95.

Xia, W., & Lan, T. (2019). Interfacial dynamics governs the mechanical properties of glassy polymer thin films. *Macromolecules*, *52*(17), 6547–6554.

Xia, W., Song, J., Hsu, D. D., & Keten, S. (2016). Understanding the interfacial mechanical response of nanoscale polymer thin films via nanoindentation. *Macromolecules*, *49*(10), 3810–3817.

Xu, J., Wang, S., Wang, G.-J. N., Zhu, C., Luo, S., Jin, L., Gu, X., Chen, S., Feig, V. R., To, J. W. F., Rondeau-Gagné, S., Park, J., Schroeder, B. C., Lu, C., Oh, J. Y., Wang, Y., Kim, Y.-H., Yan, H., Sinclair, R., … Bao, Z. (2017). Highly stretchable polymer semiconductor films through the nanoconfinement effect. *Science*, *355*(6320), 59–64.

Xu, S., O'Connell, P. A., & McKenna, G. B. (2010). Unusual elastic behavior of ultrathin polymer films: Confinement-induced/molecular stiffening and surface tension effects. *The Journal of Chemical Physics*, *132*(18), 184902.

Xu, Z., Zhao, Y., Wang, X., & Lin, T. (2013). A thermally healable polyhedral oligomeric silsesquioxane (POSS) nanocomposite based on Diels–Alder chemistry. *Chemical Communications*, *49*(60), 6755–6757.

Yamashiro, M., Inoue, K., & Iji, M. (2008). Recyclable shape-memory and mechanical strength of poly(lactic acid) compounds cross-linked by thermo-reversible Diels-Alder reaction. *Polymer Journal*, *40*(7), 657–662.

Yan, P., Zhao, W., Fu, X., Liu, Z., Kong, W., Zhou, C., & Lei, J. (2017). Multifunctional polyurethane-vitrimers completely based on transcarbamoylation of carbamates: Thermally-induced dual-shape memory effect and self-welding. *RSC Advances*, *7*(43), 26858–26866.

Yang, H., He, C., Russell, T. P., & Wang, D. (2020). Epoxy-polyhedral oligomeric silsesquioxanes (POSS) nanocomposite vitrimers with high strength, toughness, and efficient relaxation. *Giant*, *4*, 100035.

Yang, H. W. H., & Chang, E.-P. (1997). The role of viscoelastic properties in the design of pressure-sensitive adhesives. *Trends in Polymer Science*, *11*(5), 380–384.

Yang, W., Dong, Q., Liu, S., Xie, H., Liu, L., & Li, J. (2012). Recycling and disposal methods for polyurethane foam wastes. *Procedia Environmental Sciences*, *16*, 167–175.

Yang, Y., Ding, X., & Urban, M. W. (2015). Chemical and physical aspects of self-healing materials. *Progress in Polymer Science*, *49–50*, 34–59.

Yang, Y., Poessel, B., & Mülhaupt, R. (2020). Graphenated ceramic particles as functional fillers for nonisocyanate polyhydroxyurethane composites. *Macromolecular Materials and Engineering*, *305*(8), 2000203.

Yarusso, D. J. (1999). Quantifying the relationship between peel and rheology for pressure sensitive adhesives. *The Journal of Adhesion*, *70*(3–4), 299–320.

Ye, C., Wiener, C. G., Tyagi, M., Uhrig, D., Orski, S. V., Soles, C. L., Vogt, B. D., & Simmons, D. S. (2015). Understanding the decreased segmental dynamics of supported thin polymer films reported by incoherent neutron scattering. *Macromolecules*, *48*(3), 801–808.

Ying, H., Zhang, Y., & Cheng, J. (2014). Dynamic urea bond for the design of reversible and self-healing polymers. *Nature Communications*, *5*, 3218.

Zhang, B., Kowsari, K., Serjouei, A., Dunn, M. L., & Ge, Q. (2018). Reprocessable thermosets for sustainable three-dimensional printing. *Nature Communications*, *9*(1), 1831.

Zhang, L., Elupula, R., Grayson, S. M., & Torkelson, J. M. (2016). Major impact of cyclic chain topology on the tg-confinement effect of supported thin films of polystyrene. *Macromolecules*, *49*(1), 257–268.

Zhang, L., Elupula, R., Grayson, S. M., & Torkelson, J. M. (2017). Suppression of the fragility-confinement effect via low molecular weight cyclic or ring polymer topology. *Macromolecules*, *50*(3), 1147–1154.

Zhang, M., Askar, S., Torkelson, J. M., & Brinson, L. C. (2017). Stiffness gradients in glassy polymer model nanocomposites: comparisons of quantitative characterization by fluorescence spectroscopy and atomic force microscopy. *Macromolecules*, *50*(14), 5447–5458.

Zhang, M., Li, Y., Kolluru, P. V., & Brinson, L. C. (2018). Determination of mechanical properties of polymer interphase using combined atomic force microscope (AFM) experiments and finite element simulations. *Macromolecules*, *51*(20), 8229–8240.

Zhang, Q., Wang, S., Rao, B., Chen, X., Ma, L., Cui, C., Zhong, Q., Li, Z., Cheng, Y., & Zhang, Y. (2021). Hindered urea bonds for dynamic polymers: An overview. *Reactive and Functional Polymers*, *159*, 104807.

Zhang, Y., Ying, H., Hart, K. R., Wu, Y., Hsu, A. J., Coppola, A. M., Kim, T. A., Yang, K., Sottos, N. R., White, S. R., & Cheng, J. (2016). Malleable and recyclable poly(urea-urethane) thermosets bearing hindered urea bonds. *Advanced Materials*, *28*(35), 7646–7651.

Zhang, Z. P., Rong, M. Z., & Zhang, M. Q. (2018). Mechanically robust, self-healable, and highly stretchable “living” crosslinked polyurethane based on a reversible C-C bond. *Advanced Functional Materials*, *28*(11), 1706050.

Zhao, B., Wei, K., Wang, L., & Zheng, S. (2020). Poly(hydroxyl urethane)s with double decker silsesquioxanes in the main chains: Synthesis, shape recovery, and reprocessing properties. *Macromolecules*, *53*(1), 434–444.

Zheng, N., Fang, Z., Zou, W., Zhao, Q., & Xie, T. (2016). Thermoset shape-memory polyurethane with intrinsic plasticity enabled by transcarbamoylation. *Angewandte Chemie International Edition*, *55*(38), 11421–11425.

Zheng, N., Hou, J., Xu, Y., Fang, Z., Zou, W., Zhao, Q., & Xie, T. (2017). Catalyst-free thermoset polyurethane with permanent shape reconfigurability and highly tunable triple-shape memory performance. *ACS Macro Letters*, *6*(4), 326–330.

Zheng, N., Xu, Y., Zhao, Q., & Xie, T. (2021). Dynamic covalent polymer networks: A molecular platform for designing functions beyond chemical recycling and self-healing. *Chemical Reviews*.

Zheng, P., & McCarthy, T. J. (2012). A surprise from 1954: Siloxane equilibration is a simple, robust, and obvious polymer self-healing mechanism. *Journal of the American Chemical Society*, *134*(4), 2024–2027.

Zhou, D., Wang, Y., Zhu, J., Yu, J., & Hu, Z. (2019). Mechanically strong and highly efficient healable organic/inorganic hybrid dynamic network. *Polymer*, *167*, 202–208.

Ziebert, F., & Raphaël, E. (2009). Dewetting dynamics of stressed viscoelastic thin polymer films. *Physical Review E*, *79*(3), 031605.

Zou, W., Dong, J., Luo, Y., Zhao, Q., & Xie, T. (2017). Dynamic covalent polymer networks: From old chemistry to modern day innovations. *Advanced Materials*, *29*(14), 1606100.